UNIVERSIDAD NACIONAL AUTÓNOMA DE MÉXICO

P O S G R A D O E N C I E N C I A S D E L A T I E R R A

ESCUELA NACIONAL DE ESTUDIOS SUPERIORES, UNIDAD MORELIA

INVESTIGACIÓN PALEOMAGNÉTICA DE ROCAS VOLCÁNICAS < 10 KA Y DE CERÁMICAS PREHISPÁNICAS EN CONTEXTOS VOLCÁNICOS DEL OCCIDENTE DE MÉXICO

T E S I S

QUE PARA OPTAR POR EL GRADO DE

DOCTORA EN CIENCIAS DE LA TIERRA (GEOFÍSICA DE LA TIERRA SÓLIDA)

PRESENTA

NAYELI PÉREZ RODRÍGUEZ

TUTOR

DR. JUAN JULIO MORALES CONTRERAS

INSTITUTO DE GEOFÍSICA UNIDAD MICHOACÁN

MIEMBROS DEL COMITÉ TUTOR

DR. MANUEL CALVO RATHERT

UNIVERSIDAD DE BURGOS, ESPAÑA

DRA. MARIE-NOËLLE GUILBAUD

INSTITUTO DE GEOFÍSICA

MORELIA MICHOACÁN, MÉXICO, OCTUBRE 2022

Agradecimientos

Son muchas las personas que me han acompañado y apoyado durante el proceso y conclusión de este trabajo, que sin duda alguna ha sido un trayecto de mucho aprendizaje profesional y personal.

Agradezco al programa de Posgrado en Ciencias de la Tierra de la Universidad Nacional Autónoma de México, al Instituto de Geofísica Unidad Michoacán y a la Escuela Nacional de Estudios Superiores Unidad Morelia por todas las facilidades prestadas durante mis estudios doctorales.

Agradezco al CONACYT por el soporte financiero brindado durante estos cuatro años, sin el cual no hubiera sido posible la realización de este trabajo. Adicionalmente, esta investigación fue apoyado financieramente por los proyectos CONACYT No. 252149 y UNAM-PAPIIT No. IN101920.

Quiero realizar un agradecimiento especial al dr. Juan Julio Morales Contreras, por su guía y paciencia. Sin sus palabras y correcciones no hubiese podido concluir ni la mitad del trabajo que aquí se presenta. Gracias por todos sus consejos y por el conocimiento compartido, aprecio mucho todo el tiempo que dedicó para ayudarme a resolver mis dudas. Muchas gracias por depositar su confianza en mi.

De igual forma quiero agradecer la tutoría del dr. Manuel Calvo Rathert y de la dra. Marie-Noëlle Guilbaud, que junto con el dr. Avto Goguitchaisvili guiaron mi proceso de aprendijaze mediante su crítica siempre objetiva de la investigación. Muchas gracias por su tiempo, sus observaciones y sus consejos.

A mis padres, Inés Rodríguez Daza y Alfredo Pérez Sandoaval, y a mis hermanos, Teresa y Alfredo, que siempre han sido mi apoyo absoluto para poder cumplir mis objetivos personales y académicos. Gracias por su cariño incondicional que siempre ha sido mi fuerza para perseguir mis metas y sobreponerme a las adversidades.

Finalmente, aunque no menos importante, quiero agradecer a todos mis compañeros del Instituto de Geofísica, que se han vuelto grandes amigos y mi segunda familia. Rubén, Rafa, Ale, Ángela, Bere , Daniel, Marco, Ulises. Gracias por su compañía, sus consejos y las pláticas para el desestrés.

Un viaje de mil millas comienza con el primer paso (Lao Tse)

Índice

Resumen

De los diferentes tipos de estudios paleomagnéticos, la determinación de paleointensidades (PI) fidedignas representa un gran reto para la comunidad geocientífica ya que aún no existen las bases teóricas que permitan predecir de manera precisa el comportamiento general de los diferentes minerales magnéticos presentes en los materiales de estudio. Los resultados de experimentos de PI se ven afectados por factores como el tamaño de los minerales magnéticos, su composición química, estabilidad térmica, estructura interna, etc. Lo anterior ha derivado en el desarrollo de distintas metodologías para la determinación de la PI, así como de propuestas de análisis de control, criterios de selección para clasificar las muestras de acuerdo con su idoneidad, alertas sobre posibles causas que dan lugar a experimentos fallidos, y el tratamiento de muestras para aumentar la tasa de éxito de los experimentos junto con la confiabilidad de los datos obtenidos.

La investigación que se presenta en esta tesis reside en la determinación de datos de calidad de valores de intensidad del campo magnético terrestre antiguo registrado en materiales tanto geológicos como arqueológicos pertenecientes a la Faja Volcánica Transmexicana, los cuales fueron formados o elaborados durante el Cuaternario. En el desarrollo del trabajo se consideran tanto las dificultades a superar como los controles de calidad antes mencionados, en donde el análisis de las muestras a partir de un enfoque multi-metodológico toma importancia como un factor adicional para asegurar la calidad de los resultados. Esto con la finalidad de contribuir al enriquecimiento de la base de datos de PI mexicanos para el refinamiento de la curva de variación secular de la región, que por una parte permite conocer y analizar la evolución de una de las componentes del campo magnético terrestre a través del tiempo y, por la otra, permitirá desarrollar una herramienta alternativa y confiable que pueda ser empleada para la datación de materiales dentro de la temporalidad acotada.

Adicionalmente, en los distintos capítulos de la investigación se resalta la versatilidad de los estudios de paleointensidad, ya que al tratar materiales de orígenes tanto geológicos como antrópicos, la información obtenida de los experimentos paleomagnéticos permite obtener información adicional de los respectivos contextos de las muestras. Tal es el caso de las edades de ocupación determinadas para el sitio arqueológico de Tingambato obtenidas a partir de la información registrada en cerámicas prehispánicas de distintos niveles estratigráficos, así como la estimación de temperaturas asociadas al incendio que se infiere llevó al abandono de este lugar hacia el año 900 de nuestra era. Asimismo, la probable ocupación

temprana del sitio arqueológico El Caracol, en la zona del malpaís de Zacapu, determinada a partir de los valores de intensidad obtenidos de sus cerámicas; así como la estimación del tiempo de emplazamiento del volcán El Metate, y el cuestionamiento de su naturaleza monogenética, en virtud de la diferencia de edades obtenida entre sus flujos de lava, y la probabilidad de más de un periodo eruptivo en el volcán Xitle.

Abstract

Among the different paleomagnetic studies, the determination of reliable paleointensities (PI) represents a great challenge for the geoscientific community since currently there are no theoretical bases that allows an accurate prediction of the general behavior of the different magnetic minerals present in the studied materials. The results of the PI experiments are affected by factors such as the size of the magnetic minerals, their chemical composition, thermal stability, internal structure, etc. This has led to the development of different methodologies for PI determinations, as well as control analysis proposals, selection criteria to classify samples according to their suitability, alerts on possible causes that lead to failed experiments and treatment of samples to increase the success rate of the experiments and the reliability of the results.

The research presented in this thesis lies in the determination of reliable intensity values of the ancient terrestrial magnetic field strength recorded in both geological and archaeological materials belonging to the Trans-Mexican Volcanic Belt, which were formed or elaborated during the Quaternary. During the development of the work, both the difficulties to be overcome and the quality controls were considered, where the analysis of the samples from a multi-methodological approach becomes important as an additional factor to ensure the quality of the results. This with the purpose of contributing to the enrichment of the PI Mexican database for the refinement of the secular variation curve of the region, which on the one hand allows knowing and analyzing the evolution of one of the components of the terrestrial magnetic field through the time and, on the other hand, it will allow the development of an alternative and reliable tool that can be used for the dating of materials within the delimited temporality.

Additionally, in the different chapters of the research, the versatility of paleointensity studies is highlighted, since through the study of materials of both geological and anthropic origins, the information obtained from the paleomagnetic experiments allows additional information to be gathered from the corresponding contexts of the samples. That is the case of the occupation ages determined for the archaeological site of Tingambato obtained from the information recorded in pre-Hispanic ceramics of different stratigraphic levels, as well as the temperatures estimation associated with the fire that probably caused the abandonment of this place around the year 900 C.E. Likewise, the probable early occupation the El Caracol archaeological site, in the Zacapu malpaís area, determined from the intensity values obtained from its ceramics; as well as the emplacement time estimation of the El Metate volcano, and the

questioning of its monogenetic nature, due to the difference in ages obtained between its lava flows, and the probability of more than one eruptive period in the Xitle volcano.

1. Introducción

De entre las distintas ramas de las Ciencias de la Tierra, el paleomagnetismo es probablemente una de las disciplinas con mayor versatilidad. Su aplicación ha figurado como punto de apoyo para resolver problemas en diferentes áreas de las Ciencias de la Tierra, por ejemplo, en tectónica (ver Terres y Luyendyk, 1985; Darín *et al*., 2016; Ruíz-González *et al.,* 2022), estratigrafía (ver Huang *et al.,* 2015; Grabowsky *et al.,* 2016; Boschman *et al*., 2019), petrología (ver Lewchuk *et al.,* 1998; Paul *et al.,* 2008; Larson *et al.,* 1985), etc., así como en otros campos del conocimiento, con los que de primera instancia parece no tener relación alguna (p. ej., dentro de las ciencias sociales como la antropología y la arqueología).

Uno de los usos más popularizados de las técnicas paleomagnéticas es, quizás, su aplicación como herramienta de datación, en la que los patrones de inversiones de polaridad han permitido estimar edades relativas de rocas que abarcan múltiples eras geológicas (ej. Lenhardt *et al.,* 2010, Perrin *et al.,* 2013). De manera adicional, estas técnicas han ofrecido la posibilidad de estimar las edades absolutas de materiales con registro de magnetización termoremanente (TRM) gracias a la disposición de curvas de variación secular para los últimos miles de años (ej., Pérez-Rodríguez *et al.,* 2019; Morales *et al.,* 2015; Cejudo *et al.,* 2019). Para que un material registre una TRM se requiere que dentro de su proceso de formación (materiales geológicos) o elaboración (materiales arqueológicos) estén involucradas temperaturas superiores a la temperatura de Curie de los minerales ferromagnéticos que posee, propiciando que estos tengan un comportamiento paramagnético, por lo que se orientan en la dirección del campo magnético terrestre (CMT) y guardan, en principio, una intensidad proporcional a la de éste. Tales características quedan *"congeladas"* en la muestra al disminuir la temperatura y se mantienen invariables en el tiempo bajo ciertas condiciones.

Una de las ventajas que ofrece el uso de las técnicas paleomagnéticas con respecto al uso de ^{14}C, siendo este último uno de los principales métodos de datación radiométrica empleados en materiales geológicamente jóvenes, es la de datar directamente el material de análisis y no un material asociado. Para obtener la edad de una lava por ^{14}C, por ejemplo, se requiere de la presencia de materia orgánica en un nivel estratigráfico correlacionable con la lava.

Sin embargo, para asignar una edad confiable a un material haciendo uso de las curvas de variación secular se requiere de la concentración de una gran cantidad de datos paleomagnéticos, tanto direccionales como

de intensidades, para los sitios y las temporalidades de interés (Korte *et al.,* 2019). A partir de esta premisa se deben considerar algunas dificultades a superar para utilizar de forma efectiva el método paleomagnético como herramienta de datación:

1. A nivel global existe una mayor cantidad de información direccional (declinación e inclinación) del CMT que de sus valores de intensidad (Brown et al., 2021). Esto se debe, principalmente, a que las direcciones del campo geomagnético antiguo se registran de forma paralela en los materiales de estudio, por lo que, haciendo uso de las técnicas de laboratorio adecuadas, se puede realizar la determinación directa de los valores de declinación e inclinación correspondientes (salvo algunas excepciones en las que los materiales poseen un alto grado de anisotropía, ej., Tema, 2009). Por otra parte, el registro de la intensidad en los materiales es proporcional a la intensidad del CMT; su valor depende de la capacidad de magnetización de los minerales presentes en la muestra, lo cual obliga a realizar experimentos de remagnetización en campos de laboratorio conocidos que permiten establecer una constante de proporcionalidad entre la magnetización de la muestra y el campo aplicado. Por tanto, los fundamentos teóricos y los procedimientos experimentales para la determinación de intensidades son más complejos y se ven afectados por una mayor cantidad de variables (derivadas tanto de las características de los minerales portadores de la magnetización como de los protocolos experimentales) que aquellos procesos establecidos para la determinación de direcciones.

   Esto ha resultado en el desarrollo de distintas metodologías para la determinación de paleointensidades (ej., Thellier y Thellier, 1959; Wilson, 1961; Coe, 1967; Shaw, 1974; Yu *et al.,* 2004; Dekkers y Böhnel, 2006), con las que se pretende superar los problemas derivados de las propiedades intrínsecas de los minerales portadores de la magnetización (ej., tamaño de los granos ferromagnéticos; Dunlop, 2002), y/o a las alteraciones provocadas durante el proceso experimental (ej., alteración química de la mineralogía magnética por el incremento de temperatura; Riisager y Riisager, 2001), propiciando un aumento en la tasa de éxito de los experimentos de intensidades que, a menudo, pueden ser inferiores al 50%.

   Actualmente, los métodos con mayor aceptación dentro de la comunidad paleomagnética para la determinación de intensidades son los experimentos de tipo Thellier (Thellier y Thellier, 1959; Coe, 1967; Yu *et al.,* 2004). Por otra parte, durante los últimos años ha incrementado el uso de métodos diseñados para disminuir la alteración térmica de la mineralogía magnética de las muestras, como por ejemplo el método de Múltiples especímenes (Dekkers y Böhnel, 2006;

Fabian y Leonhardt, 2010) y los experimentos de la familia Shaw (Shaw, 1974; Tsunakawa and Shaw, 1994; Yamamoto et al., 2003).

2. La evaluación de la calidad de los datos paleomagnéticos disponibles es también un punto importante por considerar. En la actualidad existen diversos parámetros que permiten evaluar la calidad técnica de los datos obtenidos (ej. Coe *et al.,* 1978; Kissel and Laj, 2004; Leonhardt *et al.,* 2004). Sin embargo, no existe un consenso general sobre la cantidad de parámetros a emplear, así como de los valores precisos que deben tener dichos parámetros para establecer si una determinación de intensidad es o no de calidad (Béguin, 2020).
3. Finalmente, se debe tomar en cuenta la distribución espacial y temporal de los datos paleomagnéticos. En este sentido es importante considerar la abundancia de materiales geológicos y arqueológicos disponibles en el área de interés para poder desarrollar una curva de variación secular regional con la resolución adecuada para poder emplearla como herramienta de datación (Schnepp *et al.,* 2020).

En la investigación desarrollada en la presente tesis se realizó un análisis enfocado en los tres puntos arriba mencionados: la cantidad, la calidad y la distribución espacial y temporal de los datos paleomagnéticos disponibles en México para los últimos 10,000 años. Para alcanzar este objetivo se realizaron distintos ejercicios de aplicación tanto en materiales geológicos como arqueológicos del centro-occidente de México. Esta región del país concentra una gran cantidad de estructuras volcánicas dentro del denominado Campo Volcánico Michoacán-Guanajuato (CVMG) cuya actividad se encuentra dentro del rango temporal de interés (Hasenaka y Carimchael, 1985), además de poseer una gran riqueza cultural (Espejel, 2014), por lo que fue considerada un área idónea para la investigación propuesta. Adicionalmente, dada la interdisciplinariedad de la investigación, los resultados obtenidos no sólo conducen a la generación de información de interés dentro del área de paleomagnetismo, sino que también aportan información para una mejor comprensión de la actividad volcánica de la región y de las dinámicas poblacionales de las sociedades prehispánicas que habitaron la zona.

En los capítulos 2 y 3 se presentan los resultados obtenidos de los ejercicios realizados sobre materiales arqueológicos. En el primero de ellos: *"An inter-comparison exercise for the Mexican intensity secular variation curves: Case study of the Tingambato archaeological site (central-western Mexico)",* se presentan los resultados obtenidos para un conjunto de cerámicas localizadas dentro del sitio arqueológico de Tingambato en el estado de Michoacán. Con los resultados de este estudio se pudieron determinar edades para dichas cerámicas haciendo uso de distintas curvas de intensidad para la variación

secular en México. Por otra parte, algunas de las cerámicas estudiadas están asociadas con el incendio que se cree incitó al abandono del sitio arqueológico (Punzo-Díaz *et al.,* 2016). Gracias al análisis de las distintas componentes de magnetización registradas en estas cerámicas se pudieron estimar temperaturas asociadas a dicho incendio. Adicionalmente, el análisis de las distintas componentes de magnetización registradas en una misma cerámica permitió delimitar el rango temporal relacionado con la elaboración y uso de estos artefactos. Finalmente, en este trabajo se presenta un análisis comparativo de las características de las cuatro curvas de variación secular disponibles para México (hasta el año 2021) elaboradas exclusivamente con los valores del parámetro de intensidad del CMT. El procedimiento empleado en la elaboración de la más reciente de estas curvas se puede revisar en el Apéndice A: "*On the absolute geomagnetic intensity fluctuations in Mexico over the last three millennia"*.

Asimismo, los resultados que se presentan en el capítulo 3: *"Archaeomagnetic evidence of a likely earlier occupation of "El Caracol" lava flow (Zacapu Malpaís, Western Mesoamerica)",* siguen la misma metodología planteada en el trabajo desarrollado en el capítulo 2. En este caso la interpretación de los resultados obtenidos permitió realizar especulaciones sobre el posible poblamiento temprano de un área del Malpaís de Zacapu (Estado de Michoacán) conocida como El Caracol. En general, el crecimiento de poblaciones en esta región se considera controversial debido a las condiciones inhóspitas que presenta el terreno por sus características geológicas para el desarrollo de grupos humanos (Michelet *et al.,* 2018).

En los capítulos 4, 5 y 6 se presentan los resultados obtenidos en los trabajos realizados sobre materiales geológicos. Para estos ejercicios se siguió un enfoque distinto al empleado en el análisis de los materiales arqueológicos, dando prioridad a la aplicación de un análisis multi-metodológico que permitiera aumentar la confiabilidad de los valores de intensidad obtenidos en los distintos sitios de estudio. Los volcanes que se presentan en los tres capítulos cuentan con estudios de paleointensidades previos, por lo que en el análisis realizado se incluyó la evaluación de la calidad de dichos resultados, los cuales se compararon con los datos aquí obtenidos.

En el capítulo 4: "*A multimethod paleointensity approach applied to the historical Xitle lava flows (Central Mexico): towards the accurate paleointensity determination"* se analizan los datos obtenidos para el volcán Xitle (Ciudad de México). Este es uno de los volcanes con mayor cantidad de estudios de paleointensidades en México, los cuales iniciaron en la década de los 60's del siglo pasado (Nagata *et al.,* 1965b) y han sido controversiales debido a la dispersión en los valores de intensidad reportados, abarcando un rango desde $\sim$ 50 µT hasta más de 80 µT. Gracias al estudio realizado se determinó un valor

de intensidad con una dispersión menor, el cual además está sustentado por la aplicación de tres metodologías distintas.

Caso contrario, las tres estructuras volcánicas analizados en el capítulo 5: *"Reassessing the paleointensities of three volcanic structures of the Michoacán-Guanajuato Volcanic Field (Mexico) through a multimethodological análisis"* han sido poco estudiadas, tanto en cuestiones paleomagnéticas como vulcanológicas. Aunado a esto, los valores de intensidades previamente reportados para dichas estructuras fueron determinados con una cantidad mínima de especímenes, generando ambigüedad en la calidad de los resultados. Otro punto por destacar al considerar los estudios previos es el uso del método Shaw (Shaw, 1974) para la determinación de la intensidad de una de las estructuras volcánicas; la aplicación de este método se mantiene actualmente en debate debido al escaso sustento teórico con que cuenta y se prefiere el uso de sus variaciones posteriormente desarrolladas. Todos estos factores llevaron a plantear la necesidad de realizar nuevas determinaciones de intensidades para dichas estructuras a través del enfoque multi-metodológico antes mencionado. Con los resultados obtenidos se confirmó el valor de intensidad previamente reportado para la lava fisural del Malpaís Prieto de Zacapu haciendo uso de dos metodologías distintas, además de la previamente empleada; se descartó el valor de intensidad antes reportado para el volcán monogenético el Jabalí aportando nuevos datos de intensidades a partir de dos metodologías; y se abrió un debate con respecto a la diferencia de más de 20 µT encontrada entre los valores de intensidad reportados previamente para uno de los flujos de lava del volcán Rancho Seco con respecto a los valores determinados en el presente trabajo.

El tercer estudio realizado sobre materiales geológicos corresponde al volcán el Metate. Por las dimensiones de sus flujos de lava ha sido considerado como el volcán más grande emplazado durante el Holoceno en México. En estudios previos, tanto vulcanológicos como paleomagnéticos, se determinó que el volcán se formó durante una sola fase eruptiva continua, por lo que fue considerado de origen monogenético. Sin embargo, los resultados mostrados en el capítulo 6: "Reassessment of the eruptive chronology of El Metate shield volcano (central-western Mexico) based on a comprehensive rock-magnetic, paleomagnetic and multi-approach paleointensity survey", presentan evidencias del registro de la variación secular entre los distintos flujos de lava, indicando que el tiempo de emplazamiento del Metate fue mayor a lo antes propuesto, y probablemente en más de una etapa, poniendo en duda la naturaleza monogenética con que inicialmente se describió.

Finalmente, se plantean las conclusiones generales de la investigación en el capítulo 7.

2. An inter-comparison exercise for the Mexican intensity secular variation curves: Case study of the Tingambato archaeological site (central-western Mexico) https://doi.org/10.1016/j.quageo.2021.101195

Nayeli Pérez-Rodríguez, Juan Morales, David Rangel-Campos, Avto Goguitchaichvili, José Luis Punzo-Díaz

Quaternary Geochronology

2.1 Resumen

Se presentan los resultados obtenidos del estudio arqueomagnético de 11 fragmentos cerámicos provenientes del sitio arqueológico de Tingambato, Michoacán (México). Se realizó la caracterización de la mineralogía magnética de las muestras mediante experimentos de magnetismo de rocas: curvas de histéresis, campo inverso, magnetización remanente isotérmica y curvas termomagnéticas, así como la desmagnetización térmica y por campos alternos de especímenes representativos de cada fragmento cerámico. Dichos experimentos fueron de utilidad para estimar el potencial del uso de los materiales de estudio en experimentos de arqueointensidades mediante el tamaño de grano de los minerales magnéticos, su composición, estabilidad térmica y la cantidad de componentes de magnetización registradas en las cerámicas.

La presencia de dos componentes de magnetización en cinco de las cerámicas analizadas proporciona información puntual del comportamiento de la intensidad del campo magnético terrestre en dos temporalidades distintas; una asociada con el momento de elaboración de las cerámicas, y la otra con la última exposición al fuego que tuvo la cerámica. Los valores de intensidad se obtuvieron siguiendo criterios de calidad estrictos. Adicionalmente se consideraron procesos como el ritmo de enfriamiento y las correcciones por efectos de anisotropía. Considerando dichos criterios se obtuvieron intensidades para cuatro de los once fragmentos cerámicos analizados. Las principales causas de falla en los experimentos de arqueointensidad se asociaron con la alteración de la mineralogía magnética durante los calentamientos de los especímenes, así como con la presencia de granos de dominio múltiple.

Finalmente, tras analizar las características de las 4 diferentes curvas de variación secular actualmente disponibles para modelar la intensidad del campo magnético en México durante los últimos milenios, se eligieron las dos curvas de variación secular que presentan los datos de mayor calidad de acuerdo con los parámetros actualmente usados en la literatura. Ambas curvas se usaron para realizar un ejercicio de datación con las intensidades de calidad determinadas en las 4 cerámicas. De igual forma, y con fines comparativos, se empleó el modelo global SHA.DIF.14k.

El ejercicio de datación muestra una mejor correspondencia de los valores de intensidad con las curvas regionales que con el modelo global, especialmente para el rango temporal entre 400 – 1200 d. C., para el cual ambas curvas regionales tienen la mayor concentración de datos y una buena correspondencia entre ellas. Las edades arqueomagnéticas obtenidas concuerdan con las edades de radiocarbono reportadas en estudios previos. Gracias a los dos valores de intensidad estimados en una de las cerámicas, se estimaron por primera vez edades del probable fin de la ocupación del sitio de Tingambato.

2.2 Abstract

Dating analysis of potsherds from three of the six units recently excavated in the Tingambato archaeological site, central-western Mexico, was carried out employing two regional intensity Paleosecular Variation Curves (PSVC) and the global model SHA.DIF.14k. A complete evaluation of the ceramic fragments' magnetic characteristics was done to determine the samples' magnetic carriers and their capacity to provide reliable archaeointensity data. The presence of two magnetization components in five analyzed potsherds provides two snapshots of the Earth's magnetic field intensity behavior at different temporalities. Intensity values were obtained following strict quality criteria, including cooling rate and anisotropy corrections. The principal causes of failure in archaeointensity experiments are associated with the alteration of the magnetic mineralogy during the heating of the specimens and with the presence of MD grains. Intensities within the established quality criteria were obtained for four of the eleven ceramic fragments analyzed. The dating exercise shows a better correspondence of the intensity values with the regional curves than with the global model, especially for the temporal range between AD 400 – 1200, for which both regional curves are in good agreement. The obtained archaeomagnetic ages had a good correspondence with the radiocarbon ages reported in previous studies. By determining two archaeointensity values in one of the studied potsherds: one associated with its fabrication and the other

related to the fire (after which the site is supposed to be abandoned), archaeomagnetic ages of the probable end of Tingambato occupation were estimated.

2.3 Introduction

Understanding the Earth magnetic field (EMF) behavior is a great scientific challenge since the EMF is generated in the planet's outer core and cannot be observed directly. Additionally, the EMF behavior is non-constant on time; it exhibits fluctuations from hundreds of years (e.g., secular variation) to millions of years (e.g., paleomagnetic reversals). While the main dipolar geomagnetic field variations rates display similar patterns around the world (Valet, 2003), as the Matuyama – Brunhes geomagnetic reversal about ~773 ka ago (Suganuma *et al*., 2018; Singer *et al*., 2019), secular variation patterns are distinctive in each region of the Earth's surface due to the EMF's non-dipolar constituents (DuBois, 1975). The registers of the EMF's first direct measurements were carried out at the beginning of the nineteenth century. Hence, for the analysis of its variations before this epoch and through geological history, it is necessary to use the records logged in different materials (Aitken *et al*., 1988), like geological and archaeological materials, which are the only empirical data source recording the EMF variations in the Earth's surface.

The relevance of using EMF variation patterns as a dating tool for rocks, sediments, and archaeological samples in paleo- and archaeomagnetic studies has been featured since the pioneering studies (Thellier, 1938; Aitken, 1970). During the last years, an increasing number of EMF variation models covering the most recent millennia, have been developed, and age estimate up to the decadal resolution is now possible in some parts of Europe (Korte *et al*., 2019). The global models of the EMF variations, as the name implies, were created to encompass the entire Earth's surface. Some models employ the full available catalog of paleomagnetic inputs: sedimentary deposits, archaeological, and volcanic data (e.g., CALS3k model; Korte and Constable, 2003); others are only based on the sedimentary records (e.g., SED3k.1; Korte *et al*., 2009), and finally, a third group avoid the use of sedimentary information (e.g., SHA.DIF.14k model; Pavón-Carrasco *et al*., 2014) due to the complexities associated to their paleomagnetic records, (e.g., incomplete understanding of the detrital remanent magnetization process, possible environmental bias, and a general smoothed representation of the field; Roberts and Winklhofer, 2004). Nevertheless, the irregular coverage of the archaeomagnetic data, both in space and time, makes the magnetic field estimation untrustworthy in many areas and periods (Casas *et al*., 2018). Consequently, the construction

of regional reference models is indispensable. Such a process requires obtaining and gathering enough archaeomagnetic results from a specific area (with a radius of ~1200 km; Thébault *et al*., 2015) with a particular temporality. So, the process of regional paleosecular variation curves (PSVC) modeling entails years of work (Korte *et al*., 2019).

The ancient geomagnetic field analysis comprises the retrieval of at least one of the three geomagnetic field elements: declination (D), inclination (I), or intensity (F) (Butler, 1992), and for each one of these components, a different EMF pattern is obtained. For volcanic rocks and burned archaeological materials, the EMF direction is recorded parallel to the direction of the geomagnetic field at the time of formation (or elaboration) of the studied material (e.g., Calvo-Rathert *et al*., 2019) and is easily determined through a thermal (TH) or alternating field (AF) demagnetization. However, the intensity recorded is proportional to the EMF's strength, and numerous methodologies for its determination exist (for a review of state of the art, see Tauxe and Yamazaki, 2015), although the most widely accepted procedures are those based on the Thellier method (Thellier and Thellier, 1959). Furthermore, tests for thermal stability verification (Leonhardt *et al*., 2004), cooling rate (Chauvin *et al*., 2000), and anisotropy of remanence (Veitch *et al*.; 1984) correction procedures, developed during the last four decades, are required to warrant the quality of the data. Therefore, a careful analysis of the data quality to be used while elaborating a secular variation curve is also needed. Similarly, accurate verification of the independent dating associated with archaeomagnetic information is essential (Casas and Tema, 2019).

Owing to the scarce high-quality archaeomagnetic data available for a region, or because of the unreliability of regional PSVCs, global models are often used as a dating tool instead (e.g., Goguitchaichvili *et al*., 2015). However, as is mentioned in the previous paragraphs, most of the data used in global models are outside of these regions; thus, they do not necessarily reflect the regional field behavior, and significant dating uncertainties are expected (Roperch *et al*., 2015).

Mexico is a country with great potential for archaeomagnetic studies because of its tremendous cultural legacy (Gasco *et al*., 2016) and the large number of volcanic structures (emplaced or with activity during Holocene times) distributed throughout the country (e.g., la Virgen volcano at the north, Paricutín and Xitle in the central sector, and Chichón at the south). Therefore, Mexico has the possibility of possessing an adequate regional PSVC.

The archaeomagnetic study of potsherds of the Tingambato archaeological site (Michoacán, Mexico) is presented in this work. Differences in archaeomagnetic ages obtained with the global model SHA.DIF.14k

and two regional PSVC (Mahgoubd *et al*., 2019; García *et al*., 2020), whose main behavior differences come from the data selection and weighting, are analyzed, as well as the archaeological implications of the different temporalities associated with each model.

2.4 Archaeological context

Tingambato (19° 29’ 39.40” N, 101° 51’ 30.98” W), also known as Tinganio (the place where the fire ends, in Purhépecha language) by local people, is an archaeological site located in the municipality of Tingambato, Michoacán state (Mexico) (Figure 1). It is part of the western Mesoamerican Prehispanic cultures, which are frequently associated with the Tarascan empire, that dominated the area since the beginning of the thirteenth century and until the Spaniard conquest in the sixteenth century (Carot, 2005).

Sites occupied before this temporality, such as Tingambato (AD 0 - 900; Punzo-Díaz, 2016), are referred to as pre-Tarascan sites. Many archaeological investigations in sites with these early temporalities began only a few decades ago and are still in progress (Espejel-Carbajal, 2014).

The four chronological proposals made so far for Tingambato are described in the following paragraphs.

The first systematic research in Tingambato archaeological site was managed in 1978 (Piña-Chan and Ohi, 1982). As a result of this early intervention, two construction stages were associated with the site. The first between AD 450 and 600, in which the settlement and construction of the ceremonial center started; and the second stage, from AD 600 to 900, in which a Teotihuacan style was introduced in the place’s architecture as well as the construction of a ball court. The ages of both construction stages were associated by means of architectural characteristics and ceramic styles. Within this chronology, the idea the site was abandoned due to a fire was proposed. It has been maintained for the rest of the proposed chronologies and prevails until now; both -ashes and burned structures- were left as evidence (Piña-Chan and Ohi, 1982). Subsequently, also following an age association by the ceramic/architectonic style method, Ohi (2005) proposed the beginning of the Tingambato occupation around AD 600, concluding in the first half of the eleventh century.

On the other hand, Cruz and Landa (2013) established the occupation of Tingambato between AD 200 and 700 – 750, with three construction stages: the first stage corresponding to the construction of the eastern and western pyramidal structures, as well as an early ground leveling. For the second stage, they propose

the construction of a large platform, tombs, dipped courtyards, and the introduction of the Teotihuacan talud-tablero style. Finally, the third stage corresponds to the covering of the talud-tablero structures. The temporalities of the three chronologies described above were proposed based on their contemporaneity with other neighboring regions, principally with those of Teotihuacan and Zacapu (center and west Mexico, respectively). Such contemporaneity was assumed by the similitudes with some architectural and pottery styles. However, no direct dating studies on Tingambato materials had been conducted.

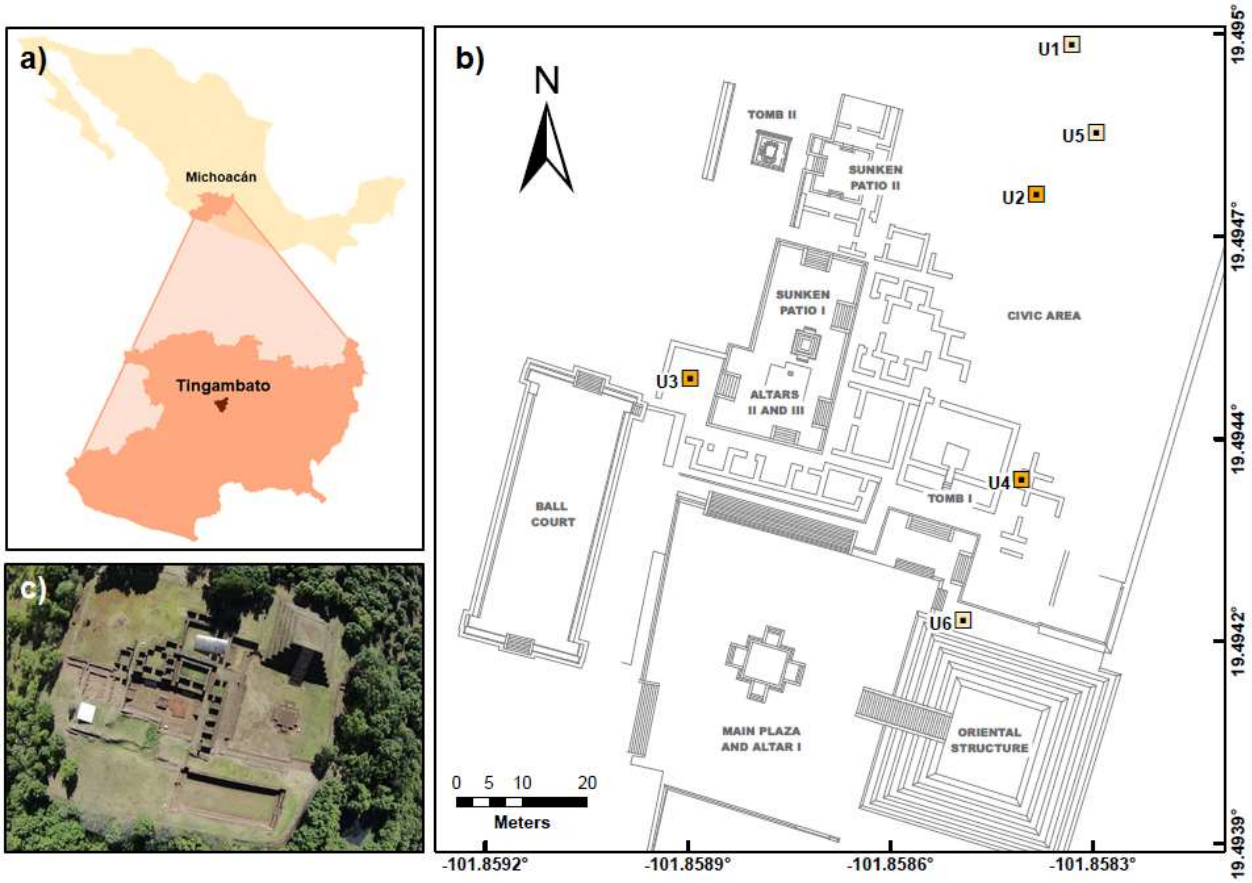

Figure 1 Location of the study area. a) Ubication of Tingambato municipality. b) Plane of Tingambato archaeological site. The names of the main structures are shown. U1-U6: Excavation areas; oranges squares: sampled excavation areas. Modified of Punzo-Díaz 2016. c) Aerial view of the archaeological site.

The last chronology proposed for Tingambato was elaborated by Punzo-Díaz (2016), who established three occupational phases: Tingambato I (AD 0 – 300); Tingambato II (AD 300 – 600); and Tingambato III (AD 600 – 900). Each phase's onset is marked in the archaeological site with a ground leveling, which was

implemented with filling materials. Compared to the past proposals, the principal advantage of this chronology is that it not only considers the ceramic styles and architectural elements to associate ages, but it is also the first one that uses radiometric (^{14}C) and collagen ages to date the different occupation stages. Accordingly, the chronology proposed by Punzo-Díaz (2016) is used as a reference for the present work.

2.5 Materials and Methods

2.5.1 Pottery sherds description and preparation

As part of the Archaeology and Landscape of the South-Central Area of Michoacán Project (PAPACSUM, by its abbreviation in Spanish), six units were excavated in Tingambato archaeological site (U1 – U6 in Figure 1b) during the years 2015 to 2017. A total of eleven pottery sherds with distinct ceramic styles were selected for archaeomagnetic purposes: Rojo Pulido (RPB2) and Rojo Escobillado (REB2) for U2. Both fragments were found in a context associated with the fire that caused the site's abandonment; they are burned, and the presence of ashes was recognized around. Café Pulido (CPF3), Cherán (CHF3), and Loma Alta Pulido (LAF3) from U3; Zacapu Café (CZD4), Tres Palos (TPE4), Unidentified-1 (UNE4), Lupe Punzado (LPD4), Unidentified-2 (UNI4) and Rojo Pulido from U4 (RPH4). A view of the different above-described ceramic types is presented in Figure 2. The two first letters of the potsherd labels represent the ceramic style. The third letter corresponds to the excavation layer, where A is the superficial layer, and B, C, etc., are consecutively deeper layers. The number in the last position of the label corresponds to the excavation site number. The ceramic style was associated according to the proposal elaborated by García-García (2017).

Potsherds preparation for Thellier experiments consisted, firstly, of setting a random reference system over one of their flattening planes. Such reference systems were signalized with a set of parallel arrows. Then, pottery sherds were cut in at least six "oriented" sub-samples with surfaces of ~1 cm^2. These were compressed into salt pellets with a non-magnetic hydraulic press to process them as standard paleomagnetic samples (22 mm long × 25 mm diameter). According to the established reference system, each subsample was embedded in a different position (±X, ±Y, ±Z). To identifying the embed direction of

the six specimens into the salt pellets during the archaeointensity experiment, the top of all pellets was marked in the +X direction.

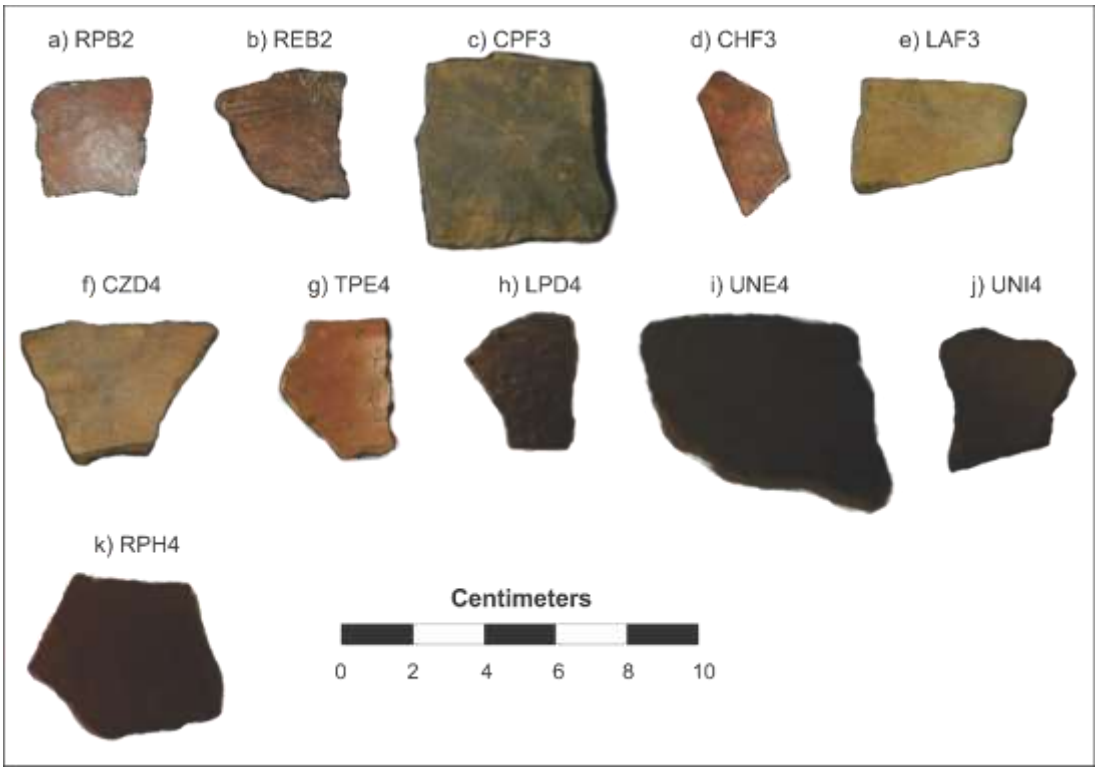

Figure 2 Tingambato potsherds worked in the present study.

2.5.2 Magnetic Mineralogy

Between 250 and 300 mg per potsherd were pulverized to complete four classical rock-magnetism experiments to characterize the magnetic mineralogy carrying the remanent magnetization and to check its thermal stability: 1) Isothermal Remanence Magnetization (IRM) acquisition curves and 2) hysteresis loops were carried out up to a maximum field of 0.7 T. The hysteresis loops were corrected for drift and high field slope. The saturation remanent magnetizations (M_{rs}), saturation magnetizations (M_s), coercivity fields (B_c), and shape (σ) parameters were determined. 3) Backfield curves after saturation was used to obtain the parameter of remanence coercivity (B_{cr}). Finally, 4) Thermomagnetic curves were acquired between room temperature and 600 °C. The Rock – Mag Analyzer 1.0 software (Leonhardt, 2006) and the

HystLab v1.0.9 MATLAB tool (Paterson *et al*., 2018) were used to evaluate the advanced variable field translation balance (AVFTB) obtained data. Due to the small size of CHF3, TPE4, and UNE4, no rock magnetism experiments could be done for these potsherds. These experiments were carried out employing an AVFTB from Magnetic Measurements Ltd.

In addition to the rock magnetic experiments, detailed tumbling stepwise alternating field (AF) demagnetization up to 50 – 100 mT, with increments of 5 to 10 mT between each step, depending on the behavior of the magnetic minerals of each potsherd, were performed using an AGICO LDA 3 equipment to isolate the characteristic remanent magnetization (ChRM) of the samples. Measurements of Natural Remanent Magnetization (NRM) and laboratory Alternating Field Demagnetizations (AFDs) were carried out with an AGICO JR6 spinner magnetometer. Data were analyzed using the MS Windows application, Remasoft 3.0, by Chadima and Hrouda (2006). The pottery sherd's suitability to get reliable archaeointensities (AI) was established based on the documented characteristics of the magnetic mineralogy.

2.5.3 Archaeointensity determinations

The AI experiments were performed following the Thellier-Coe (TC) method (Thellier and Thellier, 1959; Coe, 1967). Thirteen heating and cooling steps were performed in the air from room temperature to 560 °C, at which ~ 90% of the specimen's original NRM was erased and replaced by a partial thermoremanent magnetization (pTRM). An ASC Scientific TD48-SC furnace, with reproducibility of ~2 °C between heating steps, was used. The laboratory field strength was set to 45.0 (± 0.5) µT along the salt pallets' cylindrical axis. Every third temperature step, pTRM checks were carried out, and a pTRM tail check (Riisager and Riisager 2001) determination was implemented at 350 °C. AI determinations were completed with the ThellierTool 4.0 software (Leonhardt *et al*., 2004). The Arai Plot curvature (k) was calculated using the method suggested by Paterson (2011), with the support of the MATLAB CircleFitByPratt (XY) function (Chernov, 2020) based on Pratt's method (Pratt, 1987).

The cooling rate (CR) dependence effect was evaluated with three additional infield steps at 560 °C following a modified procedure (Morales *et al*., 2009) to that described in Chauvin et al. (2000). Between the two fast cooling steps (TRM1 and TRM3), which took ~45 min, a slow cooling step (TRM2) of ~6 h was carried out. The correction factor (f_{CR}) was calculated as the difference between the magnetizations

acquired with the first fast step (TRM1) and the slow step (TRM2). Variations in the TRM acquisition capacity were measured using the percent change between fast cooling steps. When $f_{CR} > 1$ and the normalized ratio between the magnetization acquired at TRM1 and TRM3 was ~1, CR correction was applied.

Trying to avoid the magneto-mineralogical alteration generated by at least six additional heating required for the TRM anisotropy correction (McCabe *et al*., 1985), the approach developed by Morales *et al*. (2009) was implemented. This method requires six specimens embedded in salt pellets in six different positions (±X, ±Y, ±Z) and the laboratory field's application along the pellet's Z-axis during the TC experiment. Under these conditions, the possible bias generated due to remanence anisotropy is reduced. Additionally, the low degree of anisotropy can be confirmed or rejected with the low standard deviation in the six AI values obtained for a potsherd sample (Kapper *et al*., 2020). For a more detailed analysis regarding this approach's use, see García *et al*. (2020).

2.6 Results

2.6.1 Rock magnetism experiments

The isothermal remanence magnetization (IRM) acquisition curves results (Figure 3) indicate a saturation magnetization (M_s) between 250 and 300 mT for the ceramic samples RPB2 (M_s= 6.63×10-8 Am^2/kg), REB2 (M_s= 1.23×10^{-7} Am^2/kg), LAF3 (M_s= 1.87×10^{-7} Am^2/kg), CZD4 (M_s= 7.28×10^{-8} Am^2/kg), and LPD4 (M_s= 9.24×10^{-8} Am^2/kg), which suggest the dominance of low coercivity minerals of titanomagnetite of single-domain (SD) and/or pseudo-single domain (PSD) grain size. Potsherds CPF3 (M_s= 6.05×10^{-8} Am^2/kg), UNI4 (M_s= 3.70×10^{-7} Am^2/kg), and RPH4 (M_s= 3.04×10^{-7} Am^2/kg) reach saturation near 400 mT, evincing the domination of intermediate coercivity minerals of magnetite of SD and/or PSD grain size slightly replaced with Al, Mg, or Ti as the dominant magnetization carriers. Both magnetic mineralogies are considered appropriate for AI determinations.

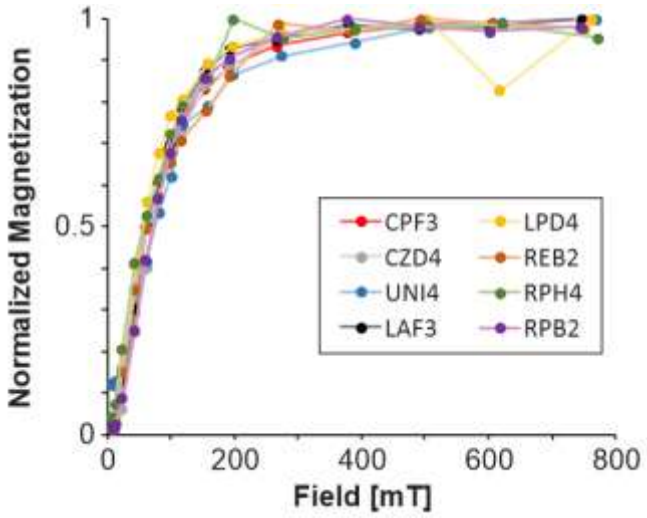

Figure 3 Representative isothermal remanent magnetization (IRM) acquisition- curves for eight pottery sherds of the Tingambato archaeological site.

The mixture of contrasting magnetic fractions coercivities was quantified according to the hysteresis loop shape parameter (σ) of Fabian (2003). The shape parameter compares the area of an ideal hysteresis curve with identical upper and lower branches (blue and red lines respectively in Figure 4b), for which a rectangular area with height 2MS and width 2BC (4MSBC, σ = 0) is formed, with the area covered for a wasp-waisted loop (> 4MSBC, σ > 0) and the area covered by a potbellied loop (< 4MSBC, σ < 0) . Ceramic fragments REB2, LAF3, RPH4, and UNI4 (Figure 4a, d, f, and g) show a wasp-waisted shape, commonly associated with the mixture of SD and large superparamagnetic (SP) particles, while potsherds RPB2, CPF3, LPD4, and CZD4 (Figure 4b, c, e, and h) exhibit the characteristic potbellied loop behavior, related to the mixture of SD and small SP particles (Tauxe *et al*., 1996). Additionally, for a broad approach about the bulk magnetic domain structure of the Tingambato potsherds, the ratio between M_{RS} / M_S and B_C / B_{CR} parameters gotten from the hysteresis loops are displayed in the Day plot (Day *et al*., 1977) with the theoretical curves for SD-MD and SP-SD magnetite mixtures proposed by Dunlop (2002) (Figure 5). As can be seen, the analyzed sherds fall within the SD -MD mixing region of Dunlop and between the PSD (RPB2, CZD4, LPD4 and LAF3) and MD (CPF3, REB2, UNI4 and RPH4) fields of Day, reflecting the mix of high and low coercivity magnetic components described before through the shape parameter.

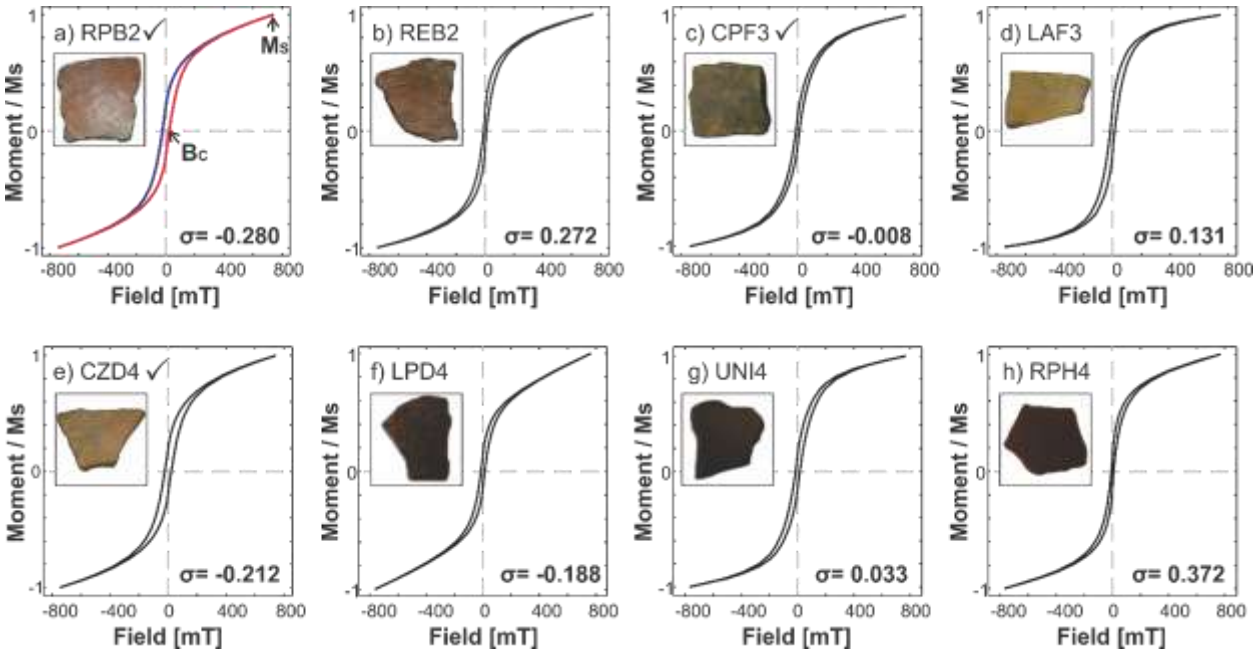

Figure 4 Representative examples of hysteresis plots for Tingambato potsherds. See description in the text. The inset in the plots are the analyzed potsherds. The checkmark in a), c) and e) indicate the samples with specimens that ended up passing the AI criteria and were used for the dating exercise.

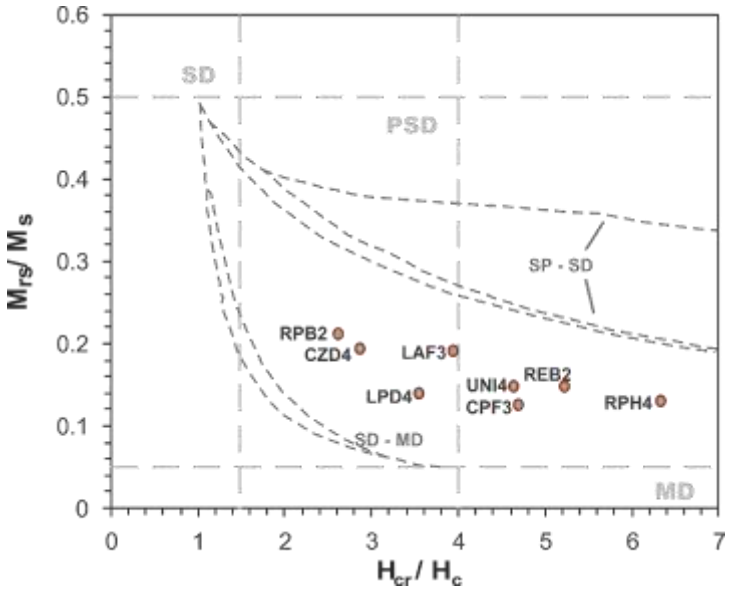

Figure 5 Day-plot with theoretical curves (Dunlop, 2002) for SD-MD and SP-SD magnetite mixtures.

Following the use of the Moskowitz method for the Curie Temperature (T_C) determination (Mozkowitz, 1981) and with the use of thermomagnetic curves classification proposed by Calvo *et al*. (2002), three

different behaviors were recognized (Figure 6): 1) Type H samples (REB2, RPB2, and LAF3 potsherds) exhibit a single ferromagnetic phase with a Curie Temperature (T_C) ~560 °C, corresponding to magnetite or a near magnetite composition. Curves are reversible with a difference in magnetization acquisition between the heating and the cooling behavior < 30%. 2) The Type H(mx) curves have similar characteristics to the type H samples; high reversibility and a main magnetic phase with T_C related to close magnetite composition, but additionally show another T_C between 450 and 500 °C associated with Ti-poor titanomagnetites, in this group are the potsherds CPF3 and CZD4. 3) Type M samples (LPD4, RPH4, and UNI4 potsherds) are characterized by irreversible curves. The heating curve of the potsherd RPH4 shows an intermediate T_C phase (~500 °C) and a high T_C phase (~560 °C), while the cooling curve only presents the high T_C phase. The heating curve of the potsherd UNI4 shows only a T_C phase at ~560 °C, while in the cooling curve additionally appears a T_C at ~450 °C. Finally, for the potsherd LPD4, a main T_C phase with near magnetite composition is observed in the heating and cooling process. The differences between the magnetization acquisition of heating and cooling curves are > 50% for the three potsherds. The sets of type H and H(mx) samples are considered as high-quality for AI determinations due to the low alteration suffered in thermal processes.

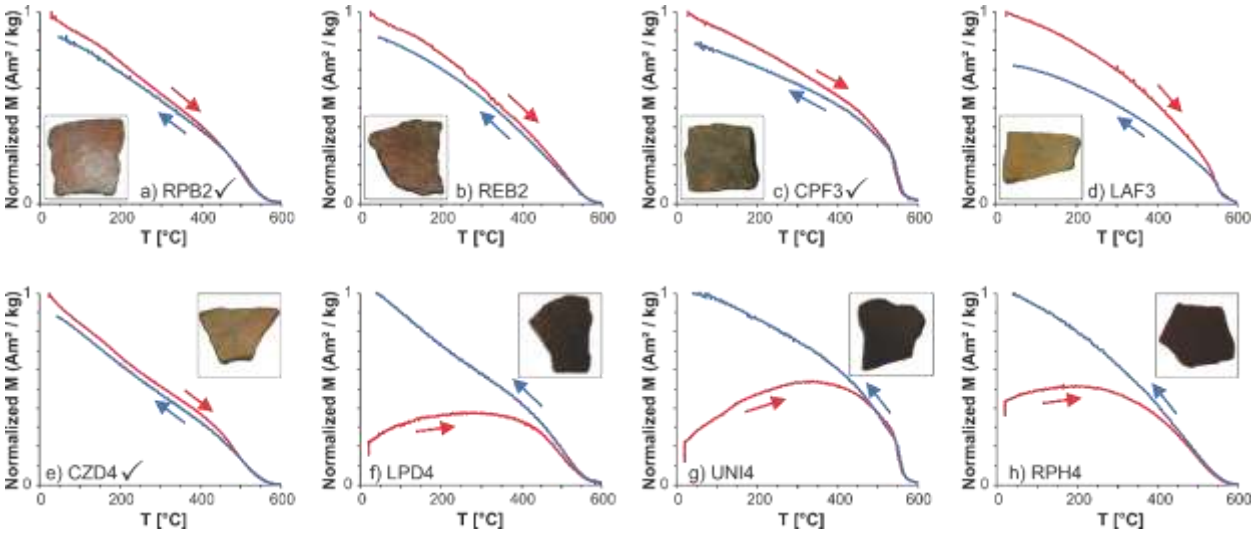

Figure 6 Thermomagnetic curves (M – T) for the Tingambato potsherds. The inset in the plots are the analyzed potsherds. The checkmark in a), c), and e) indicate the samples with specimens that ended up passing the AI criteria and were used for the dating exercise.

2.6.2 Alternating field demagnetization

Representative AFD behaviors of the analyzed ceramic fragments are presented in the Zijderveld diagrams in Figure 7. The magnetization of potsherds RPB2, CPF3, CZD4, and RPH4 (Figures 7a, 7c, 7e, and 7h) is composed by two components: the ChRM and a secondary magnetization component, which is erased at maximum fields of 40 mT.

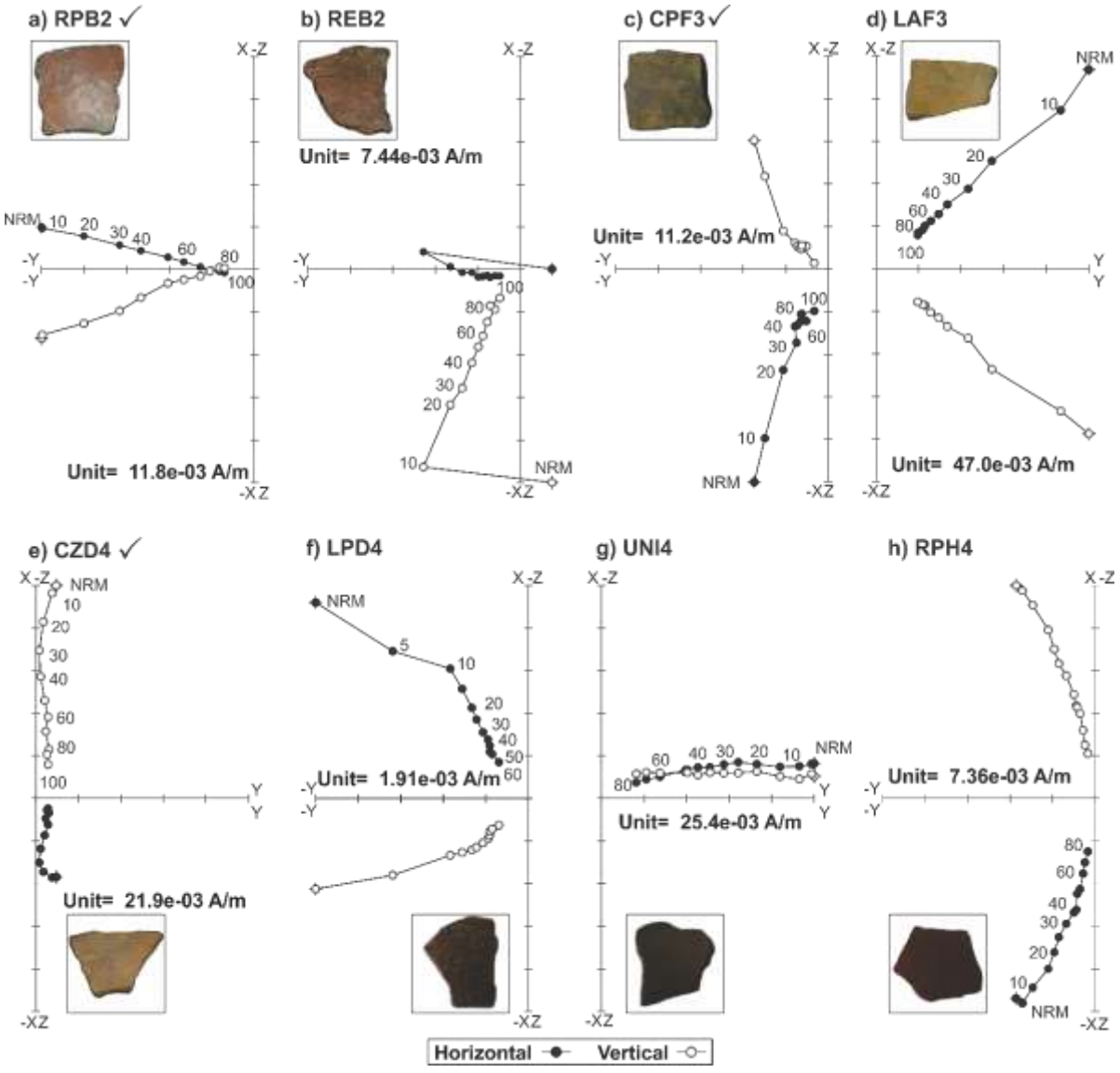

Figure 7 Representative Zijderveld (1967) plots of AF demagnetized samples. Labels along curves denote the maximum AF amplitude applied by each step. The inset in the plots are the analyzed potsherds. The checkmark in a), c), and e) indicate the samples with specimens that ended up passing the AI criteria and were used for the dating exercise.

On the other hand, the magnetization of the potsherds REB2, LAF3, LPD4, and UNI4 is characterized by a primary archaeomagnetic component towards the origin and an initial overprint of possible viscous origin, which is removable at fields between 10 and 20 mT. The residual remanence after AFD of the specimens at fields of 100 mT suggests the presence of a mineral phase of high coercivity in the potsherds, such as fine-grained hematite.

According to the results of rock magnetism and AFD experiments, unreliable results for AI determinations of RPH4, LPD4, and UNI4 samples were expected, also considering that no previous rock magnetism data were available for evaluating magnetic mineralogy quality of CHF3, TPE4, and UNE4 samples.

2.6.3 Archaeointensities

2.6.3.1 Thermal demagnetization

To start the analysis of archaeointensity data, the Thellier-Coe experiment's zero-field steps were separated and examined independently to review the specimen's TH demagnetization behavior. In general, three comportments were observed: 1) The Zijderveld diagrams show a single directional component of magnetization, i.e., the observed magnetization corresponds to the NRM acquired by the ceramic at the time of their elaboration (M1). In some cases, M1 is accompanied by a magnetization of viscous origin (VRM), which is erased by maximum temperatures of 200 °C. The potsherds in this group are REB2, LAF3, TPE4, UNE4 and UNI4 (Figures 8b, e, g, l, and j, respectively). The specimen's M1 component of REB2 and CPF3 potsherds are noisy, and for most specimens of the potsherds UNE4 and UNI4, the M1 component does not tend to the origin. 2) The Zijderveld diagrams show two main directional components. A probable potsherd's reheating is exhibited by a secondary component of magnetization (M2), which erased a fraction of M1, leaving only a portion of the original NRM (pM1). The potsherds in this group are RPB2, CPF3, CHF3, CZD4 and RPH4 (Figures 8a, c, d, f, and k, respectively). The maximum temperature reached by the M2 components is between 350 and 475 °C. The potsherds in this group coincide with those presenting double magnetization components in the AFD experiment (see section 2.5.2 Alternating field demagnetization), except for the potsherd CHF3 for which no AFD experiments could be realized.

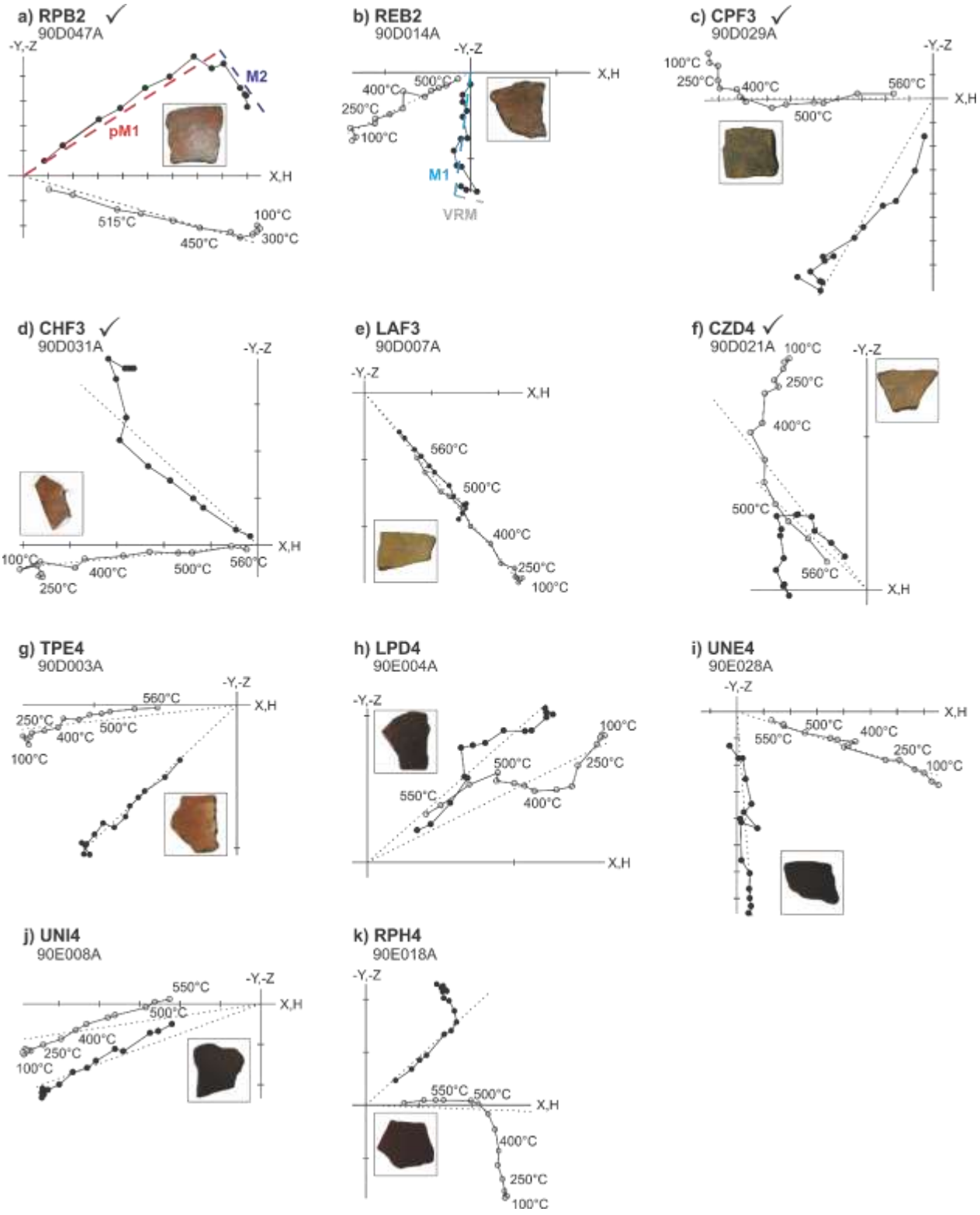

Figure 8 Representative Zijderveld (1967) plots of TH demagnetized samples. Labels along curves denote the maximum temperature applied by each step. For a) and b) M1, pM1, M2, and VRM exemplify the magnetization components employed for classifying the potsherd's behavior (see main text). The inset in the plots are the analyzed potsherds. The checkmark in a), c), d), and f) indicate the samples with specimens that ended up passing the AI criteria and were used for the dating exercise.

The secondary component is associated with minerals of maximum coercivities of 40 mT and maximum TC of 475 °C. 3) The Zijderveld diagrams of the potsherd LPD4 (Figure 8h) has a multicomponent complex behavior. Additionally, for some of the specimens of this potsherd, no tendency to the origin is observed.

2.6.3.2 Archaeointensity determination

For AI data selection, a modification of the original Thellier-Tool criteria TTA and TTB (Leonhardt *et al*., 2004) established by Paterson *et al*. (2014) was applied. According to Paterson *et al*., the modification of the parameter sets shows greater effectiveness in rejecting inaccurate results and accepting accurate results than the original sets. Similarly, the modified TTA and TTB parameters (TTAm and TTBm, see Table 1), demonstrate that while with the TTAm parameters set ~60 % of the accurate results are accepted, and ~50% of the inaccurate results are rejected, for the TTBm parameter set, 80% of the accurate results are accepted, and only ~35% of the inaccurate results are rejected. The use of either of these two parameters sets shows advantages and disadvantages. The TTAm parameters values were used initially for the data selection (the names of the specimens with values into the threshold of TTAm criteria are marked with * in Table 2), but to improve the statistics in the average calculation of intensities per ceramic, the data with values within the TTBm parameter set were also considered as reliable. Also, standard deviation (std) ≤ 5 μT for average intensity per sherd and N ≥ 5 for specimen number in mean intensity calculus were considered.

Table 1 TTAm and TTBm criteria of Paterson et al. (2014) with their threshold values used for data selection. n: number of NRM-pTRM points employed for paleointensity determination; f: the fraction of NRM utilized. β: Ratio of the standard error of the slope and the slope of the NRM-TRM plot; q: quality factor defined by Coe *et al*., (1978); MAD: Maximum angular deviation of NRM end-point directions at each step acquired during paleointensity experiments (°); α: the angle, in degrees, between the vector average of the data selected for paleointensity calculation and the principal component of the data (Kissel and Laj, 2004); δ(CK): Difference between the pTRM check and original TRM value at a specified temperature normalized to the TRM; δ(pal): cumulative check error (Leonhardt *et al*., 2004); δ(TR): relative intensity difference in pTRM-tail check; δ(t*): normalized pTRM tail (Leonhardt *et al*., 2004).

Parameters set	n	f	β	q	MAD	α	δCK	δpal	δTR	δt*
TTAm	≥ 5	≥0.35	≤0.10	≥5	≤6	≤15	≤7	≤10	≤10	≤9
TTBm	≥ 5	≥0.35	≤0.15	≥0	≤15	≤15	≤9	≤18	≤20	≤99

The archaeointensities in the specimens with evidence of reheating (pM1 + M2 components) were calculated employing the two-step method of Yu & Dunlop (2002). One archaeointensity value per magnetization component was obtained. Single-component samples' intensities were obtained using the traditional Arai plot (Nagata *et al*., 1965).

Characteristic Arai plots of Tingambato ceramics are shown in Figure 9. For the pM1 and M1 AI data, 39 of the 66 specimens belonging to 9 of the 11 analyzed potsherds present a good linear adjustment and pass the criteria sets established; 18 are into the TTAm criteria and the remaining 21 in the TTBm one (See Table 2). For three specimens of the potsherd REB2 and two specimens of the potsherd LPD4, no coherent results were obtained, and their data are not presented. The rejected samples exhibit failed pTRM checks, and a curved trend is observed between the NRM lost / pTRM gained points (e.g., Figure 9b); consequently, the high percentage of failure (~41%) in obtaining accurate archaeointensities can be attributed to the presence of MD grains in the samples and the mineralogical changes in the specimens. The mean intensity values of two potsherds have std > 5 μT (LAF3 [std = 8.08 μT] and TPE4 [std =8.68 μT]), no specimens of the REB2, and UNE4 potsherds are into the less stringed threshold values of the TTBm criteria set. The specimens of the potsherds LPD4, UNI4 and, RPH4 potsherds have N < 5 for the calculation of their mean AI value. Therefore, they were considered as unreliable results. In summary, only the AI values for the M1 / pM1 component of potsherds RPB2, CPF3, CHF3, and CZD4 were considered as quality results and thus used for archaeomagnetic dating.

The M2 intensity results are presented in Table 3. As can be observed, all the specimens have the f and β parameters with values out of the threshold established for the TTBm criteria set. This result is not surprising, considering the M2 magnetization fraction contribution to the total specimen magnetization (pM1 + M2). Additionally, 8 of the 24 analyzed specimens show notorious evidence of alteration (δpal) or significant differences between the pTRM check and the original TRM values (δCK). Except for the AI values of specimens in RPB2 and CPF3, the specimen's archaeointensity values in the potshard are not consistent, and thus, their standard deviation is considerable (near to 10 μT).

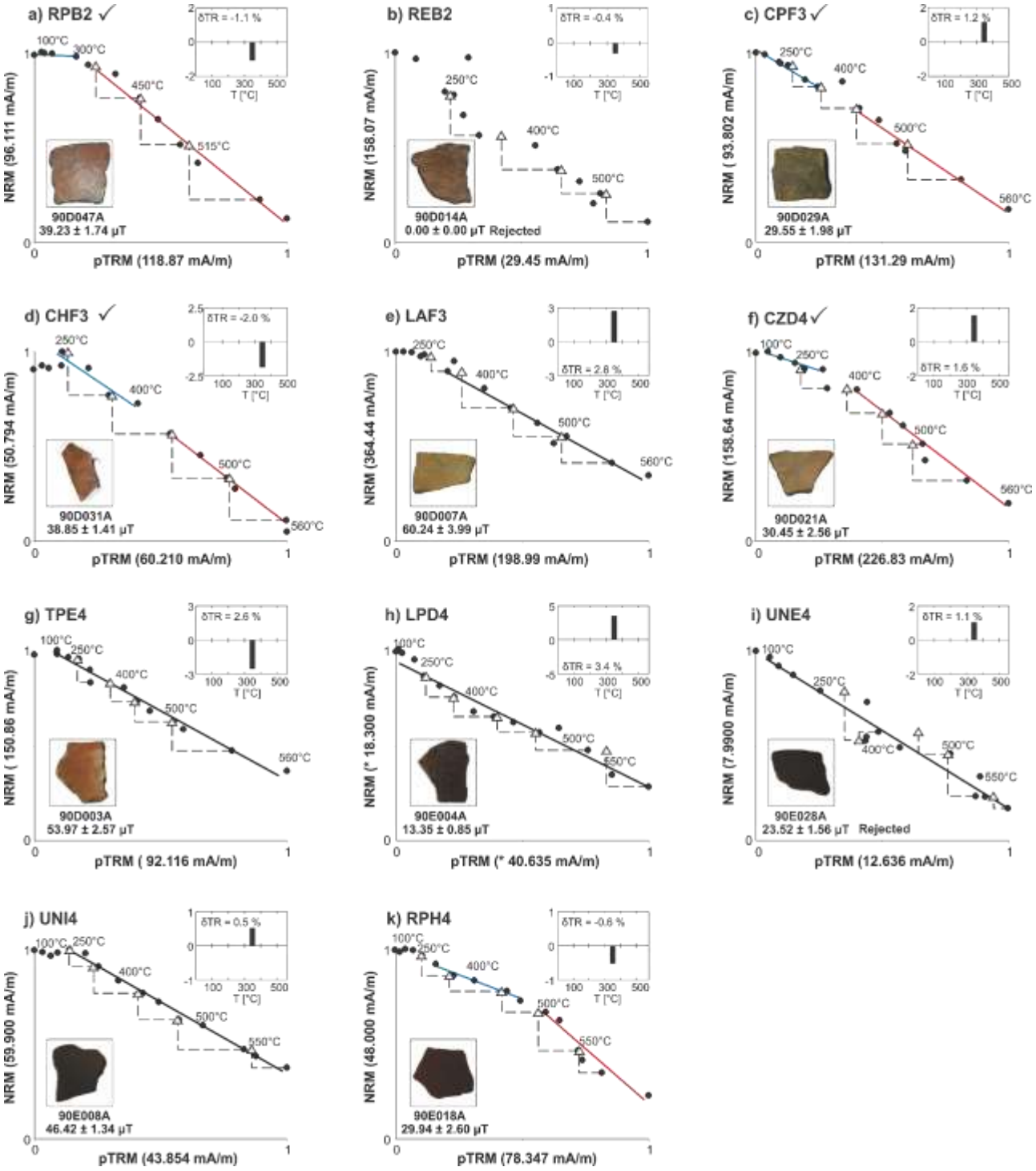

Figure 9 Representative Arai (NRM lost vs. pTRM acquired) plots for Tingambato potsherds. Filled circles represent data points gained at each double heating step. Triangles represent the pTRM checks. The linear fit for 1) M1 is signalized with black lines, 2) pM1 signalized with red lines, and 3) M2 signalized with blue lines. The insets in the upper part of the plots are the maximum absolute difference produced by the pTRM tail check at 350 °C, normalized by the NRM (δTR). The insets in the lower part of the plots are the analyzed potsherds. The checkmark in a), c), d), and f) indicate the samples with specimens that ended up passing the AI criteria and were used for the dating exercise.

Table 2 Thellier-Coe paleointensity results for M1 and pM1 components of Tingambato potshards. n, f, β, q, MAD, α, δ(CK), δ(pal), δ (TR), and δ(t*) are defined in Table 1 caption; Tmin/max: minimum/maximum temperature (°C); g: gap factor; k: curvature. k = R-1, where R is the fitted circle radius to the data set (pTRM vs. NRM); HRAW: raw archaeointensity values (μT); σ: archaeointensity standard deviation per specimen (μT); f_{CRC}: cooling rate correction factor; H_{CORR}: corrected archaeointensity values (μT) by cooling rate factor; Std: standard deviation for average intensity per sherd (μT). The specimen's name with all their values in the TTAm parameters set are marked with *. Specimens that exceed the threshold values established in the TTBm parameters set are underlined, and its respective AI value was not considered for mean intensity and standard deviation determination. The curvature parameter is double-underlined in specimens with k > 0.270.

Name	Tmin	Tmax	n	β	f	g	q	MAD	α	δCK	δpal	Drat	δt*	δTR	k	H_{RAW}	σ	f_{CRC}	H_{CRcorr}
RPB2 (pM1) ✓																			
90D043A*	400	560	7	0.07	0.60	0.81	7.3	1.8	2.1	2.2	9.4	2.6	0.00	0.2	0.345	45.22	2.85	1.02	44.33
90D044A*	400	560	7	0.06	0.60	0.81	7.9	3.6	6.1	2.6	7.0	3.3	0.10	0.1	0.256	39.06	2.07	1.03	37.91
90D045A	350	560	8	0.04	0.66	0.83	13.7	3.1	3.4	3.2	12.1	3.5	0.60	1.7	0.196	42.15	2.67	1.02	41.24
90D046A*	400	560	7	0.06	0.63	0.81	9.0	3.5	5.5	3.5	8.3	4.1	1.90	1.7	0.278	40.59	3.65	1.03	39.54
90D047A*	350	560	8	0.05	0.70	0.83	11.4	2.8	3.0	3.3	7.7	3.5	0.50	1.1	0.185	39.73	4.07	1.02	39.06
90D048A*	400	560	7	0.06	0.64	0.81	9.2	3.7	4.7	2.7	0.4	3.4	0.00	2.1	0.055	32.15	2.31	1.00	32.10
															Mean	**39.82**			**39.03**
															Std	**4.35**			**4.06**
REB2 (M1)																			
90D014A	200	540	10	0.07	0.73	0.86	9.6	4.5	0.7	8.1	23.1	7.6	0.0	0.5	0.505	47.04	3.09	-	47.04
90D016A	200	540	10	0.06	0.83	0.86	12.4	3.7	4.9	11.3	48.6	9.6	0.0	3.1	0.113	45.06	2.59	-	45.06
90D018A	200	540	10	0.08	0.79	0.84	8.1	5.3	4.3	17.0	30.8	16.0	0.0	1.9	0.296	40.36	3.31	-	40.36
															Mean	-			-
															Std	-			-
CPF3 (pM1) ✓																			
90D025A	400	560	7	0.08	0.56	0.81	6.0	8.3	10.0	2.5	7.0	3.8	3.9	4.9	0.333	28.78	3.60	-	28.78
90D026A	400	560	7	0.12	0.60	0.82	3.9	5.3	6.3	5.9	3.5	8.3	0.0	1.1	0.667	27.81	3.40	1.08	25.68
90D027A*	450	560	6	0.07	0.46	0.76	5.2	5.8	11.0	2.0	6.1	3.6	8.5	2.9	0.333	30.68	3.88	1.04	29.44
90D028A	450	540	5	0.16	0.41	0.72	1.8	5.3	9.1	5.3	17.3	11.1	0.0	3.3	0.667	22.53	2.76	1.07	21.05
90D029A*	450	560	6	0.07	0.50	0.75	5.1	5.3	8.5	3.6	8.1	6.0	0.0	1.2	0.294	28.43	2.87	1.06	26.92
90D030A	350	540	7	0.07	0.65	0.81	7.5	8.1	13.0	4.2	10.6	5.6	0.7	1.8	0.526	24.19	2.52	1.06	22.82
															Mean	**27.98**			**26.73**
															Std	**2.37**			**2.64**
CHF3 (pM1)✓																			
90D031A*	450	560	6	0.05	0.44	0.73	5.9	1.8	1.7	2.1	4.0	3.6	0.5	1.9	0.009	40.37	1.30	1.02	39.43
90D032A*	400	560	7	0.05	0.57	0.82	8.6	3.3	3.1	2.0	5.4	2.5	1.8	1.1	0.145	42.66	1.41	1.02	41.81
90D033A	450	560	6	0.06	0.42	0.78	5.5	1.7	2.4	9.8	17.3	17.3	0.0	1.2	0.238	41.35	2.02	1.00	41.23
90D034A*	450	560	6	0.02	0.40	0.77	14.3	3.3	2.2	3.3	4.9	6.5	0.0	2.9	0.038	35.61	0.99	0.98	36.18
90D035A	450	560	6	0.10	0.42	0.78	3.4	3.1	4.1	5.8	6.3	11.4	1.6	1.2	0.323	30.12	0.88	1.01	29.82
90D036A*	450	560	6	0.05	0.41	0.78	6.9	2.2	2.1	2.6	1.4	5.0	0.0	2.0	0.122	33.01	0.85	1.02	32.44
															Mean	**36.35**			**35.94**
															Std	**5.16**			**4.91**
LAF3 (M1)																			
90D007A*	350	560	8	0.07	0.54	0.83	6.8	1.0	0.8	3.8	2.9	4.2	4.3	2.9	0.093	60.24	3.99	1.03	58.53
90D008A	350	560	8	0.07	0.58	0.83	7.4	1.2	0.4	4.7	6.9	4.7	0.0	0.9	0.236	61.70	4.05	1.03	60.13
90D009A	200	540	10	0.08	0.61	0.83	6.6	1.6	2.4	9.2	21.3	7.5	0.0	0.4	0.396	77.95	5.91	1.04	74.97
90D010A	350	560	8	0.06	0.60	0.83	8.1	2.2	4.0	8.5	12.8	8.9	0.0	0.9	0.290	55.15	3.42	1.02	53.81
90D011A	350	560	8	0.05	0.58	0.84	10.7	1.3	1.4	7.5	9.1	9.5	0.0	0.5	0.187	41.55	1.89	1.04	39.97
90D012A	300	560	9	0.09	0.70	0.86	6.9	1.3	0.5	4.5	9.9	4.3	0.0	1.3	0.355	51.67	4.46	1.04	49.74
															Mean	**54.06**			**52.43**
															Std	**8.06**			**8.08**
CZD4 (pM1) ✓																			
90D019A*	450	560	6	0.08	0.40	0.76	3.8	3.4	4.7	5.8	5.7	8.0	0.0	0.4	0.278	37.27	4.50	1.01	36.91
90D020A*	450	560	6	0.08	0.42	0.76	3.9	4.5	6.5	6.4	7.0	9.9	0.0	2.2	0.286	35.66	5.80	1.01	35.33
90D021A	400	560	7	0.08	0.51	0.81	5.0	6.2	11.0	6.7	12.3	9.4	0.0	1.5	0.270	32.71	5.60	1.01	32.30
90D022A*	400	560	7	0.07	0.52	0.81	6.3	5.2	7.3	3.7	8.3	5.0	0.0	0.7	0.196	37.78	5.71	1.02	36.87
90D023A	400	560	7	0.07	0.51	0.81	6.3	6.4	9.8	2.9	6.5	4.1	0.0	2.0	0.217	36.60	6.00	1.03	35.61
90D024A*	400	560	7	0.05	0.49	0.80	7.8	3.5	2.9	2.3	3.4	3.2	0.3	1.3	0.072	38.50	5.84	1.02	37.72
															Mean	**36.42**			**35.79**
															Std	**2.06**			**1.93**
TPE4 (M1)																			
90D001A	250	560	10	0.08	0.58	0.86	5.9	1.6	2.9	5.2	3.8	6.1	0.0	3.1	0.381	48.61	4.12	1.02	47.55
90D002A	200	560	11	0.07	0.59	0.86	7.4	2.5	6.8	6.0	6.9	6.9	0.0	0.4	0.451	49.54	3.37	1.02	48.61
90D003A	150	560	12	0.05	0.62	0.88	11.4	2.4	6.2	5.3	6.6	5.5	0.0	2.6	0.295	53.97	2.57	1.02	52.78
90D004A	300	560	9	0.07	0.56	0.85	6.6	3.2	8.8	2.1	4.7	2.5	0.0	0.8	0.495	50.08	3.61	1.03	48.63
90D005A	200	560	11	0.06	0.63	0.87	9.0	3.2	8.4	1.1	0.2	1.3	1.0	1.0	0.377	41.32	2.50	1.09	37.92
90D006A	150	560	12	0.05	0.65	0.87	10.8	4.6	12.8	1.4	1.3	1.7	0.0	0.7	0.302	32.01	1.67	1.08	29.60
															Mean	**45.92**			**44.18**

															Std	**7.96**			**8.68**
LPD4 (M1)																			
90E001A	300	540	8	0.10	0.74	0.83	6.5	10.6	14.5	2.0	4.1	2.7	1.3	1.9	0.400	10.47	1.00	1.02	10.31
90E002A	100	540	12	0.04	0.83	0.89	17.6	14.5	12.3	2.7	3.8	3.1	1.2	2.8	0.169	11.27	0.47	1.02	11.02
90E003A	300	540	8	0.08	0.55	0.85	5.7	10.5	17.8	2.1	1.8	3.7	1.3	2.3	0.714	9.78	0.80	1.04	9.43
90E004A	200	560	12	0.06	0.69	0.89	9.7	6.4	11.2	5.0	6.8	6.9	0.1	3.5	0.238	13.35	0.85	1.02	13.10
															Mean	**11.70**			**11.48**
															Std	**1.49**			**1.45**
UNE4 (M1)																			
90E025A	200	560	12	0.10	0.67	0.85	5.7	2.4	1.4	12.8	6.2	14.5	1.4	0.5	0.476	38.14	3.82	-	38.14
90E026A	150	550	12	0.10	0.72	0.87	6.6	2.9	0.8	15.5	29.1	18.2	1.9	1.7	0.156	28.38	2.71	-	28.38
90E027A	200	560	12	0.08	0.66	0.88	7.7	2.3	4.1	13.8	54.5	18.2	1.9	4.8	0.013	25.32	1.92	-	25.32
90E028A	100	560	14	0.07	0.79	0.89	10.7	2.7	1.5	13.2	44.0	14.7	1.0	1.1	0.111	23.52	1.56	-	23.52
90E029A	400	560	8	0.10	0.37	0.79	3.0	5.0	9.1	13.3	63.4	34.2	1.9	3.9	0.006	14.64	1.44	-	14.64
90E030A	250	560	11	0.07	0.55	0.87	7.2	1.8	0.5	9.7	31.3	15.7	4.6	1.3	0.074	22.88	1.54	1.08	21.19
															Mean	**-**			**-**
															Std	**-**			**-**
UNI4 (M1)																			
90E007A	250	540	9	0.10	0.53	0.85	4.6	10.8	30.8	1.6	5.1	2.5	2.7	10.2	0.556	28.42	2.78	-	28.42
90E008A*	250	560	11	0.03	0.58	0.88	17.7	4.4	12.7	2.0	3.0	2.4	1.5	1.9	0.089	46.42	1.34	-	46.42
90E009A	200	560	12	0.08	0.62	0.88	7.0	14.4	33.1	3.5	3.7	5.0	2.6	2.8	0.556	23.69	1.86	-	23.69
90E010A	250	560	11	0.05	0.71	0.86	12.6	10.0	20.9	2.9	2.5	3.3	0.9	1.0	0.185	35.37	1.72	0.93	38.03
90E011A	250	560	11	0.10	0.77	0.87	7.0	11.3	21.5	6.6	12.3	7.6	0.6	0.7	0.667	23.77	2.29	-	23.77
90E012A	250	560	11	0.10	0.85	0.88	7.8	12.3	20.1	5.0	15.6	5.3	0.9	1.9	0.667	21.17	2.01	1.07	19.79
															Mean	**46.42**			**46.42**
															Std	**-**			**-**
RPH4 (pM1)																			
90E013A*	450	560	7	0.07	0.48	0.81	5.2	1.7	1.8	4.6	8.5	6.9	6.4	2.4	0.062	39.93	3.23	0.95	42.03
90E014A	475	560	6	0.15	0.38	0.76	1.9	2.2	2.8	3.5	10.3	6.2	0.8	3.8	0.244	37.47	4.40	0.98	38.23
90E015A	475	560	6	0.20	0.27	0.75	1.0	3.0	4.3	3.5	12.6	9.8	1.8	3.0	0.161	32.99	5.82	-	32.99
90E016A	475	560	6	0.15	0.29	0.77	1.5	3.6	7.3	3.5	15.0	8.9	4.9	2.6	0.476	52.62	8.08	-	52.62
90E017A	475	560	6	0.10	0.31	0.78	2.5	3.2	5.6	0.3	1.8	0.8	1.5	1.1	0.294	33.74	4.68	-	33.74
90E018A	500	575	6	0.15	0.34	0.74	1.7	1.9	2.9	2.6	4.2	6.1	0.9	0.6	0.625	29.94	2.60	-	29.94
															Mean	**38.70**			**40.13**
															Std	**1.74**			**2.68**

RPB2 ceramic is the only one that does not present determinations with high δCK and/or δpal values and presents a good within-specimens intensity-values consistency. Therefore, the M2 component intensity result was considered for archaeomagnetic dating. However, one must note that a dating obtained from an M2 component should be regarded as of lower quality than the one obtained from a pM1 component.

Table 3 Thellier-Coe paleointensity results for M2 component of Tingambato potshards. The meaning of the parameters is explained in the captions of Tables 1 and 2.

Name	Tmin	Tmax	n	β	f	g	q	MAD	α	δCK	δpal	Drat	δt*	δTR	k	H_{RAW}	σ	f_{CRC}	H_{CRcorr}
RPB2 ✓																			
90D043A	20	350	7	0.13	0.13	0.78	0.8	4.4	7.4	1.2	3.9	8.5	0.0	0.2	0.417	28.26	1.24	1.02	27.70
90D044A	20	350	7	0.11	0.12	0.78	0.9	6.1	13.3	0.7	5.4	5.1	0.1	0.1	0.051	32.98	0.92	1.03	32.01
90D045A	100	350	6	0.26	0.06	0.58	0.1	3.8	2.1	0.4	8.7	5.8	0.7	1.9	0.714	23.68	1.18	1.02	23.17
90D046A	20	300	6	0.42	0.05	0.61	0.1	4.5	2.3	0.3	3.0	5.6	2.3	0.0	1.111	23.68	1.23	1.03	23.07
90D047A	20	300	5	0.50	0.02	0.45	0.0	4.0	0.5	0.0	0.0	0.0	0.6	0.0	2.000	21.12	1.11	1.02	20.76
90D048A	20	350	7	0.13	0.18	0.78	1.0	4.9	11.6	0.6	4.9	3.0	0.0	2.6	0.061	36.16	0.88	1.00	36.11
															Mean	**27.65**			**27.14**
															Std	**5.92**			**5.96**
CPF3																			
90D025A	100	350	6	0.21	0.17	0.73	0.6	2.9	3.2	2.1	17.9	11.0	4.2	5.3	0.714	24.31	2.77	-	24.31
90D026A	20	350	7	0.20	0.30	0.77	1.1	3.4	6.8	7.2	39.3	18.3	0.0	1.0	0.370	34.52	2.67	1.08	31.88
90D027A	100	350	6	0.27	0.17	0.73	0.4	3.1	2.7	1.6	32.0	8.1	8.6	3.0	0.556	28.61	2.47	1.04	27.46
90D028A	20	400	8	0.15	0.29	0.83	1.6	1.4	1.4	2.0	25.1	5.7	0.0	2.8	0.137	31.05	3.47	1.07	29.02

90D029A	20	350	7	0.07	0.18	0.77	2.0	4.7	8.3	1.3	12.8	6.3	0.0	1.3	0.625	30.90	2.21	1.06	29.26
90D030A	20	300	6	0.26	0.13	0.72	0.4	3.3	2.4	3.2	28.2	21.7	0.7	0.0	0.833	21.34	1.40	1.06	20.13
															Mean	**28.46**			**27.01**
															Std	**4.84**			**4.18**
CHF3																			
90D031A	200	400	5	0.20	0.25	0.64	0.8	5.3	7.9	1.9	14.3	5.9	0.5	2.1	1.000	38.05	1.40	1.02	37.16
90D032A	100	350	6	0.19	0.19	0.63	0.6	3.5	5.3	1.3	7.8	5.6	2.2	1.2	0.667	32.61	0.78	1.02	31.96
90D033A	200	400	5	0.20	0.25	0.70	0.9	5.2	8.0	2.6	1.9	7.5	0.0	1.3	1.000	43.96	2.12	1.00	43.83
90D034A	200	400	5	0.28	0.13	0.65	0.3	4.1	3.2	2.0	1.7	14.4	0.0	3.4	1.429	18.78	0.80	0.98	19.08
90D035A	150	400	6	0.22	0.23	0.75	0.8	5.9	13.1	5.1	2.2	19.2	1.8	1.3	0.833	27.17	0.86	1.01	26.90
90D036A	200	400	5	0.14	0.21	0.68	1.0	4.3	5.4	2.4	2.5	9.8	0.0	2.1	1.000	33.15	0.86	1.02	32.57
															Mean	**32.29**			**31.92**
															Std	**8.71**			**8.48**
CZD4																			
90D019A	100	400	7	0.58	0.03	0.21	0.0	7.7	7.3	1.0	6.5	28.7	0.0	0.6	0.667	7.92	2.72	1.01	7.84
90D020A	100	400	7	0.26	0.12	0.81	0.4	9.9	45.3	2.5	8.6	21.2	0.0	2.9	0.217	19.41	4.32	1.01	19.23
90D021A	100	300	5	0.17	0.10	0.74	0.4	5.8	3.8	0.8	9.4	7.5	0.0	0.0	0.625	25.75	3.48	1.01	25.42
90D022A	100	350	6	0.18	0.13	0.75	0.5	7.6	12.5	0.2	0.7	1.4	0.0	1.0	0.278	29.69	3.20	1.02	28.97
90D023A	100	350	6	0.19	0.18	0.75	0.7	7.4	14.7	0.6	0.7	3.0	0.0	2.6	0.625	33.92	3.86	1.03	33.00
90D024A	100	350	6	0.21	0.09	0.70	0.3	8.5	14.0	0.2	0.3	1.9	0.4	1.7	0.556	31.09	4.10	1.02	30.46
															Mean	**24.63**			**24.16**
															Std	**9.61**			**9.31**
RPH4																			
90E013A	200	400	5	0.10	0.16	0.74	1.2	7.4	9.2	2.6	12.3	15.5	9.3	3.4	0.588	36.71	1.81	0.95	38.64
90E014A	250	450	5	0.11	0.16	0.70	1.1	10.6	19.2	1.1	7.9	6.3	1.3	4.2	0.357	34.66	2.13	0.98	35.37
90E015A	200	450	6	0.19	0.35	0.78	1.4	14.0	34.8	2.1	7.6	5.3	2.5	0.3	1.429	31.07	2.93	-	31.07
90E016A	250	450	5	0.07	0.17	0.74	1.8	7.8	10.2	0.6	3.9	3.3	7.9	0.2	0.016	19.38	2.18	-	19.38
90E017A	250	450	5	0.12	0.14	0.75	0.9	7.7	8.5	0.1	0.5	0.5	2.2	1.6	0.149	19.53	1.37	-	19.53
90E018A	300	475	5	0.09	0.19	0.74	1.5	9.7	17.1	0.8	6.9	3.9	1.2	0.8	0.001	18.98	1.38	-	18.98
															Mean	**26.72**			**27.16**
															Std	**8.33**			**8.95**

As could be noted in the AI results of this work, and as in previous works has been pointed out (e.g., Kosterov and Prévot, 1998; Krása *et. al*., 2003; Carvallo *et al*., 2006), one of the principal causes of failure in the AI experiments is the presence of MD grains. The k parameter of Paterson (2011) was proposed as an easy way of calculating the curvature of the Arai plot. Specimens within an optimum value of $k \leq 0.164$, and a more relaxed one of $k \leq 0.270$, are supposed to yield reliable paleointensities and exclude the inaccuracies associated with the effects of MD and large PSD grains. However, these values were determined on synthetic samples, and as Paterson himself mentions, these values are very strict for most natural specimens and may reject reliable results. All the specimens with $k > 0.270$ are double-underlined in tables 2 and 3. For specimens in which the Arai plot was used to calculate a single magnetization component (M1), 18 of the 31 results present k values over the established limit value. Half of these results are also associated with high values of δpal, δCK, or α (the k parameter fulfills its function). Still, this is the only parameter with values outside of the established thresholds for the other half.

On the other hand, for the specimens with k values < 0.270, six are into the TTBm criteria set, but the seven-remaining do not. The use and analysis of the k parameter values in pots with overheating evidence is more complex. As shown in Figure 9, the different magnetization segments (pM1 and M2) in the Arai diagram can have different slopes. When both segments are analyzed together, a curvature that is not

necessarily associated with the MD grains' presence is formed. Nevertheless, k values calculated for each magnetization component in the specimens, which are reported in Tables 2 and 3, are also high in general: $0.009 \leq k \leq 0.667$ for the pM1 components (with $k > 0.270$ for 14 of 30 specimens), and $0.001 \leq k \leq 2.000$ for the M2 components (with $k > 0.270$ for 18 of 30 specimens). One of the disadvantages of using a low data number for calculating k is that the deviation of a single NRM/pTRM data point has a greater weight to increase the curvature's value than when using a more significant data amount. Additionally, for the case of the M2 data, the VRM data trend at the beginning of the magnetization tends to generate higher curvature values. The pTRM tail check values at 350 °C, quantified with the parameter δTR, are < 6% for all the samples (see upper insets in Figure 9), so the curvature trend in the M2 component is not associated with the presence of multidomain grains.

The comparison of the data that pass the TTAm and TTBm critical values, with the data that pass the k critical value was unsuccessful, so the parameter k was not considered within the final data selection.

2.7 Discussion

2.7.1 Secular Variation Curves for México

From the time the SHA.DIF.14k global model (Pavón-Carrasco *et al*., 2014) was published, a growing number of archaeomagnetic dating has been carried out in Mexico (e.g., Terán-Guerrero *et al*., 2016; Goguitchaichvili *et al*., 2017; Cejudo-Ruiz *et al*., 2019; Pérez-Rodríguez *et al*., 2020; Morales *et al*., 2020). However, it is worth nothing that the SHA.DIF.14k database is biased to the European region, and no evaluations of their effectiveness in Central America have been done yet.

According to Korte et al. (2019), "for an adequate age association to material utilizing archaeomagnetic dating, is fundamental a reliably determined paleomagnetic data from the material to be dated, and the existence of a high-resolution regional palaeomagnetic reference record that is robustly constrained in time".

In the last years, four Mexican intensity PSVCs (restricted to archaeological baked clays and lava flows information) have been developed: Goguitchaichvili *et al*., 2018 (G_2018); Mahgoub *et al*., 2019 (M_2019); Hervé *et al*., 2019b (H_2019), and García *et al*., 2020 (G_2020). Although the database used in

all the studies is essentially the same, the differences observed in the PSVC's behavior come mainly from the data selection and weighting. The principal characteristics of the Mexican archaeointensity data PSVC are described below and are synthesized in Table 3:

- G_2018: Constructed with 84 data distributed between Mexico, Guatemala, El Salvador, and the southern part of the United States. Data were primarily recovered from GEOMAGIA50.v3 (Brown *et al.,* 2015) and ArcheoInt (Genevey *et al.,* 2008). The PSVC was modeled using Bootstrap algorithms (Thébault and Gallet, 2010). For data selection, the presence of cooling rate and anisotropy correction, specimen number for average intensity (N) ≥ 4, and std ≤ 10 μT were considered. The temporality covered by the G_2018 intensity PSVC ranges from 1000 BC to AD 2000. Two major temporal gaps of 195 years are observed between 775 – 580 BC and AD 1350 – 1545. The largest age error of the independent association dating is of 280 years.
- M_2019: This PSVC was created using 79 archaeointensity data (38 previously published and 41 new data) for the last 3600 years (1600 BC – AD 2000) utilizing the bootstrap approach. Previously published data were obtained from the GEOMAGIA50.v3 database and were evaluated according to the following parameters: 1) For the data selection obtained with Thellier type (THE) and Microwave (MW) (Hill and Shaw, 2000) methods were checked: a) the presence of thermal alteration tests by pTRM criteria (δCK and/or δpal), b) the evaluation of the stability of NRM direction in the archaeointensity experiment (MAD, α, and/or DANG), c) the presence of anisotropy (anisotropy TRM tensor determination) and cooling rate corrections (for archaeological materials), d) N ≥ 2, and e) the std ≤ 5 μT. 2) For the data obtained with the multiple-specimen method (MS) (Dekkers and Böhnel, 2006), it was verified that the temperature chosen was below the thermal alteration temperature and that the domain-state correction (Fabian and Leonhardt, 2010) was completed. Additionally, 22 historical data between AD 1840 and 1898 listed in the gufm1 model (Jackson *et al.,* 2000) and geomagnetic observatory data (Teoloyucan, Mexico City observatory) between AD 1923 and 1985 were also considered. Three major temporal gaps are observed. The first of 815 years (1000 – 285 BC), the second of 425 years (AD 975 – 1400), and the third of 331 years (AD 1435 – 1766). The biggest age error of the independent association dating is of 280 years.
- H_2019: Modeled using a Bayesian framework (Lanos, 2004). The period considered in this curve goes from 1500 BC to AD 200, for which 63 Mexican archaeointensity data were used (50 of previous works and 13 new data). In addition to the GEOMAGIA50.v3 database, archaeointensity data published in 18 papers were contemplated (for more details, see Hervé *et al.,* 2019a and

2019b). For data-selection were considered: N ≥ 4, std ≤ 15%, AI determination obtained by Thellier – Thellier or Microwave method, pTRM checks, presence of cooling rate correction and, anisotropy correction by the TRM tensor and the Morales *et al.* (2009) approach performed on six specimens. Two major temporal gaps are observed; the first between 1550 – 1300 BC, and the second between 950 – 600 BC. The biggest age error of the independent association dating is of 300 years.

- G_2020: As to M_2019 PSVC, this curve covers the last 3600 years. 110 out of 243 compiled data from the GEOMAGIA50.v3 database and recent research (for details, see García *et al.,* 2020) were selected as reliable archaeointensity data. Parameter-selection criteria for Thellier type and Microwave intensity data were separated into two groups. One corresponds to the data published in recent studies, where thermal alteration quantification (δCK / δpal) was carried out. In this group are considered the following parameters: N ≥ 3, f ≥ 0.4, q ≥ 5, MAD ≤ 10, δCK ≤ 10, and std ≤ 5 μT. The second group involves intensity data evaluated following conventional parameters: the presence of pTRM checks, N ≥ 5, f ≥ 0.5, q ≥ 5, and std ≤ 5 μT. Both groups consider the presence of cooling rate and anisotropy corrections. This last obtained either from the TRM anisotropy tensor or using the method suggested by Morales *et al.* (2009) obtained from six specimens. On the other hand, multi specimen data selection should include all steps of Fabian and Leonhardt's (2010) extended protocol. Also, more than 400 intensity data for historical times (since 1587) published in Goguitchaishvili *et al.* (2020) were employed in the PSVC construction. A major gap of 250 years is observed (1550 – 1300 BC), and the biggest age error of the independent association dating is 400 years.

Table 4 Principal characteristics of the four Mexican PSVC's. For the data selection parameters section: THE – MW: Thellier and Microwave methods for PI determinations, MS: Multispecimen method for PI determination, 1. pTRM: the presence of pTRM checks, 2. CRC: cooling rate correction, 3. Ani: Anisotropy correction. 4. N: specimen number used in mean intensity calculus. The meanings of 5 to 9 are explained in the captions of Tables 1 and 2. 10. T < TA: The selected temperature T for the multispecimen method lower than the alteration temperature of the specimens TA. 11. Ext. P: Extended protocol for multiple-specimen method. The cross marks (✗) indicate the absence of data or the lack of information in the original files where the PSVC's were published. For the parameters data 1. - 9. of the G_2020 curve, two different values are presented (a. and b.), each one corresponds with a distinct parameter set established for classify the paleointensity data (for more details, see explanation in the main text).

Characteristics	**Mexican PSVC**			
	G_2018	**M_2019**	**H_2019**	**G_2020**
Temporal coverage	1000 BC – AD 2000	1600 BC – AD 2000	1500 BC – AD 200	1600 BC – AD 2000
Modeling Method	Bootstrap	Bootstrap	Bayesian	Bootstrap

N° Paleointensity data		111	79	63	110
N° Historical data		0	22	0	455
Observatory data		×	✓	×	✓
Major temporal gaps		775 – 580 BC AD 1350 – 1545	1000 – 285 BC AD 975 – 1400 AD 1435 – 1766	1550 – 1300 BC 950 – 600 BC	1550 – 1300 BC
Major uncertainty error		280 years	280 years	300 years	400 years
Data selection parameters	**a) THE - MW**	**1. pTRM**	×	✓	✓	a. ✓ b. ✓
		2. CRC	✓	✓	✓	a. ✓ b. ✓
		3. Ani	✓	✓	✓	a. ✓ b. ✓
		4. N	≥ 4	≥ 2	≥ 4	a. ≥ 3 b. ≥ 5
		5. f	×	≥ 0.5	×	a. ≥ 0.4 b. ≥ 0.5
		6. q	×	≥ 5	×	a. ≥ 5 b. ≥ 5
		7. MAD	×	≤ 10	×	a. ≤ 10 b. ×
		8. δCK	×	≤ 10	×	a. ≤ 10 b. ×
		9. Std	≤ 10 μT	≤ 5 μT	≤ 15 %	a. ≤ 5 μT b. ≤ 5 μT
	b) MS	**10. T < TA**	×	✓	×	✓
		11. Ext. P	×	✓	×	✓

Figure 10 displays the behavior of the Mexican intensity PSVC restricted to the temporality of interest for the present study (AD 0 – 1600). Since only the last 200 years of the H_2019 PSVC fall within the temporality selected, it will not be considered for dating purposes. Similarly, the G_2018 PSVC was discarded for the dating evaluation because the parameters for quantifying the quality of intensity data were not considered. Besides that, being the first curve built, the new quality data published together with the H_2019 and M_2019 curves were not used.

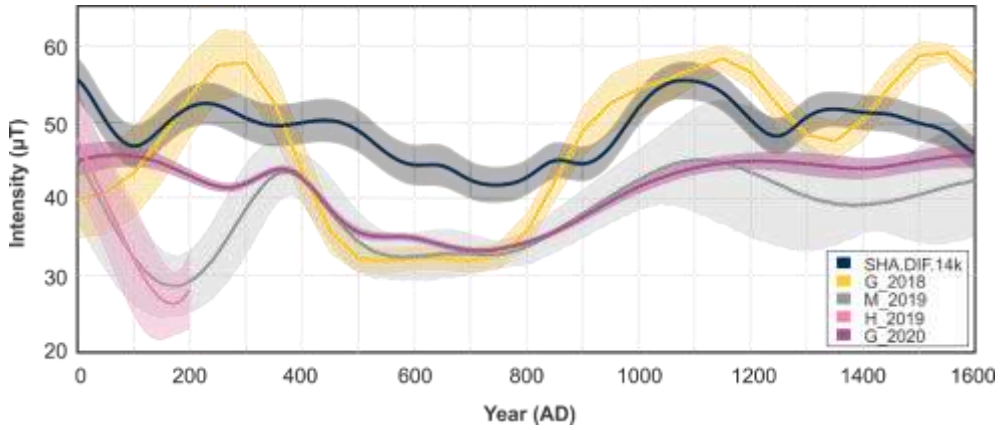

Figure 10 Comparison of intensity PSVCs developed for Mexico calculated for Tingambato archaeological site. Solid lines show the paleointensity data. Shaded curves are the corresponding 95% confidence limits of each curve. G_2018, M_2019 and G_2020 curves are coincident for the AD ~ [400 – 800] interval, while M_2019 and G_2020 are in good agreement for AD ~ [400 – 1200] interval. In general, for the selected temporality, M_2019 and G_2020 curves show lower intensity values than the values observed in the SHA.DIF.14k model.

Although the behaviors in M_2019 and G_2020 PSVC are different for some temporalities, the trends are very similar for the range between AD ~400 and ~1200. More than 40% of the total data (45/110 data) employed for constructing the G_2020 curve and almost a quarter of the M_2019 curve data (21/79 data) are within this ~800 years interval. With the data available until today, reliable dating could be anticipated for materials with expected temporalities in such age range, with their corresponding differences associated with each curve's uncertainty.

2.7.2 Archaeomagnetic dating and archaeological implications

Four potsherds were dated with two regional PSVCs: M_2019 and G_2020, and with the global model SHA.DIF.14k. The minimum intensity value of the SHA.DIF.14k model in the temporality bounded for dating is ~40 μT (see Figure 10). Hence, for the potsherds with intensities below this value (considering their uncertainties), the dating with the SHA.DIF.14k model were discarded.

The potsherds were analyzed according to their archaeological context and the ^{14}C dates (at 95% or 2σ uncertainty range) reported in Punzo-Díaz (2016) and Rangel-Campos (2018) to select the best age interval for each ceramic fragment.

The RPB2 potsherd was recovered from the most superficial layers of unit 2. It is associated with the last occupational stage of Tingambato, more specifically, with the fire that supposedly caused the site abandonment at AD 900. Within the excavation of unit 2, in a layer also associated with the fire, two radiocarbon ages (AD 600 - 660 and AD 620 - 670 obtained from a room beam and a carbon lenticule, respectively) were reported by Punzo-Díaz (2016). The entire context locates the ceramic fragment in the Tingambato III phase (AD 600 – 900), so archaeomagnetic dating with the M_2019 and G_2020 curves was carried out using the AD 1000 upper limit.

The intensity values used for the archaeomagnetic dating of the RPB2 sample were determined using the two-step method. This method was initially used to estimate emplacement ages of plutonic rocks in Canada (Yu & Dunlop, 2002). Recently, with this methodology, Scotland was confirmed as the place of provenance of ancient bricks of an Australian furnace (Lisé-Pronovost *et al.,* 2020).

In the case of archaeological material, a history of multiple heating for the ceramic pieces, evidenced as secondary components in the Zijderveld plots, likely reflects recurrent use of the pots for cooking or other ceremonial activities involving heat, as mentioned by Morales *et al.* (2012).

Also, as Fránces-Negro *et al.* (2019) propose, the analysis of thermal demagnetization components in potsherds helps infer their use. Pots with a single component could have been used for storage; potteries with multiples magnetization components probably were used for cooking.

Therefore, using the two-step method, it is proposed in this work the determination of the EMF intensity at the moment of the ceramics baking (pM1) and the intensity present during their last use (M2). However, due to the RPB2 archaeological context, the M2 component could have instead registered the Earth's magnetic field intensity during the fire.

The dating of RPB2 potsherd using the different PSVCs, with their respective probability density functions, is presented in Figures 11a and 11b for pM1 and M2, respectively. According to the context, the best age intervals for the baking's potsherd are AD 600 – 1000 for the M_2019 curve, AD 721 – 994 for the G_2020 curve, and AD 494 – 972 for the SHA.DIF.14k model. The best age interval associated with the M2 components is AD 446 – 913 for the M_2019 curve, and the G_2020 only offers the interval AD 418 – 917.

The potsherds CPF3 and CHF3 were recollected from the same unit (3) and layer (F). The intensity values recorded in pM1 of both ceramics are close within their error limits: 35.94 ± 4.91 μT (CHF3) and 26.73 ± 2.64 μT (CPF3). Also, layer F, which was excavated at 2.40 m below the surface, has a radiocarbon age of AD 570 to 655 (Punzo – Díaz, 2016), corresponding to the end of the Tingambato II phase and the onset

of the Tingambato III phase. Archaeomagnetic dating was carried out for the period between AD 0 – 1000 (Figure 11c). The best age range obtained for the potsherd CPF3 goes from AD 507 to 781 with the M_2019 curve, while the G_2020 curve does not present such low-intensity values for the temporality selected, and the intensity value obtained does no match with the curve. Although the temporal range AD 525 – 830 brought with the G_2020 curve has a good coincidence whit the M _2019 curve range, the G_2020 dating is considered less reliable. On the other hand, ages obtained for the potsherd CHF3 (Figure 11d) are similar for the M_ 2019 (AD 398 – 1000) and the G_2020 (AD 366 – 994) curves. Similarly, SHA.DIF.14k model dating provides a comparable age (AD 491 – 973). Nevertheless, solely the upper error limit matches with the master curve.

Radiocarbon age for unit 4, corresponding to the same layer where the CZD4 potsherd was recollected, has the eldest age reported for the Tingambato archaeological site (AD 41 – 114; Rangel – Campos, 2018), which suggest that this ceramic fragment is part of the first occupational stage (Tingambato I). However, archaeological research indicates that the layer from which the potsherd was recovered is the last filler layer of the site (Rangel-Campos, 2018; Punzo-Díaz, in press). Therefore, it is at the base of the Tingambato III phase's constructions, and materials of different temporalities could be mixed into the layer. The ceramic style Zacapu Café had been recognized in neighboring areas such as Pátzcuaro and Zacapu (García – García, 2017), and it has been associated to the Loma Alta phase III (AD 350 – 550) according to the temporal North – Central Michoacán sequence established by Michelet (1988). Archaeomagnetic dating in pM1 was carried out for the period between AD 0 – 1000 (Figure 11e). Three age-ranges were obtained for the M_2019 curve; the first (AD 22 – 125) is in good agreement with the ^{14}C age, while the last (AD 426 – 951) coincides with the ceramic style's age-associated. On the other hand, one of the range ages obtained with the G_2020 curve (AD 443 – 707) supports the ceramic style's temporal proposal.

The best age ranges selected for each ceramic fragment with the different PSVCs are shown in Figure 12.

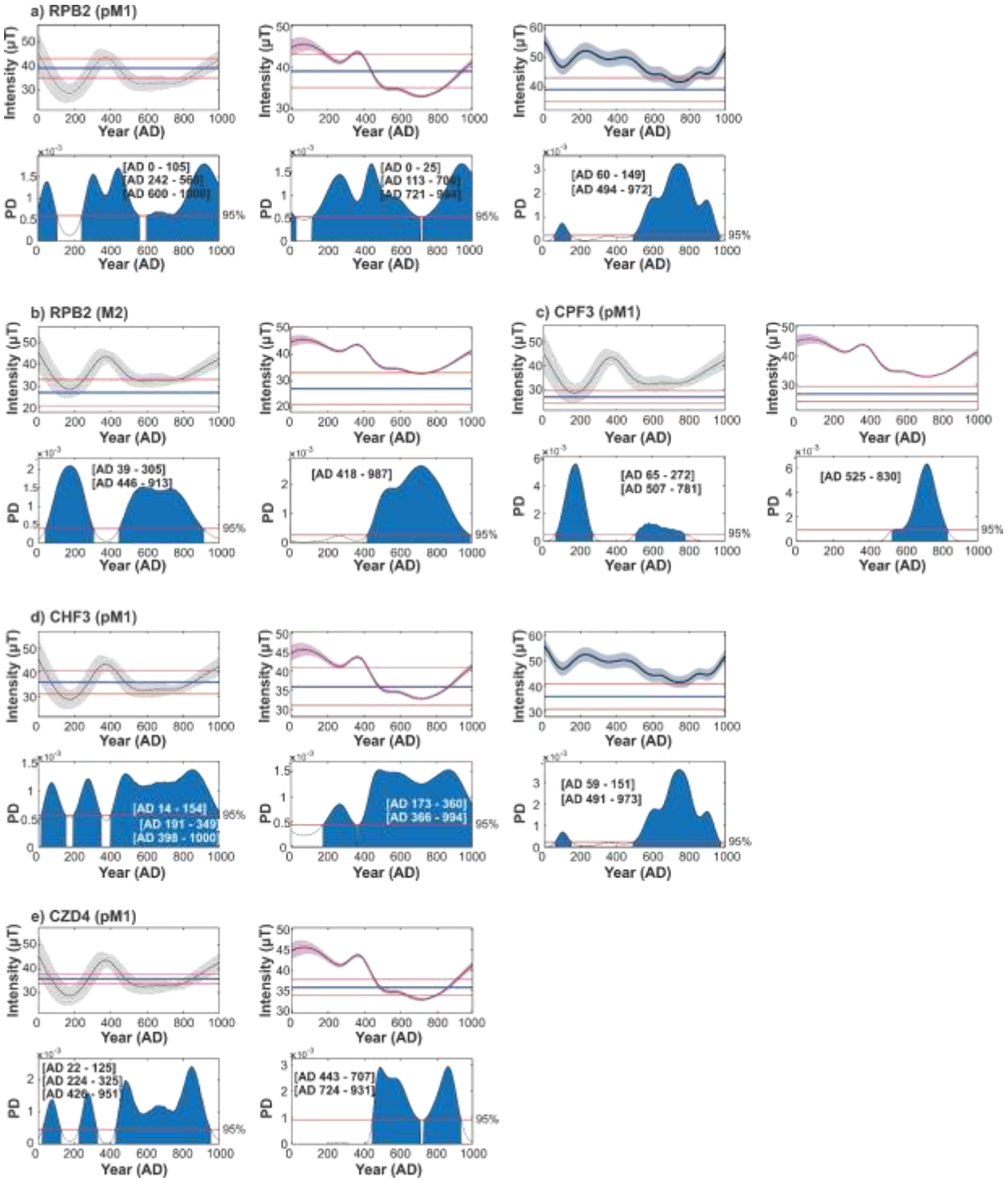

Figure 11 Archaeomagnetic dating of Tingambato potsherds with two Mexican PSVC's and the global model SHA.DIF.14k. The PSVC colors correspond with the colors used in Figure 10: Grey for the M_2019 curve, purple for the G_2020 curve, and blue for the SHA.DIF.14k model.

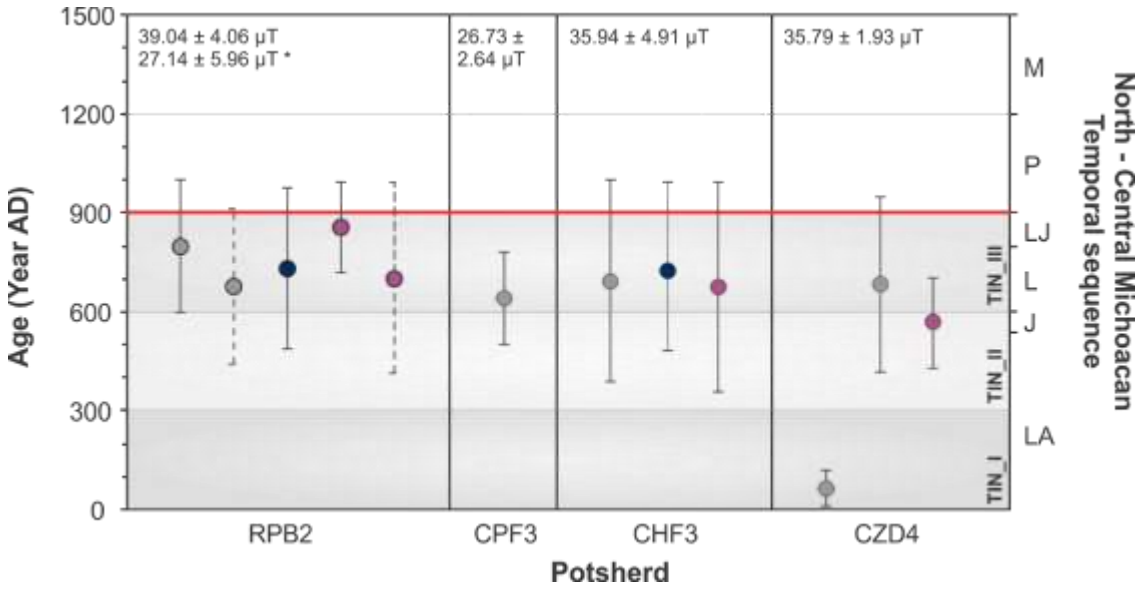

Figure 12 Age ranges obtained per potsherd with the different PSVCs: Grey circles M_2019; Blue circles SHA.DIF.14k; Purple circles G_2020 PSVC. The age ranges with dotted lines in the first column are the ages obtained for M2 in RPB2. Shaded horizontal sectors with labels TIN_I, TIN_II, and TIN_III correspond to the three occupational stages of Tingambato (see 2. Archaeological context section). In the right axis are labeled the phases and subphases of the temporal sequence used for the North-Central Region of Michoacán state: Loma Alta phase (LA), Jarácuaro subphase (J), Lupe Phase (L), La Joya subphase (L J), Palacio phase (P) and Milpillas (M). The red line at AD 900, indicates the most accepted age for the fire by the archaeological community (see section 2.3 Archaeological context). The numbers at the top of each column are the archaeointensity values used for dating. The number with * in the first column corresponds to the archaeointensity value of M2.

Although the potsherds were recollected from different units and depths, all present a coincident age range at AD ~700 (see Figure 10). Archaeological research suggests building the last stage structures required a significant grounded-leveling effort (Punzo-Díaz, in press). The filler layer has varying thicknesses (of 2.5 to 3.2 m) around the archaeological site. Therefore, finding similar temporality materials at different depths, as well as old materials coming from the first stage construction in very superficial layers, is not surprising (as it is probably the carbon-dated case near the CZD4 ceramic). This seems to reasonably explain the CHF3, CPF3, and CZD4 potsherds' contemporaneity.

The determination of two intensities, and their corresponding age intervals, linked with two different processes recorded by potsherd RPB2, could help narrow the age intervals obtained for this potsherd since the ceramic manufacture's lower limit age could also be regarded as the age lower limit associated with the fire. Similarly, the ceramic age-upper limit associated with the fire allows reducing the manufacture age's upper limit.

Following this reasoning, the age ranges AD 600 – 913 for the M_2019 curve and AD 721 – 987 for the G_2020 curve would represent the maximum time intervals within which the RPB2 ceramic was elaborated and recorded the fire of the Tingambato site. Both age ranges are similar and tend to be higher than the ages obtained by radiocarbon (AD 600 - 660 and AD 620 - 670) in the same layer that the ceramic was recovered.

As noted by Punzo-Díaz (in press), *"Although the archaeological zone of Tingambato has been studied on different occasions, the complexity of this important city in western Mesoamerica is just beginning to be understood"*. Therefore, refined ages of the occupational stages of Tingambato and the age of its collapse could only be obtained with future investigations.

For this last purpose, the use of archaeomagnetic technics provides not only ages, but it could also detect areas of greater exposure to fire during a conflagration by analyzing the thermal magnetization components of different archaeological materials associated with it and distributed around the place. A more detailed fire scenario could be recreated with the temperature distribution knowledge (within limits established by the Curie temperatures of the magnetization carrier minerals in ceramics) and get closer to its origin.

2.8 Conclusions

Four excellent-quality archaeointensity data were obtained for the Tingambato archaeological site, which were used for dating purposes using the two most recent Mexican regional models (M_2019 and G_2020) and the global model SHA.DIF.14k. As Batt (1988) mentioned, *"an archaeomagnetic date is only as reliable as the calibration curve from which it is derived."* The dating exercise demonstrates that western Mexican archaeological site data better correspond with the regional models than with the global model. Therefore, better dates are obtained with regional models.

For the analyzed temporal sector, the SHA.DIF.14k model shows a similar trend to the regional curves, but with higher intensity values, and with differences >20 μT in comparison with the M_2019 curve (e.g., intensities for the year AD 200) and >10 μT with the G_2020 curve (e.g., intensities for the year AD 500). Comparisons with other global models (e.g., Pfm9k by Nilsson *et al.,* 2014; CALS10k by Korte *et al.,* 2011; and HFM.OL1.AL1 by Panovska *et al.,* 2015), realized in the original publications of the M_2019 and G_2020 curves, shown a similar trend to the SHA.DIF.14k model for the analyzed period. On the other

hand, although the two regional models have significant differences at different temporalities, the period AD 400 – 1200, which is the focus of this study, seems to be the best defined for the 3600 years interval the curves cover due to the high data concentration and the similitudes between both curves. However, the period between AD 400 – 800 is also characterized by minimal EMF intensity variations. Thus, more defined dating requires an extra EMF component (declination and/or inclination), achievable with in-situ samples such as bricks, furnaces, and burned soils.

Regional models archaeomagnetic dating of Tingambato's potsherds shows a good relationship with the radiocarbon ages.

Regional curves in other parts of the world, with similar temporal coverage, have comparable data quantity to the G_2020 and M_2019 curves (e.g., the Iberian curve of Molina Cardin *et al.* (2018) and the Italian curve of Tema and Lanos (2020)) but better distribution. Hence, a higher density data for specific age ranges is still necessary to construct an adequate regional model. A revaluation of ages obtained for Mexican materials through the SHA.DIF.14k model will be required once the expected temporalities for each material have a better definition within the regional curves.

3. Archaeomagnetic evidence of a likely earlier occupation of "El Caracol" lava flow (Zacapu Malpaís, Western Mesoamerica)

https://doi.org/10.1016/j.ringps.2021.100029

Nayeli Pérez-Rodríguez, Juan Morales, Avto Goguitchaichvili, José Rosas-Elguera

Results in Geophysical Sciences

3.1 Resumen

Se presentan los resultados de la investigación arqueomagnética integral realizada en siete fragmentos cerámicos recuperados del flujo de lava "El Caracol", localizado en el Malpaís de Zacapu, Michoacán (México). Para la caracterización de la mineralogía magnética de las muestras se llevó a cabo un conjunto de experimentos de magnetismo de rocas (los cuales incluyen curvas termomagnéticas, curvas de histéresis, curvas de campo inverso y curvas de adquisición de magnetización remanente isotérmica). La metodología experimental también considera la detección de alteraciones magnetoquímicas en los experimentos de arqueointensidades, correcciones por ritmo de enfriamiento y correcciones por los efectos de anisotropía de remanencia para garantizar la confiabilidad de las determinaciones de arqueointensidad.

Con la desmagnetización térmica de los tiestos I, II, V y VII se determinaron entre dos y tres componentes de magnetización: una de ellas asociada con la fabricación del tiesto, la segunda con el recalentamiento de la muestra y la tercera (cuando está presente) con una componente de magnetización viscosa. Para cada una de las dos primeras componentes se calculó un valor de intensidad. Cinco de los siete fragmentos cerámicos: una cazoleta de una pipa (fragmento I), dos soportes de vasija (fragmento II y V), el fragmento de la pared de una vasija (fragmento III) y la boquilla de una pipa (fragmento VII), arrojaron resultados de arqueointensidad dentro de los criterios de aceptación establecidos. Los tiestos I, II, III y VII arrojaron valores de intensidad del campo geomagnético antiguo de entre 30 y 40 μT, mientras que el tiesto V tuvo un valor menor de ~20 μT. Aunque las curvas sintéticas de variación secular (regionales y globales) no predicen intensidades tan bajas para los últimos milenios en la región, se han encontrado valores similares en materiales arqueológicos del centro y sur de México, lo cual podría indicar la falta de resolución de las

curvas de variación secular para dicha temporalidad, así como la necesidad de una mayor generación de información que cubra esta deficiencia.

La datación arqueomagnética de las cerámicas analizadas se realizó empleando dos curvas de variación secular regionales. Los resultados obtenidos sugieren que algunas de las piezas encontradas sobre el flujo de lava “El Caracol” tienen una edad más temprana (AD 900) a la que se había estipulado anteriormente para la ocupación humana del sitio (AD 1200), abriendo la posibilidad de más de una etapa ocupacional del lugar.

3.2 Abstract

A comprehensive archaeomagnetic investigation was carried out on seven ceramic fragments recovered at the "El Caracol" lava flow in the Zacapu Malpaís –Michoacan state, Mexico –. A full set of magnetic-mineralogy experiments (encompassing thermomagnetic curves, hysteresis loops, backfield curves, and isothermal remanent magnetization acquisition measurements) were carried out. The experimental methodology also considers magneto-chemical alteration detection, cooling rate, and remanence anisotropy effects to ensure reliable archaeointensity determinations. Five of the seven ceramic fragments – a pipe (potsherd I), vessel's supports (potsherd II and V), a vessel's wall-fragment (potsherd III), and a pipe's nozzle (potsherd VII) – yielded archaeointensity results within the acceptance established criteria to guarantee quality data. Thermal demagnetization of potsherds I, II, V, and VII shows between two and three magnetization components: one associated with potsherd's fabrication, the second with sample's reheating, and the third one, when present, with a viscous component. For each of the first two components, an intensity value was calculated. Potsherds I, II, III, and VII yielded archaeointensity values between 30 and 40 μT, while potsherd V had a much lower value <20 μT. Although secular variation models do not predict such low intensities, similar values are reported for the center and south of Mexico. Archaeomagnetic dating was carried out with two regional Paleosecular Variation Curves. The "El Caracol" lava flow is an area with human occupation reported from AD 1200. The results obtained in this work, on the contrary, envision the possibility of an early occupation of the site.

3.3 Introduction

Mesoamerican cultural heritage has been the focal point of many studies around the world (ej. Butzer, 2013; Santiny *et al.,* 2022; Gyarmati *et al.,* 2022; Berger, 2019). Nonetheless, a high percentage of the investigations carried out focused on a select group of cultures and temporalities considered greatly important by their popularity (for example the Mayan and Aztec cultures vs the Tarascan culture), leaving aside other cultures. These disregarded cultures were considered less important due to their apparently lower development (justified by the size of their constructions and/or by their crafts' limited complexity) (Williams, 2005). Western Mesoamerican cultures belong to this unattended group. The Tarascan Empire dominated such region at the Spaniard's arrival in AD 1522, so it is considered the representative pre-Hispanic culture of the area. This region has a little-known past that began to be systematically studied until the last decade of the twentieth century (Espejel-Carbajal, 2014). Despite the evident advances in the Western region investigations in previous years, different circumstances (e.g., limited historical registers, looting of archeological sites, scarcity of resources for archeological rescues and corresponding laboratory analysis, etc.) have led to know only small information windows of specific temporalities and spatial distributions. Therefore, a more significant effort that allows unraveling these cultures' history more fluidly is needed. In this sense, the use of archaeomagnetism in archeological studies offers the possibility to get a better understanding of the population dynamics through the age association to different archeological materials in varied contexts (e.g., Morales *et al.,* 2013 and López-Delgado *et al.,* 2019).

This work presents an archaeomagnetic study conducted on seven superficial ceramic potsherds recovered at "El Caracol", a lava flow belonging to the Zacapu's Malpaís located in Michoacán state (Mexico). Zacapu region represents a strategic investigation area for western Mexican archeological studies, since it is considered the starting point of the human group that founded the Tarascan empire (see details in Section 3.3 Geological and archeological background).

The investigation comprises the magnetic-mineralogy characterization of the potsherds and considers most of the correction factors that are currently used in archaeomagnetic research worldwide to ensure the obtaining of high-quality data (i.e., monitoring of magnetomineralogical changes during AI experiments (pTRM checks); dependence of the magnetization acquisition capacity due to differences between laboratory-used and similar to normal cooling times employed at the ceramics manufacture

(cooling rate correction); and determination of the anisotropy tensor of the samples for anisotropy corrections).

Based on the archaeointensity (AI) values obtained, two likely potsherd groups are recognized. The first group with AI values between 30 and 40 μT, and the second group with values lower than 20 μT. The age differences obtained associating the intensity values acquired with two of the four regional intensity Paleosecular Variation Curves (PSVC) published for Mexico until now are discussed.

3.4 Geological and archeological background

The Zacapu Malpaís (19◦50'45.98'' N, 101◦48'21.64'' W) is a set of Pleistocene and Holocene lava flows situated in the septentrional portion of Michoacán State, Mexico. It is located within one of the most extensive monogenetic volcanic fields worldwide; the Michoacán-Guanajuato Volcanic Field (MGVF) (Valentine and Connor, 2015). The Malpaís lava flows have a mean thickness of 100 m and a rough, blocky surface covering an approximate area of 50 km2 (Darras, 1998). The first geological study in the area was realized by Demant (1992), who determined that lavas of andesitic composition are the main component of the Malpaís. However, he also observed basaltic andesite and dacite composition lava flows. Radiometric dating (Reyes-Guzmán *et al.,* 2018) and paleomagnetic dates (Mahgoub *et al.,* 2017) suggest two emplacement stages; the initial stage (composed of five lava flows: Las Cabras, Las Florecitas, Mesa del Bolsón, El Caracol, and Milpillas) between ~30, 000 and ~21,300 BCE and the second one between ~1500 BCE and AD ~900. The last emplacement phase is composed of four lava flows: El Infiernillo (1492–1379 BCE), Malpaís las Víboras (1333–1239 BCE), El Capaxtiro (193–84 BCE), and Malpaís Prieto (AD 829–962) (Figure 13). The Zacapu lava flow complex has been considered of great interest to the archeological investigations due to the human occupation evidence, localized in distinct lava flows, and to the contemporaneity of some of the lava flows' emplacement with such populations.

From the archaeology's point of view, the Zacapu region represents a starting point for the research because of its relevance described in the most ancient ethnohistorical document, "La Relación de Michoacán" (RM), which was written at the beginning of the Spanish conquest. This document mentions that the Tarascan empire founders (the dominant culture in western México since AD ~1200 and until the Spaniard's arrival) initially arrived on a pilgrimage to the Zacapu area for later establishment their main city at ~55 km to the SE in the Pátzcuaro lake shores (Alcalá, 1977). However, as Michelet (2018) mentions,

"The image that one can make of the Tarascan realities from the RM is not exempt from probable imperfections, so it is essential to resort to other sources and the information field that would make it possible is the archeological record."

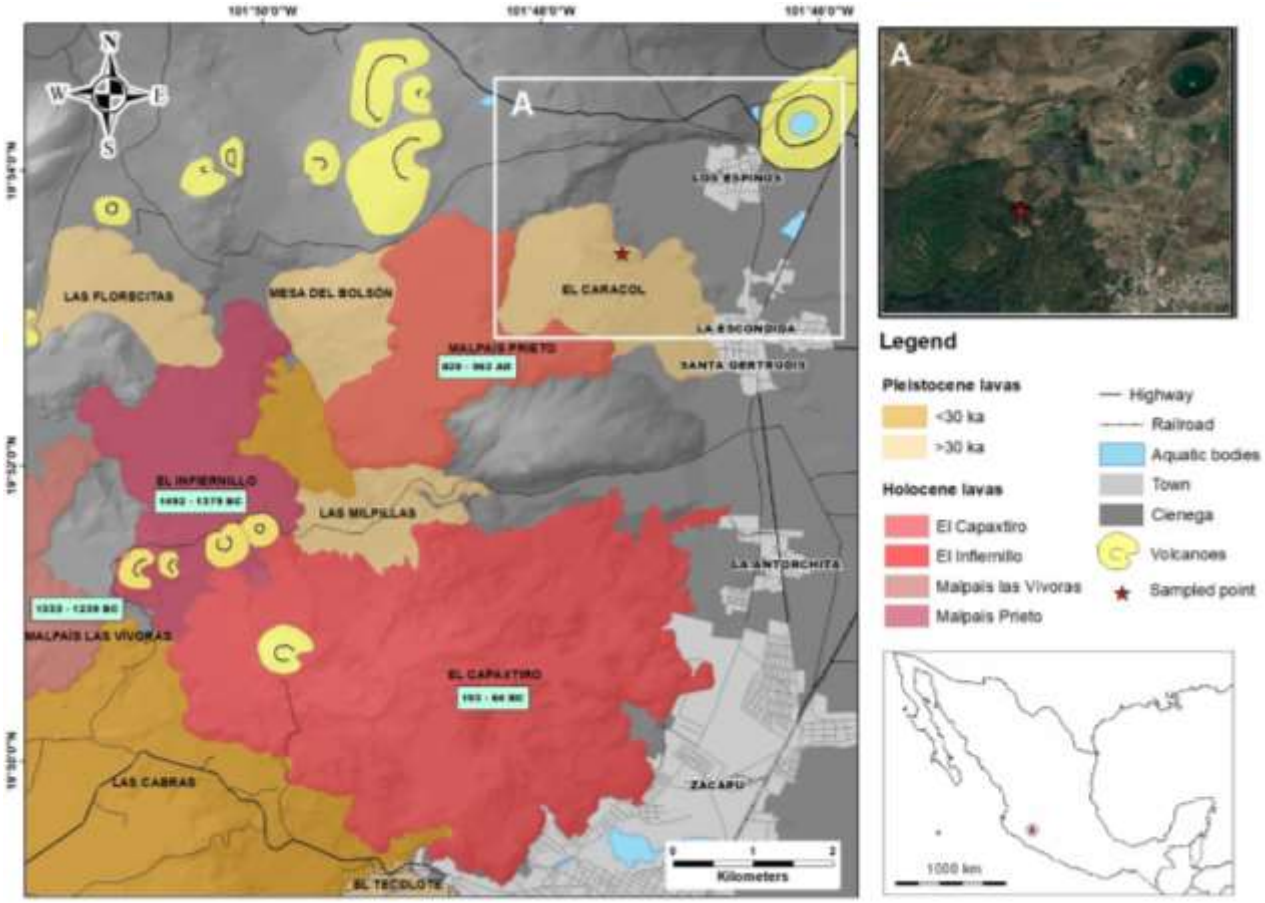

Figure 13 Digital elevation model of the north area of Zacapu Malpaís. Pleistocene and Holocene lava flows are highlighted. The A box presents a satellite view of the remarked area in the digital elevation model. Dates presented were taken from Mahgoub *et al.* (2017). Geological lava flows sequence was proposed by Reyes- Guzmán *et al.* (2018).

On the other hand, archeological evidence suggests a great cultural continuity in Zacapu from the year 100 BCE and until AD 1450 (Michelet, 1988) based on the distinct pottery styles located in the area. This period is divided into four phases and two subphases: Loma Alta phase (100 BCE – AD 550), Jarácuaro subphase (AD 550 – 600), Lupe phase (AD 600 – 850), La Joya subphase (AD 850 – 900), Palacio phase (AD 900 – 1200) and Milpillas phase (AD 1200 – 1450) (Michelet, 1992; Arnauld *et al.,* 1993). Although the cultural continuity is evidenced, two ruptures mark the sequence. The first (AD 550) is characterized by

the end of the apogee in the pottery culture, *i.e.,* the complexity in the designs and decorations of the ceramics had a setback (Carot, 2005), and the second (AD 900) is represented by a sudden population increase (Migeon, 1998, 2016), which could be associated with the aforementioned pilgrimage described in the RM. Both phenomena, the occupation, and the abandonment of the Malpaís, occur suddenly, so they represent events without precedents in the region. Additionally, settlement of lands with hostile conditions, characteristics of a badland, for the population development is an uncommon phenomenon with many questions without answers yet.

Recently, one of the most significant discoveries within the archeological investigations of the Mesoamerican West, particularly about pre- Tarascan cultures, was the urban area of the Malpaís Prieto (see Figure 13), also known as "the lost city" (Michelet, 2018 and references therein). So, within the Zacapu lava complex, the area corresponding to Malpaís Prieto has represented a focus of interest, and the rest of the lava flows have been poorly studied. Such is the case of the "El Caracol", a Pleistocene structure located to the east of Malpaís Prieto (Figure 13). The "El Caracol" lava flow settlements are only referred to in the literature as a neighborhood belonging to Malpaís Prieto, with occupation within the Milpillas phase (Migeon, 2016). No more information has been recovered about the settlements of this area.

3.5 Methodology

3.5.1 Materials

Seven surface ceramic fragments were recovered from "El Caracol" lava flow (see Figure 13 and Figure 14). A visual archeological recognition associates the "Milpillas Pulido" and the "Milpillas Inciso" styles to the ceramic fragments; both styles are frequently observed in domestic contexts. These potteries are made of a fine reddish paste and have a polished engobe produced by an oxidant atmosphere at baking (Migeon, 2016). The pottery fragments were associated with different utensils through their shape. Potsherd I was identified as a pipe; potsherds II and V correspond to vessel supports; potsherd III was related to a vessel's wall; potsherd IV seems to be part of a vessel's handle; potsherds VI could not be precisely identified; by their dimensions, shape, and color, potsherd VII could be part of the nozzle of potsherd I.

3.5.2 Laboratory procedures

Pottery shards recovered in the field were cut into six specimens, which were pressed into salt pellets of paleomagnetic standard size (22 mm long and 25 mm diameter). In this way, a total of 42 archaeomagnetic specimens were obtained. Four rock-magnetic experiments (progressive isothermal remanence magnetization (IRM) acquisition curves, hysteresis loops, backfield curves, and thermomagnetic curves) were realized utilizing an advanced variable-field translation balance (AVFTB) from Magnetic Measurements Ltd. The data obtained from these experiments allowed us to determine the remanence carriers, estimate the magnetic mineralogy's thermal stability, and ascertain the potteries' capacity to achieve reliable AI determinations. IRM curves and hysteresis loops were carried out up to a maximum field of 0.7 T. Hysteresis loops were corrected for slope and drift contributions. Subsequently, saturation remanent magnetizations (MRS), saturation magnetizations (MS), and coercivity fields (BC) parameters were recovered. Coercivities of remanence (BCR) were set using gradually increasing backfields after saturation. Thermomagnetic curves were acquired between room temperature and 600 ◦C. AVFTB data were analyzed through the Rock – Mag Analyzer 1.0 software by Leonhardt (2006) and the HystLab v1.0.9 MATLAB tool by Paterson et al. (2018).

Figure 14 View of the pottery shards collected during fieldwork.

The Thellier method (Thellier and Thellier, 1959), as modified by Coe (1967), was used for AI determinations. The experiments were held employing a TD48-SC furnace from ASC Scientific. Heating and cooling steps were carried out in the air. Thirteen temperature steps were distributed from room temperature up to 560 ◦C, and the laboratory field strength was established to 45 ± 0.5 μT. Partial thermoremanent checks (pTRM) every third step and pTRM tail checks at 350 and 450 ◦C were executed to analyze the results' reliability (Riisager and Riisager, 2001). Natural remanent magnetization (NRM) and laboratory-induced magnetizations (TRMs) were measured using a JR6 dual-speed spinner magnetometer from AGICO. All determinations were accomplished with the ThellierTool 4.0 software (Leonhardt et al., 2004). Additionally, Arai Plot curvature (k) was calculated using the method suggested by Paterson (2011).

Three additional infield steps at 560 ◦C were carried out at the end of the Thellier – Coe (TC) protocol to evaluate the cooling rate (CR) effect in the specimens based on a modified method to that outlined by Chauvin *et al.* (2000). The first and third additional steps (TRM1 and TRM3) were carried out with the same time conditions as those steps in the TC protocol (cooling time ~ 45 min). The second step (TRM2) as performed using a prolonged cooling time (~ 6 h) based on the findings of a thermal evolution study carried out on different Mexican pottery kilns (Rojas-Navarrete, 1995), as reported by Morales *et al.* (2011). The cooling rate factor (f_{CR}) was computed as the ratio between TRM2 and TRM1, while variations in the TRM gaining capacity were assessed via the percent change between TRM3 and TRM1. CR correction was used when changes in TRM gain capacity were below 15% and $f_{CR} > 1$ (Morales *et al.,* 2009).

As noted by Chauvin et al. (2000), magnetic anisotropy deviates the TRM's direction acquired during manufacture and modifies the TRM's intensity acquired depending on the direction of the geomagnetic field applied. Accordingly, a six-step anisotropy of anhysteretic remanent magnetization (AARM) protocol was carried out to balance the effects of the magnetic anisotropy' shape. An anhysteretic remanent magnetization (ARM) was induced on each specimen by the simultaneous application of AC and DC magnetic fields (180 mT and 0.30 mT, respectively) at 6 axial directions (± X, ± Y, ± Z) employing an LDA5 AF demagnetizer, attached to a PAM1 anhysteretic/pulse magnetizer from AGICO. The C–mode procedure outlined in the Anisotropy of Magnetic Remanence – A Brief Practical Guide application note (AGICO, 2018) was followed. At the beginning of the experiment, and between each ARM directional stage, an AF demagnetization at 200 mT was performed to be utilized as a baseline. The AARM tensor was determined with the Anisoft5 software (Chadima, 2018). The procedure described by Veitch et al. (1984) for anisotropy correction was applied, correction factors were determined, and AI values were corrected accordingly.

3.6 Results

3.6.1 Rock magnetism experiments

On the one hand, isothermal remanent magnetization (IRM) acquisition curves for potsherds I, II, and V (Figure 15) revealed the dominance of low-coercivity (< 250 mT) (titano-) magnetite minerals of pseudo-single domain (PSD) grain size. Corresponding curves for potsherds III, IV, and VI got saturation at fields ~ 400 mT, suggesting the dominance of medium-coercivity Al, Mg, or Ti-substituted magnetite minerals of single domain (SD) and/or PSD grain size. On the other hand, the ratio between M_{RS} / M_S and B_{CR} / B_C, displayed in a Day-plot (Day *et al.,* 1977), depicts a first approach to the bulk magnetic domain structure. Potsherds I, II, IV, and V show a predominant PSD behavior (Figure 16a), while potsherds III and VI tend to the multidomain (MD) behavior. In the same sense, the comparison of the sample's parameters behavior with theoretical mixing curves for magnetite of Dunlop (2002) in a Day-plot, locate all the potsherds in the field of SD-MD mixing lines. However, due to the lack of consensus about the interpretation of the grain sizes trend in the Day diagram (Morales *et al.,* 2013), and to the possible improper use of this diagram in the analysis of natural samples, suggested by Roberts *et al.* (2018), the results obtained from the Day plot are compared against the alternative information generated from the rock magnetism experiments to get a more accurate interpretation of the domain states structures within the analyzed samples.

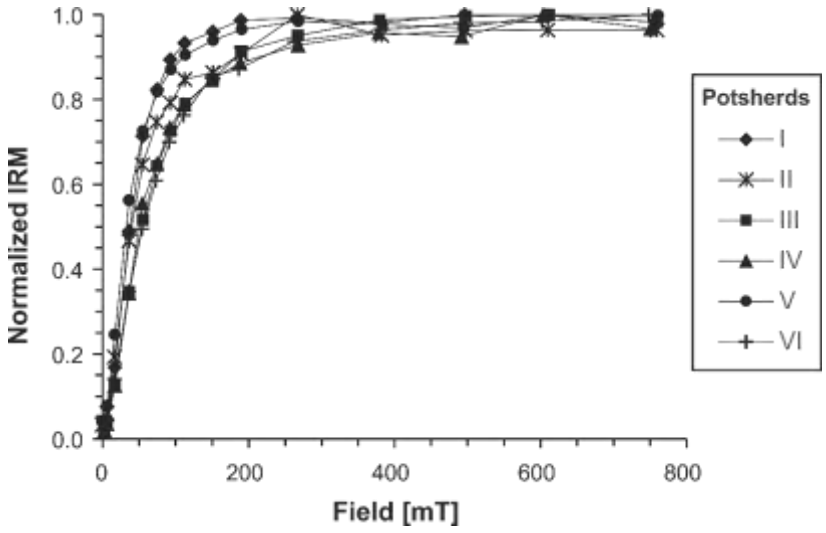

Figure 15 Demonstrative cases of isothermal remanent magnetization (IRM) acquisition curves for the six potsherds.

The parameter's shape (σ) of hysteresis curves (Fabian, 2003) shows a wasp-waisted behavior (σ > 0) for potsherds V and VI, associated with the mixture of SD and large superparamagnetic (SP) particles. On the contrary, a potbellied behavior (σ < 0), typical in samples with a mixture of SD and small SP particles, is observed from the hysteresis plot of potsherds I, II, and III. The combination of high and low coercivity magnetic components (Tauxe *et al.,* 1996), observed in the Day-plot, is supported with the shape parameter data for the potsherds before described. Finally, the σ = 0 suggests a constricted magnetic coercivity population for potsherd IV.

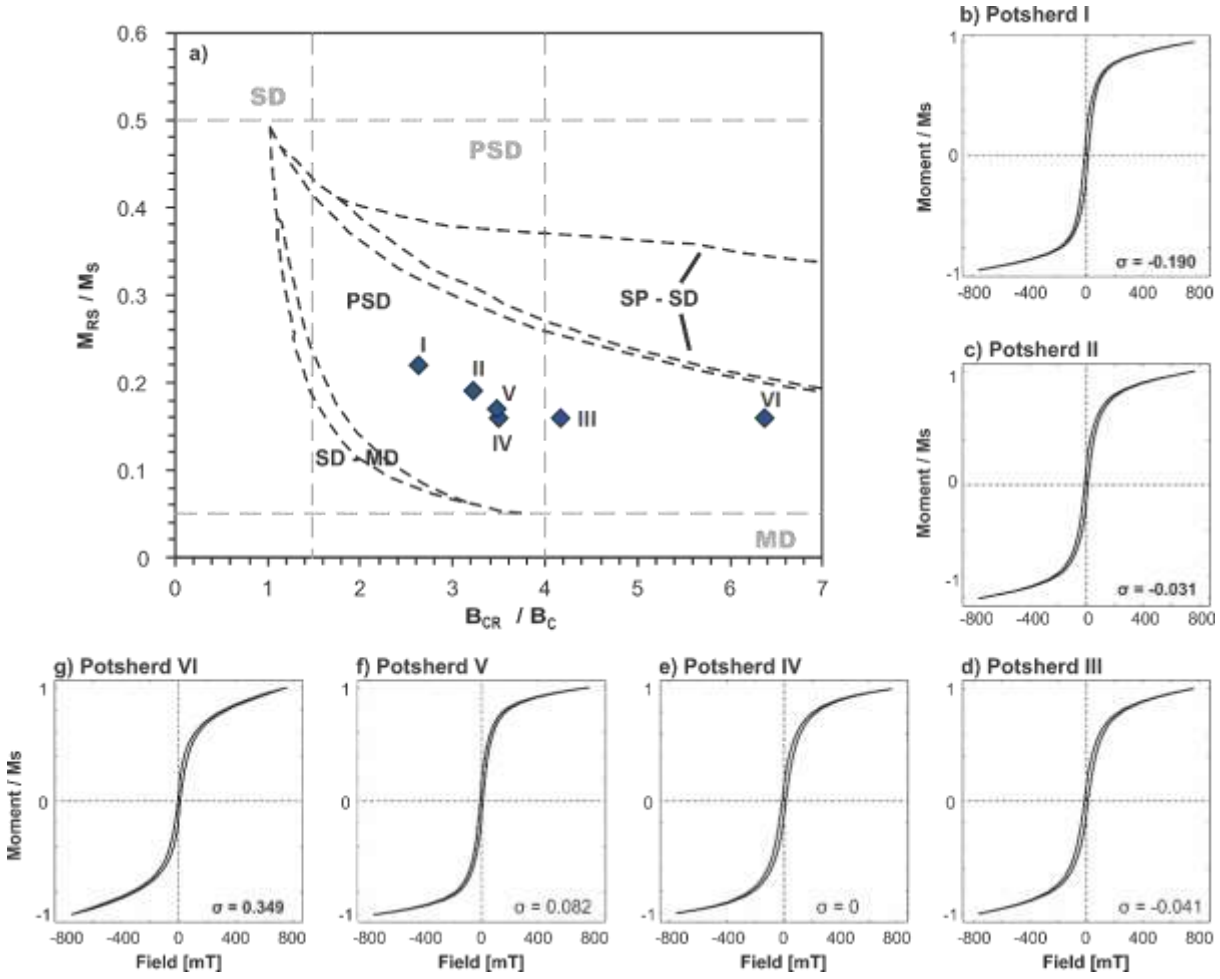

Figure 16 Hysteresis curve results. (a) Day-plot with theoretical curves (Dunlop, 2002) for SD-MD and SP-SD magnetite mixtures. (b–g) representative hysteresis curves of potsherds.

Thermomagnetic curves (M_S – T curves) for analyzed potsherds are quite reversible – type H(mx) behavior according to Calvo *et al.* (2002) – except for potsherd IV (Figure 17). For H(mx) M_S – T curves, the main

magnetic phase has a Curie temperature (T_C) that matches that of pure magnetite or close to magnetite composition (540 ± 10 ◦C) and displays no sign of alteration in the cooling curve (a difference between initial and final magnetization within ±10%). Additionally, H(mx) curves show another T_C between 400 and 450 ◦C associated with Ti-poor titanomagnetites. On the other hand, the thermomagnetic curve of potsherd IV (Figure 17d) shows three T_C (at low [250 ◦C], medium [400 ◦C] and high [510 ◦C] temperatures) in the heating branch, while the cooling one shows only two T_C (510 and 350 ◦C, respectively) and is described as a type L sample (Calvo 2002), *et al.,* which suggests a mineralogical change in the heating process. Therefore, an unfavorable result for AI experiments can be expected.

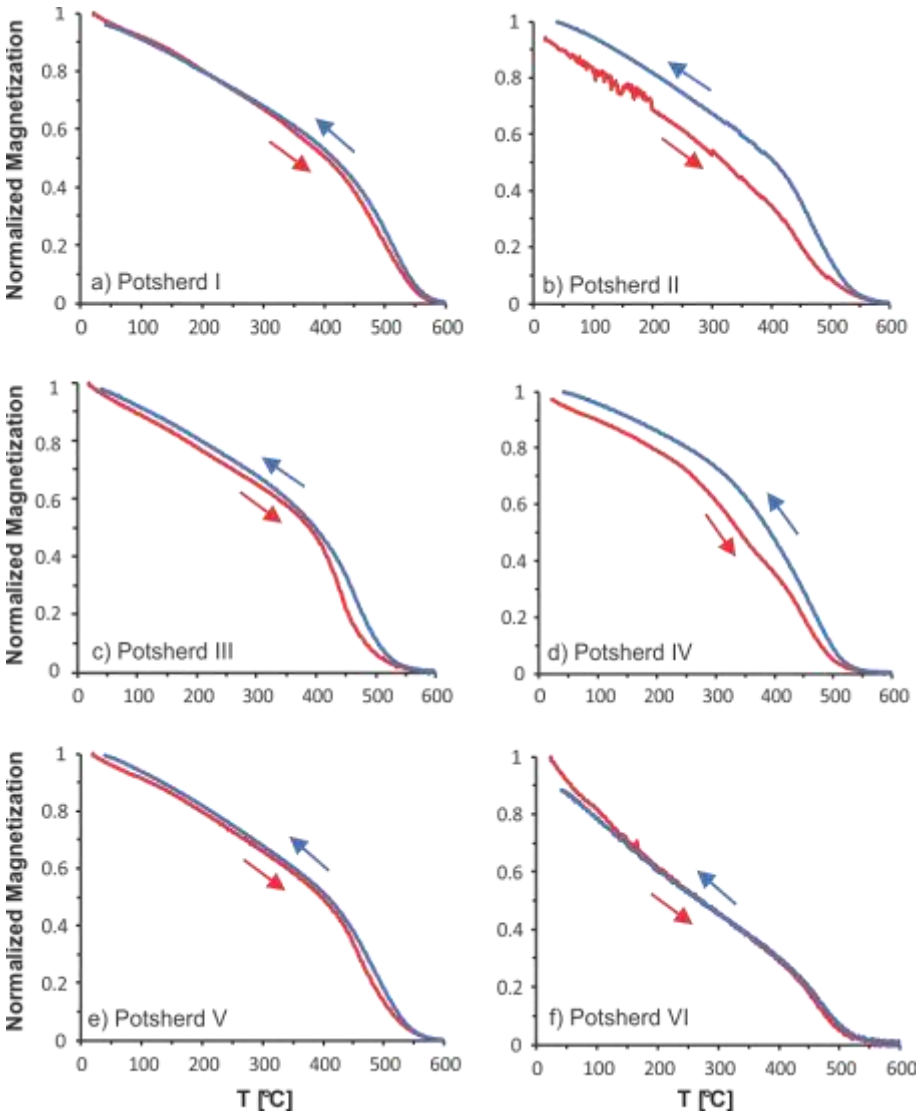

Figure 17 Thermomagnetic curves (M_S – T). The heating curve is shown in red, and the cooling curve in blue.

Results of rock-magnetism on the ceramic fragments I-VI are presented in Figure 17. These experiments were not carried out on the ceramic VII due to the small amount of available material. However, at the end of the AI experiments, one of the six ceramic fragments was extracted from the salt pellet of each analyzed potsherd (including potsherd VII) to replay the rock magnetism experiments and verify the magnetochemical changes before and after the thermal intensity experiment. The results are presented in Figure S1 of the supplementary material.

3.6.2 Archaeointensities

The 42 archaeomagnetic specimens were treated with the TC protocol for AI determinations. Quality checks, statistical parameters of the linear fit, and a correlation between the chosen temperature portion for intensity determination and the temperature range that keeps the characteristic remanent magnetization of the samples were considered to warrant the reliability of the antique geomagnetic field recorded.

Figure 18 shows representative orthogonal diagrams of thermal demagnetization (THD) of the ceramic fragments. As can be observed, the different THDs behaviors can be explained as follow: (1) Specimens with the register of the Earth's magnetic field magnetization at the moment of their elaboration (M1), in some cases accompanied with a secondary component of probable viscous origin (VRM), which is erased at maximum temperatures of 150 °C (e.g., specimens of potsherds III and VI; Figure 18c and f). (2) Specimens with evidence of reheating (between 300 – 450 °C) after potsherds elaboration. The reheating is noted by a secondary component (M2) which erased a portion of the original magnetization component (M1), leaving only the magnetic minerals with TC higher than the reheat temperature with the characteristics of the first magnetization (pM1). As in the previous group, some specimens show a VRM component. Examples of the multi-component magnetization specimens could be noted in Figure 18a, b, e, and g.

For the specimens with two magnetization components (pM1 + M2 components), one archaeointensity value per each magnetization component was obtained with the two-step method of Yu and Dunlop (2002). This method has been used successfully to determine intensity values in specimens with multiple magnetization components in bricks (Lisé-Pronovost *et al.,* 2020), ceramics (Pérez-Rodríguez *et al.,* 2021), and metamorphic rocks (Yu and Dunlop, 2002). In specimens with a single magnetization component, the

intensity value was obtained straightforward using the Arai plot (Nagata *et al.,* 1965). Representative Arai plots to illustrate the AI determination process are shown in Figure 19. The concave-up trend of potsherd IV (Figure 19d) is indicative of multidomain particles dominance as the principal remanence carriers (Fabian, 2001). As mentioned by Hodgson *et al.* (2018), the concave-up form is a non-ideal behavior caused by the cumulative alteration in magnetic particles of large grain/domain size, originated during the repeated heating of the TC experiment. Consequently, incongruent or no AI results at all were obtained. On the contrary, a good linear adjustment was obtained for the other ceramics, so their slopes were considered to calculate the AI values of the ceramics.

A modification of the Thellier-Tool A and Thellier-Tool B parameters (Leonhardt *et al.,* 2004), with different stringency levels proposed by Paterson *et al.* (2014) (TTAm and TTBm parameters, respectively), were used as a selection criterion to validate the results. The meaning and the threshold values for the different classes used are shown in Table 5. Additionally, a minimum of four specimens per potsherd (N = 4) was considered for calculating the mean intensity value in a ceramic sample. For the pM1 and M1 components, 24 out of 42 specimens (8 within the TTAm threshold parameters -Class A data- and 16 within the TTBm threshold parameters -Class B data), corresponding to six out of seven potsherds analyzed, yielded successful determinations (~57% success). Results with their related quality parameters are recorded in Table 6. Calculated raw AI values (H_{RAW}) are presented, as well as the values corrected by the cooling-rate and anisotropy factors (H_{CORR}). The specimens that exceed the quality values established in Table 5 are also presented, but the parameters with the values that exceed the threshold values are underlined; these data are distinguished in the class column as C class. These unreliable data were not considered for the average AI calculations.

Due to the low portion of the magnetic minerals that were magnetized by the reheating of the potsherds, f and β parameters for the M2 component do not reach the minimum value established in the quality parameters sets. Hence, all data are in the C class (see Table 6). However, as was suggested by Pérez-Rodríguez *et al.* (2021), if the rest of the parameters are into the established parameters sets and the specimen's intensity values are consistent by ceramic, the intensity mean value could be calculated and used for dating purposes. According to that, intensity mean values for the M2 component of potsherds I (six specimens), II (five specimens), and V (five specimens) were calculated.

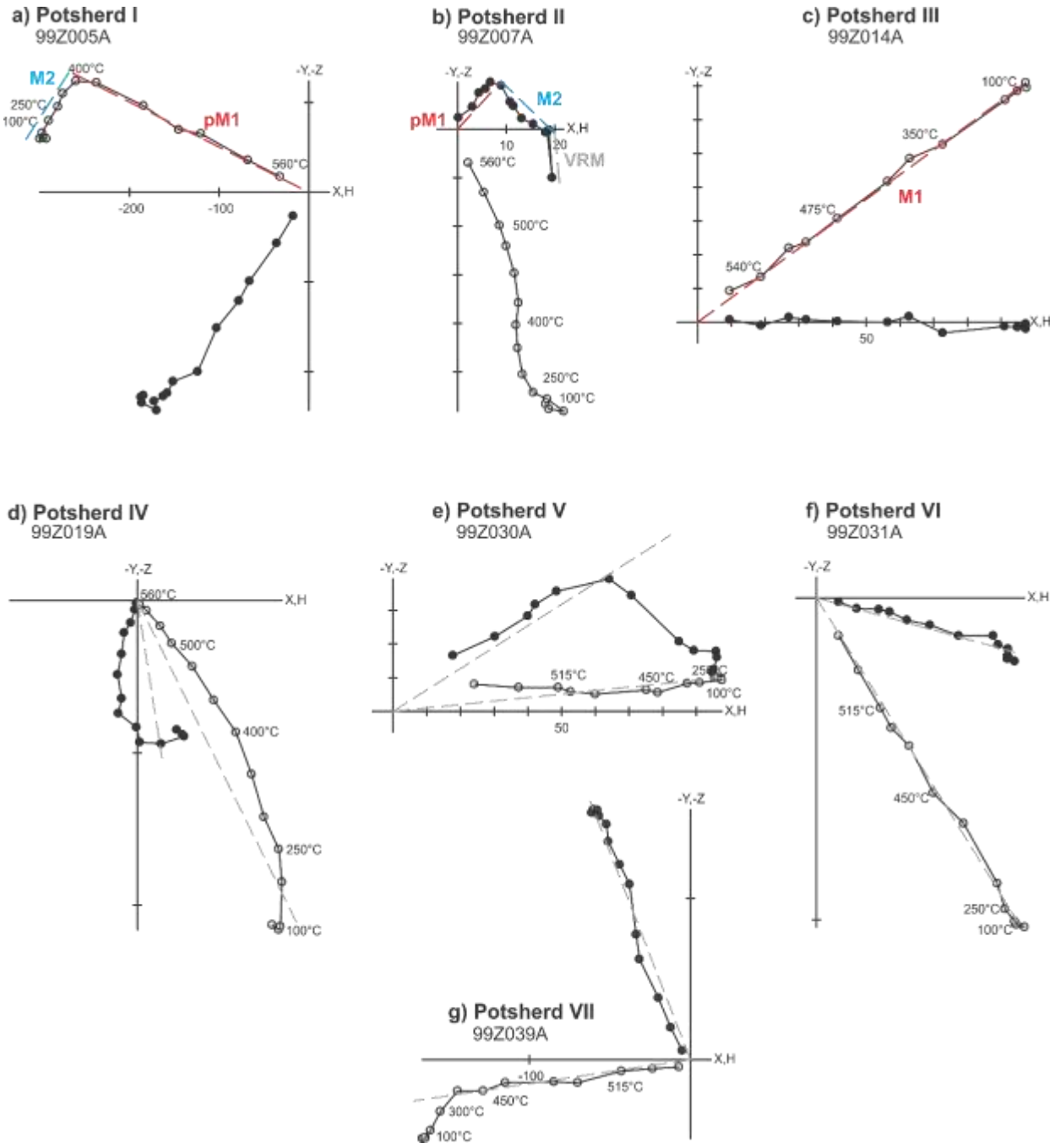

Figure 18 Illustrative (Zijderveld, 1967) plots of thermal demagnetized samples from the examined potsherds. Markers in the curves designate the temperature steps through the demagnetization. For (a–c) M1, pM1, M2, and VRM exemplify the magnetization components employed for classifying the potsherd's behavior (see main text).

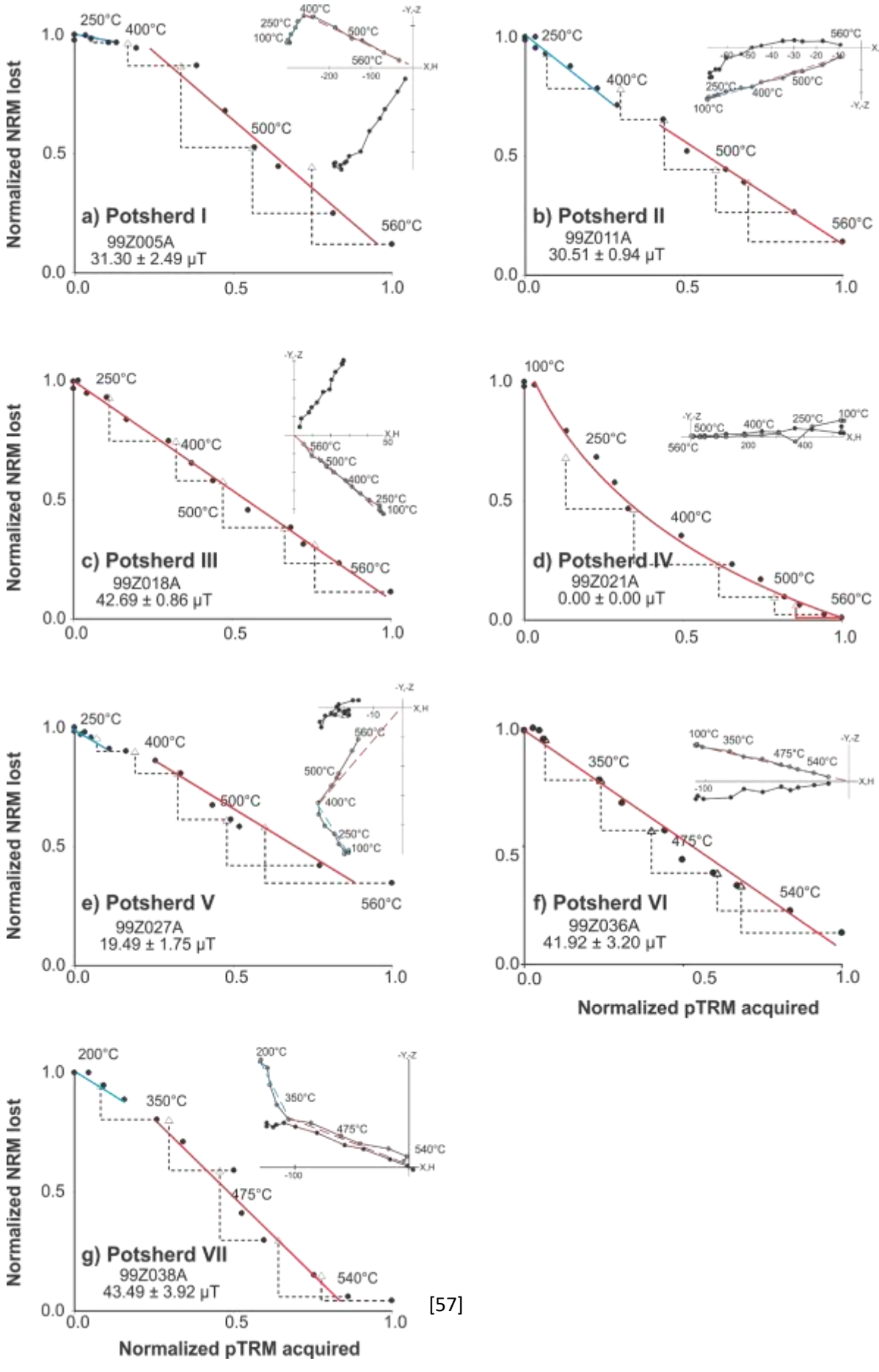
Normalized NRM lost
Normalized pTRM acquired
a) Potsherd I
99Z005A
31.30 ± 2.49 μT
b) Potsherd II
99Z011A
30.51 ± 0.94 μT
c) Potsherd III
99Z018A
42.69 ± 0.86 μT
d) Potsherd IV
99Z021A
0.00 ± 0.00 μT
e) Potsherd V
99Z027A
19.49 ± 1.75 μT
f) Potsherd VI
99Z036A
41.92 ± 3.20 μT
g) Potsherd VII
99Z038A
43.49 ± 3.92 μT

[57]

Figure 19 Representative Arai (NRM lost vs. pTRM acquired) plots. Red lines correspond to the pM1 portion or the M1 magnetization component. Blue lines correspond to the M2 portion of the magnetization component. Directional demagnetization plots are presented at the upper right-hand corner of the Arai diagrams.

Table 5 Selection criteria and threshold values used in this work following the Thellier Tools A and B parameters (Leonhardt *et al.,* 2004) modified by Paterson *et al.* (2014). n: number of NRM-pTRM points employed for paleointensity determination; f: the fraction of NRM utilized. β: Ratio of the standard error of the slope and the slope of the NRM-TRM plot; q: quality factor defined by Coe *et al.* (1978); MAD: Maximum angular deviation of NRM end-point directions at each step acquired during paleointensity experiments; α: the angle between the vector average of the data selected for paleointensity calculation and the principal component of the data (Kissel and Laj, 2004); δ(CK): Difference between the pTRM check and original TRM value at a specified temperature normalized to the TRM; δ(pal): cumulative check error (Leonhardt *et al.,* 2004); δ(TR): relative intensity difference in pTRM-tail check; δ(t*): normalized pTRM tail (Leonhardt *et al.,* 2004).

Class	n	f	β	q	MAD	α	δ(CK)	δ(pal)	δ(TR)	δ(t*)
TTAm	≥ 5	≥0.35	≤0.10	≥ 5	≤6	≤15	≤7	≤10	≤10	≤9
TTBm	≥ 5	≥0.35	≤0.15	≥0	≤15	≤15	≤9	≤18	≤20	≤99

Table 6 Thellier-Coe paleointensity results for Zacapu potsherds. n, f, β, q, MAD, α, δ(CK), δ(pal), δ(TR) and δ(t*) are defined in Table 5 caption; T_{MIN}/$_{MAX}$: minimum/maximum temperature; Class: A for values within TTAm parameters, B for values within TTBm parameters, C for values out of established parameters; H_{RAW}: raw archaeointensity values, f_{CR}: cooling rate correction factor; f_{ANI}: anisotropy correction factor; H_{CORR}: corrected archaeointensity values by cooling rate and anisotropy factors.

Name	T_{MIN}	T_{MAX}	N	β	f	g	q	w	MAD	α	δ(CK)	δ(pal)	δ(t*)	δ(TR)	k	Class	H_{RAW}	f_{CR}	f_{ANI}	H_{CORR}
Potsherd I (pM1)																				
99Z001A	350	560	7	0.11	0.77	0.77	5.4	2.4	1.6	0.9	3.0	0.2	2.9	1.3	0.148	B	38.39	1.02	0.94	35.31
99Z002A	350	560	8	0.02	0.78	0.81	36.5	14.9	2.4	1.3	9.2	37.8	3.3	6.8	-0.059	C	37.22	1.06	0.97	33.99
99Z003A	350	560	7	0.03	0.81	0.75	20.0	8.9	2.1	1.4	8.3	4.3	10.7	3.2	-0.020	B	37.18	1.05	0.86	30.48
99Z004A	400	560	6	0.10	0.75	0.79	6.1	3.1	2.8	1.5	10.2	17.5	7.0	2.4	-0.027	C	34.06	1.05	0.89	28.85
99Z005A	400	560	7	0.08	0.72	0.82	7.4	3.3	1.8	0.8	9.8	7.8	6.8	6.6	0.100	C	30.79	1.06	0.92	26.80
99Z006A	400	560	7	0.05	0.68	0.81	11.4	5.1	1.1	0.8	11.0	41.4	6.2	5.8	0.135	C	37.86	1.07	0.98	34.59
																Mean =	37.79			**32.90**
																Std =	0.86			**3.42**
Potsherd I (M2)																				
99Z001A	20	300	5	0.29	0.05	0.58	0.1	0.1	4.6	2.0	0.4	8.0	3.2	0.0	-0.420	C	42.98	1.02	0.94	39.53
99Z002A	20	300	5	0.30	0.07	0.63	0.2	0.1	3.7	2.5	0.7	2.5	3.6	0.0	-0.411	C	42.36	1.06	0.97	38.68
99Z003A	20	300	5	0.45	0.03	0.37	0.0	0.0	3.1	0.4	0.2	2.7	11.9	0.0	-0.339	C	28.72	1.05	0.86	23.55
99Z004A	20	350	6	0.17	0.07	0.70	0.3	0.1	4.1	4.1	0.4	8.8	8.4	2.1	-0.197	C	35.77	1.05	0.89	30.30
99Z005A	100	350	5	0.13	0.04	0.69	0.2	0.1	4.2	1.5	0.2	6.9	8.3	0.4	-0.068	C	28.09	1.06	0.92	24.45
99Z006A	100	350	5	0.10	0.10	0.72	0.7	0.4	3.6	3.4	0.7	3.6	6.6	0.1	-0.103	C	36.30	1.07	0.98	33.16
																Mean =	35.70			**31.61**
																Std =	6.39			**6.83**
Potsherd II (pM1)																				
99Z007A	400	540	6	0.05	0.46	0.78	8.0	4.0	4.7	7.4	5.8	9.2	4.2	3.7	-0.024	A	34.95	1.06	0.99	32.56
99Z008A	400	540	6	0.05	0.45	0.79	6.6	3.3	4.3	7.7	6.0	4.5	0.0	4.2	0.046	A	37.32	1.05	1.00	35.45
99Z009A	450	560	5	0.04	0.52	0.74	9.6	5.5	2.1	1.9	7.0	2.1	4.1	3.8	-0.082	B	33.72	1.07	1.00	31.48
99Z010A	450	560	6	0.03	0.53	0.79	14.3	7.1	1.7	0.5	7.8	10.6	4.5	2.2	-0.076	B	34.01	1.30	0.99	25.92
99Z011A	450	560	6	0.06	0.50	0.78	6.5	3.2	2.9	3.9	6.5	2.0	3.3	0.9	0.185	A	30.78	1.06	0.91	26.49
99Z012A	400	560	7	0.06	0.58	0.82	8.2	3.7	4.6	6.0	3.9	0.8	4.3	2.5	0.024	A	29.87	-	0.91	27.14
																Mean =	33.44			**29.84**
																Std =	2.74			**3.89**
Potsherd II (M2)																				
99Z007A	100	350	5	0.06	0.25	0.71	3.0	1.7	4.9	8.1	1.0	5.0	4.1	0.9	0.097	C	43.11	1.06	0.99	40.16
99Z008A	20	350	6	0.05	0.23	0.72	3.3	1.6	1.0	1.9	0.6	0.9	0.0	0.2	-0.010	C	38.77	1.05	1.00	36.83
99Z009A	20	400	8	0.05	0.28	0.77	3.9	1.6	3.0	9.9	6.1	16.1	4.1	0.3	0.304	C	31.91	1.07	1.00	29.79

99Z010A	20	400	8	0.04	0.28	0.78	5.8	2.4	3.2	10.4	5.2	15.5	4.5	0.7	0.064	C	34.87	1.30	0.99	26.57
99Z011A	100	400	7	0.06	0.29	0.77	3.5	1.6	3.3	9.1	7.4	20.9	3.3	0.7	-0.057	C	37.06	1.06	0.91	31.90
99Z012A	20	350	6	0.08	0.25	0.44	1.3	0.7	2.1	3.1	2.9	12.5	4.1	0.3	0.047	C	36.37	-	0.91	33.05
																Mean =	37.01			**33.28**
																Std =	4.22			**5.41**
Potsherd III (M1)																				
99Z013A	100	560	11	0.03	0.88	0.87	26.7	8.9	3.3	5.2	5.7	16.7	5.2	1.0	0.174	B	39.17	1.03	0.96	36.53
99Z014A	100	560	11	0.04	0.90	0.88	17.9	6.0	1.2	0.9	7.7	10.2	3.1	4.6	0.035	B	44.42	-	0.94	41.91
99Z015A	100	560	12	0.06	0.88	0.89	14.1	4.5	1.3	1.1	12.9	12.3	3.3	4.6	0.072	C	44.17	1.06	0.99	41.24
99Z016A	200	560	11	0.01	0.83	0.88	68.1	22.7	2.6	4.3	4.2	13.7	5.0	4.6	0.062	B	40.28	-	0.98	39.35
99Z017A	150	560	11	0.03	0.89	0.87	28.3	9.4	1.2	0.9	14.3	28.3	8.2	8.4	0.027	C	44.75	1.02	0.98	42.82
99Z018A	20	560	14	0.02	0.90	0.90	40.3	11.6	1.4	1.6	3.1	8.6	6.2	2.6	0.091	A	42.32	1.17	0.96	34.76
																Mean =	41.55	-		**38.14**
																Std =	2.32			**3.15**
Potsherd V (pM1)																				
99Z025A	400	515	5	0.03	0.32	0.72	8.7	5.0	4.5	7.5	2.4	1.5	4.2	6.8	0.473	C	24.97	1.10	0.97	22.09
99Z026A	350	540	7	0.07	0.56	0.79	6.1	2.7	7.2	13.8	9.0	11.2	2.3	7.4	0.414	B	17.97	1.08	0.98	16.30
99Z027A	350	540	7	0.07	0.47	0.77	5.2	2.3	5.9	14.2	6.3	10.1	4.5	4.2	0.419	B	17.35	1.07	0.91	14.86
99Z028A	400	560	7	0.08	0.53	0.79	5.1	2.3	3.2	6.1	4.8	2.8	2.6	3.2	0.422	A	19.28	1.10	0.98	17.20
99Z029A	475	560	5	0.13	0.39	0.69	2.0	1.2	4.4	7.9	4.8	1.9	5.3	2.6	0.573	B	17.33	1.07	0.90	14.46
99Z030A	400	560	7	0.12	0.57	0.8	3.7	1.6	5.3	10.2	5.5	6.4	2.9	2.5	0.445	B	19.40	1.06	0.88	15.99
																Mean =	18.27			**15.76**
																Std =	1.01			**1.11**
Potsherd V (M2)																				
99Z025A	20	350	7	0.10	0.08	0.70	0.6	0.2	5.7	9.8	0.4	4.0	5.0	0.2	0.188	C	10.75	1.10	0.97	9.51
99Z026A	100	300	5	0.05	0.12	0.58	1.4	0.8	2.3	1.5	0.4	0.1	2.1	0.0	-0.625	C	21.33	1.08	0.98	19.34
99Z027A	20	300	6	0.15	0.08	0.53	0.3	0.2	2.8	1.8	1.3	8.1	4.8	0.0	-0.059	C	20.53	1.07	0.91	17.58
99Z028A	20	350	6	0.07	0.18	0.60	1.4	0.6	4.8	11.8	1.1	6.2	2.6	0.0	-0.349	C	22.44	1.10	0.98	20.02
99Z029A	20	400	7	0.13	0.26	0.62	1.3	0.6	5.0	14.3	1.6	7.8	4.4	0.0	0.374	C	32.00	1.07	0.90	26.70
99Z030A	20	300	6	0.28	0.10	0.63	0.2	0.1	2.2	1.6	1.2	30.1	2.8	0.0	-0.286	C	22.57	1.06	0.88	18.61
																Mean =	21.41			**18.63**
																Std =	7.54			**6.16**
Potsherd VI (M1)																				
99Z031A	100	500	9	0.06	0.63	0.78	8.1	3.1	1.2	1.5	12.2	20.1	2.1	0.9	0.397	C	55.40	1.07	0.94	48.46
99Z032A	100	515	9	0.05	0.66	0.77	10.0	3.8	1.9	3.5	11.0	15.3	0.6	1.7	0.329	C	51.77	1.05	0.95	46.95
99Z033A	100	515	10	0.05	0.66	0.83	11.1	3.9	1.4	1.1	10.2	22.4	5.0	0.5	0.418	C	54.51	1.11	0.95	46.84
99Z034A	20	540	12	0.05	0.77	0.84	13.7	4.3	1.2	1.3	10.8	10.6	4.9	1.4	0.230	C	53.04	1.09	0.93	45.03
99Z035A	20	540	11	0.03	0.75	0.86	19.5	6.5	1.5	3.0	4.5	11.3	1.6	0.5	0.214	B	50.09	1.09	0.80	36.85
99Z036A	20	560	12	0.04	0.91	0.88	18.6	5.9	1.1	0.3	4.0	1.7	2.7	1.8	0.760	A	46.38	1.05	0.82	36.32
																Mean =	48.24			**36.58**
																Std =	2.62			**0.38**
Potsherd VII (pM1)																				
99Z037A	350	540	7	0.07	0.62	0.83	7.6	3.4	9.4	13.5	2.9	0.9	4.2	4.8	0.103	B	36.52	1.03	0.93	32.80
99Z038A	350	540	7	0.09	0.66	0.82	6.1	2.7	3.4	3.9	5.3	8.4	2.5	2.5	0.420	A	42.60	1.04	0.91	37.30
99Z039A	400	560	7	0.09	0.67	0.82	6.4	2.8	3.6	4.0	6.5	12.7	2.3	0.8	0.335	B	39.13	1.05	0.93	34.82
99Z040A	400	560	7	0.05	0.61	0.83	9.6	4.3	4.6	5.7	6.5	16.3	1.4	1.8	0.298	B	44.45	1.04	0.95	40.78
99Z041A	350	560	8	0.07	0.76	0.84	9.5	3.9	4.3	5.3	7.0	34.2	1.4	0.7	0.381	C	26.39	1.07	0.95	23.32
99Z042A	400	560	7	0.06	0.59	0.81	8.6	3.8	1.4	1.0	4.9	17.0	51.2	16.1	0.103	B	43.78	1.03	0.99	42.07
																Mean =	41.30			**37.55**
																Std =	3.37			**3.90**
Potsherd VII (M2)																				
99Z037A	20	250	4	0.21	0.03	0.61	0.1	0.1	1.3	0.1	0.0	0.0	4.7	0.0	-0.320	C	10.19	1.03	0.93	9.15
99Z038A	20	300	4	0.19	0.12	0.62	0.4	0.3	2.1	0.8	0.9	9.3	2.8	0.0	-0.543	C	30.34	1.04	0.91	26.57
99Z039A	100	350	5	0.06	0.15	0.69	1.7	1.0	3.2	3.0	0.1	4.9	2.4	0.3	0.558	C	33.53	1.05	0.93	29.84
99Z040A	20	350	6	0.09	0.23	0.74	2.0	1.0	3.5	6.7	0.3	1.8	1.4	1.9	-0.364	C	41.98	1.04	0.95	38.51
99Z041A	20	300	6	0.17	0.11	0.64	0.4	0.2	2.6	2.4	0.0	1.1	1.4	0.0	-0.722	C	21.45	1.07	0.95	18.95
99Z042A	20	350	7	0.10	0.20	0.75	1.5	0.7	4.0	10.3	0.0	0.0	58.2	1.6	-0.491	C	32.54	1.03	0.99	31.27
																Mean =	28.34			**25.72**
																Std =	11.06			**10.32**

As the last parameter for the quality evaluation of the archaeointensity data, the k (curvature) parameter was proposed, which was determined in MATLAB using the CircleFitByPratt(XY) function (Chernov, 2020) based on Pratt's method (Pratt, 1987). k data are displayed in Table 2, while Fig. 8 shows characteristic plots of the fitted circles to the Arai plots data. For the specimens with two magnetization components, a k value by component was calculated. According to Paterson (2011), a positive curvature (concave-up shape) (Fig. 8a and c) is indicative of MD contributions. In contrast, a concave down shape or negative curvature is indicative of magnetic mineralogy alteration by temperature and/or noisy data. In the same sense, Paterson (2011) proposed the limit value of $k \leq 0.164$ as indicative of SD particles as the principal carriers of remanence, and $k \leq 0.270$ as indicatory of PSD particles as the principal carriers of remanence. These values were defined using synthetic samples with known grain sizes.

Figure 20e summarizes the curvature results for the 60 data presented in Table 6 (36 for M1 or pM1 magnetization components, and 24 for M2 magnetization component), along with the corresponding threshold values mentioned above. Data are compared with the established classes in Table 5. As can be observed, for this specific set of samples, there is no relationship between the quality of the specimens assigned by the TTAm / TTBm parameters and the curvature. While 36 data were rejected for exceeding the TTAm / TTBm parameters' limits, 28 exceeded the curvature's critical values, of which only 19 coincide with the previously rejected values. On the other hand, the specimen with the highest curvature values (99Z036A: $k = 0.760$) is within the data with the best quality according to the TTAm / TTBm parameters. Although k is a valuable tool to quantify the curvature in the Arai plots, the lack of refinement in its threshold values (Paterson, 2011) led us to provide further weight to the rest of the quality criteria for the final determination of archaeointensities data quality.

Finally, seven quality AI values corresponding to five of the seven analyzed potsherds were obtained: the AI values obtained for potsherds I (M2), II (pM1 and M2), III (M1), and VII (pM1) have intensity values between ~30 and 40 μT, while both components of potsherd V (pM1 and M2) have lower AI values (< 20 μT).

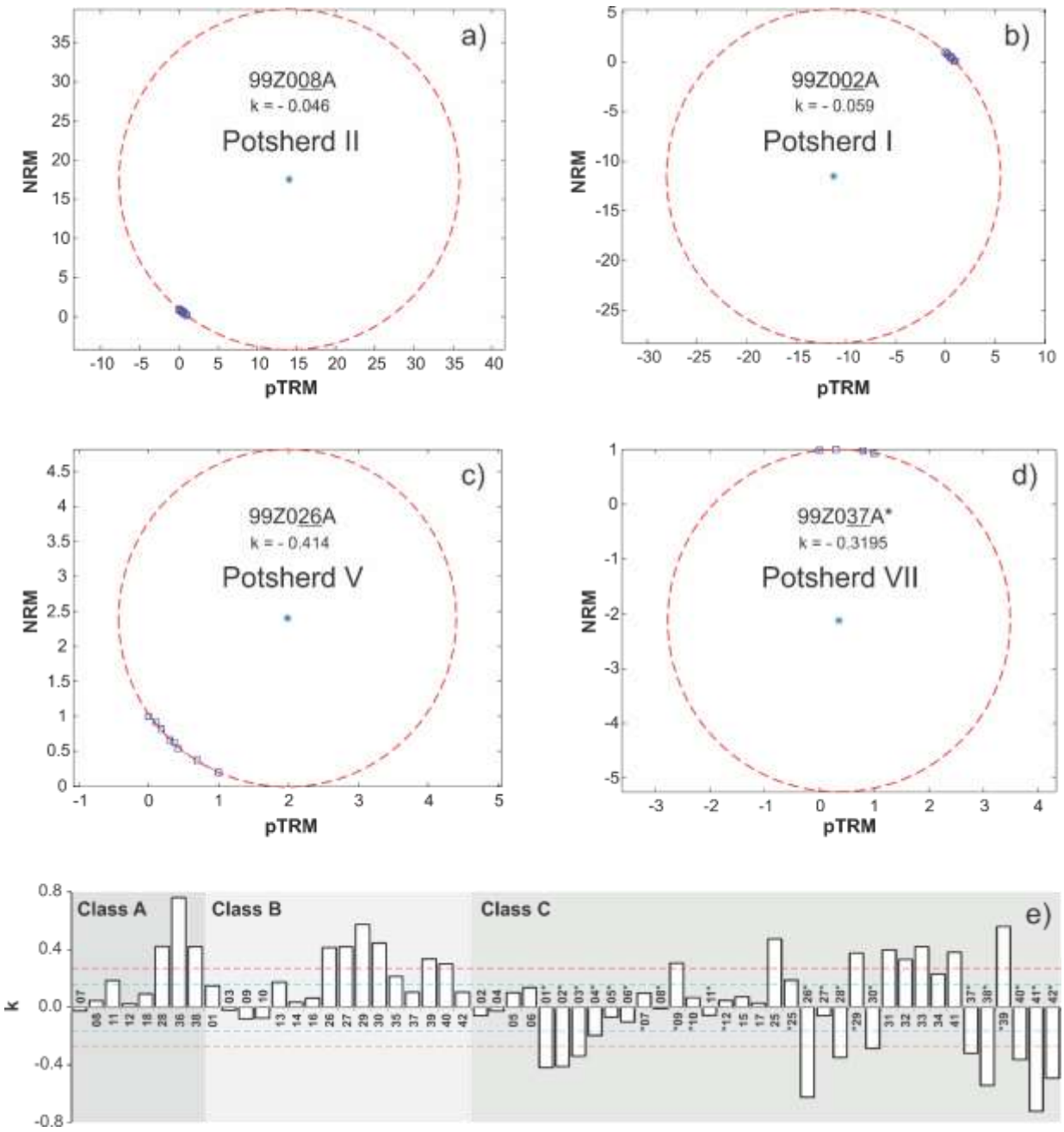

Figure 20 Representative plots of the fitted circles to the data of the Arai plots. a) and b) show data with curvature within the limit established by Paterson (2011), where SD particles are the dominant remanence carriers ($k \leq 0.164$). a) Shows positive curvature and b) negative curvature. c) and d) show data with curvature $k > 0.164$ with positive and negative curvatures, respectively. e) Synthesis of the 60-curvature data for archaeointensity estimations displayed in Table 6. Labels indicate to which specimen each bar corresponds. For the sake of simplicity, only the last two digits of the name assigned to each specimen are shown (digits underlined in a) – d)). Specimens name with an asterisk (*) denote the k value for the M2 component. Dotted blue lines indicate the curvature limit value established for the dominance of SD particles as the principal carriers of remanence ($k \leq 0.164$). Dotted red lines indicate the curvature limit value set for the dominance of PSD particles as the main carriers of remanence ($k \leq 0.270$). A, B, and C correspond to the classes described in the main text and are associated with each specimen in Table 6. (For interpretation of the references to color in this figure legend, the reader is referred to the web version of this article.)

3.6.3 Archaeomagnetic dating

The most likely age for the elaboration (or last heating) of the analyzed potsherds through the ancient intensity values obtained (archaeointensity dating) was established by the valuation of the probability density function (PDF), estimated by the use of the Matlab-tool archaeo_dating (Pavón-Carrasco *et al.,* 2014). Although the SHA.DIF.14k global model (Pavón-Carrasco *et al.,* 2014) has been widely used for dating Mexican archaeological materials (e.g., García-Pimentel *et al.* 2020; Torreblanca *et al.* 2020; Morales *et al.* 2015; Goguitchaichvili *et al.* 2017; and Olay Barrientos *et al.* 2020), overestimated intensity values have been observed for the period AD 0 – 1600 (Pérez-Rodríguez *et al.,* 2021; Alva-Valdivia *et al.,* 2021). Such temporality covers since the first human occupations registered in western Mexico and until the arrival of the Spaniards to the region. For this temporal range, the minimum intensity value projected in the SHA.DIF.14k model is ~ 40 µT. As mentioned in the previous section *3.5.2 Archaeointensities*, the intensities determined as reliable for the ceramics of "El Caracol" lava flow have intensity values between ~15 and 40 µT. This fact predicts an unreliable dating process with the global model for the potsherds shown in the present work (See Figure S2 of the supplementary material).

During the last years, four Mexican paleointensity PSVCs have been published (Goguitchaichvili *et al.,* 2018; Hervé *et al.,* 2019; Mahgoub *et al.,* 2019; García *et al.,* 2021). Their characteristics such as the temporal coverage, the quality parameters employed for data selection, modeling method, total data used for the model, temporal gaps, etc., as well as the advantages of using these regional models instead of global models to dating Mexican archaeological artifacts, were published in Pérez-Rodríguez *et al.,* 2021. Generally, the main differences in the curve behaviors are associated with the parameters, their thresholds values used for data selection, and the quantity of data available in the publication age. Following the PSVC descriptions presented in Pérez-Rodríguez 2021, it *et al.,* was decided that the use of the Mexican PSVC of 2019 (Mahgoub *et al.,* 2019) and 2021 (García *et al.,* 2021) were the most adequate for the dating exercise of "El Caracol" potsherds.

The dating results are summarized in Figure 21. Between one and four probable age intervals are presented for each potsherd.

As mentioned in section *3.4.1 Materials,* according to the visual recognition of the analyzed ceramic fragments, potsherds I and VII seem to come from the same artifact: a pipe. Both potsherds exhibit two magnetization components with a probable reheating between 350 – 400 °C. The Al results obtained for

the pM1 component of potsherd I (32.9 ± 3.42 μT, N = 2) are in good agreement with the pM1 results for potsherd VII (37.55 ± 3.90 μT, N = 5) within their error limits. However, the number of specimens used for calculating the mean intensity in potsherd I is not enough to be considered reliable. On the other hand, the M2 component of potsherd I have a lower mean intensity value than the pM1 magnetization component (31.61 ± 6.83 μT, N = 6). Archaeomagnetic age association for the M2 component of potsherd I shows two probable age ranges (AD 137 – 1193 and AD 1222 – 1495 (Figure 21a)) with the regional intensity PSVC of 2021 and three likely age ranges with the PSVC of 2019 (AD 10 – 352, AD 395 – 1016, and AD 1184 – 1600 (Figure 21b)). For the pM1 component of potsherd VII, a single age range was obtained with the PSVC of 2021 (AD 136 – 1497 (Figure 21m)) and three probable ages with the PSVC of 2019 (AD 9 – 119, AD 227 – 1053, and AD 1142 – 1600 (Figure 21n). According to archaeological evidence, it is known that pipes were widely used in western Mesoamerica during the Lupe (AD 600 – 850) and La Joya (AD 850 – 900) phases. Later they reappeared in the archaeological record in the Milpillas phase (AD 1200 – 1450) and remained until the Spaniard's arrival (Jadot and Testard, 2020). Considering this information, and whether both fragments are part of the same object or not, the earliest temporality associated with the elaboration (for pM1 of potsherd VII) or the reheating (for M2 of potsherd I) of the artifact are restricted to AD 600 and extends until AD 1495 (PSVC 2021), or AD 1600 (PSVC 2019) for potsherd I. Potsherd VII's upper limit could extend to 1497 (PSVC 2021) or AD 1600 (PSVC 2019).

For the vessel support labeled as potsherd II were obtained reliable AI data of both magnetization components, corresponding to the elaboration (pM1, AI = 29.84 ± 3.89 μT, N = 6) and to the reheating (M2, AI = 33.28 ± 5.41 μT, N = 5) of the sample. Using the PSVC of 2021, an age interval of AD 461 – 898 for the M1 component was obtained (Figure 21c), while for the M2 component, two probable age ranges were obtained: AD 143 – 1159 and AD 1258 – 1484 (Figure 21e). Since the pM1 component should have been acquired before the M2 component associated with a reheating, the lower age range obtained for pM1 can restrict the inferior temporal limit of the M2 range, and the upper age ranges obtained for M2 can restrict the superior temporal limit of pM1. So, the second temporal range for M2 could be discarded, and the age of the potsherd is restricted to AD 461 – 1159. When the PSVC of 2019 is used for dating the potsherd II, four temporal ranges for the pM1 component (AD 26 – 315, AD 437 – 924, AD 1262 – 1417, and AD 1489 – 1507; Figure 21d) and three for the M2 component were obtained (AD 12 – 346, AD 401 – 1007, and AD 1189 – 1600; Figure 21f). With all these probable intervals, it is challenging to restrict the temporality of the potsherd.

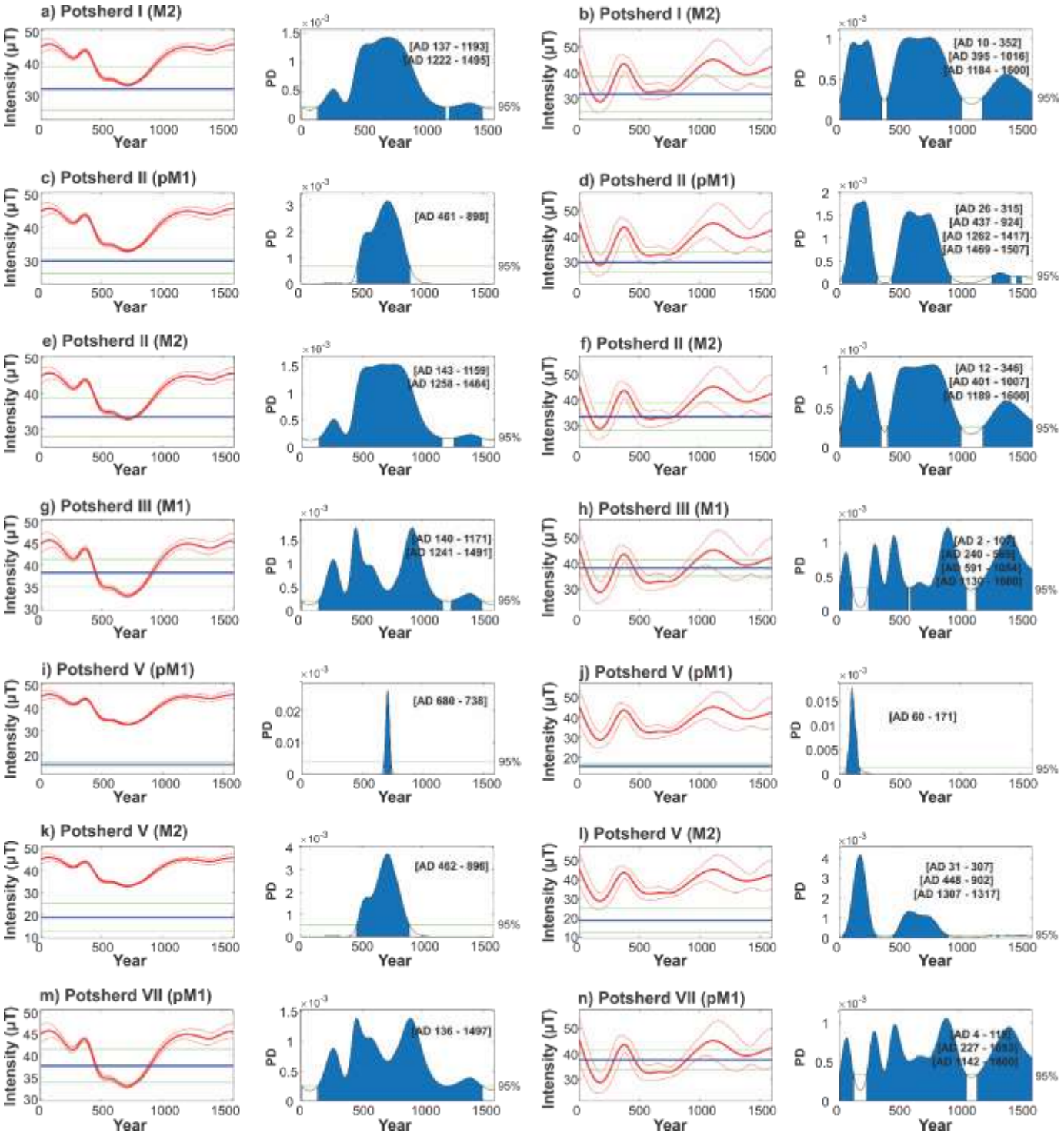

Figure 21 Archeointensity dating of "El Caracol" potsherds. Left boxes: Red wide-curves display the secular variation curve as established by the regional model of García *et al.* (2021) for a), c), e), g), i), k) and m); or Mahgoub *et al.* (2019) regional model for b), d), f), h), j), l) and n). The ancient geomagnetic field values determined for potsherds are denoted with blue horizontal lines; curves and lines are presented with their corresponding 95% confidence intervals, which are represented with thin lines above and below the corresponding broad line. Right boxes: Probability density for each intersection of the determined values of ancient geomagnetic field with secular variation curve, horizontal green lines represent the 95% confidence level, and the

probable age intervals are in the upper right corner. (For interpretation of the references to color in this figure legend, the reader is referred to the web version of this article).

Potsherd III's magnetization is characterized by a single component with an archaeointensity value of 38.14 ± 3.15 μT (N = 4). While two temporal ranges (AD 140 – 1171, and AD 1241 – 1491; Figure 21g) were obtained with the 2021's PSVC, four age ranges (AD 2 – 107, AD 240 – 569, AD 591 – 1054, and AD 1130 – 1600; Figure 21h) were obtained with the 2019's PSVC. Unfortunately, no extra information is available to confine the age of this potsherd.

Finally, both intensity values obtained for potsherd V are quite below the intensity values observed in both used regional curves (for pM1 AI = 15.76 ± 1.11 μT, N = 5; for M2 AI = 18.63 ± 6.16 μT, N = 5). An age per magnetization component is obtained with the PSVC of 2021 (AD 680 – 738 for pM1, Figure 21i, and AD 462 – 896 for M2, Figure 21k). The age interval for potsherd V with this PSVC is restricted to AD 680 – 896. As with the ceramics described above, the PSVC of 2019 presents a wide age range. For pM1 is obtained an age of AD 60 – 171 (Figure 21j), while for the M2 component, three age ranges are suggested AD 31 – 307, AD 448 – 902, and AD 1307 – 1317 (Figure 21l). For the year AD 0 to present, similar intensity values are reported for Ichkaantijo (16.1 ± 4.3, AD 750 ± 150 years) by Goguitchaishvili *et al.* (2018) and for Teotihuacan (16.40 ± 3.90, AD 750 ± 150 years) by Mahgoub *et al.* (2019). The age range obtained with the PSVC of 2021 is in good agreement with these data.

In Figure 22 are summarized the best temporal ranges elected for each potsherd.

3.7 Discussion

Based on the ability of magnetic particles found in baked (or burned) archaeological materials to acquire a magnetic remanence in the presence of the geomagnetic field at their last heating, archaeomagnetism stands as an excellent dating method in archaeology. Archaeomagnetism is a practical and economical technique for the age association to materials within archaeological contexts. However, many factors must be considered for a successful archaeomagnetic experiment.

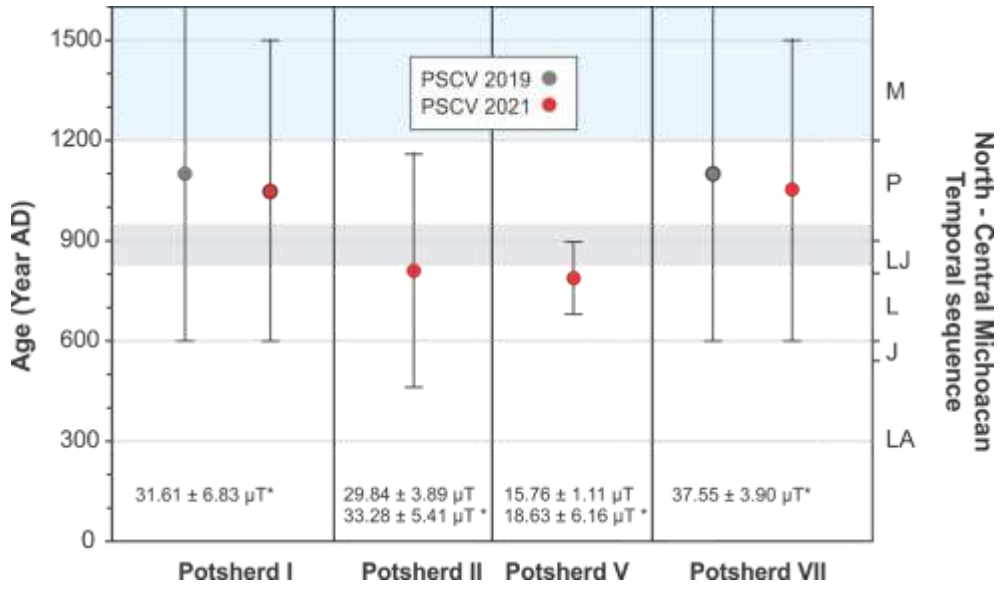

Figure 22 Age ranges obtained for potsherds within the established quality parameters. At the bottom of each box are shown the AI values of each potsherd with their error limits. The numbers with * correspond to the archaeointensity values of M2. Grey fringe represents the age eruption of Malpaís Prieto lava flow. Blue fringe represents the before human occupational age-associated to "El Caracol". In the right axis are labeled the phases and subphases of the North Central Michoacan Temporal sequence. LA: Loma Alta; J: Jarácuaro; L: Lupe; LJ: La Joya; P: Palacio; M: Milpillas.

Appropriate control of magneto-chemical alterations in the samples caused by repeated laboratory heating to high temperatures (Selkin and Tauxe, 2000) was quantified using the described parameters in Leonhardt *et al.* (2004). Additionally, a set of strict quality parameters (Table 5) was applied, ensuring that only values with no significant magneto-chemical alterations were selected for the AI calculation.

As highlighted in previous studies, determining the influence of anisotropy and changes in the cooling rate for AI determinations is essential for appropriate information processing (Aitken *et al.,* 1981; Aitken, 1983; Veitch *et al.,* 1984; Lanos, 1987; Tema, 2009; Kovacheva *et al.,* 2009; Morales *et al.,* 2011; Fox and Aitken, 1980). In the case of the ceramics analyzed during this study, it can be observed (Table 6) how archaeointensity values calculated without considering these corrections (H_{RAW}) are overestimated (H_{CORR}), generating incorrect age associations to the ceramics. Differences between $\sim$3 and 26% relative to the uncorrected intensity value are observed. The potsherd VI specimens that pass all AI criteria (99Z035A and 99Z036A) are the specimens that exhibit the strongest dependence with the effects of cooling rate and anisotropy on the intensity of TRM. Once these factors are considered, the AI results obtained can be regarded as reliable records of the Earth Magnetic Field (EMF) strength present at the time of elaboration or the last heating of the ceramics studied.

The next step to consider is choosing the best PSVC model to obtain an adequate age association. The use of global models to analyze EMF behavior through the Earth's history is a valuable tool. However, due to the inhomogeneity in paleomagnetic data distribution, regional models represent a better option than the global models to obtain a reliable dating (Pérez-Rodríguez *et al.,* 2021). Nevertheless, the construction of a PSVC for a specific area requires enough quality intensity data for such a region. Until December 2020, a total of 240 intensity data obtained of volcanic rocks (33 data) and archaeological burned material (207 data), corresponding to the last 3600 years, had been published for Mexico. Forty-four data were published between AD 1965 and 1999. Only the 4 data published in the '90s consider pTRM checks and cooling rate corrections (when is the case) as quality selection parameters. One data was obtained by the Shaw method (Shaw, 1974) and the rest by Thellier type methods. Between AD 2000 – 2010, 61 data were published; 3 data were determined by the Microwave method (Hill and Shaw, 2000). Two of them do not consider pTRM checks. Seven were obtained by the original protocol of the multispecimen method (Dekkers and Böhnel, 2006, and the other 51 were calculated with a Thellier type method. In this last case, all data consider pTRM checks, cooling rate, and anisotropy corrections when applicable. Finally, for the period 2011 – 2020, 135 data were published. Only one data was obtained by the multispecimen method; the others were determined by Thellier-type methods. For this data group, in addition to pTRM checks, cooling rate, and anisotropy corrections, the MAD parameter was reported as a quality parameter (except for 45 data).

As exposed by Béguin *et al.* (2020), the lack of a consensus in paleomagnetism that allows homogenizing the parameters used for the quality data selection makes this a semi-arbitrary process, where each author select a before published parameters set to classify their data or generate their own parameters set. Although the databases used by Mahgoub *et al.* (2019) and García *et al.* (2021) for their intensity PSVC are practically the same, the parameters set chosen by each one (see parameters set in the original publications) consider 79 and 115 data, respectively, within their quality parameters to model their regional curves.

Within the temporality chosen for dating, the results obtained for potsherds I, III, and VII present a wide age range. Additionally, because the ceramics were recollected on the lava flow's surface, no stratigraphic control allows restricting the age range mentioned before. On the other hand, age ranges obtained for potsherds II and V are better restricted: AD 461 – 1159 and AD 680 – 896, respectively. These ranges correspond to an earlier temporality than the previously associated with the "El Caracol" site. As mentioned before, the occupation of "El Caracol" Malpaís has been considered contemporary to that of

the Malpaís Prieto, within the Milpillas phase (AD 1200 – 1450). However, research within "El Caracol" is still scarce and is limited to few evidence. Two probable hypotheses arise on the ages obtained for these ceramics: 1) As mentioned In Section 3.3: Geological and archaeological background, the Malpaís Prieto erupted between AD 829 – 962 (see Figure 22). Consequently, it could be suggested a double occupation into "El Caracol" lava flow; the first one before the eruption, and corresponding to the dates reported in this work, while the last one after the eruption, when the lava flow cooled, and corresponding to dates proposed in earlier works (Migeon, 2016). 2) One must bear in mind, however, that the recovered material is surface material. Therefore, it may be decontextualized or could come from neighboring areas with early occupations. There is, in fact, occupation evidence at Las Florecitas lava flow –northwestern sector of the Zacapu Malpaís (see Figure 13)– at the Epiclassic period (AD 650 – 1000) (Pereira *et al.,* 2019).

In any case, this likely early occupation here suggested should promote further investigations at "El Caracol" and neighboring flows at the Zacapu Malpais for a better knowledge of the Tarascan empire's population dynamic.

3.8 Conclusions

This paper highlights the importance of considering the effects of magnetic anisotropy and the cooling rate factors within an archaeomagnetic study for a correct determination of archaeointensities and the corresponding dating derived from them.

AI dates were obtained for five out of the seven ceramic fragments studied. Although few results, they are high-quality absolute archaeointensity results and deserve some credit. The age intervals for potsherds II and V, obtained with Mexican regional intensity PSVC, show earlier temporalities for the "El Caracol" occupation. Although this result does not change the Tarascan empire's history, it does provide essential data for a better knowledge of its population dynamics.

Conditioned to the findings obtained in future investigations within the study area, ages obtained in this work allows proposing the presence of early material at the "El Caracol" site, which could be either of local or foreign origin.

3.9 Supplementary material.

Figure S1 shows a comparison between MRS/MS vs. HCR/HC data before and after applying the TC protocol. Except for potsherd III (III and III* in Figure A.1), the rest of the ceramics maintain a behavior within the SD - MD field. So, it is considered that the magnetic mineralogy of potsherd VII (VII* in Figure A.1), which could not be evaluated before starting the TC protocol (see main text), maintains a consistency with the rest of the analyzed potsherds.

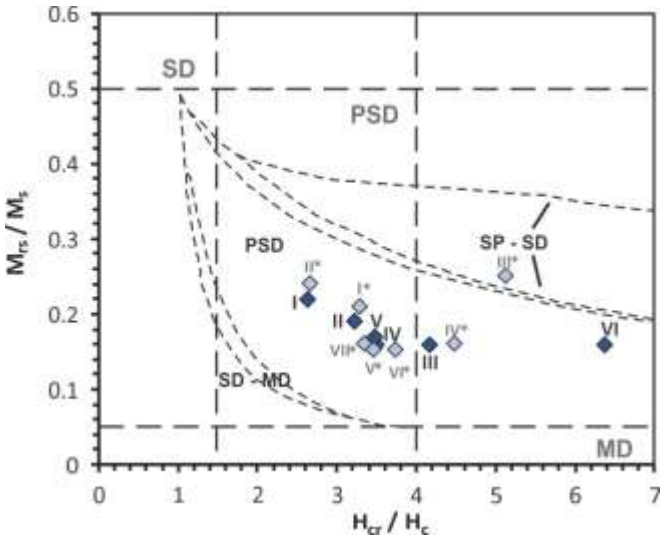

Figure S 1 Day plot with theoretical curves of Dunlop [31] for comparison between data before (dark blue diamonds) and after (light blue diamonds) carrying out the TC protocol for archaeointensity determinations.

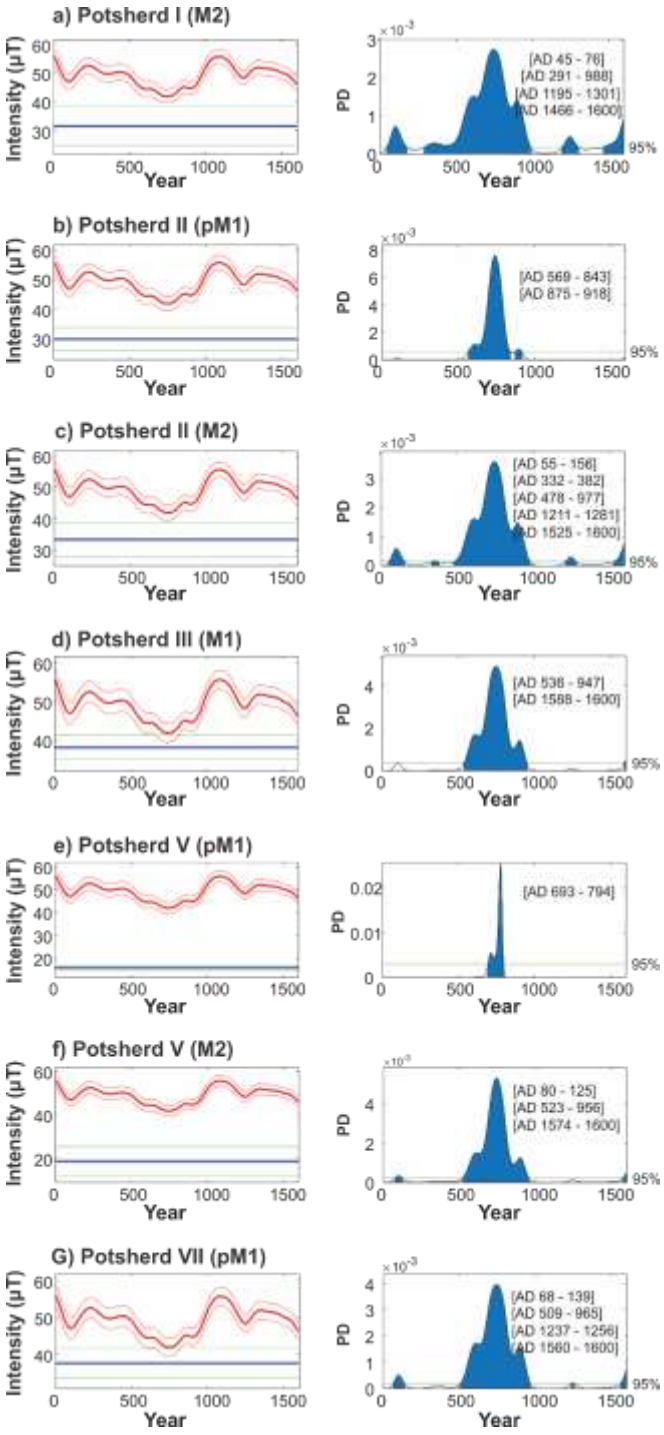

Figure S 2 Archeointensity dating of potsherds of "El Caracol" Malpaís. Left boxes: Red wide curves display the secular variation curve as established by the SHA.DIF.14k model [43]. The ancient geomagnetic field values determined for potsherds are denoted with blue horizontal lines; curves and lines are presented with their corresponding 95% confidence intervals, which are represented with thin lines above and below the corresponding wide line. Right boxes: Probability density functions for each intersection of determined values of ancient geomagnetic field with secular variation curve, horizontal green lines represent the 95% confidence level, and the probable age intervals are in the upper left corner. The intensity values of potsherds I, II, III, and V do not intersect the SHA.DIF.14k model.

4. A multimethod paleointensity approach applied to the historical Xitle lava flows (Central Mexico): towards the accurate paleointensity determination https://doi.org/10.1186/s40623-020-01232-z

Juan Morales, **Nayeli Pérez-Rodríguez**, Avto Goguitchaichvili and Miguel Cervantes-Solano

Earth, Planets and Space

4.1 Resumen

Con la finalidad de evaluar la fidelidad de los registros paleomagnéticos grabados en flujos de lava frescos, ampliamente expuestos y bien conservados, se llevó a cabo un estudio de paleointensidades absolutas y magnetismo de rocas en una secuencia de lavas del volcán Xitle, localizado en la cuenca sur de la ciudad de México, y cuya erupción se estima que ocurrió hace aproximadamente 2 ka.

Las muestras paleomagnéticas estudiadas, obtenidas de seis flujos de lava distintos, se sometieron al análisis de paleointensidades a través de un enfoque multimetodológico, para el cual se emplearon los métodos de Thellier-Coe, IZZI y múltiples especímenes. Los valores medios de PI de los flujos 4 a 6 arrojaron valores de 68,4 μT (σ = ± 5,6 μT), 63,9 μT (σ = ± 5,8 μT) y 61,5 μT (σ = ± 4,3 μT) para los métodos Thellier-Coe, IZZI e IZZI con corrección por ritmo de enfriamiento, respectivamente. Aunque de manera general los resultados de paleointensidades obtenidos por el método de múltiples especímenes fueron inferiores a los valores de intensidad obtenidos con los otros métodos para los mismos flujos, los resultados para el Flujo 5 (61,8 μT) fueron muy similares a los determinados con los métodos tipo Thellier, por lo que se considera que dichos valores son los más confiables de toda la secuencia analizada.

Con base en los resultados obtenidos, la secuencia de flujos de lava analizada podría corresponder a dos períodos eruptivos: uno relacionado con el volcán Xitle (flujos 3-6), y otro con una erupción más antigua (flujos 1 y 2). La datación arqueomagnética combinada de los diferentes flujos refuerza esta hipótesis, así como la distribución multimodal reportada en la literatura desde hace dos décadas para la edad del volcán Xitle. La aplicación de criterios de aceptación más estrictos y la consideración de la corrección por ritmo de enfriamiento reducen ligeramente la dispersión de los valores de intensidad determinados.

Finalmente, el enfoque multimetodológico empleado en este estudio, combinado con los experimentos detallados de magnetismo de rocas, definitivamente incrementan la precisión de las determinaciones de paleointensidad.

4.2 Abstract

An inclusive rock-magnetic and absolute paleointensity survey of the ~2-ka-old Xitle volcano (southerly Basin of Mexico) was undertaken to assess the faithfulness of the paleomagnetic log carried by fresh, widely exposed and well-preserved lava flows. Paleomagnetic samples from six lava flows were subjected to paleointensity analysis with a multi-method approach: the Thellier–Coe, IZZI, and multi-specimen methods. Overall mean flow PI values from flows 4–6 obtained by the Thellier-type methods used yielded 68.4 μT (σ = ± 5.6 μT), 63.9 μT (σ = ± 5.8 μT) and 61.5 μT (σ = ± 4.3 μT) for the TC, IZZI, and IZZI with CR correction methods, respectively. Although multi-specimen paleointensity results were, in general, lower than that obtained with the other methods for the same flows, that for Flow 5 (61.8 μT) was very similar to those obtained with the Thellier-type methods. Based on the results obtained, this lava flows sequence could correspond to two eruptive periods: one related with the Xitle volcano (flows 3–6), and another older (flows 1 and 2). The combined archeomagnetic dating of the different flows reinforces this hypothesis, as well as the multi-modal distribution for the age of the Xitle, proposed two decades ago. The application of stricter acceptance criteria and consideration of cooling-rate correction could slightly reduce the scattered observations. The multimethod approach employed under this study, combined with detailed rock-magnetic experiments, may definitively increase the accuracy of paleointensity determinations.

4.3 Introduction

The Xitle volcano belongs to the Chichinautzin Quaternary volcanic field. It is located south of the Valley of Mexico (Herrero-Bervera *et al.,* 1986; Urrutia-Fucugauchi and Martin-del Pozzo 1993). It is a monogenetic cone whose lavas overlay an area of approximately 80 km^2 in which seven flow-units are identified (Figure 23; Delgado- Granados *et al.,* 1998). The largest flow to the north is more than 13 km

long, encompassing an area of 70 km^2 (Martin-del Pozzo *et al.,* 1997; Delgado-Granados *et al.,* 1998) and covering the first urban settlements of the Valley of Mexico (Heizer and Bennyhoff 1958)—the archeological center of Cuicuilco.

Being one of the youngest volcanoes, charred material (charcoal from pottery level below lava) by its eruption was used during the development of the innovative radiocarbon method for dating organic materials (Arnold and Libby 1951; Libby 1955), obtaining a date of 2422 ± 250 years BP. After this, more than 30 further studies have been reported, yielding a breadth age interval for the Xitle's eruption. Through a comprehensive review of the available radiometric dates, Urrutia-Fucugauchi (1996) identified three apparent clusters roughly around 4000, 2375, and 2000 years BP. The older cluster is mainly associated with the early archeological occupation Tlalpan stages (Fergusson and Libby 1963), while the other two to the age for the Xitle eruption, respectively. Moreover, an age of 1670 years BP was proposed (Siebe 2000).

Likewise, its different lavas have aided to appraise the reliableness of the paleomagnetic log carried by fresh, widely exposed, and well-preserved lava flows (Urrutia- Fucugauchi 1996). In the case of paleointensity (PI) determinations, it seems to be also a matter of controversy. Pioneer estimations of Nagata et al. (1965a) yielded a mean PI value of 56.11 ± 5.89 μT (*n* = 8), while those of González-Huesca (1992), Morales-Contreras (1995) and Urrutia-Fucugauchi (1996) yielded mean PI values of 66.83 ± 10.09 μT (*n* = 6), 59.2 ± 11.0 (*n* = 9) and 60.04 ± 9.62 μT (*n* = 6), respectively. It is worth mentioning that all these studies were carried out on sites from different flows of the Xitle volcano.

Moreover, variations in the PI values are observed across vertical sections within a single flow (e.g., Urrutia- Fucugauchi 1996; Böhnel *et al.,* 1997; Alva-Valdivia 2005; Morales *et al.,* 2006). Given its monogenetic nature and considering that recent historical eruptions of similar volcanoes in the Mexican volcanic belt point to brief activity periods, around a decade or so (e.g., Paricutin 1943–1953 or the 1759–1774 Jorullo eruptions; Bullard 1976) no such PI differences should be obtained. Attempts to correlate the observed PI variation to rock-magnetic properties, different oxidation states, etc., have not been able to account for these inter-flow variations.

The refinement of PI methods and the proposal of stricter acceptance criteria have arisen with time, as well as new PI methods, which could contribute to a better understanding of the causes for such variations. Even more, multi-method approaches have been recently applied to the study of volcanic rock (e.g., Calvo-Rathert *et al.*, 2016 and Calvo-Rathert *et al.,* 2019) as an alternative criterion of reliability.

In the present study, we report the paleointensity results from six different lava effusion episodes from unit V of the Xitle volcano obtained with the multi-specimens and IZZI methods, considering also cooling rate correction. Likewise, we carried out a reassessment of the Thellier–Coe paleointensity results previously reported on sister samples using stricter acceptance criteria.

4.4 Material and rock-magnetic results from the previous study

The paleomagnetic sampling of lava flows was done previously and results were reported by Cervantes-Solano *et al.* (2019). Sampling was completed at the *Ciudad Universitaria Basaltic Lava member (BCU)*, at the site known as La Cantera (19° 18′ 47.10″ N, 99° 10′ 19.01″ W)—a quarry at the neighborhood of the UNAM facilities (Figure 23). At this site is the most complete exposure of lava flows with a thickness of 40 m, which corresponds to the unit V described by Delgado-Granados *et al.* (1998), in which seven individual lava units with thicknesses of 2 to 8 m each are distinguished (Figure 24). Lava-flow sampling was realized using a hand-held water-cooled gasoline powered drilling device with a diamond bit; all samples were oriented using a precision core orienting accessory with a magnetic compass mounted on it. Fifty-four standard paleomagnetic cores (8 to 10 samples per flow) were obtained from the exposed-interiors of six flows, which were consecutively numbered according to their stratigraphic position (i.e., 95X001AL–95X054L; L: A, B or C, the outermost specimen, the one at the middle, or the innermost specimen), with Flow 1 the one at the bottom and Flow 6 the one at the top of the exposure. Because of its inaccessibility, Flow 7 was unable to be sampled.

Thermomagnetic curves indicate the existence of a magnetic phase during heating with Curie temperature between 520 °C and 560 °C, suggesting magnetite or titanomagnetite with low titanium content as responsible for the magnetization. Cooling curves are similar to heating ones, showing a decrease in initial susceptibility less than 15%, which is likely due to oxidation produced during heating (Figure 25). For details of the opaque mineralogy, the reader is referred to the paper by Alva-Valdivia (2005).

In most samples studied (60%), two magnetization components are observed, the first of which is removed during the first steps of demagnetization (fields from 5 mT to 10 mT) and represents less than 10% of the value of the total magnetization of the samples and is likely to be of viscous origin. Once this component was removed, the behavior was linear towards the origin in the orthogonal Zijderveld (1967) diagrams. Another group of samples (31%), corresponding to flows 2 and 5, retain about 40 to 50% of the initial magnetization after having applied magnetic fields of 90 mT, however, a linear behavior towards

the origin of coordinates is also observed. In the remaining 9% of samples, a single stable component was identified with a single behavior towards the origin.

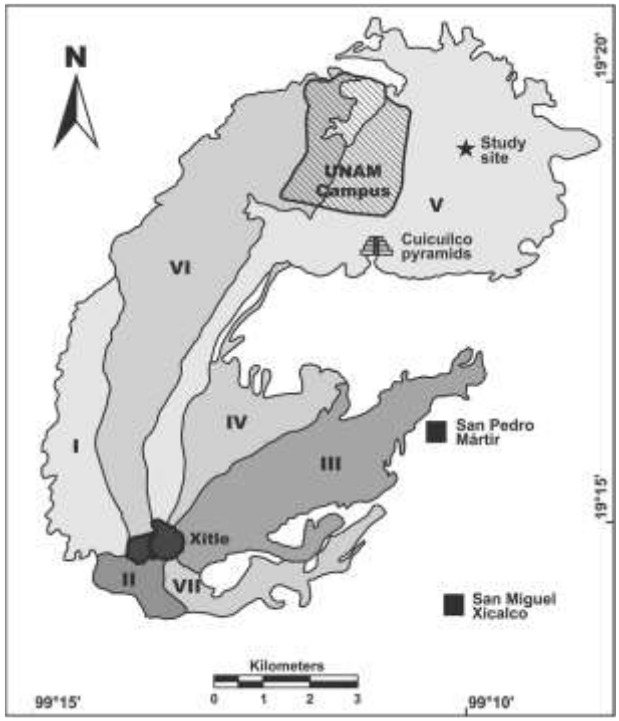

Figure 23 Location map of Xitle volcano and the spatial distribution of its different lava flows (modified from Delgado-Granados *et al.,* 1998)

Paleointensity experiments were carried out on six to seven specimens per flow (40 in total) using the Thellier double-heating method (Thellier and Thellier 1959) as modified by Coe (Coe 1967), here thereafter called Thellier–Coe (TC). Heating and cooling were done in a TD48 thermal demagnetizer from ASC Scientific. Once the specimens reached the desired temperature at each heating step, they were left for an idle of 20 min at that temperature so that all specimens got thermal equilibrium. Afterward, the fan was turned on emitting the samples to cool down. The laboratory field (45.0 ± 0.5 μT) remained on for infield steps during the whole heating– cooling cycle. Thirteen temperature steps were distributed between room temperature and 580 °C, and pTRM checks were carried out at every third heating step, except at the last one. Natural and laboratory-induced remanent magnetizations were both measured through a JR6 dual-speed spinner magnetometer from AGICO.

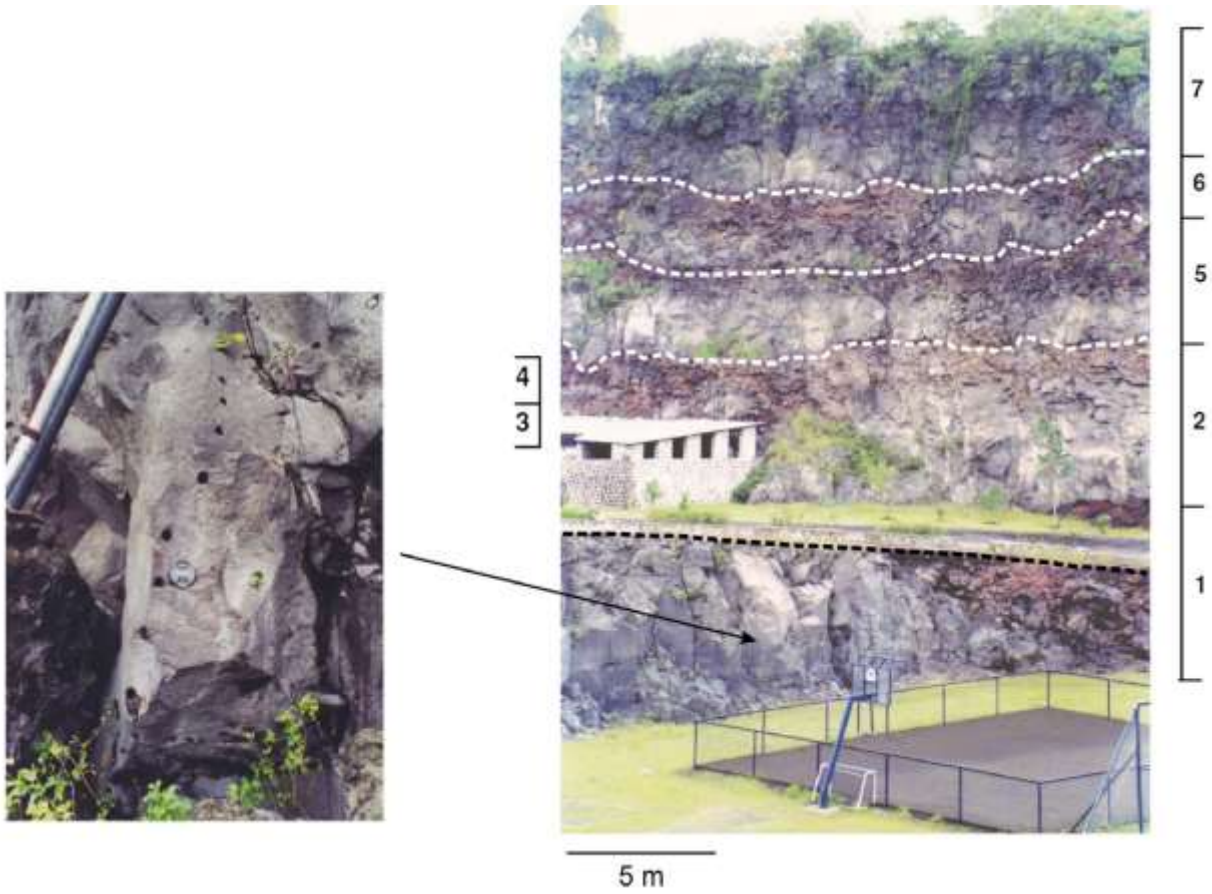

Figure 24 Right: view of the 7 flows exposed at BCU quarry (adopted from Alva-Valdivia 2005). Left: a closer view of the paleomagnetic sampling

4.5 Experimental procedure

The experiments were performed with material left from the former study (Cervantes-Solano *et al.,* 2019), and the original numbers of the specimens were preserved, but for the sake of simplicity, the initial number (95) in the specimen's ID was eliminated. This enabled us to analyze sister samples, minimizing the possibility of within-flow heterogeneities, as well as the application of a multimethodological exercise on almost the same material.

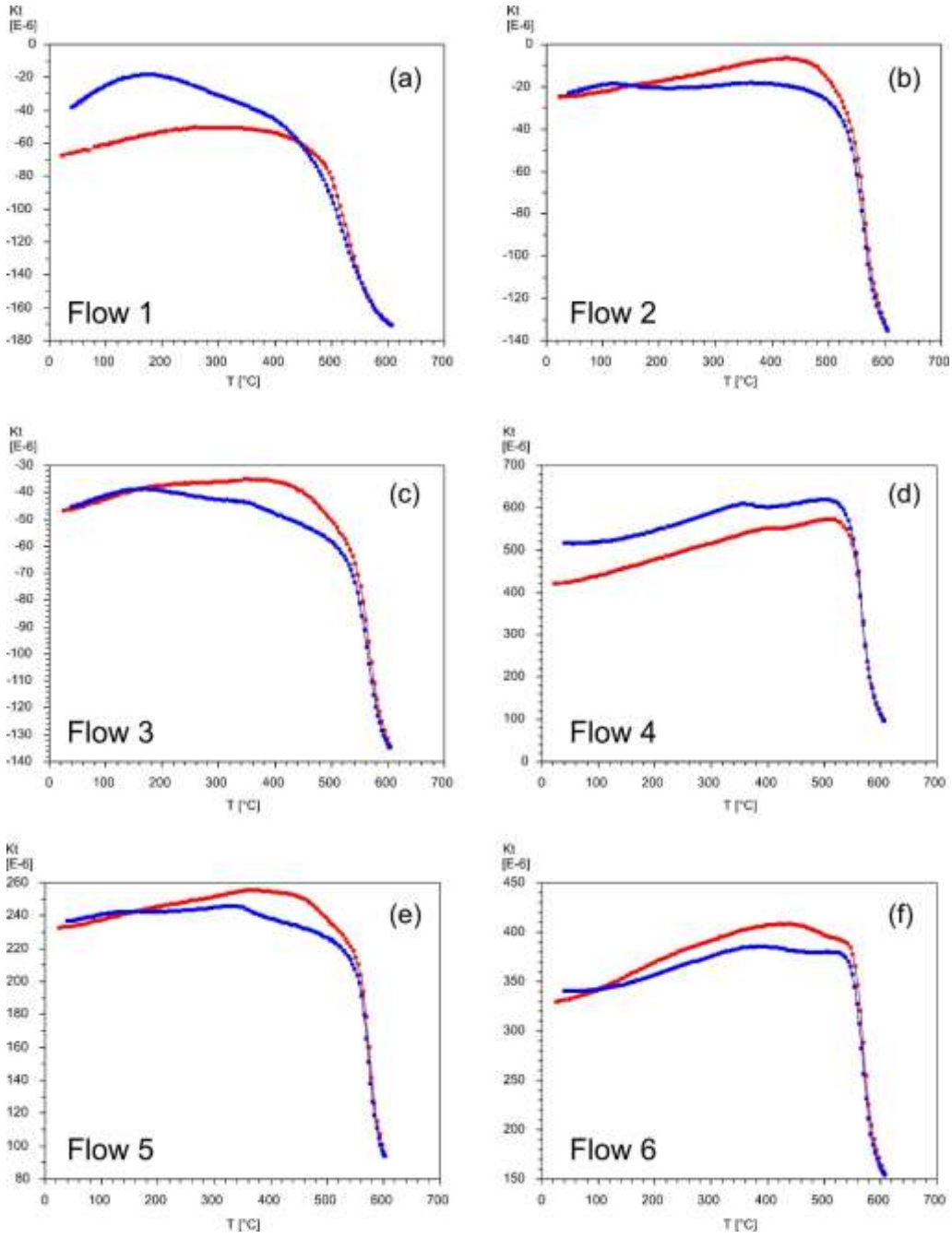

Figure 25 Representative thermomagnetic (κ-T) curves for the different flows analyzed, obtained in the previous study (Cervantes-Solano *et al.* 2019). Curves in red correspond to the heating, while those in blue to the cooling

4.5.1 Rock-magnetic experiments

Stepwise low-field susceptibility (κ-T) curves were obtained for precise monitoring of the onset of the magneto-chemical alteration of the magnetic mineralogy. This monitoring was done using an MFK1B

Kappabridge from AGICO in an argon atmosphere. A four-step procedure, initiating at 100 °C and with an opening return temperature of 350 °C, was followed up to a maximum final temperature of 500 °C. Temperature increments of 50 °C were set for the following return-temperatures (i.e., 350, 400, 450, and 500 °C).

4.5.2 Paleointensity determinations

Absolute paleointensity determinations were accomplished employing two different methodologies. The first set of paleointensity experiments was performed with the multi-specimen (MS) technique proposed by Hoffman *et al.* (1989) as modified by Dekkers and Böhnel (2006). Protocols for fraction correction (FC) and domain-state correction (DSC)—proposed by Fabian and Leonhardt (2010)—were also included. Three different standard paleomagnetic cores per flow were used for these experiments. Each standard paleomagnetic core was cut into eight specimens, which were pressed into standard dimension cylindrical salt pellets and labeled from 1 to 8 (e.g., X001-C-1–X001-C-8), obtaining 144 specimens. The multi-specimen method was carried out at a temperature of 450 °C—a temperature below the lowermost Curie temperature observed from κ-T curves but enough to create a pTRM. Experiments were performed sing a TD48-SC furnace (ASC Scientific) with laboratory fields varying from 10 to 70 μT, and increments of 10 μT. The following measurement sequence was applied to the specimens subjected this methodology: (i) the natural remanent magnetization (NRM) of the different specimens were measured; (ii) six specimens were oriented so that their corresponding NRM directions lay parallel to the axis of the heating compartment and heated at 450 °C using the first laboratory field selected (10 μT). After cooled down, their remanences were measured; (iii) specimens were set and heated as in the previous step but inverting the laboratory field direction. Then, their remanences were measured; (iv) specimens were reheated in zero field and cooled infield, and their remanences measured; (v) Step (ii) was repeated. Once finished this five-step procedure, another set of six specimens was worked, musing the next laboratory field (20 μT) up to 70 μT.

All calculations (relative differences between pTRMs and NRMs) and corresponding correction factors were accomplished following Fabian and Leonhardt (2010).

The so-called 'IZZI' method (Tauxe and Staudigel 2004; Yu *et al.,* 2004) was employed for the second set of paleointensity experiments, using one or two standard paleomagnetic cores per flow, which were previously cut, pressed into salt pellets and numbered consecutively (e.g., X014C-1–X014C-4). 32

specimens were treated using the following measurement sequence: (i) The NRM of the specimens was measured. (ii) The specimens were heated to temperature *T*1 in a close to zero (~ 50 nT) magnetic field strength and then their remanences were measured. (iii) The specimens were heated again to temperature *T*1, but this time in the presence of a magnetic field (50.0 ± 0.5 μT), and then their remanences were measured. (iv) The next heating step is performed at a temperature T2 (with *T*1 < *T*2) in the presence of a magnetic field. (v) The *T*2 temperature step is repeated in the absence of a magnetic field. (vi) The temperature is increased further to a *T*3 value, the samples were heated in the absence of a magnetic field. (vii) A pTRM check is performed from *T*3 to *T*1. (viii) The specimens are then reheated to *T*3 in the presence of a magnetic field. (ix) A pTRM tail check is performed. (x) Steps (iv) to (ix) were repeated as often as necessary to cover the entire Curie temperature range of the ferromagnetic minerals present in specimens under analysis.

Although cooling rate (CR) effects on volcanic rocks are not normally considered in most paleointensity experiments (Morales *et al.,* 2006), we have decided to consider it at the end of this experiment. Cooling rate dependence on TRMs was studied using a modified procedure to the one outlined by Chauvin *et al*., (2000) (e.g., Morales *et al.,* 2006). Finally, to account for non-ideal multidomain (MD) behavior, the curvature k of the individual Arai plots was estimated.

4.6 Results

4.6.1 k-T curves

Stepwise low-field susceptibility vs temperature (κ-T) curves helped to evidence the temperature range at which mineral alteration took place. In the cases of Flow 1 and Flow 3, evident magneto-chemical alteration seems to start at moderate temperatures, between 350 and 400 °C (Figure 26). On the contrary, alteration appears to start at higher temperatures (400 °C and 450 °C) in the case of Flow 6. The analysis of the susceptibility curves was accomplished using the Cureval 8.0.2 software (Chadima and Hrouda 2012).

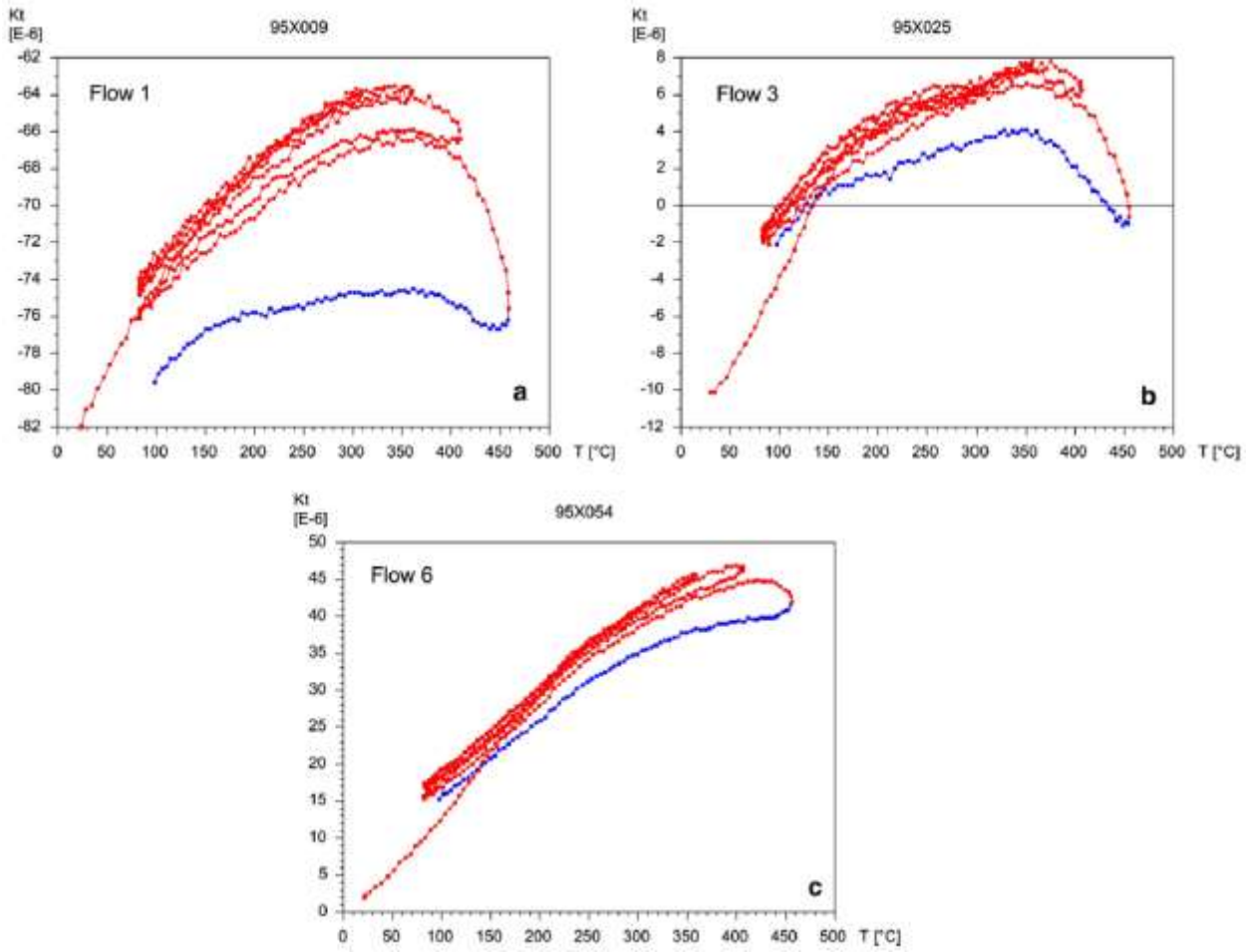

Figure 26 Representative stepwise thermomagnetic (κ-T) curves for the different flows analyzed, obtained in this study. Peak heating steps used: 350, 400, 450, and 500 °C. Curves in red correspond to the heating, while those in blue to the cooling.

4.6.2 Paleointensity determinations

4.6.2.1 Reassessment of the Thellier–Coe results from the previous study

Different factors play significant roles in the reliability of a paleointensity determination—quality of the experimental conditions, the occurrence of alteration, and the presence of remanent magnetization carried by MD grains (Calvo-Rathert *et al.,* 2016). On the other hand, several statistical parameters and different reliability criteria for paleointensity determinations have been proposed to take into account for

these experimental situations (e.g., Selkin and Tauxe 2000; Kissel and Laj 2004), however, no specific criteria and parameter set is normally applied (Calvo-Rathert *et al.,* 2016).

Accordingly, we carried out a reassessment of the Thellier–Coe paleointensity results previously reported by Cervantes-Solano *et al.,* (2019) on sister samples using the same stricter acceptance criteria used for the results obtained in this multi-methodological exercise.

Acceptance criteria of different strictness (A, B, or C, as proposed by Leonhardt *et al.,* 2004) were employed to label successful paleointensity determinations according to specific quality levels, which are summarized in Table 7.

Table 7 Selection criteria and threshold values for the three determination classes (A, B, and C) for Thellier–Coe experiments. N, number of points in the Arai plot used for the linear best-fit; σ/slope, the ratio of the standard error of the slope of the selected segment in the Arai plot to the absolute value of the slope; f, NRM fraction used for the best-fit calculation; q, quality factor (Coe *et al.,* 1978); MAD-anc, anchored maximum angular deviation; α, the angular difference between the anchored and non-anchored best-fit; δ(CK), relative check error; δ(pal), cumulative check error (Leonhardt *et al.,* 2004); δ(TR), relative intensity difference in pTRM tail check; δ(t*): the normalized tail of pTRM (Leonhardt *et al.,* 2004)

Class	**A**	**B**	**C**
N	≥ 5	≥ 5	≥ 5
***σ*/slope**	≤ 0.10	≤ 0.15	≤ 0.15
f	≥ 0.5	≥ 0.3	≥ 0.3
q	≥ 3	≥ 2	≥ 2
MAD-anc	≤ 5	≤ 10	≤ 10
α	≤ 15	≤ 15	≤ 15
***δ*(CK)**	≤ 5	≤ 9	≤ 15
***δ*(pal)**	≤ 5	≤ 10	≤ 15
***δ*(*t**)**	≤ 3	≤ 30	≤ 30

Additionally, concave-up shape Arai plots are rejected for the PI calculations because, in such cases, the remanence is very likely carried by MD grains (Levi 1977). Its contribution was assessed estimating the curvature k of the selected data points of the Arai plot (Paterson 2011). Following Paterson (2011), threshold values for $k = 0.164$ and $k \leq 0.270$, defined using samples with known grain sizes, were used. The curvature k was determined in MATLAB using the function CircleFit-ByPratt (XY) (Chernov 2019) which

uses the method proposed by Pratt (1987) for fitting a circle to a set of data points on a plane. Estimation of paleointensity values was performed using the ThellierTool4.0 software (Leonhardt *et al.,* 2004).

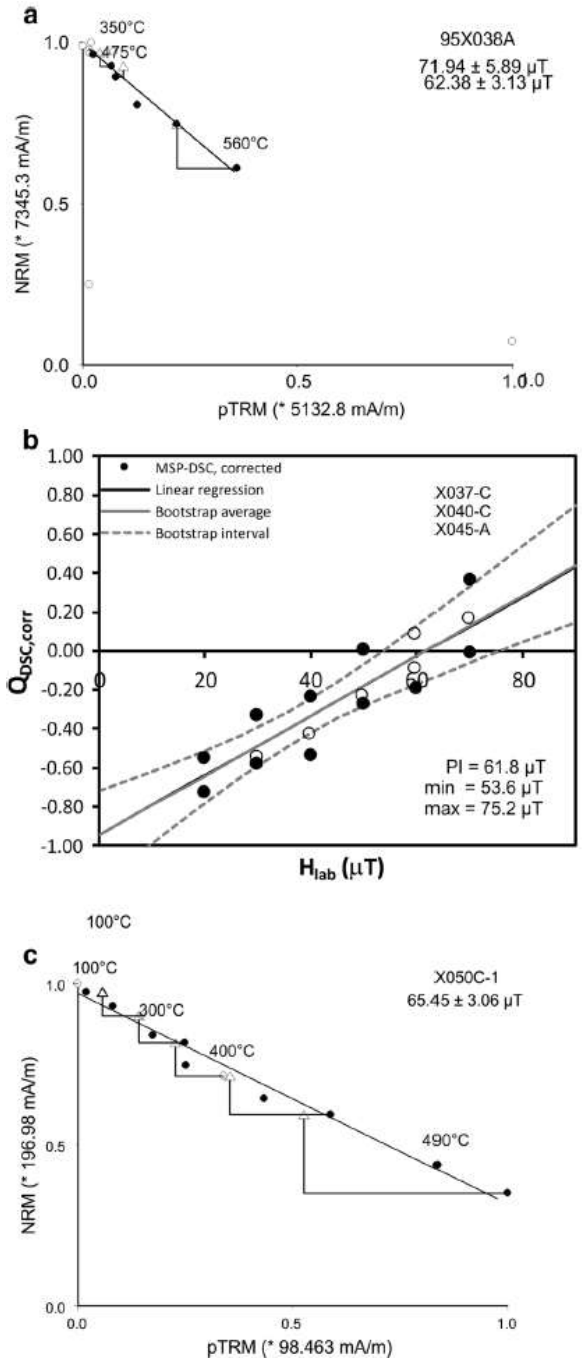

Figure 27 a Representative Arai plot (Nagata *et al.,* 1965b) obtained from the TC experiments. **b** Representative plot obtained from the MS experiments. **c** Representative Arai plot (Nagata *et al.,* 1965b) obtained from the IZZI CRcorr experiments

Based on the above-mentioned criteria, no reliable paleointensity determinations could be gathered from flows 1 and 2, except for one specimen from Flow 1 (X004A).

Most specimens showed very scattered Arai plots and negative pTRM checks even at low temperatures. Given the negative pTRM checks and the irreversible κ-T behavior of the curves obtained on sister samples, this misbehavior could be attributed to significant thermochemical alteration during the paleointensity experiments. On the contrary, although with a very low success-rate, reliable PI determinations were obtained from flows 3 to 6. A representative Arai plot (Nagata *et al.,* 1965b) is shown in Figure 27a.

Table 8 Thellier–Coe paleointensity results for all six studied flows. T_{min}/T_{max}: lower/upper temperature step used to determine the archeointensity. Terms from column 4 ("N") to column 16 ("δ(TR)") as defined in Table 7. k: curvature. k = R−1, where R is the radius of the fitted circle to the data set (pTRM vs NRM); PI: paleointensity; σ: standard deviation of paleointensity. Specimen names in italic face correspond to specimens rejected for the average intensity calculation because of exceeding of at least one of the threshold values (underlined) set for the corresponding assigned Class

Name	T_{min} [°C]	T_{max} [°C]	N	slope	β	f	g	q	MAD-anc	α	Class	CK-error	CK-diff	Drat [deg]	d(t*)	d(TR)	k	PI	σ
Flow 1																			
X004A	20	540	10	-1.4	0.1	0.8	0.8	10.1	1.1	1.0	C	4.5	10.6	3.2	11.1	6.6		62.4	4.1
Flow 3																			
95X017A	350	540	6	-1.9	0.05	0.7	0.8	11.1	3.3	3.3	C	1.5	10.5	1.1	2.3	2.8	0.112	86.20	4.02
95X018A	350	540	6	-1.8	0.07	0.4	0.7	4.2	2.3	4.2	C	32.8	1.7	37.8	1.9	2.0	0.470	80.00	5.77
95X019A	350	540	6	-1.7	0.05	0.6	0.7	8.2	3.2	4.8	C	44.2	20.0	38.7	1.6	0.5	0.299	76.02	3.70
																	Mean =	**N/A**	
																	σ=	**N/A**	
Flow 4																			
95X022A	300	560	8	-1.3	0.03	0.9	0.8	20.7	1.8	1.1	B	7.0	3.9	4.6	5.5	4.9	0.078	59.68	2.05
95X023A	20	450	7	-1.5	0.06	0.5	0.6	5.2	1.8	2.5	B	1.7	5.8	1.8	0.6	0.0	0.190	69.49	4.06
95X024A	20	475	8	-1.4	0.14	0.5	0.7	2.5	1.2	0.7	B	6.7	4.2	7.8	1.0	4.6	0.308	64.28	8.84
95X027A	300	560	8	-1.5	0.05	0.5	0.8	8.7	1.7	2.2	C	10.3	3.8	10.7	2.9	2.1	0.008	68.74	3.25
95X028A	300	540	7	-1.4	0.04	0.5	0.8	8.5	1.3	1.8	C	17.4	43.3	20.5	5.3	2.1	0.012	61.08	2.73
																	Mean =	**66.0**	
																	σ =	5.5	
Flow 5																			
95X030A	300	560	8	-1.4	0.05	0.5	0.8	7.7	1.1	1.3	B	1.9	8.9	2.4	1.9	2.7	0.108	62.38	3.13
95X033A	20	450	7	-1.9	0.13	0.3	0.7	1.8	0.9	0.8	B	2.2	8.0	3.4	7.6	2.4	0.178	86.91	10.88
																	Mean =	**N/A**	
																	σ =	**N/A**	
Flow 6																			
95X036A	300	560	8	-1.6	0.05	0.4	0.8	6.5	2.4	2.5	C	12.6	12.4	17.3	1.5	1.9	0.186	70.25	3.33
95X037A	300	560	8	-1.2	0.06	0.6	0.8	7.6	2.7	4.9	C	14.9	7.9	16.1	0.9	2.3	0.282	54.11	3.38
95X038A	200	560	9	-1.6	0.08	0.4	0.7	3.4	1.0	0.6	B	3.8	3.8	5.3	0.0	1.8	0.167	71.94	5.89
95X039A	350	560	7	-1.2	0.09	0.7	0.8	6.1	2.8	3.5	C	25.9	36.8	24.5	3.9	3.5	0.540	55.16	4.85
95X040A	100	450	6	-1.7	0.11	0.3	0.7	2.1	0.7	1.0	B	0.6	0.3	1.0	3.3	1.8	0.037	76.15	8.00

Mean =	72.8
σ =	3.0

It is observed that flows 4 and 6 yielded slightly similar PI of 66.0 ± 5.5 μT (*n* = 3) and 72.8 ± 3 μT (*n* = 3), respectively. For flows 3 and 5, however, only one specimen per flow yielded an acceptable result, 86.2 ± 4.0 μT, and 62.4 ± 3.1 μT, respectively. Results are summarized in Table 8 and are graphically presented in Figure 28. This means that only 8 out of the 40 previously reported results (20%) can be considered as reliable. If the curvature parameter is also considered, only five results survive (12.5%).

Representative Arai (Nagata *et al.,* 1965b) and associated vectorial (Zijderveld, 1967) plots for the six flows analyzed are shown as Additional file 1: Figure S3.

4.6.2.2 Multi-specimen method

As above-mentioned, two magnetization components were observed in almost 60% of the samples studied. These soft overprints were also observed at the vectorial plots obtained from the Thellier-type double-heating method, which were eliminated at temperatures between 200 and 350 °C. Thus, the chosen heating temperature of 450 °C seems to be suitable to remove these overprints on the one hand and locates somewhat below the Curie temperature observed from M-T curves on the other hand, so that thermochemical alteration on the specimens due to heating should be less likely. Calculations were performed through the VBA software of Monster *et al.* (2015a).

Reliability criteria applied for this methodology was based on: (i) a maximum acceptable angular deviation (AAD) of 10°; (ii) the "overprint?" check and (*Δ*dec and *Δ*inc) < 10°; (iii) the amount of progressive alteration (*ε*alt) ≤ 10%; (iv) the intersection with the y-axis (*Δ*b = −1 at Hlab = 0), and (*v*) the linear least-squares fit (R^2).

All PI determinations fulfill with the criterion of *δ*b between (0, 1) and show *r*2 values ≥ 0.9, except one case (Flow 5). However, despite the low enough chosen heating temperature of 450 °C, Avg *ε*alt range between 6 and 12%. In general, the original DBc, fraction, and domainstate- corrected determinations with alignment correction (FCc and DSCc, respectively) yield higher R^2 values than the corresponding uncorrected values.

Flow 1 yielded a significantly lower mean PI value (21.6 μT; min = 17.9 μT, max = 23.8 μT), compared with those obtained from the other flows, and no significant differences between the results of the original DBc and the extended protocols FCc and DSCc are observed. Flow 2 and Flow 4 yielded undistinguishable PI values of 52.9 μT and 49.5 μT, while Flow 3 and Flow 5 PI values of 58.2 μT and 61.8 μT, respectively. In the case of Flow 6, a PI value of 51.9 μT was obtained, although with a higher Avg. *ε*alt of − 17.6%. A summary of the results is provided in Table 9, and a representative plot is shown in Figure 27b. Plots for the six flows analyzed are shown as Additional file 1: Figure S4.

Table 9 Multi-specimen (Q_{DSC}) paleointensity results for the different flows studied. Min and Max: estimated minimum and maximum paleointensity values. Reliability criteria: (i) the amount of progressive alteration ε_{alt}—a systematic (alteration-induced) error; (ii) the intersection with the y-axis ($-1 < \delta b < 1$) and (iii) r2: correlation coefficient of the linear regression. Data in italic represent the mean PI value calculated from the three specimens used in MS experiments.

Specimens **Flow**	PI [μT]	Min [μT]	Max [μT]	Avg ε_{alt} [%]	Δb	r^2
X001-C	25.0	22.5	26.2	11.8	-0.08	0.985
X005-C	21.1	18.2	23.1	8.9	0.03	0.994
X009-C	20.6	13.4	26.3	20.0	-0.04	0.941
Flow 1	**21.6**	**17.9**	**23.8**	**10.7**	**0.06**	**0.952**
X0015-B	73.4	71.3	78.0	-3.2	-0.02	0.983
X0017-B	48.7	44.7	51.9	-20.0	-0.17	0.948
X0019-B	52.9	51.5	54.2	-12.4	-0.03	0.995
Flow 2	**52.9**	**51.4**	**54.3**	**-12.4**	**-0.03**	**0.995**
X0020-B	31.1	35.1	37.2	-9.2	0.11	0.993
X0022-C	58.2	56.5	61.1	-6.1	-0.02	0.986
X0026-C	30.8	29.0	33.9	-6.9	0.12	0.991
Flow 3	**58.2**	**56.4**	**61.4**	**-6.1**	**-0.02**	**0.986**
X0028-B	31.7	28.8	36.9	-9.0	-0.48	0.932
X0033-C	47.1	42.2	54.8	-9.8	0.15	0.886
X0036-C	49.7	48.4	50.6	-13.3	-0.07	0.997
Flow 4	**49.5**	**46.8**	**52.3**	**-11.0**	**0.04**	**0.954**
X0037-C	51.4	49.4	54.5	-12.5	0.11	0.982
X0040-C	71.9	69.2	76.6	-9.1	-0.03	0.974
X0045-A	64.9			-16.2	-0.05	0.997
Flow 5	**61.8**	**53.6**	**75.2**	**-10.5**	**0.05**	**0.758**

X0047-C	36.4	34.8	39.9	-14.9	-0.23	0.979
X0049-C	39.2	38.6	39.5	-9.4	-0.07	0.999
X0052-A	52.2	49.8	54.7	-18.6	-0.07	0.986
Flow 6	**51.9**	**49.6**	**55.1**	**-17.6**	**0.00**	**0.974**

4.6.2.3 IZZI method

For this type of experiment, a similar acceptance criterion to that used for the TC experiments was considered, and paleointensity estimations were performed also with the ThellierTool4.22 software (Leonhardt *et al.,* 2004). No reliable results could be obtained from Flow 1 (specimens X003 and X007), except for one sub-specimen (X003C-2). Negative pTRM checks due to alteration, even at temperatures below 400 °C, and a zig− zag type behavior of the magnetization component observed at the Zijderveld plot precluded the estimation of PI values for this flow. One must note, however, that corresponding κ-T plot seems to be quite reversible up to a temperature of ~ 450 °C (Figure 25) and provided no clue for these unsuccessful results. Flow 2 (specimens X014 and X017) yielded consistent and quite reliable specimen's mean results of 49.4 ± 4.4 and 49.5 ± 3.6 μT, respectively, with a flow mean result of 49.4 ± 3.7 μT (*n* = 8). Flows 3 and 4 (specimens X029 and X032, respectively) yielded also consistent and quite reliable specimen's mean results of 76.5 ± 3.2 and 63.9 ± 1.5 μT, respectively, although significantly higher than the underlying flow. For Flow 5 (specimens X041 and X042) two somewhat different specimen's mean results of 68.2 ± 6.0 and 59.4 ± 3.6 μT, respectively, were obtained, with a flow mean result of 63.8 ± 6.6 μT (*n* = 8). In case of Flow 6 (specimens X047 and X050) quite similar specimen's mean results of 63.9 ± 10.2 and 64.0 ± 2.3 μT, respectively, with a flow mean result of 63.9 ± 6.9 μT (*n* = 8). A representative Arai plot (Nagata *et al.,* 1965b) is shown in Figure 27c. Results are summarized in Table 10 and are graphically presented in Figure 28.

Representative examples of the Arai plots (Nagata *et al.,* 1965b) for the six flows are shown as Additional file 1: Figure S5. The corresponding vectorial plots (Zijderveld, 1967) are shown as Additional file 1: Figure S6.

From the different individual specimen's results from flows 4–6, an overall Xitle's PI value of 63.9 ± 5.8 μT (*n* = 20) was estimated. Corresponding cooling rate corrected values yield an overall PI value of 61.5 ± 4.3 μT (*n* = 19). As noted, the cooling rate correction of PI results slightly reduced the raw value and, in some cases, also the dispersion. Half of the 32 analyzed specimens showed k values < 0.164, seven 0.164 < *k* <

0.270 and only one a $k > 0.270$. Representative plots of the fitted circles to the data of the Arai diagrams are shown as Additional file 1: Figure S7.

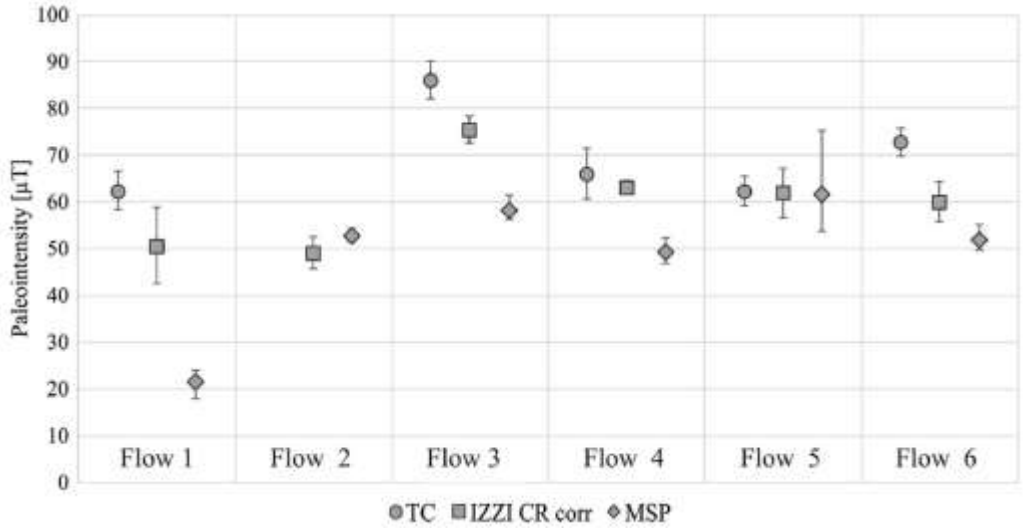

Figure 28 Comparison of PI results obtained by the different methodologies used (TC, IZZI CRcorr, and MS) for the 6 flows analyzed. Error bars represent the corresponding standard deviations in the case of TC and IZZI CRcorr results, while for the MS data to the Min and Max values obtained

Table 10 IZZI CRcorr paleointensity results for all six studied flows. Columns as defined in Table 8.

Specimen	Tmin [°C]	Tmax [°C]	N	slope	β	f	g	q	Mad anc [deg]	α	Class	CK-error	CK-diff	Drat	d(t*)	d(TR)	k	PI [µT]	σ [µT]	f_{CR}	PI $_{CRC}$ [µT]
Flow 1																					
X003C-2	20	460	10	-1.14	0.14	0.51	0.85	3.1	3.0	2.1	B	5.9	5.1	7.6	12.8	12.0		57.27	8.05	1.13	50.7
Flow 2																					
X014C-1	340	490	6	-0.92	0.02	0.49	0.65	20.8	2.6	1.4	B	4.9	2.9	7.3	6.0	0.9	0.0508	46.21	0.71	0.991	46.6
X014C-2	20	490	11	-0.95	0.03	0.58	0.72	12.6	4.6	3.3	B	5.1	5.7	6.4	3.7	1.5	0.1780	47.64	1.56	0.987	48.3
X014C-3	300	490	7	-0.96	0.03	0.54	0.70	14.8	2.0	0.9	B	4.2	0.0	5.6	12.6	0.8	0.1694	47.80	1.21	0.993	48.1
X014C-4	20	490	11	-1.12	0.03	0.59	0.76	14.1	3.7	2.8	B	5.1	0.9	5.7	6.1	3.7	0.0357	55.82	1.79	1.030	54.2
																Mean =		**49.4**			**49.3**
																σ =		**4.4**			**3.3**
Flow 2																					
X017C-1	20	460	10	-0.95	0.09	0.46	0.66	3.5	5.4	2.4	B	2.4	0.0	3.8	9.7	8.8	-0.0483	47.42	4.11	1.021	46.4
X017C-2	20	460	10	-0.95	0.08	0.43	0.71	3.7	4.0	1.0	B	1.6	6.6	2.7	12.2	7.2	-0.0302	47.72	3.98	1.011	47.2
X017C-3	20	460	10	-0.96	0.09	0.39	0.70	2.9	4.7	1.8	B	0.8	2.4	1.6	13.4	8.8	-0.0885	47.91	4.49	1.018	47.1
X017C-4	20	460	10	-1.10	0.10	0.40	0.75	3.1	6.5	3.0	B	3.2	9.4	5.4	13.0	4.1	0.0836	54.87	5.33	0.993	55.3
																Mean =		**49.5**			**49.0**
																σ =		**3.6**			**4.2**
															Flow mean (n = 8) =			**49.4**			**49.1**
																σ =		**3.7**			**3.5**
Flow 3																					
X029C-1	100	510	11	-1.55	0.03	0.55	0.85	16.3	3.7	4.4	B	3.5	4.8	3.4	10.5	3.2	-0.2467	77.55	2.24	0.986	78.7
X029C-2	300	510	8	-1.47	0.03	0.51	0.83	12.5	4.3	3.5	B	4.0	5.9	4.4	7.8	2.6	-0.0736	73.27	2.52	1.004	73.0
X029C-3	20	510	12	-1.50	0.02	0.61	0.87	21.6	5.6	5.9	B	5.1	1.9	4.6	8.5	2.6	0.0364	74.90	1.84	1.025	73.1
X029C-4	20	510	12	-1.61	0.07	0.53	0.86	6.6	5.4	5.8	B	2.4	3.8	2.4	6.1	2.0	0.0357	80.47	5.50	1.039	77.4
																Mean =		**76.5**			**75.5**
																σ =		**3.2**			**2.9**
Flow 4																					

X032C-1	20	460	10	-1.31	0.15	0.37	0.77	2.0	10.5	1.3	B	2.1	7.9	3.5	5.8	4.2	-0.0614	65.58	9.55	1.062	61.8
X032C-2	20	460	10	-1.29	0.07	0.40	0.81	4.7	4.0	1.2	B	2.2	4.9	3.5	5.0	3.3	0.8330	64.64	4.38	1.004	64.4
X032C-3	100	460	9	-1.26	0.12	0.39	0.75	2.4	6.0	2.2	B	5.4	9.2	8.6	8.0	4.0	0.2563	63.06	7.43	0.980	64.3
X032C-4	200	460	8	-1.25	0.13	0.41	0.73	2.3	5.8	2.9	B	4.6	8.5	7.0	8.3	4.2	0.1987	62.25	8.04	1.001	62.2
																Mean =		**63.9**			**63.2**
																σ =		**1.5**			**1.4**
Flow 5																					
X041C-1	20	460	10	-1.32	0.05	0.70	0.82	10.8	4.5	3.5	B	6.0	6.7	5.2	5.8	2.7	0.0331	66.01	3.48	1.023	64.5
X041C-2	20	460	10	-1.36	0.04	0.71	0.84	15.6	4.2	3.5	B	1.9	0.9	1.6	5.0	2.3	0.0006	68.18	2.63	1.033	66.0
X041C-3	20	460	10	-1.24	0.03	0.70	0.82	18.0	4.3	2.9	B	0.9	0.1	0.8	6.4	1.6	0.1558	62.13	1.98	1.036	60.0
X041C-4	20	460	10	-1.53	0.05	0.74	0.83	11.6	3.1	2.5	B	6.1	1.8	4.5	7.1	2.7	0.0933	76.38	4.04	1.075	71.1
																Mean =		**68.2**			**65.4**
																σ =		**6.0**			**4.6**
Flow 5																					
X042C-1	20	490	11	-1.14	0.05	0.77	0.78	12.2	3.6	1.9	B	2.1	0.6	1.8	8.4	3.4	0.2122	56.80	2.80	1.013	56.1
X042C-2	340	490	6	-1.16	0.05	0.60	0.73	8.7	1.6	1.5	B	3.0	9.9	3.2	11.6	1.9	0.2140	58.12	2.93	1.009	57.6
X042C-3	100	460	9	-1.30	0.09	0.56	0.76	4.7	4.1	1.9	B	2.6	3.2	2.8	10.1	2.4	0.1808	64.80	5.92	1.022	63.4
X042C-4	20	490	11	-1.16	0.05	0.74	0.79	12.9	3.4	1.9	B	1.5	2.4	1.3	10.1	1.4	0.0671	57.97	2.62	1.024	56.6
																Mean =		**59.4**			**58.4**
																σ =		**3.6**			**3.4**
																Flow mean (n = 8) =		**63.8**			**61.9**
																σ =		**6.6**			**5.3**
Flow 6																					
X047C-1	400	510	5	-1.09	0.01	0.41	0.73	21.9	4.8	2.8	B	3.7	3.6	6.1	6.5	2.2	-0.0659	54.37	0.75	1.027	52.9
X047C-2	300	510	8	-1.21	0.11	0.54	0.82	4.1	4.3	3.3	B	5.7	9.7	6.7	4.4	3.2	0.2978	60.32	6.53	1.078	56.0
X047C-3	20	460	10	-1.57	0.10	0.41	0.85	3.6	3.9	0.4	B	1.9	8.3	2.5	4.2	3.9	0.4380	78.35	7.49	1.143	
X047C-4	200	510	10	-1.25	0.06	0.55	0.85	8.2	5.4	4.3	B	4.3	9.9	4.9	4.2	2.1	0.2307	62.57	3.55	1.011	61.9
																Mean =		**63.9**			**56.9**
																σ =		**10.2**			**4.5**
Flow 6																					
X050C-1	20	510	12	-1.31	0.05	0.66	0.87	12.2	4.9	6.2	B	4.2	5.7	3.9	5.0	3.1	0.2857	65.45	3.06	1.033	63.4
X050C-2	20	510	12	-1.29	0.04	0.62	0.87	14.8	5.4	6.2	B	2.3	5.3	2.3	5.6	2.2	0.0568	64.71	2.35	1.017	63.6
X050C-3	100	510	11	-1.21	0.05	0.62	0.86	11.7	4.9	4.8	B	4.2	10.0	4.3	5.4	4.1	0.1401	60.46	2.76	1.026	58.9
X050C-4	20	510	12	-1.30	0.03	0.64	0.87	21.1	3.5	3.7	B	2.3	7.6	2.2	7.9	2.8	0.0745	65.19	1.71	1.017	64.1
																Mean =		**64.0**			**62.5**
																σ =		**2.3**			**2.4**
																Flow mean (n = 8) =		**63.9**			**60.1**
																σ =		**6.9**			**4.3**
																Flows 4 - 6 Mean (n = 20) =		**63.9**			**61.5**
																σ =		**5.8**			**4.5**

4.7 Discussion and concluding remarks

The comparison between the results obtained by the three methods used (TC, IZZI CRcorr, and MS) shows some differences (Table 11). TC type results are in most cases higher than corresponding IZZI CRcorr values, except for Flow 5. On the contrary, MS data are in most cases significantly lower than the corresponding Thellier type values, except for Flow 2 and Flow 5. For this last flow, a PI of 61.8 μT, compatible with those obtained from Thellier-type methods, was obtained. In general, the thermochemical alteration—attested by Avg ε_{alt} > 10% seems to be the main cause for the inter-method differences observed.

Table 11 Summary of the mean PI values from three methods for the six flows. TC Thellier–Coe method, IZZI CRcorr IZZI method with cooling rate correction, MS multispecimen method, n number of specimens used for PI calculation.

Flow	TC [μT]	± σ	n	IZZI CR $_{corr}$ [μT]	± σ	n	MS [μT]	Min [μT]	Max [μT]

		[μT]			[μT]				
Flow 1	62.4	4.1	1	50.7	8.1	1	21.6	17.9	23.8
Flow 2	N/R	–	–	49.1	3.5	8	52.9	51.4	54.3
Flow 3	86.2	4.0	1	75.5	2.9	4	58.2	56.4	61.4
Flow 4	66.0	5.5	3	63.2	1.4	4	49.5	46.8	52.3
Flow 5	62.4	3.1	1	61.9	5.3	8	61.8	53.6	75.2
Flow 6	72.8	3.0	3	60.1	4.3	7	51.9	49.6	55.1

Taking into account that consistent results obtained with methodologies relying on dissimilar physical bases can be regarded as an alternative means to support the reliability of paleointensity determinations (e.g., De Groot *et al.,* 2015; Enterpinar *et al.,* 2016; Monster *et al.,* 2015b; Calvo-Rathert *et al.,* 2016), similar results for Flow 5 obtained by the three methodologies should be considered as the most reliable PI value for this flow. A mean multi-method PI flow value of 62.1 ± 5.9 μT (*n* = 12) was obtained for Flow 5.

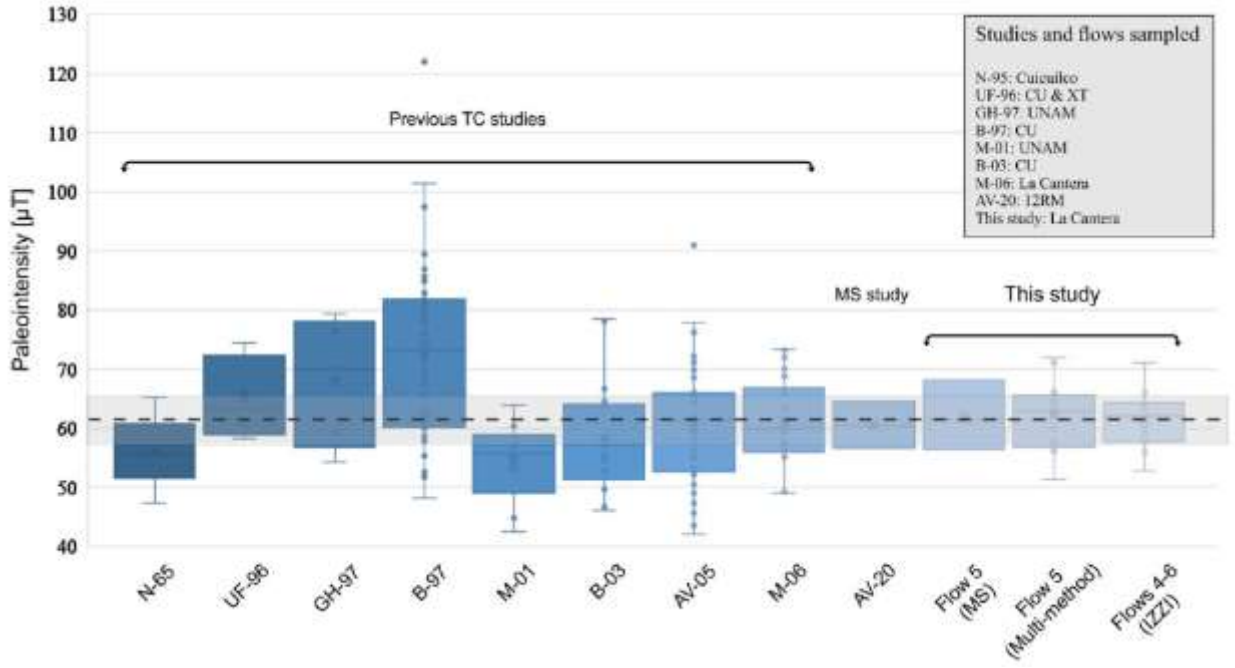

Figure 29 Box-and-whisker plots showing the available lava PI data for Xitle, together with those obtained in this investigation. N-65: Nagata *et al.* (1965a); UF-96: Urrutia-Fucugauchi (1996); GH-97: Gonzalez *et al.* (1997); B-97: Böhnel *et al.* (1997); M-01: Morales *et al.* (2001); B-03: Böhnel *et al.* (2003); M-06: Morales *et al.* (2006); AV-20: Alva-Valdivia *et al.* (2020); Flow 5 (MS): mean PI result for Flow 5 obtained with the MS method; Flow 5 (multi-method): mean PI result for Flow 5 obtained with the TC, IZZI CRcorr and MS methods; flows 4–6 (IZZI): mean PI result from flows 4–6 obtained with the IZZI CRcorr method. The dotted line

and shaded area correspond to the Xitle's mean IZZI CRcorr paleointensity value obtained in this study, and its associated standard deviation.

The results obtained from the Thellier-type methodologies are very similar in the cases of Flow 4 and Flow 5, and slightly different in the case of Flow 6 (Figure 28). Overall mean PI flow values from flows 4 to 6 obtained by the TC methods used yielded 68.4 ± 5.6 μT and 61.5 ± 4.3 μT for the TC and IZZI CRcorr methods, respectively. Therefore, the cooling rate-corrected IZZI result could be considered as the most reliable PI result for the flows 4–6 sequence of the Xitle.

As a support for the reliability of the obtained results, Alva-Valdivia *et al.* (2020) recently carried out a reassessment of paleointensity estimated of a single lava flow from Xitle volcano by means of the multispecimen domain-state-corrected method, obtaining nearly identical paleointensity results of 60.5 ± 4 μT. Figure 29 shows a summary of the results obtained in this investigation, together with the results obtained in previous studies on lavas of the Xitle volcano. We must mention that previous studies on potteries or baked sediments found beneath Xitle's lavas were excluded since this would inevitably add another factor (anisotropy of thermoremanence) to be considered in the study.

At this point, a comparison of our results against the different model predictions available—CALS10k.1b (Constable *et al.,* 2016), SHA.DIF.14 k (Pavón-Carrasco *et al.,* 2014), A_FM (Licht *et al.,* 2013), etc.—seems natural. Nonetheless, the different model predictions available show, for some intervals, significant differences.

On the other hand, even though the Xitle is one of the youngest volcanoes, a breadth age-interval for the Xitle's eruption does (still) persist, as mentioned above. Moreover, among the different age intervals proposed so far, that of Siebe (2000) and Gonzalez *et al.* (2000) (1670 BP) would seem to be the more reliable one. However, Urrutia-Fucugauchi *et al.* (2016) recently carried out a bootstrap analysis of radiocarbon dates and paleomagnetic data—by correlating full vector data with the geomagnetic secular variation reference model (SHA.DIF.14 k)—for the Xitle lava flows to constrain the best date estimates, from which new age estimates (2041 BP and 2035 BP, respectively) for the eruption were determined. Therefore, an attempt to correlate PI estimates with the different model predictions would seem to be somewhat meaningless at this stage.

Another interesting result observed from Figure 28 is that the IZZI CRcorr PI values for flows 1 and 2 are quite similar between them, but also quite different from those for flows 4–6. Cervantes-Solano *et al.*

(2019) have suggested that this lava-flow sequence could represent, at least, two eruptive periods; one related to the Xitle volcano (flows 4–6), and other older (flows 1−2) of an unknown source. Nonetheless, Delgado-Granados *et al.* (1998) had already speculated the ages of the ~4000 yr cluster identified by Urrutia-Fucugauchi (1996) could represent the age of Tenantongo Basaltic Andesite, being geomorphologically very similar to Xitle volcano lavas, and thus, very easy to confuse.

Whether or not the mean paleodirections of flows 1 and 2 are statistically different from those of flows 3 to 6 is difficult to ascertain. However, a simple look at the corresponding equal-area projections suggests slightly different mean paleodirections (Figure 30). Separated equal area projections for flows 1 and 2 and for flows 3 to 6 are shown as Additional file 1: Figure S8.

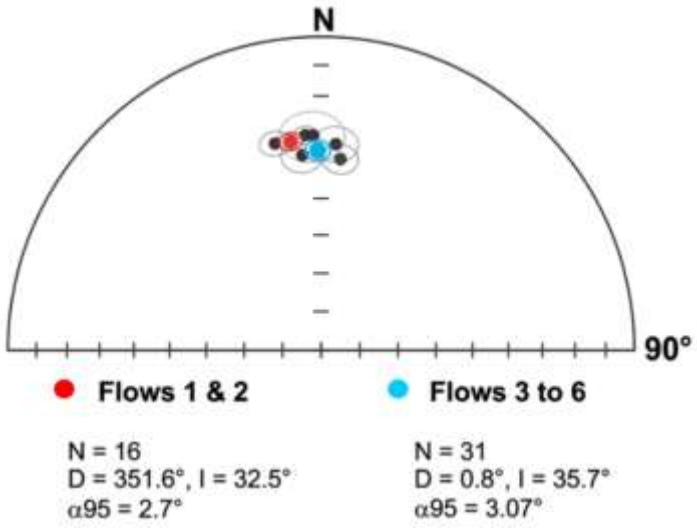

Figure 30 Equal area projection showing the corresponding mean paleomagnetic directions for flows 1 and 2 (red dot), and for flows 3 to 6 (blue dot), together with their corresponding alpha_95 intervals

The reassessment of the archeomagnetic dating of the different flows through the reference model SHA.DIF.14 k, using the reliable IZZI CR_{corr} PI data obtained in this study, yield the following periods as the most probable ages: [1620 BC–1520 BC] (3570 BP- 3470 BP) for Flow 1; [1749 BC–1597 BC] (3699 BP- 3547 BP) for Flow 2; [61 BC–5 BC] (2011 BP- 1955 BP) for Flow 3; [55 BC–1 AD] (2005 BP–1949 BP) for Flow 4; [24 BC–270 AD] (1974 BP–1680 BP) for Flow 5; [322 BC – 37 AD] (2272 BP–1913 BP) for Flow 6, thus, supporting the likely different origin for the first two flows (Flow 1 and Flow 2) of the sequence on the one hand, and the multi-modal age distribution obtained by Urrutia-Fucugauchi (1996) on the other hand.

Dating of a burnt wood fragment found beneath a lava flow from Unit V yielded and age of 1960 ± 65 yr BP (Ortega-Guerrero *et al.,* 1993), in good agreement with the archeomagnetic dating results. Archeomagnetic dating plots for the different flows are shown as Additional file 1: Figures S9.1–S9.6.

As evidenced from the results obtained, the large scatter of PI values obtained in previous studies should be attributed to the use of relaxed acceptance criteria on the one hand, and on the undetected non-ideal behavior— mainly MD effects and alteration during laboratory heating—on the other hand. This is comprehensible since those studies were carried out before stringent protocols— including extra experimental steps for the quantification and, when possible, the correction of non-ideal behavior (Paterson 2011)—were proposed, and due to the lack of standard tests.

From the results obtained in this investigation, the practice of stricter acceptance criteria, together with CR correction and curvature estimation, would help to eliminate the "enigmatic" character to the Xitle's lava flows.

4.7 Additional file 1

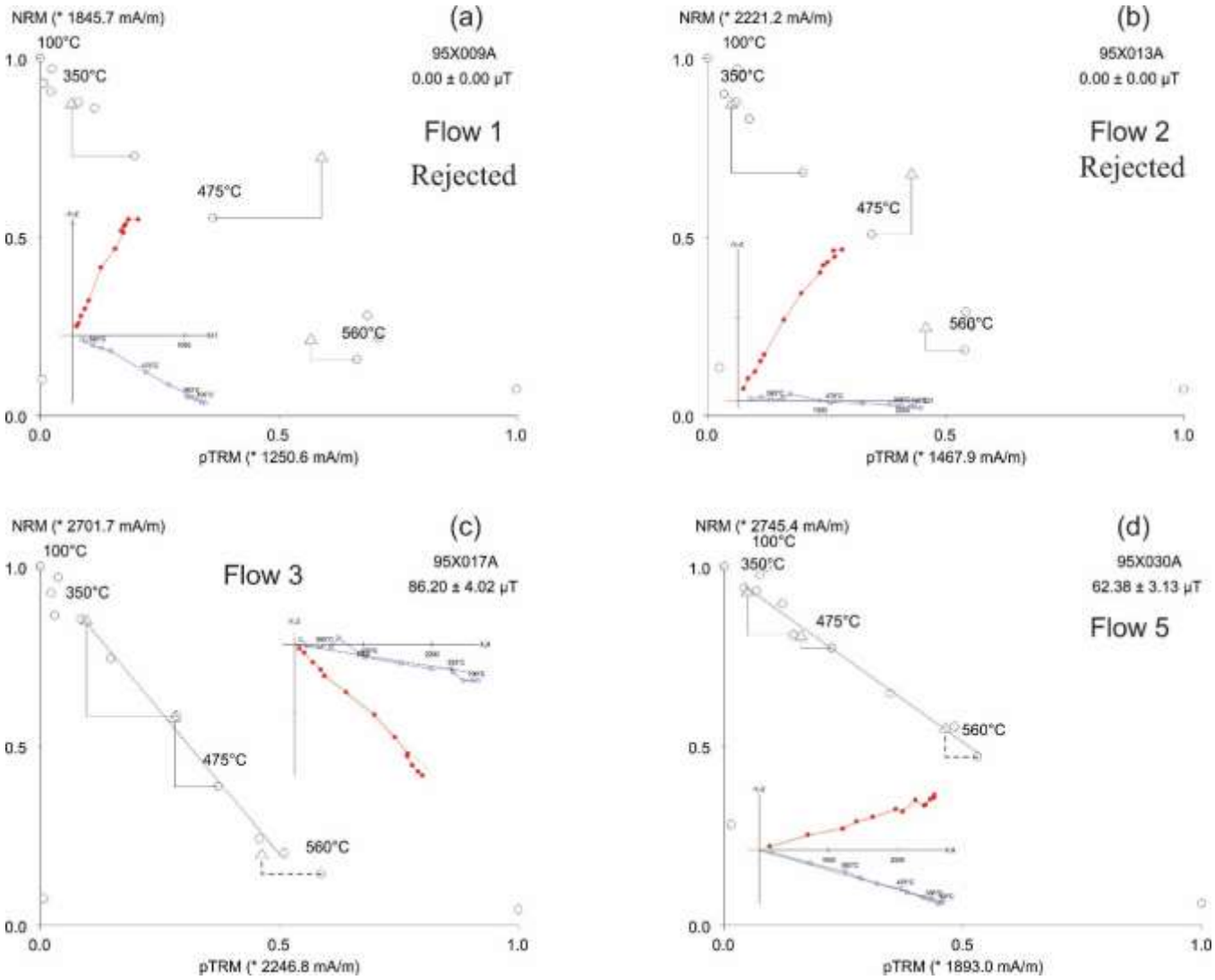

Figure S 3 Representative Arai (Nagata *et al.,* 1965b) plots of rejected (a) & (b) and successful (c) & (d) TC paleointensity determinations. Also shown are the associated vectorial (Zijderveld, 1967) plots.

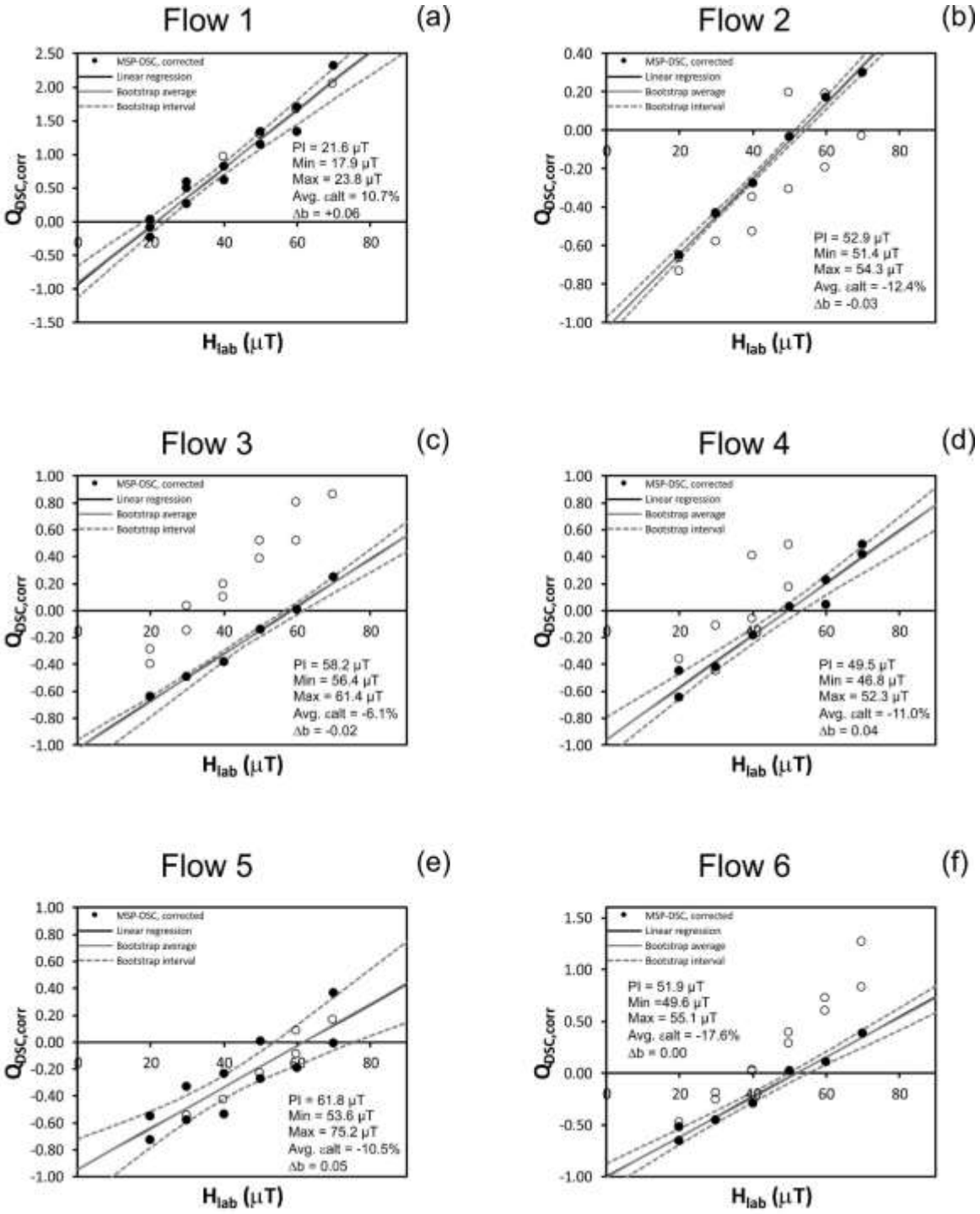

Figure S 4 Representative multispecimen (QDSC,corr) plots for the six lava flows studied.

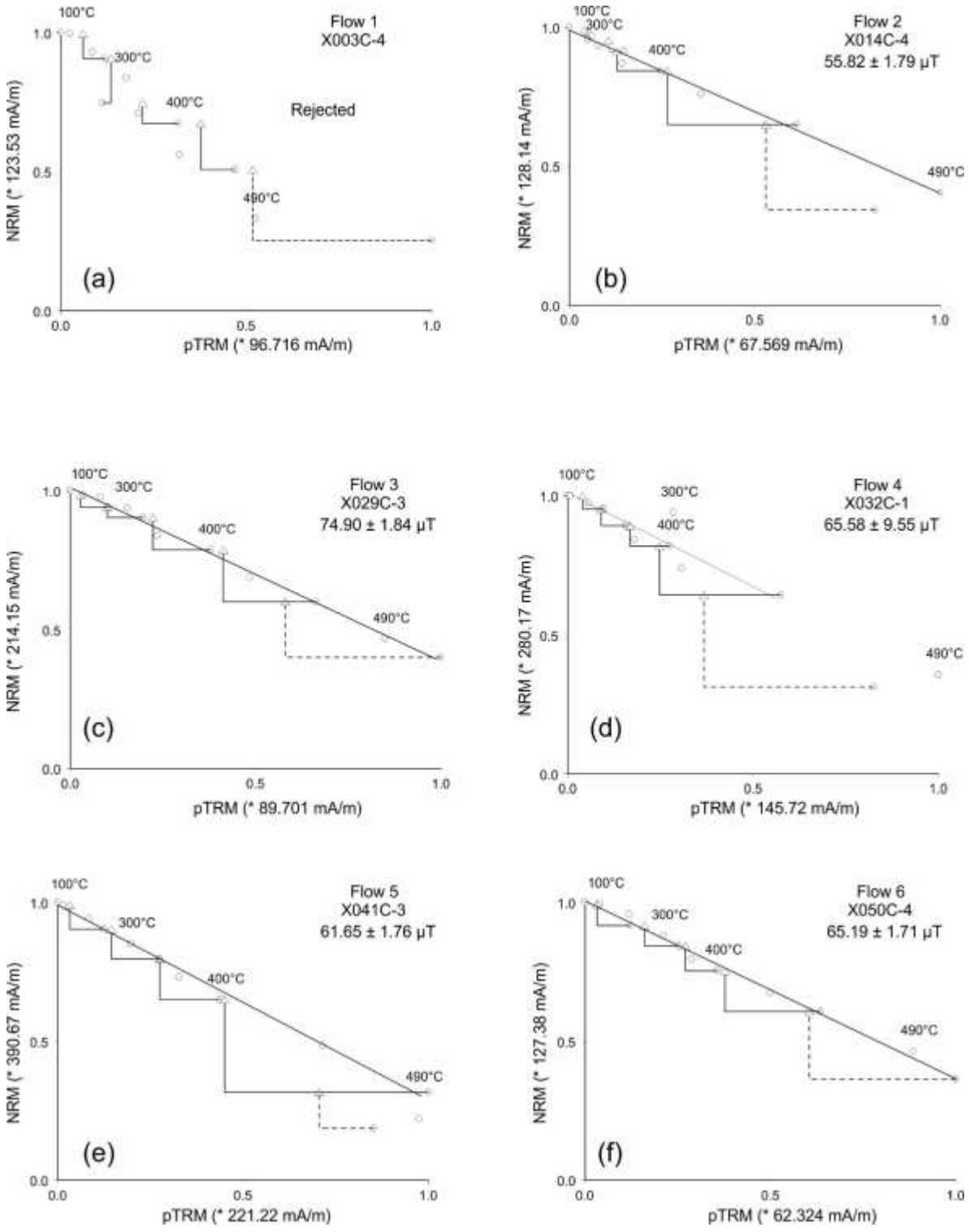

Figure S 5 Representative Arai plots (Nagata *et al.,* 1965b) of rejected (a) and successful (b) - (f) IZZI CRcorr PI determinations.

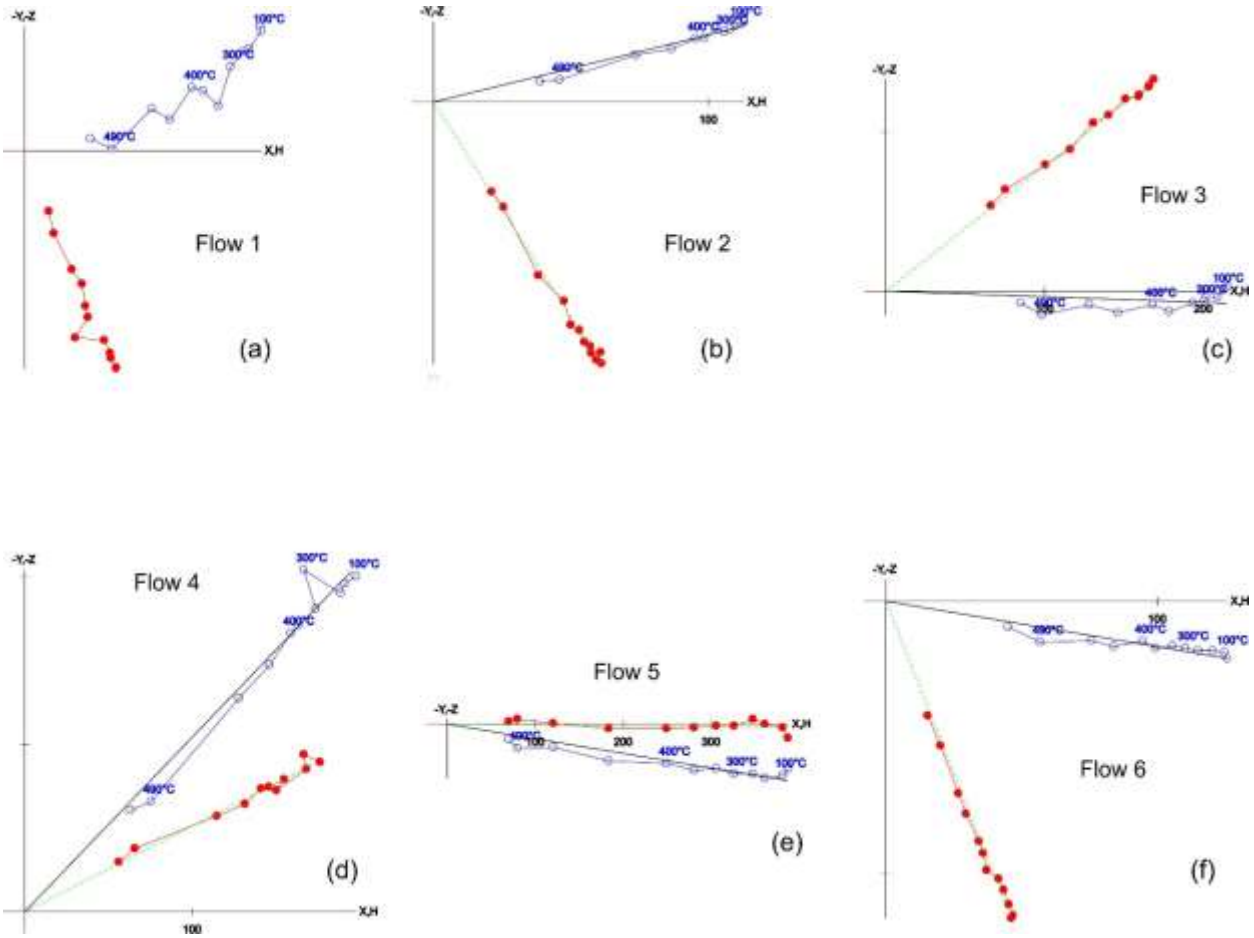

Figure S 6 Representative IZZI associated vectorial (Zijderveld, 1967) plots.

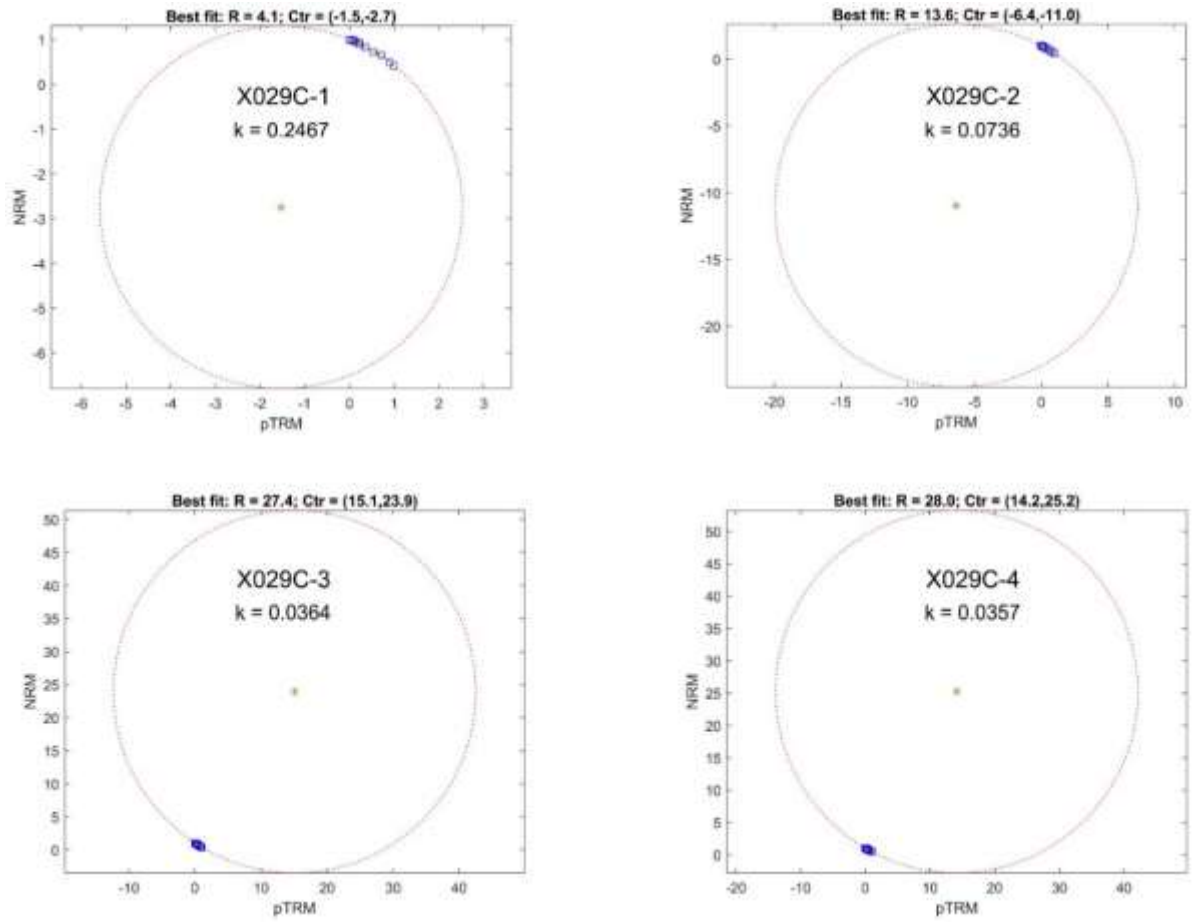

Figure S 7 Representative plots of the fitted circles to the data of the Arai diagrams.

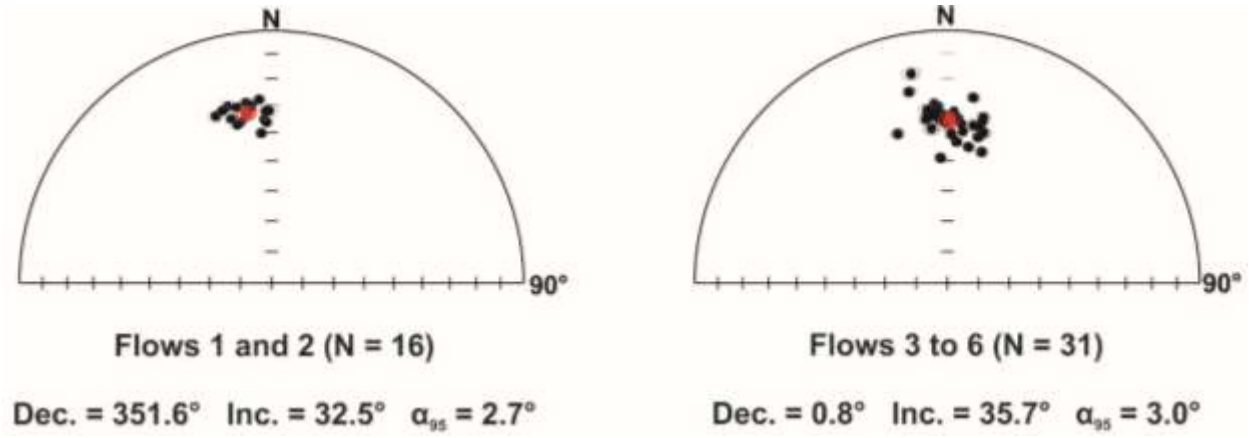

Figure S 8 Equal area projections for flows 1 and 2 (left) and flows 3 to 6 (right). Black dots represent individual specimen directions, while the red dot corresponds to the combined mean paleomagnetic direction, together with their corresponding alpha_95 intervals.

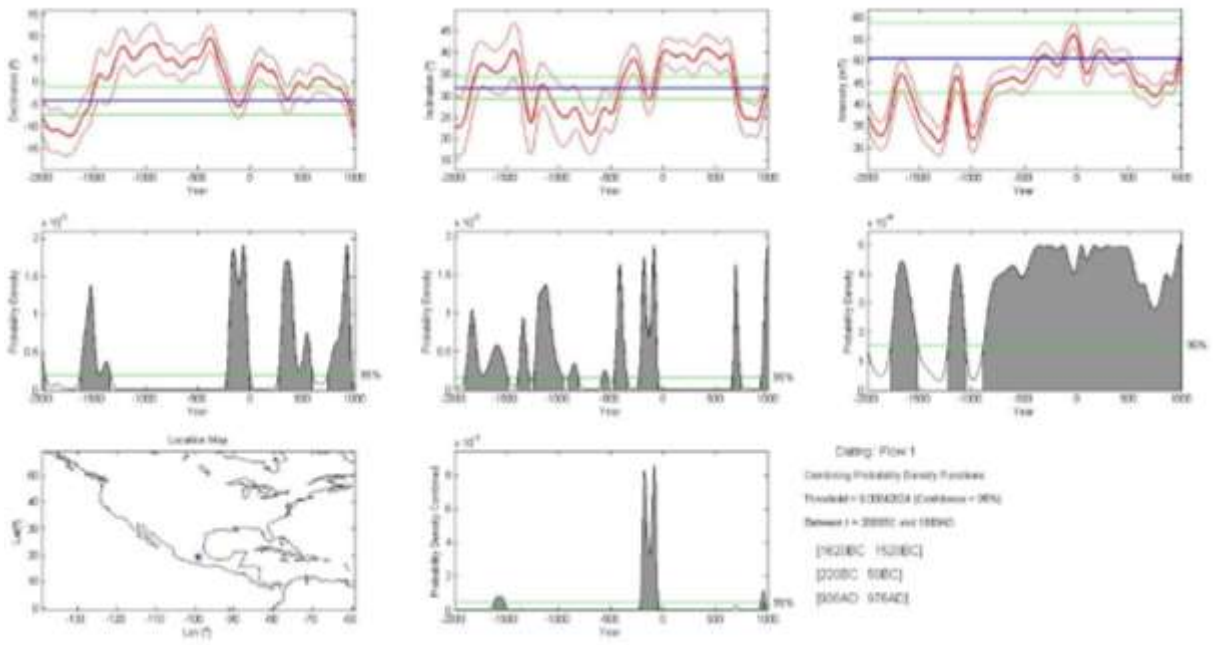

Figure S9. 1 Archeomagnetic plots for the Lava flow 1. Upper panels: Red curves show the variation in time of the three components of the paleomagnetic field as determined from the SHA.DIF.14k model, while blue horizontal lines are the components of the full vector (direction and intensity) determined for Xitle volcano; all curves and lines are shown with their corresponding 95% confidence intervals. Central panels: The corresponding probability densities derived from the declination, inclination, and intensity data are shown as shaded peaks and the 95% confidence level by horizontal green lines. Right lower panel: The combined probability density (shown as shaded peaks) and the 95% confidence level (horizontal green lines).

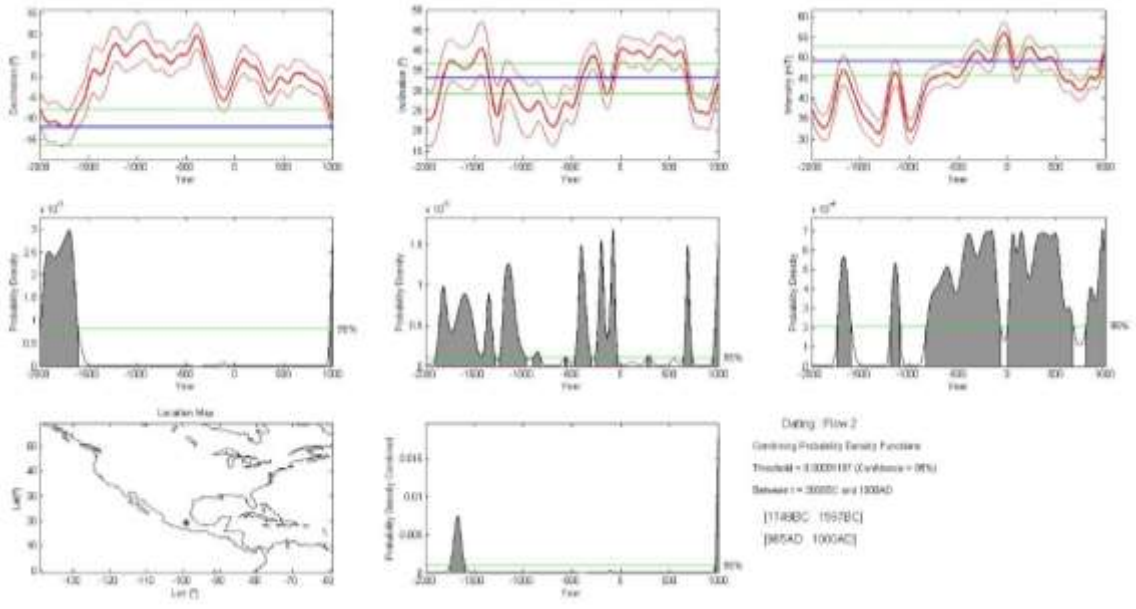

Figure S9. 2 Archeomagnetic plots for the Lava flow 2. Upper panels: Red curves show the variation in time of the three components of the paleomagnetic field as determined from the SHA.DIF.14k model, while blue horizontal lines are the components of the full vector (direction and intensity) determined for Xitle volcano; all curves and lines are shown with their

corresponding 95% confidence intervals. Central panels: The corresponding probability densities derived from the declination, inclination, and intensity data are shown as shaded peaks and the 95% confidence level by horizontal green lines. Right lower panel: The combined probability density (shown as shaded peaks) and the 95% confidence level (horizontal green lines).

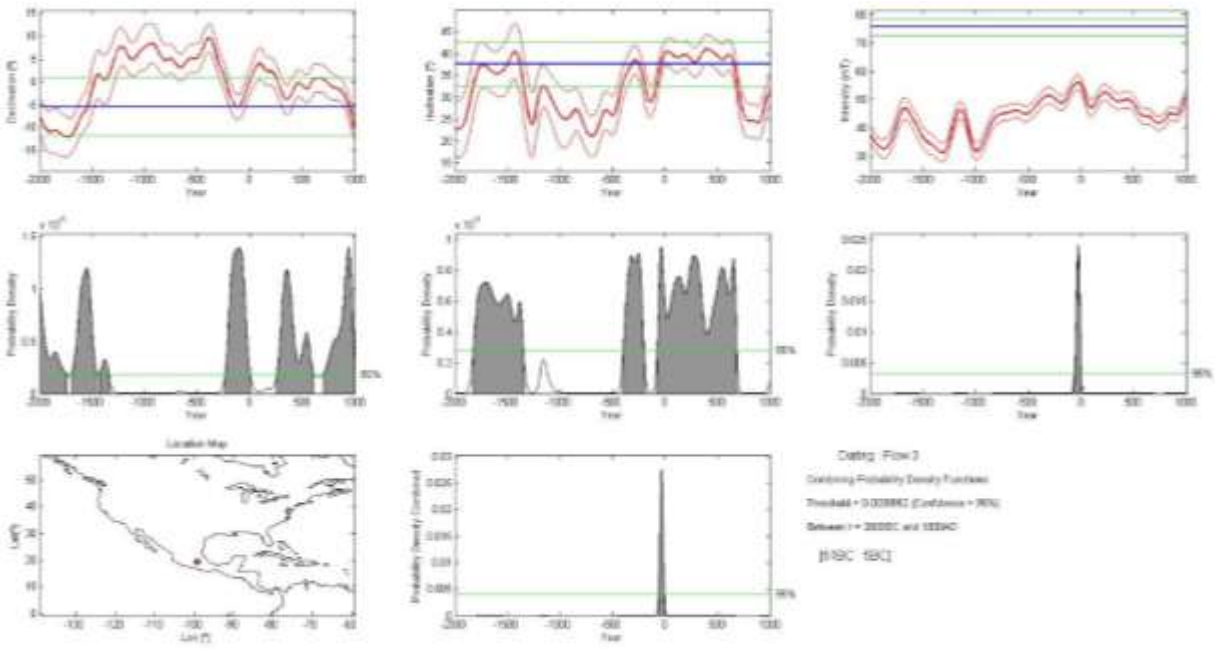

Figure S9. 3 Archaeomagnetic plots for the Lava flow 3. Upper panels: Red curves show the variation in time of the three components of the paleomagnetic field as determined from the SHA.DIF.14k model, while blue horizontal lines are the components of the full vector (direction and intensity) determined for Xitle volcano; all curves and lines are shown with their corresponding 95% confidence intervals. Central panels: The corresponding probability densities derived from the declination, inclination, and intensity data are shown as shaded peaks and the 95% confidence level by horizontal green lines. Right lower panel: The combined probability density (shown as shaded peaks) and the 95% confidence level (horizontal green lines).

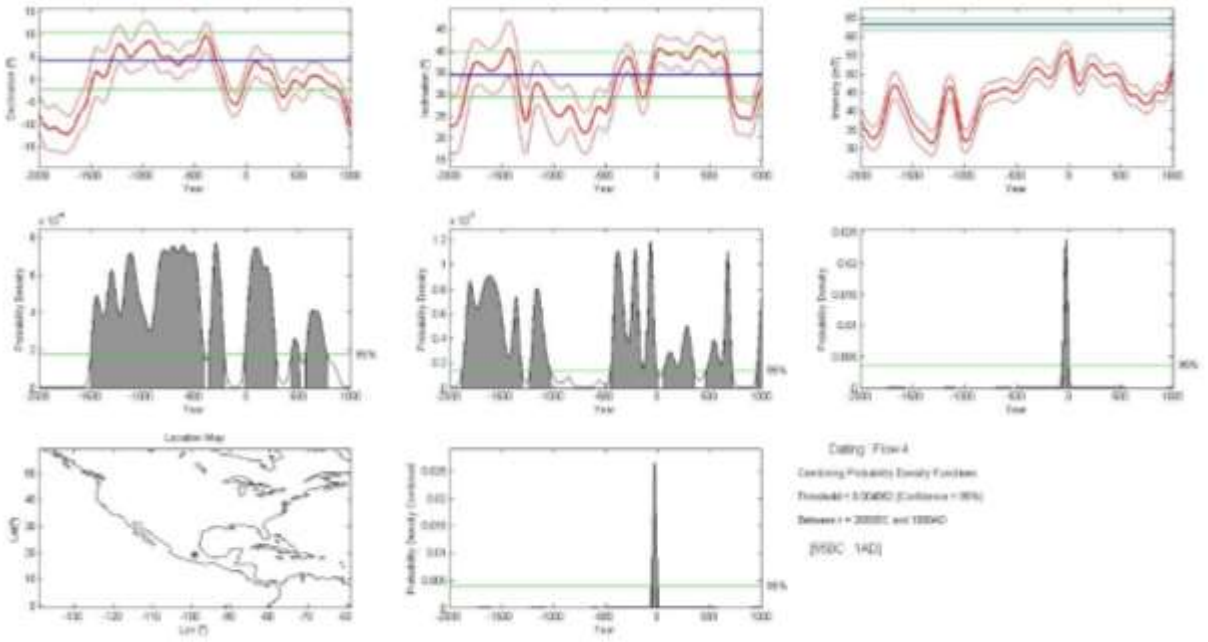

Figure S9. 4 Archeomagnetic plots for the Lava flow 4. Upper panels: Red curves show the variation in time of the three components of the paleomagnetic field as determined from the SHA.DIF.14k model, while blue horizontal lines are the components of the full vector (direction and intensity) determined for Xitle volcano; all curves and lines are shown with their corresponding 95% confidence intervals. Central panels: The corresponding probability densities derived from the declination, inclination, and intensity data are shown as shaded peaks and the 95% confidence level by horizontal green lines. Right lower panel: The combined probability density (shown as shaded peaks) and the 95% confidence level (horizontal green lines).

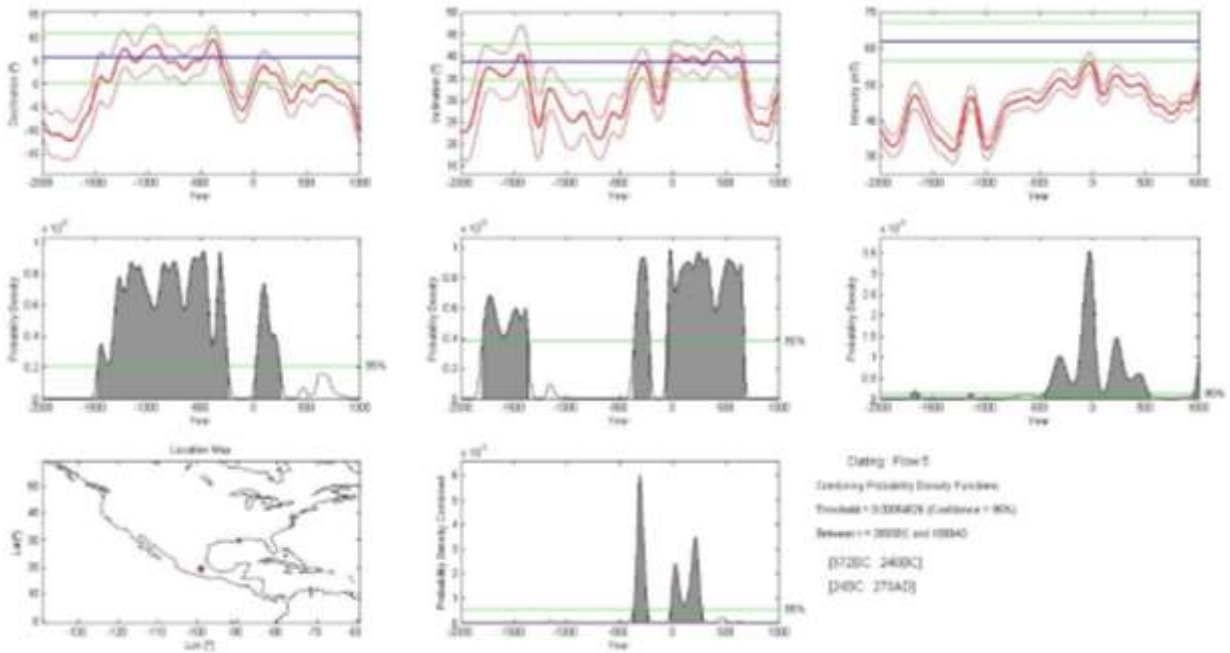

Figure S9. 5 Archeomagnetic plots for the Lava flow 5. Upper panels: Red curves show the variation in time of the three components of the paleomagnetic field as determined from the SHA.DIF.14k model, while blue horizontal lines are the

components of the full vector (direction and intensity) determined for Xitle volcano; all curves and lines are shown with their corresponding 95% confidence intervals. Central panels: The corresponding probability densities derived from the declination, inclination, and intensity data are shown as shaded peaks and the 95% confidence level by horizontal green lines. Right lower panel: The combined probability density (shown as shaded peaks) and the 95% confidence level (horizontal green lines).

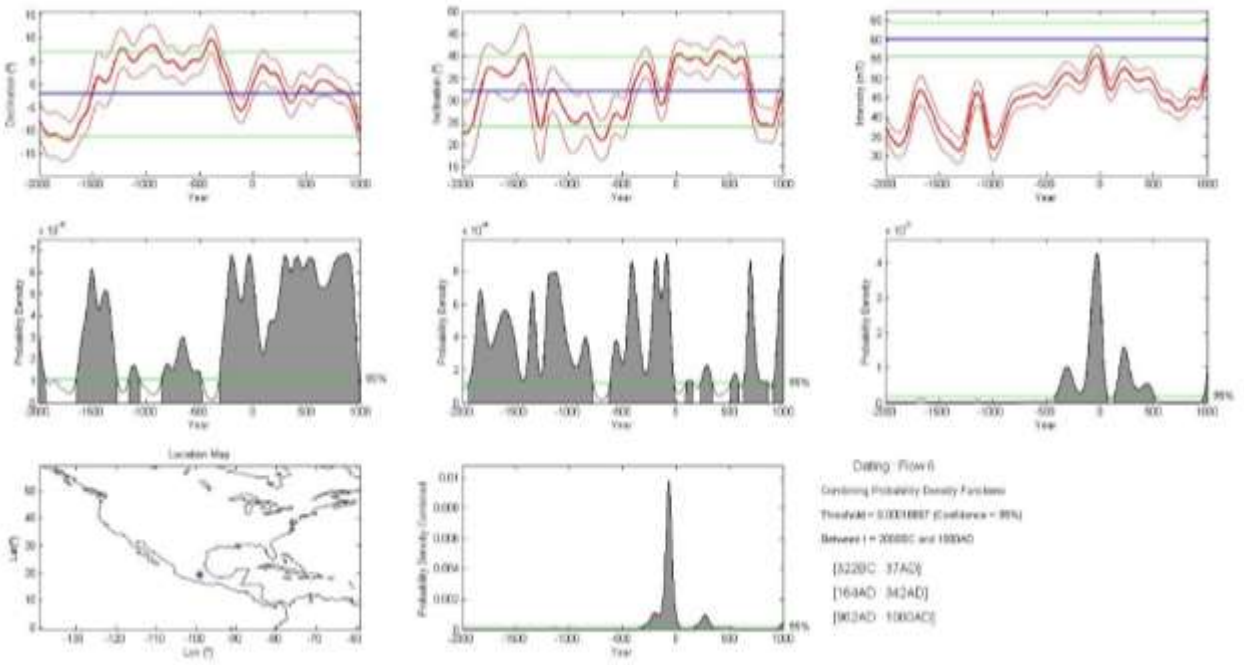

Figure S9. 6 Archeomagnetic plots for the Lava flow 6. Upper panels: Red curves show the variation in time of the three components of the paleomagnetic field as determined from the SHA.DIF.14k model, while blue horizontal lines are the components of the full vector (direction and intensity) determined for Xitle volcano; all curves and lines are shown with their corresponding 95% confidence intervals. Central panels: The corresponding probability densities derived from the declination, inclination, and intensity data are shown as shaded peaks and the 95% confidence level by horizontal green lines. Right lower panel: The combined probability density (shown as shaded peaks) and the 95% confidence level (horizontal green lines).

5. Reassessing the paleointensities of three volcanic structures of the Michoacán-Guanajuato Volcanic Field (Mexico) through a multimethodological analysis

https://doi.org/10.1016/j.pepi.2022.106927

Nayeli Pérez-Rodríguez, Juan Morales, Rubén Cejudo, Marie-Noëlle Guilbaud, Avto Goguitchaichvili

Physics of the Earth and Planetary Interiors (Submitted)

5.1 Resumen

Un enfoque que ha adquirido popularidad en la última década para aumentar la confiabilidad de las determinaciones de paleointensidad es el uso de análisis multimetodológicos, especialmente cuando se comparan valores de intensidad obtenidos mediante el uso de métodos basados en distintas propiedades físicas, como por ejemplo, los resultados obtenidos de experimentos convencionales de tipo Thellier, contra los resultados de métodos de la familia Shaw, o del más reciente protocolo de múltiples especímenes.

Esta investigación presenta la reevaluación de las intensidades del campo geomagnético registradas en tres estructuras volcánicas monogenéticas: los conos y lavas de los volcanes Rancho Seco y el Jabalí, y el flujo de lava fisural conocido como Malpaís Prieto, todas ubicadas en el campo volcánico Michoacán-Guanajuato (centro de México). Este análisis está acompañado del estudio exhaustivo de las propiedades obtenidas mediante experimentos de magnetismo de rocas, que permiten obtener una caracterización completa de los portadores de magnetización, así como una mejor comprensión de los resultados de intensidad. Las tres estructuras volcánicas analizadas han sido estudiadas de manera previa, por lo que se cuenta con información en la literatura de sus paleointensidades. Para el caso de uno de los volcanes se determinaron paleointensidades con el método original de Shaw , el cual actualmente se considera poco confiable debido a que no cuenta con monitoreos de la alteración térmica durante el experimento, por lo que dichos valores fueron descartados del análisis final. Para los datos publicados de las otras dos estructuras volcánicas, se discute su calidad y se comparan con los resultados obtenidos en el presente trabajo mediante métodos tipo Thellier, el protocolo de múltiples especímenes (MSP), y el método de Shaw modificado por Tsunakawa.

Los resultados obtenidos muestran una buena concordancia entre las determinaciones de paleointensidades estimadas con el uso de más de una metodología para muestras del volcán Jabalí y el flujo de lava Malpaís Prieto, obteniendo valores de intensidad promedio de 43,7 ± 5,1 µT y 47,8 ± 3,1 µT, respectivamente. Sin embargo, para el volcán Rancho Seco se encontró una diferencia de casi 30 µT entre los resultados obtenidos en el presente trabajo con el método de MSP (50,9 ± 2,8 µT) y los datos publicados previamente usando el protocolo IZZI (20,0 ± 1,4 µT). Para dar una explicación a este controvertido resultado, se emplearon curvas de susceptibilidad contra temperatura realizadas a pasos con incrementos progresivos de temperatura, así como los resultados de paleointensidades obtenidos al aplicar el método de Tsunakawa-Shaw a un conjunto de muestras. Las observaciones finales sugieren que los valores de paleointensidad bajos se encuentran asociados con la alteración térmica de la mineralogía magnética de las muestras, descartándolos como el valor de intensidad representativo de la temporalidad de emplazamiento del volcán Rancho Seco.

5.2 Abstract

An approach that has acquired popularity in the last decade to ensure the quality of paleointensity determinations is the use of multimethodological analysis, especially when comparing intensity values obtained by methods with different physical bases such as the conventional Thellier-type experiments against the Shaw-family methods and the most recent multispecimen protocol. This research presents the reevaluation of the intensities of three monogenetic volcanic structures: the Rancho Seco and Jabalí cones and lavas, and the Malpaís Prieto fissure lava flow, all located in the Michoacán-Guanajuato volcanic field (central Mexico). This analysis is accompanied by an exhaustive study of rock-magnetic properties to obtain a complete characterization of the magnetization carriers and a better understanding of the intensity results. The three volcanic structures have previously published intensity data; one of them was obtained with the original Shaw method that nowadays is considered unreliable due to the absence of monitoring of thermal alteration during the experiment. The quality of the previously published data is discussed to be compared to our intensity values, which were obtained employing Thellier-type methods and the multispecimen protocol (MSP). A good concordance was found for the data obtained by more than one methodology for samples from the Jabalí volcano and the Malpaís Prieto lava flow, obtaining average intensity values of 43.7 ± 5.1 µT and 47.8 ± 3.1 µT, respectively. However, a difference of almost 30 µT was found between our MSP results (50.9 ± 2.8 µT) and previously published data using the IZZI

method (20.0 ± 1.4 μT) for Rancho Seco volcano. An attempt was made to clarify this controversial result with the support of stepwise susceptibility against temperature curves analysis and the results obtained from a set of samples treated with the Tsunakawa-Shaw paleointensity method. The results obtained indicate that the low paleointensity values are associated with the thermal alteration of the magnetic mineralogy of the samples.

5.3 Introduction

Since the first half of the past century, the development of techniques for an accurate determination of the paleointensity (PI) record in geological and archeological materials has been a point of interest for the paleomagnetic community. According to the theoretical background, the materials that acquire a magnetization through thermal remanence follow an almost linear relationship with the magnetic field that produced it, as long as the field is of low intensity, such as the Earth's Magnetic Field (EMF) (Selkin and Tauxe, 2000). This principle is considered in all the protocols developed to determine the paleointensity value recorded in different materials over the Earth's surface. A brief but complete revision of the methodologies developed until now can be reviewed in Tauxe and Yakamazi (2015).

Until a decade ago, the classic Thellier-Coe (TC) method (Coe, 1967) was the most used protocol for PI determinations, as mentioned by Tauxe (2010). In the TC protocol, the natural remanent magnetization (NRM) of the samples is progressively replaced by partial termoremanences (pTRMs) applying increasing temperatures until the Curie Temperature (Tc) is reached. The sample is heated twice at each temperature step, first in the absence of an external magnetic field (zero-field, Z step) to erase a portion of the NRM, and then in the presence of a laboratory field (in-field, I step) to create a pTRM (ZI protocol). With this protocol the relation between the magnetization acquired by the sample and the intensity of a known laboratory field is established, so a proportionality constant that relates both parameters can be determined. Once this constant is obtained, it can be used to determine the strength of the ancient EMF that produced the original NRM of the sample. For a correct calculation of the sample's paleointensity, the three Thellier's laws should be accomplished: reciprocity, independence, and additivity (for a detailed explanation see Yu et al., 2004), so the success in estimating paleointensity using Thellier-type methods is directly related to the grain size distribution of the magnetic minerals in the analyzed samples (the lower the number of multidomain (MD) particles, the better), and to the thermal stability of these minerals

during heating. In the Thellier-Coe protocol, the pTRM check and the pTRM tail checks (Riisager and Riisager, 2001) have been implemented, which are useful to monitor the thermal stability of the samples and estimate the proportion of MD grains that they possess respectively.

The IZZI paleointensity method (also a Thellier type protocol) developed by Yu et al. (2004) has been widely used. For this protocol, the double heating steps are alternated. At the first temperature, the sample is initially heated in-field and then in zero-field (IZ), and for the next double heating, realized at a higher temperature than the previous one, samples are heated inversely: first in zero-field, then in-field (ZI), and so on until cover all the Tc's of the magnetic minerals of the sample. The IZZI protocol has the advantage of being particularly susceptible to the presence of pTRM tails attributed to the presence of a large quantity of MD grains, which is reflected in a zig-zag trend of the double heating steps projected in the Arai plot (Yu et al., 2004; Yu and Tauxe 2005). This allows the detection of unsuitable specimens and excludes their data from the analysis. However, the high quantity of heating steps used in the Thellier type protocols is, by itself, a cause of failure in the experiment since it tends to produce a progressive thermal alteration of the magnetic mineralogy of the specimens.

Considering this problem, different methodological proposals have been realized, among which can be highlighted the Shaw-type methods (Shaw, 1974) and the multispecimen protocol (Dekkers and Böhnel, 2006). As an additional advantage over Thellier-type experiments, the Shaw and multispecimen experiments are assumed to be independent of the domain state of the magnetic particles (Biggin and Poidras, 2006; Biggin and Paterson, 2014).

The paleointensity data obtained with the Shaw-type methods are the result of the comparison of the NRM alternating field demagnetization coercivity spectra of the samples with their demagnetization coercivity spectra obtained after the application of a laboratory thermal remanent magnetization (TRM1) (Shaw, 1974). Alterations caused by the laboratory heating are estimated by comparing the demagnetization spectra of two anhysteretic remanent magnetizations (ARMs), measured before (ARM1) and after (ARM2) the TRM step (Rolph and Shaw, 1985). The use of ARM is justified because, in many ways, it is analogous to the natural acquisition of TRM in the samples (Dunlop and Özdemir, 2015). To verify the reliability of the experiment and ensure the quality of the paleointensity determination, a second termoremanence (TRM2) and a third ARM (ARM3) with their corresponding demagnetization coercivity spectra measurements are added to the protocol. The comparison of ARM2 vs ARM3 spectra is useful to quantify the trend of chemical alteration in the samples (Tsunakawa and Shaw, 1994; Yamamoto et al., 2003). Although the paleointensity results obtained with the original Shaw protocol are considered

unreliable due to the lack of thermal stability control, recent studies have demonstrated the utility of the Tsunakawa – Shaw protocol to obtain accurate paleointensity determinations (Cromwell et al., 2015; Kitahara et al., 2018; Yamamoto and Yamaoka, 2018).

On the other hand, based on the technique by Hoffman et al. (1989), Dekkers and Böhnel (2006) proposed the so-called multispecimen parallel differential pTRM (MSP) method. The idea behind the MSP protocol is to overprint a portion of the sample's NRM, assumed as a thermoremanence, with a laboratory pTRM induced parallel to the NRM at a definite temperature using different laboratory fields in each specimen. It is therefore accepted, that the final remanence in the specimen is smaller than the NRM when the field used in the laboratory is lower than the EMF strength at which the sample acquired its magnetization, and higher when the laboratory's field is superior to EMF intensity. MSP protocol allows, therefore, a PI estimation with only one heating per sample. The heating temperature is selected according to the mineralogical characteristics of the samples; it should be enough to unblock a considerable portion of the magnetization carriers (> 20%) while keeping the sample below the temperature that produces thermo-chemical alteration. After testing the MSP protocol on samples of different sites (e.g., Michalk et al., 2008; 2010; Böhnel et al., 2009), a constant overestimation of the PI values due to the presence of pseudo-single domain (PSD) and MD particles was detected. To correct the domain state contributions, Fabian and Leonhardt (2010) proposed an extended MSP protocol, which was successfully tested in synthetic samples and has also shown good results in natural samples (e.g., Muxworthy and Taylor, 2011; Tema et al., 2016; Schnepp and Brüggler, 2016; Hervé et al., 2017).

It is important to consider that the analysis of paleointensities for a given site, comparing the results obtained using different methodologies, allows to better constrain the true value of the intensity of the ancient geomagnetic field. Additionally, the concordance of paleointensity determinations obtained from different methods can be considered as a proof of the fidelity of the results (e.g., de Groot et al., 2013; Calvo-Rathert et al., 2016; Morales et al., 2020; Sánchez-Moreno et al., 2021).

In the present work, the comparison of previously published and new paleointensity data of three volcanic structures belonging to the Michoacán-Guanajuato volcanic field (Mexico) is presented. The results were obtained using different paleointensity protocols. The study is accompanied by an exhaustive rock magnetic analysis of the sites sampled to obtain a better understanding of the results. The work carried out allows us to confirm or reject the intensity values previously published for the study sites, increasing the confiability of the data. In addition, the information obtained is useful for the construction of a

regional secular variation curve, as well as to test the effectiveness of different paleointensity methodologies in geological materials of varied compositions.

5.4 Geological context

The center of Mexico is crossed from east to west by a continental volcanic arc known as the Trans-Mexican Volcanic Belt (TMVB). It is formed by the subduction of the Cocos and Rivera plates beneath the North-American plate along the middle American trench (Gómez-Tuena et al., 2005). The area with the highest concentration of volcanic edifices along the TMVB is the Michoacán-Guanajuato Volcanic Field (MGVF), which is composed of more than a thousand volcanic structures dominated by cinder cones and medium-size shields, but which also include maars, domes, fissure lava flows, and two stratovolcanoes (Connor, 1987). The MGVF covers an area of ~40,000 km^2 (Hasenaka and Carmichael, 1985; Ban et al., 1992). Its volcanic activity started in the Early Pliocene (between ~6 or 5 Ma ago; see Guilbaud et al., 2012 and Osorio-Campos et al., 2018) and has continued until the Holocene, forming two volcanoes in the last three hundred years: the Jorullo in AD 1759 – 1774 (Guilbaud et al., 2011) and Paricutín in AD 1943 – 1952 (Luhr et al., 1993), which is indicative of the frequency of volcanic activity in the area.

The three analyzed volcanic structures in the present study are part of the MGVF (Figure 31a). Two of them are cinder cones that emitted a series of lavas and the other one is a fissure lava flow.

Of the three structures, the oldest is Rancho Seco (19°37’03’’ N, 101°28’21’’ W), with a ^{14}C associated age at 30,010 ± 929 years BC (2σ calibrated; Ramírez-Uribe et al., 2019). It is a scoria cone of andesitic composition, constructed during a single eruption in the vicinity of the Pátzcuaro lake (Ramírez-Uribe et al., 2019). Studies of this volcano started in the past decade due to the discovery of thousands of Prehispanic buildings near the edges of several lava flows. This set of ancient constructions has been named the Angamuco City (Bush, 2012). The available data indicates that the site was occupied from the Classic period (AD ~300) to the Spanish conquest (AD 1530) (Cohen, 2016), hence associated with the Tarascan empire (which dominated the western region of Mexico from AD ~1250 to the arrival of the Spaniards) and with their ancestors. Thanks to LiDAR images analysis, the seven lava flows emplaced during the effusive phase of the eruption, which was preceded by the violent Strombolian activity that formed the cinder cone (Figure 31b) were mapped; it has been estimated that the entire eruption lasted between 2 and 6 years (Ramírez-Uribe et al., 2021).

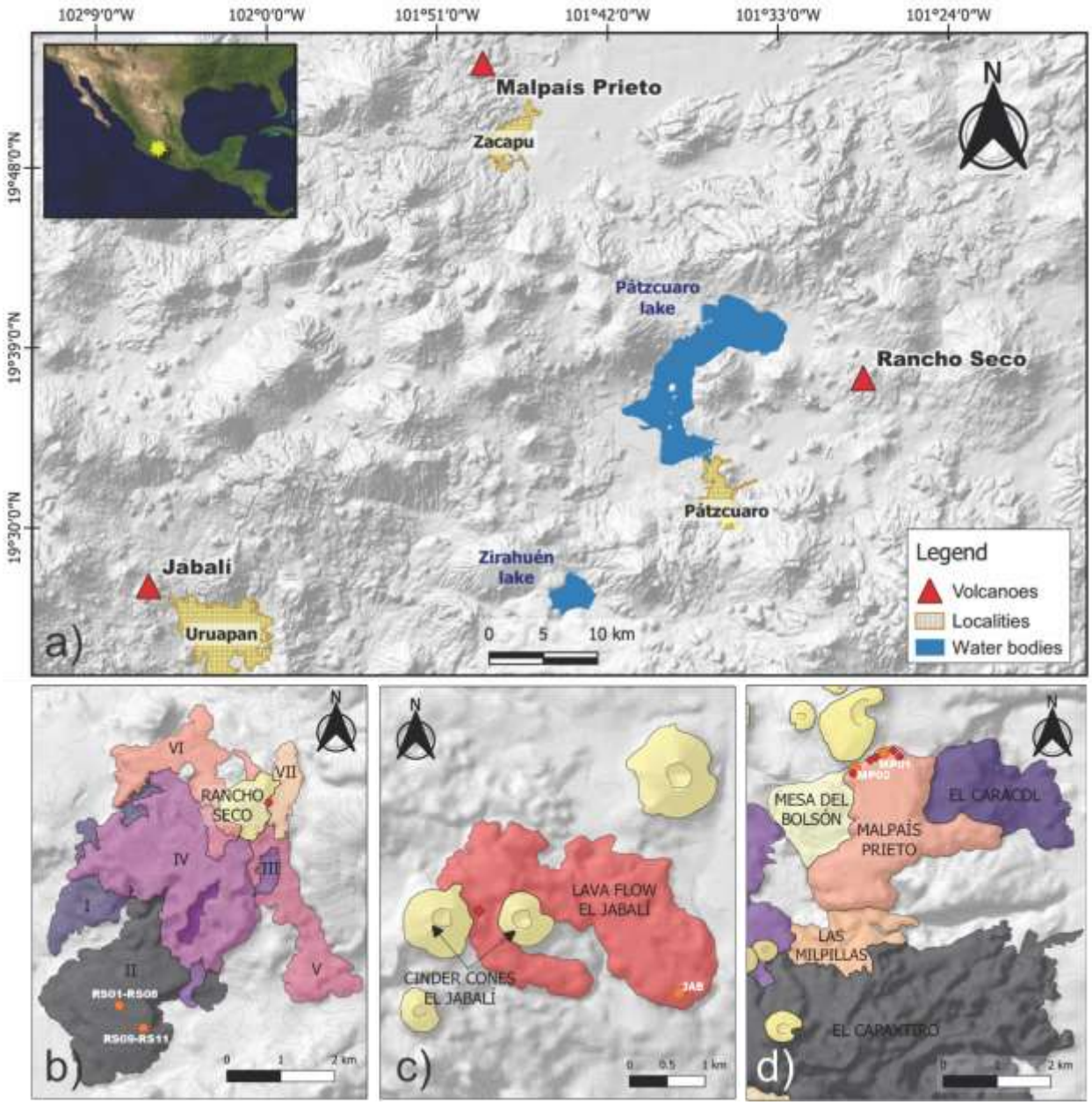

Figure 31 Geology of the study areas. a) General geographic location of the three volcanic structures analyzed in the present study with respect to lakes and current cities (in yellow). b) Geological map of the seven lava flows and the cinder cone of Rancho Seco volcano, modified from Ramírez-Uribe et al., 2021. Orange circles indicate the sampling sites of the present study; the red diamond locates the site sampled by Mahgoub et al. (2019b). c) The two youngest cinder cones and the last emplaced lava flow of El Jabalí cones (see main text for details). The orange circle indicates the site sampled in the present study, the red diamond locates the site sampled by González et al., 1997. d) Northeast sector of the Zacapu Malpaís, modified from Reyes-Guzmán et al., 2018. The sites sampled in the Malpaís Prieto lava flow by the present study are marked with orange circles and, red diamonds correspond to the sites sampled by Mahgoub et al., 2017.

The studied volcano that is intermediate in age is part of the El Jabalí cone cluster (19°27'00"N, 102° 06'08"W). This set of volcanoes is poorly studied and is located at ~7 km northwest of the Uruapan City

center. According to Williams (1950), the cluster is formed by five cinder cones that must have grown in quick succession. The bulk composition of the lavas varies from olivine basalt, for the older ones, to basaltic-andesite for the youngest. Figure 31c shows the last two cinder cones formed during this eruption, with the western one being the most recent and the eastern one being the next oldest. Additionally, the limits of the lava flows associated with the youngest cone are shown. Hasenaka and Carmichael (1985) obtained an age of 2,279 ± 398 BC (2σ calibrated) for this cone, determined from charcoal recovered from a paleosol under ash and lapilli layers associated with this eruption. According to Newton et al. (2005), the Jabalí tephra has been found in lacustrine sediments inside Pátzcuaro and Zirahuén lakes (Figure 31a).

Finally, the youngest studied volcano is the Malpaís Prieto. It is part of the Zacapu Malpaís (19°50'46" N, 101°48'22" W), a set of Pleistocene and Holocene lava flows of mainly andesitic composition (Demant, 1992). In the Zacapu Malpaís have been recognized two eruptive stages by radiometric and paleomagnetic datings (Reyes-Guzmán et al., 2018; Mahgoub et al., 2017). The first stage occurred between ~30,000 and ~21,300 BC and corresponds with the emplacement of Las Cabras, Las Florecitas, Mesa del Bolsón, El Caracol, and Milpillas lava flows. The second stage took place in the Holocene and ended with the eruption of the studied lava (in chronogical order: El Infiernillo, 1492 – 1379 BC; Malpaís las Víboras, 1333 – 1239 BC; El Capaxtiro, 193 – 84 BC; and Malpaís Prieto, AD 829 – 962). The Malpaís Prieto lava flow has a mean thickness of 90 m and covers an area of ~5.7 km2 (Mahgoub et al., 2017). Figure 31d shows the morphology of this lava flow and some of the other surrounding ones that are part of the Zacapu Malpaís. Although evidence of prehispanic human occupations has been found in distinct lava flows of the Zacapu Malpaís (Migeon, 2016), the human settlements discovered in the Malpais Prieto are the largest of the area. This urban trace was named "the lost city" and was occupied during the period AD 1250 – 1450 by those who have been assumed in ethnoarchaeological archives as the ancestors of the founders of the Tarascan empire (Michelet, 2018).

5.5 Sampling methods and sample preparation

For paleomagnetic sampling, two techniques were used: the traditional procedure using a Stihl portable rock coring drill cooled with water, and the so-called "big sample plaster method" of Thellier (1981).

For the Rancho Seco volcano sampling, the big sample plaster method was employed. Once the outcrop portion of interest was selected, a plaster-layer horizontal surface at the top of the sample was created, which was leveled with a non-magnetic flat acrylic surface and a spirit level before the plaster hardened. By using this procedure, a zero-dip sample was created, while the sample's azimuth (North magnetic pole direction, for convenience) was marked at the top of the plaster surface using a magnetic compass. Compared to the conventional core-drilling method, the plaster technique has better precision of the sample orientation in the field (Principe et al., 2004, and references therein). Besides, it allows obtaining enough material to carry out further experimental tests. A total of eleven oriented rock blocks from the south section of the lava flow II (see Figure 31c) were collected, eight for Site 1 (samples RS01 – RS08), and three for Site 2 (samples RS09 – RS11). A collection of photographs from the sampling of the three volcanic structures is shown in Figures S1.1 – S1.3 of Supplementary Material 1. In the laboratory, the oriented blocks were partially embedded into a concrete base to reproduce the in-situ dip and the azimuth recorded in the field. At least 10 standard paleomagnetic sized cubic (1" × 1") and/or cylindrical (1" diameter) specimens per sample were cut in the laboratory.

Also using the big sample method, two blocks were extracted from the Malpaís Prieto lava flow (MP01 and MP02, respectively, see Figure 31d) and one from El Jabalí volcano (see Figure 31c). As in Rancho Seco volcano, a minimum of 10 standard paleomagnetic sized cubic and/or cylindrical specimens per sample were obtained. Additionally, in these two volcanic structures, a traditional sampling was carried out in the field by using a portable rock coring drill. Between 10 and 35 standard-diameter paleomagnetic cores (6–12 cm long) were obtained per sampling site. The paleomagnetic cores were cut into specimens of 2.2 cm in length with the help of an ASC Scientific dual-blade rock saw.

5.6 Laboratory procedures

To characterize the magnetic mineralogy of the samples of the three volcanic structures studied and to select the best protocols to determinate the paleointensity values, four classical rock magnetism experiments were carried out (Isothermal Remanent Magnetization [IRM] curves, hysteresis loops, back-field curves, and magnetization of saturation vs temperature [Ms – T] curves) in representative specimens of each sampling site. The experiments were achieved in the air in a variable field translation balance (VFTB). The IRM and the hysteresis curves were obtained from a zero-field until 0.8 T. For the analysis, the

hysteresis loops were corrected for slope and drift effects. The Ms – T curves were performed from room temperature to 600 °C. Once the rock magnetism experiments were completed, the main magnetization carriers in the samples, their particles size, and their stability after a heating process were determined with the help of the RockMag Analyzer 1.0 software by Leonhardt (2006) and the HystLab MATLAB tool by Paterson et al. (2018).

Because of the low reversibility of the Ms – T curves (see section 5.1 “Rock magnetic behavior”), stepwise susceptibility vs. temperature curves (κ – T) were determined using an AGICO MFK1B Kappabridge equipped with a furnace to establish in a precise way the onset of the chemical alteration of the magnetic minerals caused by the temperature increases in the Rancho Seco samples. The experiments were realized in an inert argon atmosphere. The temperature was increased in a six-step protocol. The curve of the first step was run from room temperature to 350 °C and back. The next five cycles had estimated peak temperatures at 400, 450, 500, 550, and 600 °C, respectively. After each peak temperature step, the temperature was reduced to ~100 °C to detect potential alterations. For data analysis, the Cureval 8.0.2 program of Chadima and Hrouda (2012) was employed.

To isolate the characteristic remanent magnetization (ChRM) of the samples, the stepwise alternating field demagnetization (AFD) laboratory procedure via an AGICO LDA 5 AF demagnetizer was employed. At least six specimens per sample were elected to be treated with the AFD procedure. Maximum fields between 80 and 200 mT (according to the characteristics of the specimens) were necessary to complete the specimen’s demagnetization. The direction and the intensity of the remaining Natural Remanent Magnetization (NRM) at each AFD step were measured with an AGICO JR6 dual-speed spinner magnetometer. The analysis of the directional components of the magnetization recorded in the specimens was accomplished with the Remasoft Windows application by Chadima and Hrouda (2006).

Based on the main characteristics of the magnetic carriers of the samples obtained from the rock magnetism experiments (see section 5.6.1 “Rock magnetic behavior”), it was decided to employ: (1) two Thellier-type methods: the Thellier-Coe (Coe, 1967) and the IZZI (Yu et al., 2004) protocols; (2) the Multispecimen method (MSP-DB) (Dekkers and Böhnel, 2006) in its extended version by Fabian and Leonhardt (2010), which considers domain state (DSC) and fraction (FC) corrections; and (3) the Tsunakawa – Shaw method (Tsunakawa and Shaw, 1994) to determinate the intensity values of the ancient geomagnetic field recorded in the examined volcanic structures. The three types of protocols for paleointensity determinations were carried out using an ASC TD48 Scientific furnace. In addition, for the MSP protocol, a special sample holder that allows aligning the specimen’s NRM with the magnetic field

created into the heating chamber of the laboratory furnace in a parallel way was employed. For the Tsunakawa – Shaw method, an AGICO LDA 5 AF demagnetizer equipped with an anhysteretic / pulse magnetizer unit (PAM1) was also used.

For the Thellier-Coe and the IZZI protocols, thirteen increasing temperature steps were distributed from room temperature to 560 °C with reproducibility better than ±2 °C between two heating runs at the temperature in turns. The laboratory field strength was set to 45.0 ± 0.5 μT. Additionally, partial thermoremanent magnetization (pTRM) checks, every third temperature step, as well as pTRM tail checks (Riisager and Riisager, 2001) at 350 °C and 475 °C were added to the Thellier-Coe protocol. At the end of the Thellier-Coe experiments, three in-field heating at 560 °C were added to assess the cooling rate (CR) effects in the samples. A modification of the method described by Chauvin et al. (2000) was employed (see Morales et al., 2006). For the first and the last heating (TRM1 and TRM3), identical time conditions to those used in the Thellier type protocols steps were applied (cooling time ~ 45 min), while for the middle heating (TRM2) a prolonged cooling time (~ 6 h) was used. Due to the low dependence in the determination of the intensity with the cooling time, see results section 5.6.3.1 Thellier-type experiments, no cooling rate corrections were applied in the samples treated with the IZZI protocol. The IZZI and Thellier-Coe protocols were used in samples of the Jabalí volcano. However, for the paleointensity determinations of the Malpaís Prieto lava flow, only the Thellier-Coe protocol was used due to the scarce availability of the material. For paleointensity determinations, Thellier Tool 4.0 by Leonhardt et al. (2004) was utilized.

Due to the changes in the magnetic mineralogy caused by the temperature increase in the Rancho Seco volcano samples (described in section 5.6.1 Rock magnetic behavior), the MSP protocol was selected for the paleointensity determination of this set of samples. This protocol was also carried out in samples of the Jabalí volcano and Malpaís Prieto lava flow. For the MSP protocol, the samples were heated at different temperatures: 150 °C (specimens of the samples RS01-RS03 and RS08 of Rancho Seco volcano), 220 °C (specimens of the samples RS04-RS07 and RS11 of Rancho Seco volcano), and 525 °C (specimens of the samples RS09 and RS10 of Rancho Seco volcano, MP01 and MP02 of Malpaís Prieto lava flow, and samples of Jabalí volcano) according to the thermal stability of their magnetic minerals established with the help of the Ms - T curves. Following the Fabian and Leonhardt (2010) MSP extended protocol, five steps in each sample were realized; 1) initially the NRM of the specimens was measured; 2) then, the specimens were heated at the selected temperature in a laboratory field (from 10 to 70 μT with field increments of 10 μT) employing the special sample holder to align the specimens; 3) the specimens were

reheated in the same position and with the same temperature as in the preceding step but with the laboratory field direction inverted; 4) the specimens were heated in zero-field and then cooled in the laboratory field; 5) to check thermal stability of the samples, the second step was repeated. As described in section 5.6.2 “Stepwise demagnetization”, the AFD process of Rancho Seco samples is characterized by a multi-component behavior, therefore, before each heating step of the MSP protocol, a demagnetization field between 10 and 40 mT was applied to remove the contributions of the secondary components. Although the cooling rate method could be added to the experimental protocol as in the Thellier-type experiments to assess its effect, different studies suggest that due to the lower temperatures employed for paleointensity determinations in the MSP protocol, the effect could be negligible (see Tema et al., 2015; Calvo-Rathert et al., 2019; Schnepp et al., 2020). Due to the low thermal stability of the analyzed samples, we decided to avoid the application of the cooling rate protocol in order not to add additional heating steps to the experiment that could favor the alteration of the magnetic mineralogy. For paleointensity calculations, the VBA software of Monster et al. (2015) was used.

As can be observed in the discussion of the Rancho Seco volcano paleointensity results (see section 5.6.1), a difference of near to 30 µT between the results obtained in the present work with the MSP protocol, and the results before reported by Mahgoub et al. (2019b) obtained with the IZZI protocol was found. Trying to explain this issue, pilot specimens of the samples RS03, RS05, RS08, and RS10 were treated with the Tsunakawa – Shaw method at different temperatures (200 °C, 300 °C, and 600 °C). The maximum alternating fields applied were 100 mT (RS08), 120 mT (RS03), and 180 mT (RS05 and RS10). The DC field for the ARM acquisition was set to 100 µT. The application of the TRMs was carried out in a magnetic field of 45 µT and the hold time in the first heating was half the time employed in the second heating (20 and 40 minutes, respectively). After these tests, it was established that the only set of specimens with sufficient thermal stability and with the potential to be treated with the Tsunakawa – Shaw method are those corresponding to sample RS08 (at 300°C). Therefore, additional specimens of sample RS08 were treated at 300 °C to obtain a mean paleointensity value. The results obtained for the pilot specimens and the extra RS08 specimens are presented in Table S2.1, and Figure S2.1 of Supplementary Material 2.

5.7 Results

5.7.1 Rock magnetic behavior

Representative IRM curves of the analyzed volcanic structures are presented in Figure 32. To facilitate the visual review of the information, the IRM results are presented in three insets: Figure 32a shows the curves of site 1 of Rancho Seco volcano, Figure 32b displays the results of Rancho Seco volcano site 2, and Figure 32c presents the IRM curves of the Jabalí volcano and Malpaís Prieto lava flow. As can be observed, the samples RS01 – RS07, RS11, and JAB reach a saturation magnetization (Ms) > 95% at fields between 180 and 250 mT, which suggests that the predominant magnetic minerals in samples are of low coercivity like titanomagnetite with low titanium content or magnetite. On the other hand, samples RS08 – RS10, MP01, and MP02 have Ms > 95% at fields upper to 300 mT, suggesting the presence of remanence carriers of major coercivity like hematite. Remanence coercivity (Bcr) values of the samples obtained from the back-field curves (see bottom left of figures 32a-c) indicate similarly the presence of a soft magnetic mineral with values less than 40 mT, except for samples RS10, JAB, and MP01, which are between 60 and 90 mT.

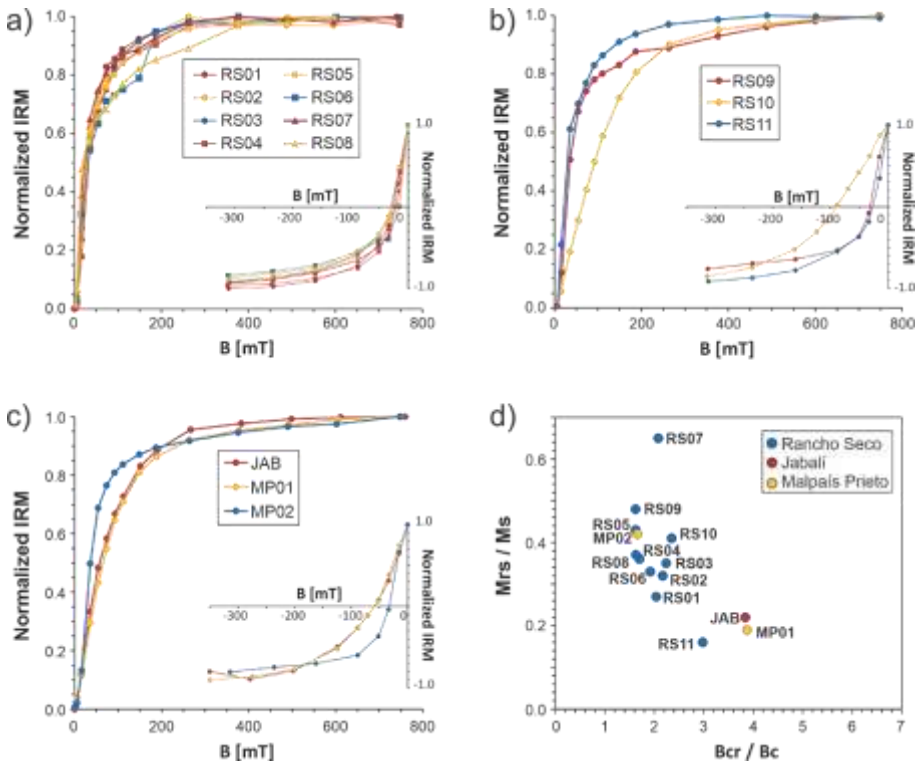

Figure 32 a) – c) Representative Isothermal Remanent Magnetization and back-field IRM curves. d) Samples displayed in a Day plot. RS: Rancho Seco samples; JAB: Jabalí samples; MP: Malpaís Prieto samples.

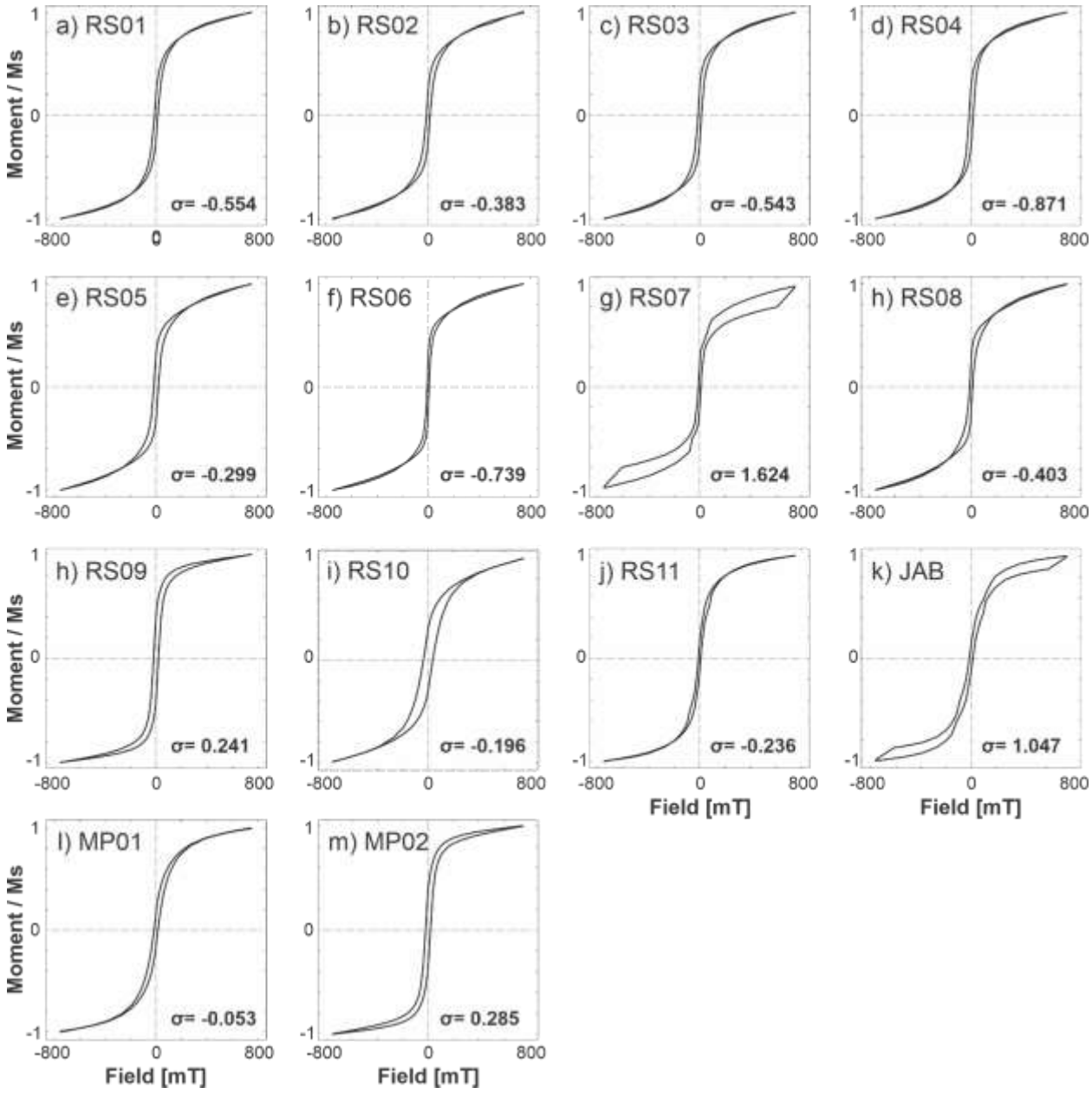

Figure 33 Representative hysteresis loops of the samples of the three analyzed volcanoes. RS: Rancho Seco samples; JAB: Jabalí samples; MP: Malpaís Prieto samples.

Characteristic hysteresis loops are shown in Figure 33. The shape parameter (σ) by Fabian (2003) shows a potbellied behavior (σ < 0) for most of the analyzed samples excluding RS07, RS09, JAB, and MP02, which are defined by a wasp-waisted behavior. The two shapes of hysteresis loops mentioned above can be associated with two different phenomena: 1) mixing in the sample of various grain sizes of magnetic

minerals, where a combination of SD and small superparamagnetic (SP) particles are related to potbellied behavior, while the mixing of SD and large SP grains conduit to a wasp-waisted behavior (Tauxe et al., 1996); or 2) the mixture of magnetic minerals with contrasting mineralogy, for example, the mixture of low coercivity magnetite and high coercivity hematite produce wasp-waisted loops (Frank and Nowaczyk, 2008). Saturation-remanence to saturation-magnetization (Mrs / Ms) and coercivity of remanence to coercivity (Bcr / Bc) ratios were plotted in a Day diagram (Day et al., 1977) to have a first approach to their relations (Figure 32d). In general, it is observed that the samples RS01 – RS06, RS08 – RS10, and MP02 are well grouped within Bcr / Bc values of 1.62 – 2.35 and Mrs / Ms values of 0.27 – 0.48. While samples RS11, JAB, and MP02 exhibit lower values of Mrs / Ms (0.16 – 0.22) and higher values of Bcr / Bc (2.98 – 3.88). Finally, sample RS07 has the higher Mrs / Ms ratio (0.65).

The Ms, Mrs, Bc, Bcr, and σ parameters obtained of the IRM curves, back-field curves, and hysteresis loops for the different analyzed samples can be consulted in Table 12.

Table 12 Results of rock-magnetism experiments. Sample: sample name. Mrs: saturation remanent magnetization; Ms: saturation magnetization; Bc: coercivity; Bcr: coercivity of remanence; σ: shape parameter (Fabian, 2003); TC: Curie Temperature. For sample column; RS: Rancho Seco samples; JAB: Jabalí samples; MP: Malpaís Prieto samples.

Sample	Mrs	Ms	Bc	Bcr	σ	TC (heating curves)				TC (cooling curves)			
	(Am^2/kg)	(Am2/kg)	(mT)	(mT)		1	2	3	4	1	2	3	4
RS01	9.70E-05	3.57E-04	12.86	26.25	-0.554	560	370	130	-	546	-	-	-
RS02	9.30E-05	2.90E-04	13.86	30.02	-0.383	553	315	228	58	503	-	-	-
RS03	8.20E-05	2.37E-04	13.06	29.25	-0.543	478	113	-	-	544	-	-	-
RS04	1.08E-04	2.94E-04	15.86	25.93	-0.871	483	203	-	-	524	-	-	-
RS05	9.30E-05	2.17E-04	18.39	29.80	-0.299	493	183	-	-	513	-	-	-
RS06	1.16E-04	3.47E-04	8.01	15.35	-0.739	223	97	-	-	323	135	-	-
RS07	1.60E-04	2.47E-04	10.42	21.62	1.624	503	293	128	-	523	224	126	-
RS08	1.09E-04	3.03E-04	10.93	18.63	-0.403	206	76	-	-	455	275	115	-
RS09	1.74E-04	3.63E-04	19.36	31.43	0.241	478	367	-	-	489	214	-	-
RS10	7.60E-05	1.84E-04	38.08	89.66	-0.196	503	305	-	-	523	351	-	-
RS11	1.19E-04	7.23E-04	9.07	27.01	-0.236	463	227	-	-	483	-	-	-
JAB	1.15E-04	5.28E-04	15.42	59.27	1.047	518	303	-	-	528	373	-	-
MP01	1.18E-07	6.25E-07	15.22	58.98	-0.053	486	326	86	-	514	344	264	-
MP02	2.07E-07	4.89E-07	19.60	32.61	0.285	486	206	-	-	564	474	234	184

Regarding the Ms – T curves, an irreversible behavior is observed for 7/11 samples of Rancho Seco volcano and the two samples of Malpaís Prieto lava flow (see Figure 34a – 34d). With the help of the Moskowitz method (Moskowitz, 1981) the Curie temperatures (TC) of the samples were calculated. Four distinct behaviors can be recognized for the irreversible samples: 1) Samples RS01 and RS02 exhibits similar behavior with three TC's during the heating (the first of low temperature < 250 °C, the second of medium temperature > 300 °C, and the third of high temperature > 500°C), while during the cooling, only the high-temperature phase is appreciated (Figure 34a). The magnetization value at the end of the cooling curve is ~40% larger than the magnetization value at the beginning of the experiment in both samples. 2) Another group of samples with similar behavior are samples RS03, RS04, RS05, and RS11. This set of samples is characterized by two TC's during the heating, one of ~500 °C and the second between 100 and 200 °C. For the cooling process, only the high-temperature phase is observed (Figure 34b). A difference of 25% – 45% between both magnetizations is observed, being higher after the sample was subjected to high temperatures. 3) Sample RS08 has a high decrease of the magnetization in the first 100 °C during the heating cycle, losing close to 100% of its magnetization. Two TC's are observed in the heating curve, the first at 76 °C and the second at 206 °C. At the cooling process, a high TC phase at 455 °C is created and the two phases observed throughout the heating are maintained (Figure 34c). For sample RS08, no significant differences in the magnetization at the beginning and the end of the experiment were observed. 4) The last two samples with irreversible behavior are MP01 and MP02. As the temperature increases, the magnetic minerals magnetize in both samples up to 250 °C and 350 °C respectively, above these temperatures the magnetization decay. For sample MP01 three TC's were determined for the heating and three for the cooling process (Figure 34d), being higher the temperatures determined for the cooling process (see values in Table 12). Sample MP02 has two TC's heating temperatures at 486 °C and 206 °C, and two more at 560 °C and 180 °C appear during the cooling. The higher magnetization values in the cooling processes could probably be associated with the forming of new magnetic minerals.

Reversible samples RS06 and RS07 have a high decrease of the magnetization at the beginning of the heating process (Figure 34e), like the described for sample RS08. TC's determined for these samples are presented in Table 12. The samples RS09 and RS10 have two TC during the heating and cooling, one of high temperature > 450 °C and the other of medium temperature > 300 °C (Figure 34f). The differences between the magnetizations of both curves are less than 20%. Finally, the sample of the Jabalí volcano is the most reversible of the complete samples set. It has a main TC > 500 °C and a phase of ~350 °C in

heating and cooling curves (Figure 34g). Insignificant differences between the magnetization values of both branches are observed.

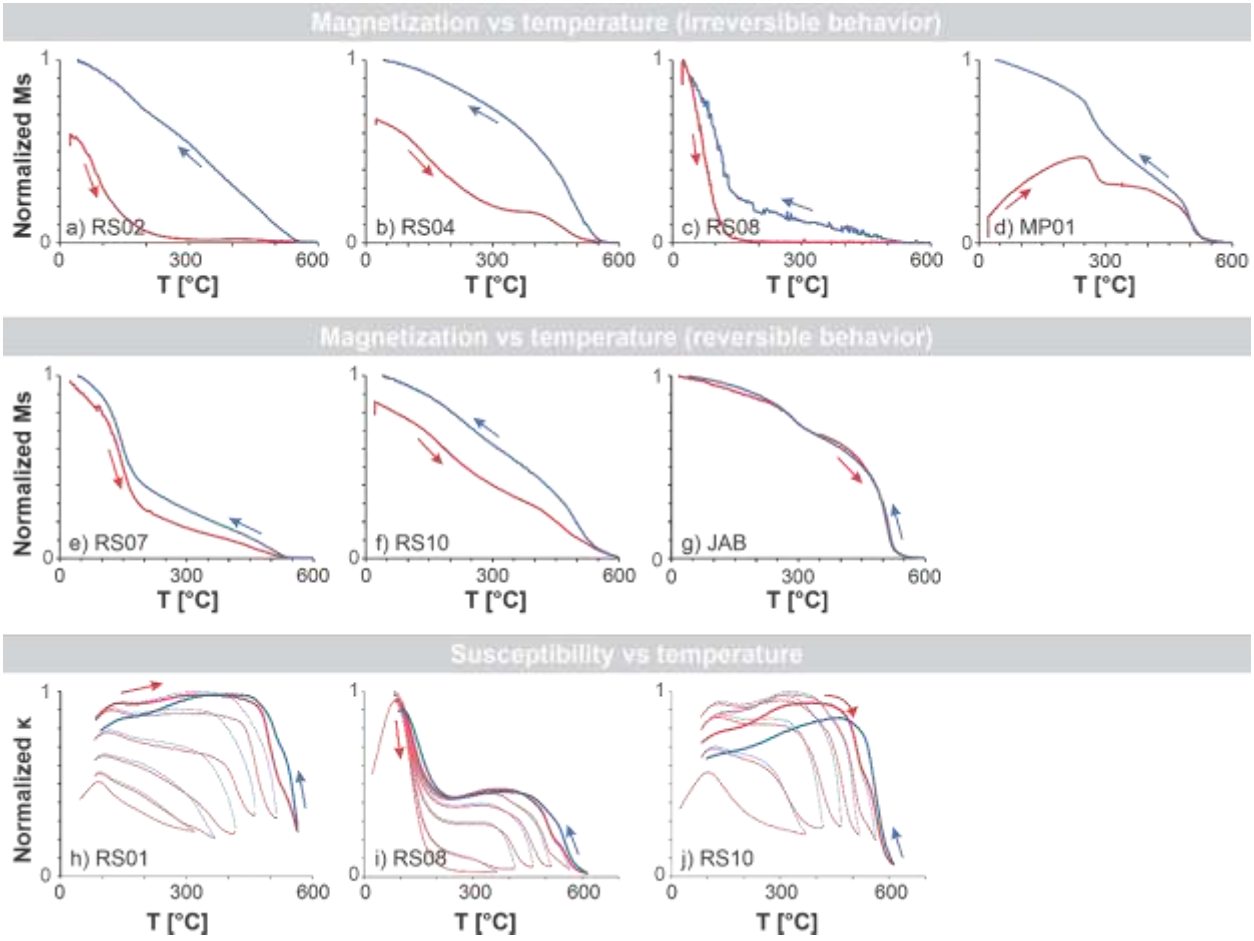

Figure 34 a) – g) Representative thermomagnetic (Ms – T) curves. h) – j) Stepwise low-field susceptibility against temperature (κ – T) curves. RS: Rancho Seco samples; JAB: Jabalí samples; MP: Malpaís Prieto samples.

The highest TC phases (>450 °C) are associated with low Ti-titanomagnetite mineral phases. The medium phases (between 200 – 350 °C) correspond to Ti-rich titanomagnetite phases, while the lowest ones (<150 °C) could be associated with goethite. Curie Temperatures of the analyzed samples are synthesized in Table 12 and representative thermomagnetic and κ - T curves are presented in Figure 34.

To estimate the temperature range at which chemical alteration occurs in the minerals, stepwise low-field κ – T curves were performed. The sample's low thermal stability shows an irreversible behavior in the magnetic mineralogy since the first temperature step (300 °C), which grows as the temperature increases

(Figure 4h-j). On the other hand, it is worth noting that the changes observed in the magnetic susceptibility values of samples RS01 and RS10 show that although an apparent reversibility is observed in the behavior of their magnetic mineralogy at the end of the experiment (600 °C), the susceptibility values are duplicated with respect to their initial values, so the mineralogy observed at the end of the experiment does not correspond to the one originally found in the samples. Even for the RS10 sample after the first heating to 300 °C, an increase of ~50% in its initial susceptibility value regarding the NRM susceptibility value of the sample is observed. Therefore, the reversible behavior observed in the Ms – T curve also could be associated with a mineralogical transformation. It is important to consider these results when performing the analysis of paleointensity values in the experiments based on the use of high temperatures.

5.7.2 Stepwise demagnetization

With the use of principal component analysis (Kirschvink, 1980), three paleomagnetic components were determined in the pilot specimens selected from Rancho Seco volcano (Figures 35a – 35e). The first component is associated with a remanent magnetization of viscous (VRM) origin, this component only affects the magnetic minerals of low coercivity and can be removed at fields between 2 and 10 mT. The magnetic minerals with VRM carry a maximum of 20% of the total magnetization of the samples. The next is a secondary magnetization component which covers the magnetic minerals with coercivity ranges between 10 – 40 mT, after removing the secondary component of the samples, the remaining magnetization has a value between 20 and 40% of the original total magnetization, this percentage is associated with the primary magnetization of the sample, i.e., the magnetization at the formation moment of the samples.

The magnetization components of the samples from the Jabalí volcano and Malpaís Prieto lava flow, are characterized by having a single main component directed to the origin and a weak initial overprint of probably viscus origin, which is removable in maximum fields of 5 mT (Figure 35f – 35h). As can be noted in Figure 5f, the samples for the Jabalí are not fully demagnetized in a 100 mT field; near 30% of the total magnetization of the sample is still present after applying such a field, evidencing the presence of a high coercivity component (e.g., hematite) in the magnetic mineralogy of the samples.

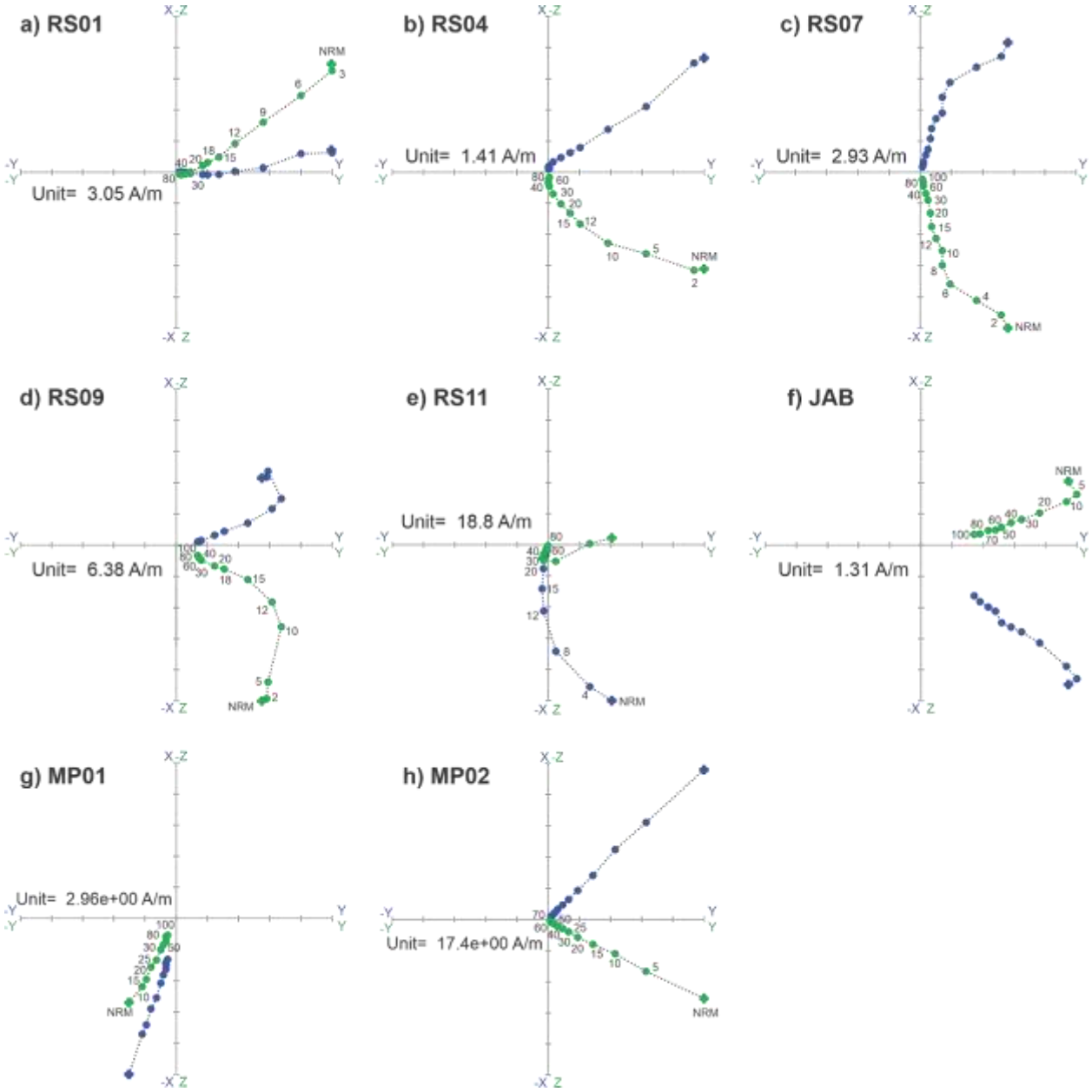

Figure 35 Representative Zijderveld plots (Zijderveld, 1967) of the AFD experiment of samples of the three sites studied. Labels along curves indicate the field applied at the point during the demagnetization process. RS: Rancho Seco samples; JAB: Jabalí samples; MP: Malpaís Prieto samples.

5.7.3 Paleointensities

5.7.3.1 Thellier-type methods

The Thellier-Coe and the IZZI protocols were carried out on a set of samples of the Jabalí volcano and Malpaís Prieto lava flow. Results of these experiments are presented in Table 13 and representative Arai diagrams (Nagata et al., 1963) are shown in Figure 36.

It is worth noting the fact that, for the Jabalí Thellier-Coe experiment shown in Fig. 36a, just under 50% of the remanence remains after at least 560 °C, suggesting a high unblocking component (e.g., hematite) is present. Although fitting is done to a low unblocking component (e.g., magnetite), it could be possible that in this case, the fit for the Thellier-Coe experiment would not fit the ChRM, and the results should be taken with caution. However, the almost undistinguishable corresponding directions estimated gives confidence that this is not an issue here. Likewise, uncoherent results were discarded and are not displayed in the table (e.g., the results obtained for the specimens of MP02 site of Malpaís Prieto, where the Arai diagrams show a curve trend characteristic of samples with dominancy of MD particles, see Figure 36d).

The specimen information was categorized into three groups: “A”, “B”, and “C”, following the criteria set established by Paterson et al., (2014), where the data into the “A” group have the best quality. The threshold values for the parameters of the specimens in category "A" are: $N \geq 5$, $f \geq 0.35$, $\beta \leq 0.10$ (≤ 0.15), $q \geq 5$ (≥ 0), $MAD \leq 6$ (≤ 15), $\alpha \leq 15$, $\delta CK \leq 7$ (≤ 9), $\delta pal \leq 10$ (≤ 18), $\delta TR \leq 10$ (≤ 20), $\delta t^* \leq 9$ (≤ 99). The values marked in parentheses are the threshold values used in the category “B”. For parameters with a single value, the threshold is the same in the "A" and "B" categories. The specimen with parameters values out of the thresholds before established were classified into the “C” category and specimens in this category were not used for the calculation of the mean paleointensity per site.

As an additional selection criterion, the k' parameter by Paterson (Paterson, 2011; Paterson et al., 2015) was employed to quantify the curvature of the specimens in the Arai plot. The curvature was determined employing the MATLAB CircleFitByPratt (XY) function by Chernov (2020), based on Pratt’s method (Pratt, 1987). Paterson suggests two threshold values with different stringency levels to ensure that the k' parameter removes all samples with evidence of MD and large PSD grains effects. The strictest limit value is $k' < 0.164$ and the most relaxed is $k' < 0.270$. Both values were used to classify our data into the “A” and “B” classes respectively.

On the other hand, correction of the paleointensity values by the cooling rate correction factor shows changes of 1.4 to 3.2 % between the magnetization values obtained from the slow and fast cooling. This

implies that the effects of the cooling rate are not significant for the set of samples analyzed in the present study.

Of the 41 results obtained for the two volcanic structures, 16 are into the "A" class, 8 in the "B" class, and 17 were rejected and grouped into "C" class. The failure in the Thellier-type experiments is associated with the presence of a large portion of multidomain grains, evidenced by the curve tendency of the points in the Arai diagrams and quantified with the k' parameter, as well as by the alteration in the magnetic mineralogy of the samples shown by the pTRM checks.

Table 13 Thellier type paleointensity results for Jabalí and Malpaís Prieto volcanoes. $T_{MIN/MAX}$: minimum/maximum temperature; N: number of NRM-pTRM points employed for paleointensity determination; β: Ratio of the standard error of the slope and the slope of the NRM-TRM plot; f: the fraction of NRM utilized; q: quality factor defined by Coe et al. (1978); MAD: Maximum angular deviation of NRM end-point directions at each step acquired during paleointensity experiments; α: the angle between the vector average of the data selected for paleointensity calculation and the principal component of the data (Kissel and Laj, 2004); δ(CK): Difference between the pTRM check and original TRM value at a specified temperature normalized to the TRM; δ(pal): cumulative check error (Leonhardt et al., 2004); δ(t*): normalized pTRM tail (Leonhardt et al., 2004); δ(TR): relative intensity difference in pTRM-tail check; k': curvature parameter (Paterson, 2011; Paterson et al., 2015); Class: A, B, and C, see explanation in the main text; HRAW: raw paleointensity values; σ: standard deviation at specimen level; f_{CRC}: cooling rate correction factor; H_{CORR}: corrected paleointensity values by cooling rate factor; std: standard deviation at site level. Specimens' names and parameters with values out of the limits settled in the B parameters set are underlined, its corresponding paleointensity value was not used for mean intensity calculation.

Site	Name	T_{min}	T_{max}	N	β	f	q	MAD	α	δ(CK)	δ(pal)	δ(t*)	δ(TR)	k'	Class	H_{RAW}	σ	f_{CRC}	H_{CORR}
Jabali Thellier-Coe	99J001A	20	560	14	0.07	0.70	8.1	2.1	5.8	20.0	41.1	1.4	4.8	0.151	C	63.94	4.19	0.982	65.09
	99J003A	20	540	13	0.07	0.36	4.2	2.2	11.0	5.8	7.6	0.0	2.3	0.019	B	50.81	3.64	0.995	51.06
	99J006A	20	565	15	0.07	0.55	4.7	0.7	1.1	4.3	5.6	1.9	2.0	0.283	C	62.47	4.27	1.014	61.61
	99J009A	20	515	12	0.04	0.59	13.5	1.6	4.4	3.3	4.6	1.4	3.5	0.123	A	52.87	1.93	1.000	52.87
	99J012A	20	565	15	0.11	0.32	1.9	3.7	20.1	10.6	36.1	3.6	0.5	0.172	C	66.94	7.67	1.004	66.68
	99J014A	20	500	11	0.04	0.32	5.8	2.2	9.5	4.0	17.9	1.2	2.1	0.181	C	44.70	1.86	1.000	44.70
	99J015A	20	515	12	0.04	0.40	8.1	1.5	5.9	9	18.2	5.3	2.6	0.035	C	52.33	2.12	1.000	52.33
	99J018A	200	515	9	0.03	0.52	15.1	1.3	2.8	1.3	9.0	7.1	1.4	0.051	A	45.30	1.30	1.000	45.30
	99J019A	250	565	11	0.04	0.65	15.6	2.5	5.6	4.9	12.3	4.3	1.7	0.095	B	35.27	1.31	1.000	35.27
	99J020A	200	560	11	0.08	0.77	8.0	1.9	3.9	4.3	8.3	5.3	3.5	0.101	A	40.08	3.24	1.008	39.75
															Mean	**44.87**			**44.85**
															Std	**5.75**			**5.87**
Jabali IZZI	99JA01A	20	410	9	0.05	0.62	8.7	2.8	6.7	2.7	3.7	3.8	2.7	0.377	C	42.54	2.17	1.000	42.54
	99JA02A	20	350	8	0.04	0.34	4.6	1.9	6.2	2.1	7.8	3.0	1.5	0.175	C	50.20	2.19	1.000	50.20
	99JA03A	20	410	9	0.05	0.62	9.3	2.7	6.4	3.3	1.0	5.1	3.4	0.066	A	40.33	2.06	1.000	40.33
	99JA04A	20	475	10	0.11	0.27	1.6	0.9	2.4	5.6	9.5	7.4	5.2	0.057	C	59.37	6.67	1.000	59.37
	99JA05A	240	580	8	0.08	0.90	8.6	1.1	1.1	9.2	12	7.5	6.7	0.163	C	61.38	4.90	1.000	61.38

	99JA06A	20	475	10	0.03	0.31	7.7	1.2	4.7	10.4	42.7	21.6	3.1	0.084	C	60.01	1.81	1.000	60.01
	99JA07A	20	525	11	0.03	0.74	22.3	1.9	3.5	14.7	27.9	3.9	5.2	0.086	C	53.35	1.36	1.000	53.35
	99JA08A	20	475	10	0.07	0.31	3.3	0.9	2.6	8.6	72.5	5.8	3.8	0.098	C	59.85	4.09	1.000	59.85
															Mean	**40.33**			**40.33**
															Std	**-**			**-**
Malpaís Prieto Thellier-Coe	80G001A	200	515	9	0.06	0.53	6.6	2.7	7.4	9.7	38.3	0.5	1.1	0.170	C	42.68	2.71	1.005	42.45
	80G002A	200	540	10	0.08	0.74	7.1	3.7	7.1	6.9	5.7	5.5	1.1	0.080	A	43.31	3.58	0.994	43.56
	80G003A	200	560	11	0.07	0.87	10.5	3.6	4.1	6.8	1.9	3.4	2.1	0.037	A	46.20	3.17	0.993	46.53
	80G004A	150	515	10	0.14	0.66	3.8	3.5	8.3	4.9	8.6	3.8	1.2	0.113	B	40.63	5.79	0.996	40.80
	80G005A	200	560	11	0.07	0.85	10.4	3.0	4.3	5.9	3.0	4.3	0.5	0.141	A	48.97	3.26	1.007	48.64
	80G006A	200	560	11	0.07	0.84	9.5	3.3	3.6	5.2	2.3	2.8	1.6	0.201	B	52.49	3.83	1.001	52.42
	80G008A	400	560	7	0.04	0.82	16.8	2.9	2.7	13.8	23.2	1.3	0.9	0.132	C	54.91	2.09	0.998	55.04
	80G009A	350	560	8	0.09	0.74	6.6	3.4	2.5	17.4	22.8	16.7	10.9	0.331	C	60.42	5.44	0.999	60.46
	80G010A	150	560	12	0.06	0.89	11.8	3.2	3.7	13.1	19.4	2.4	1.0	0.236	C	48.47	3.07	0.999	48.53
	80G011A	150	560	12	0.07	0.91	11.7	4.0	3.7	8.9	9.7	2.8	1.1	0.126	B	47.48	3.14	0.995	47.71
	80G012A	150	560	12	0.07	0.93	11.2	3.1	3.1	5.5	1.4	0.0	0.5	0.043	A	49.36	3.40	0.981	50.30
	80G013A	150	560	12	0.07	0.93	10.3	4.2	3.9	7.7	4.4	2.0	2.4	0.075	B	45.79	3.36	0.990	46.25
	80G014A	20	560	13	0.07	0.97	12.2	3.7	3.9	6.7	4.8	0.0	1.7	0.069	A	45.31	3.03	0.992	45.68
	80G015A	20	560	13	0.07	0.99	11.4	3.7	3.1	7	3.8	0.1	2.0	0.117	B	47.13	3.50	0.978	48.18
	80G016A	450	560	6	0.02	0.82	26.9	1.9	1.4	6.5	1.7	0.0	1.4	0.119	A	54.27	1.26	0.990	54.83
	80G017A	20	560	13	0.06	0.98	14.6	2.6	3.1	6.3	1.9	0.0	0.5	0.112	A	51.36	2.93	0.983	52.27
	80G021A	20	560	13	0.06	0.91	12.8	3.8	5.4	6.1	0.9	1.4	0.6	0.126	A	45.68	2.79	0.984	46.41
	80G022A	400	560	7	0.05	0.75	13.0	2.8	2.4	13.4	10.0	4.0	2.0	0.108	C	53.30	2.50	0.996	53.49
	80G024A	20	560	13	0.08	0.83	9.0	4.3	4.1	4.2	6.3	0.0	1.7	0.092	A	54.66	4.42	1.030	53.05
	80G025A	450	560	6	0.03	0.59	13.6	0.8	0.9	2.5	1.3	2.3	1.1	0.070	A	51.42	1.66	1.029	49.98
	80G046A	150	560	12	0.06	0.86	12.4	1.5	1.4	8.8	7.4	3.2	0.5	0.142	B	50.01	2.86	1.017	49.18
	80G047A	450	560	6	0.04	0.56	12.3	0.9	1.1	6.6	8.4	0.2	0.5	0.098	A	42.86	1.52	1.013	42.32
	80G049A	475	560	5	0.01	0.73	34.9	1.3	0.2	5.8	5.0	0.5	1.6	0.087	A	45.19	0.67	1.033	43.76
															Mean	**47.90**			**47.88**
															Std	**3.26**			**3.10**

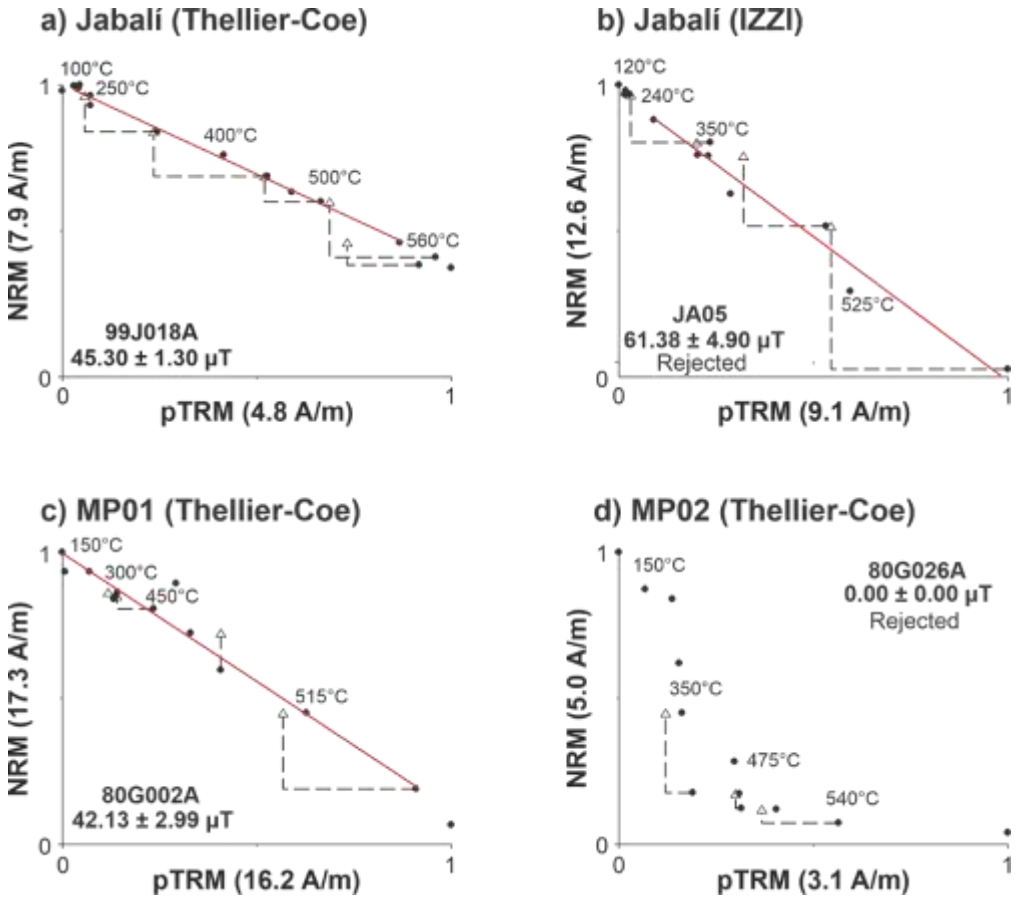

Figure 36 Representative Arai plots (NRM lost vs pTRM gained) for the different studied volcanic structures employing Thellier-type methos for paleointensity determinations. Circles represent the data obtained for each double heating step. Triangles correspond to the pTRM checks. MP: Malpaís Prieto samples.

5.7.3.2 Multispecimen method

Samples from the three volcanic structures analyzed in the present work were processed following the MSP method. For Rancho Seco volcano, one paleointensity value per each one of the eleven samples was calculated; for the Jabalí volcano, two sets of samples were analyzed, one corresponding with the cores sampled in the field (data presented as Jabalí in the "Sample" column of Table 14) and the other with specimens obtained by the big-sampler plaster method (data presented as JAB in the "Sample" column of Table 14); and finally, for the Malpaís Prieto lava flow, one experiment was realized with specimens of MP01 site and another with the specimens of MP02 site.

Table 14. Paleointensity results obtained with the MSP protocol by sample. FLOW: flow name. Multispecimen results. MSP-DBc, MSP-FCc, and MSP-DSCc: alignment-corrected standard, fraction corrected and domain-state corrected multispecimen determination. H: paleointensity result. HMin and HMax: paleointensity determination uncertainty bounds. N(r): number of used and rejected specimens for paleointensity determination. εalt: average alteration parameter. Δb: ordinate axis intercept of the linear fit. R^2: quality of the linear least-squares fit. Data corresponding to the protocol selected for each flow is shown in bold. Parameters with values out of the limits settled into the main text are underlined.

SITE	FLOW	PROTOCOL	H	H_{min}	H_{max}	N(r)	ε_{alt}	Δb	R^2
Rancho Seco	RS02	MSP-DBc	25.8	19.6	34.4	6(0)	-2.0		0.807
	RS02	MSP-FCc	30.2	27.7	31.3	4(2)	-2.9	-0.97	0.954
	RS02	MSP-DSCc	29.0	26.4	30.5	4(2)	-2.9	-1.00	0.954
	RS03	MSP-DBc	57.6	53.3	64.2	8(0)	-2.1		0.932
	RS03	MSP-FCc	55.8	52.6	60.9	8(0)	-2.1	0.05	0.976
	RS03	**MSP-DSCc**	**55.0**	**51.3**	**60.4**	**8(0)**	**-2.1**	**0.07**	**0.966**
	RS05	MSP-DBc	47.6	44.9	50.3	8(2)	-2.6		0.977
	RS05	MSP-FCc	47.7	45.0	50.3	8(2)	-2.6	-0.02	0.975
	RS05	**MSP-DSCc**	**47.7**	**44.9**	**50.9**	**7(3)**	**-1.9**	**-0.02**	**0.974**
	RS08	MSP-DBc	52.2	47.3	55.8	8(2)	-4.8		0.962
	RS08	MSP-FCc	50.9	47.1	55.1	8(2)	-4.8	-0.03	0.965
	RS08	**MSP-DSCc**	**49.9**	**46.0**	**54.1**	**8(2)**	**-4.8**	**-0.01**	**0.964**
	RS09	MSP-DBc	75.7	N.A.	N.A.	5(3)	-2.7		0.994
	RS09	MSP-FCc	75.2	N.A.	N.A.	5(3)	-2.7	0.01	0.993
	RS09	MSP-DSCc	75.2	N.A.	N.A.	5(3)	-2.7	0.01	0.993
	RS10	**MSP-DBc**	**18.4**	**16.8**	**19.9**	**5(3)**	**-7.3**		**0.997**
	RS10	MSP-FCc	19.0	16.6	24.2	5(3)	-7.3	-0.47	0.973
	RS10	MSP-DSCc	17.4	14.9	20.6	5(3)	-7.3	-0.41	0.985
Jabalí	JAB	MSP-DBc	46.7	43.9	48.7	4(3)	-8.3		0.992
	JAB	MSP-FCc	46.9	44.2	48.8	4(3)	-8.3	0.03	0.993
	JAB	**MSP-DSCc**	**46.0**	**42.5**	**48.5**	**4(3)**	**-8.3**	**0.05**	**0.986**
	Jabalí	MSP-DBc	43.5	39.2	50.3	4(3)	-3.4		0.961

	Jabalí	MSP-FCc	42.5	36.5	50.3	5(2)	-3.8	-0.04	0.823
	Jabalí	**MSP-DSCc**	**39.1**	**34.5**	**45.5**	**5(2)**	**-3.8**	**-0.04**	**0.894**
Malpaís Prieto	MP01	MSP-DBc	49.9	46.9	52.1	5(3)	-0.8		0.980
	MP01	MSP-FCc	50.3	48.0	51.8	5(3)	-0.8	0.02	0.987
	MP01	**MSP-DSCc**	**49.9**	**47.3**	**51.7**	**5(3)**	**-0.8**	**0.03**	**0.985**
	MP02	MSP-DBc	38.6	34.2	41.2	4(2)	-7.5		0.960
	MP02	MSP-FCc	37.9	34.2	40.0	4(2)	-7.5	0.05	0.973
	MP02	**MSP-DSCc**	**36.4**	**32.0**	**38.6**	**4(2)**	**-7.5**	**0.06**	**0.970**

To calculate the contribution of the multidomain particles in the extended MSP protocol the α parameter is employed, which ranges from 0 to 1, where zero means no contribution of MD grain effects in the intensity value measured and 1 is the maximum contribution of MD grains. Fabian and Leonhardt (2010) recommend choosing a value of α between 0.2 and 0.8, so that the mean quadratic deviation χ^2 among the site data and the linear fit is minimal. All suggested α values were tested in the VBA software by Monster et al. (2015) for the analyzed samples to achieve the minimal χ^2 value, α = 0.8 was the best election for the samples RS02 and RS10 of Rancho Seco volcano, while the rest of the samples were treated with α = 0.2. As in the Thellier-type methods, a set of criteria was used to select the best paleointensity results. A minimum of 4 specimens per sample were used ($N \geq 4$), the quantity of rejected specimens (r) are also reported in Table 14. The quality of the linear least-squares fit (R^2) should be ≥ 0.85. The maximum average alteration value accepted was 10 ($\varepsilon alt \leq |10|$). For the results of the experiments with fraction correction (FC) and domain state correction (DSC), was verified that the linear fit intersects the ordinate axis through (0, -1) within an error $\Delta b \leq |0.10|$. The best intensity data was selected of the three results obtained by sample (i.e., between the intensity value estimated with the original MSP protocol, the intensity corrected by the fraction of the NRM used, and the intensity corrected by domain state contributions) also considering the alignment correction by Monster et al. (2015), when more than a result for a sample were into the established quality limits, were preferred such results that consider both the fraction and domain state corrections.

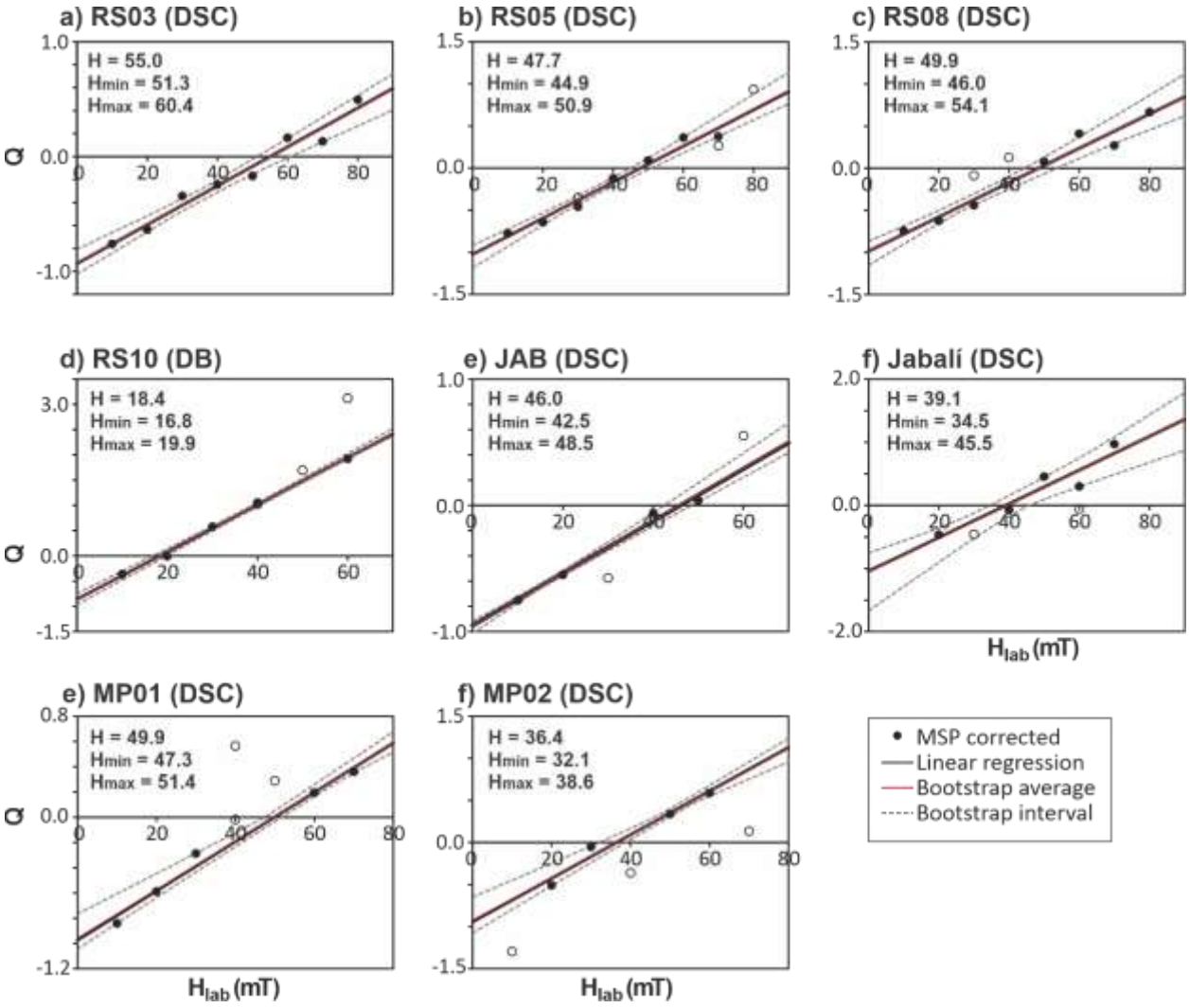

Figure 37 Paleointensity determinations obtained by the MSP method for the different samples of Rancho Seco volcano (RS), Jabalí volcano (JAB), and Malpaís Prieto lava flow (MP), according to the selection parameters established in the main text. The label in parentheses indicates the multispecimen protocol used for paleointensity determination; DB: Dekkers and Böhnel protocol; DSC: Domain state correction protocol.

Coherent results were obtained for 10 of the 15 samples analyzed, six for Rancho Seco volcano, two for the Jabalí volcano, and two for the Malpaís Prieto lava flow. The paleointensity results obtained for the multispecimen method are reported in Table 14. However, the results for samples RS02 and RS09 of Rancho Seco volcano do not meet the established quality criteria and were discarded from the final paleointensity analysis. The plots for the eight successful paleointensity determinations carried out with the multispecimen method are presented in Figure 37. It is important to consider that more than a result per site was obtained, and since all samples coming from the same site are considered contemporary, a single intensity value per site was calculated by averaging the different quality results obtained. Unlike

the results obtained for the Thellier-type experiments, in which a determination of the intensity value of the ancient geomagnetic field per specimen is obtained, in the MSP experiment only one intensity value is determined for a set of specimens (for example, 8 specimens were used to calculate one intensity value of RS08 sample, see Table 14 and Figure 37a). Therefore, the mean intensity values for Malpaís Prieto (43.2 ± 9.6μT) and El Jabalí (42.6 ± 4.9 μT) were obtained by averaging two intensity values for each one (see independent values in Table 14). While for Rancho Seco volcano, 3 intensities were averaged (50.9 ± 2.8 μT, obtained with the intensity values of samples RS03, RS05, and RS08). Since the value obtained for sample RS10 differs considerably from the rest of the values obtained for Rancho Seco, it was not considered for the calculation of the final mean value of the volcano. Mismatches in these values are covered in detail in the discussion.

For a detailed analysis of the paleointensity values, the raw and analyzed data obtained in the present research applying different paleointensity methodologies were placed in a public repository (see Supplementary Material 3).

5.8 Discussion

The application of a multimethodological approach to estimate the paleointensity recorded in a determined geological structure has been of great utility to ensure the quality of the data obtained. Direct tests of the reliability of multimethodological approximates have been carried out in different materials that recorded a known field, for example, the 20th century basaltic lava flows from Iceland presented in Muxworthy and Taylor (2011) and the experimental potteries exposed in Calvo-Rathert et al. (2019). Also, successful research has been carried out in materials for which the intensity of the Earth's magnetic field at the time of its formation or elaboration is unknown; the Xitle volcano in Mexico City is an example. This volcano has been the object of study for more than half a century, the research show discrepancies in the paleointensity values calculated for the lava flows, finding intensity values from ~40 μT (Morales et al., 2001; Alva-Valdivia, 2005) until more than 100 μT (Böhnel et al., 1997) at specimen level. The multimethodological approach carried out by Morales et al. (2020) using the IZZI method, the Thellier-Coe protocol, and the Multispecimen technique allows to determine a restricted intensity value which “help to eliminate the enigmatic character to the Xitle’s lava flows”. Following a similar methodological proposal, based on the use of different paleointensity methodologies, this paper aims to offer reliable

paleointensity values for three structures of the Michoacán-Guanajuato volcanic field, which is still an area with scarce studies. Additionally, the new intensity data obtained are compared with the results previously published in different research for these volcanoes, which also allows an interlaboratory data appraisal. The comparison of paleointensity values is presented in brief form in Figure 38.

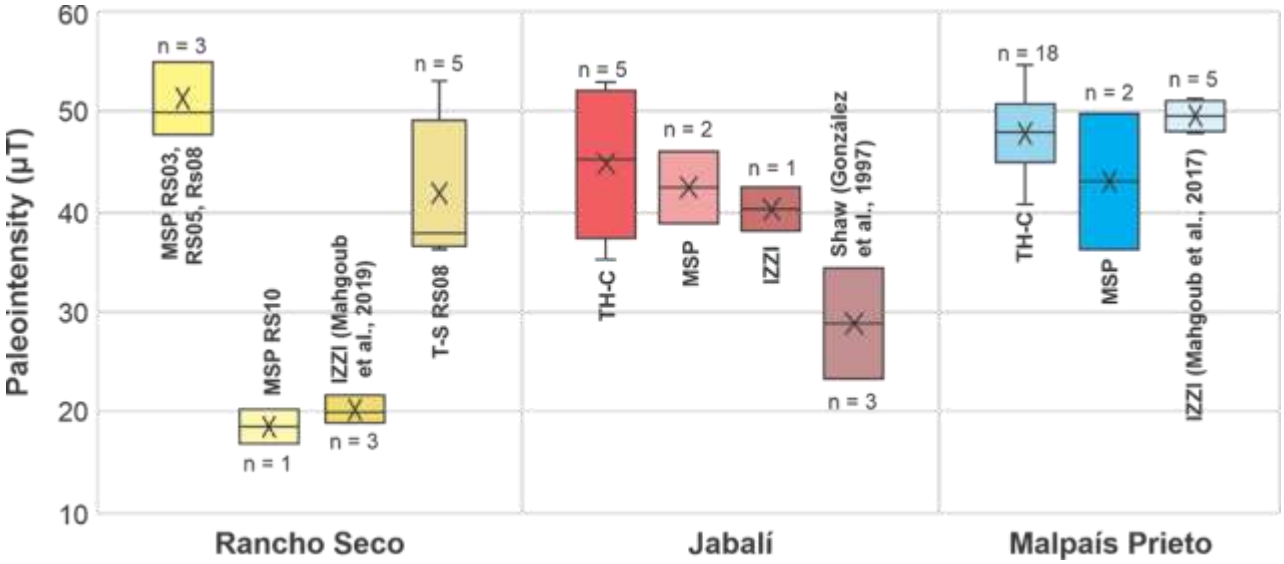

Figure 38 Comparison of the paleointensity values obtained in the present work for Rancho Seco volcano, Jabalí volcano, and Malpaís Prieto lava flow, together with the paleointensities reported in previous research. Whisker plots were graphed using the different intensity values obtained per sample, except for the MSP results of the RS10 sample and IZZI results for Jabalí volcano, for which only one intensity value was obtained per each experiment. The errors of these samples were plotted using the minimum and maximum paleointensity values presented in table 3 for RS10, and the specimen-level standard deviation for the IZZI result. TH-C: Thellier-Coe method; MSP: Multispecimen protocol; T-S: Tsunakawa – Shaw protocol. Previous research references are noted.

5.8.1 Rancho Seco volcano intensities

As was mentioned in section 4. Laboratory procedures, due to the mineralogical characteristics of Rancho Seco, initially only the MSP protocol was tested in the samples taken in the southern lava of this volcano for paleointensity determinations. For samples RS03 (PI = 55.0 μT; min = 51.3 μT; max = 60.4 μT), RS05 (PI = 47.7 μT; min = 44.9 μT; max = 50.9 μT), and RS08 (PI = 49.9 μT; min = 46.0 μT; max = 54.1 μT) similar intensities were estimated, so an average intensity value of 50.9 ± 2.8 μT (n = 3) was calculated for the intensities obtained for the three samples using the MSP protocol with domain state correction. Instead, an intensity value of 18.4 μT (min = 16.8 μT; max = 19.9 μT) was obtained for the sample RS10. The distance

between the outcrop where samples RS03, RS05, and RS08 were obtained and the one corresponding to sample RS10 is less than 1 km, and both outcrops locate in the middle of one of the volcano's lava flows (see Figure 31b). Therefore, the probability that the samples come from different volcanic structures as a possible explanation for the differences in intensity is ruled out.

Between the thresholds established in the selection parameters criteria for the MSP protocol in section 5.6.3.2 Multispecimen method, a value ≤ |0.10| was defined for the ordinate axis intercept of the linear fit parameter (Δb). In sample RS10 the MSP-FC and MSP-DSC protocols exceeded this value (Δb = -0.47; -0.41, respectively), so the intensity value with the best quality was obtained from the MSP-DB protocol. However, although the fraction parameter (f), Δb, and εalt are calculated for the MSP-DSC protocol, these parameters may be also taken to MSP-DB, since it is assumed that the generation process of the errors occurs systematically during the complete experiment (Sanchez-Moreno et al., 2021). Therefore, the Δb ≥ |0.10| of RS10 could indicate an erroneous result for the MSP-DB intensity estimation of this sample. Nevertheless, Mahgoub et al. (2019b), using the IZZI protocol, estimated an intensity value (PI = 20.0 ± 1.4 μT; n = 3) in one of the northern lavas of the volcano (near the cinder cone) comparable to the found in RS10 sample.

Unfortunately, for the temporality of the volcano (30,010 BC), the availability of paleointensity data for materials in the same geographic area (considering a radius of 1200 km to avoid the influence of the non-dipole field components; Thébault et al., 2015) which allows supporting any of the intensity values obtained for Rancho Seco, is limited. Considering a temporal range of ± 1 kyr to the age of Rancho Seco, only two paleointensity data were founded in the literature, both published in Mahgoub et al. (2019b) and obtained using Thellier type experiments (IZZI and TH-C protocols): Cd Serdán (29,700 ± 1100 BC; PI = 31.1 ± 1.5 μT; n = 5), and El Caracol (30,422 ± 1179 BC; PI = 62.8 ± 5.5 μT; n = 3). The age and paleointensity values with their uncertainties for Cd. Serdán, El Caracol, and Rancho Seco (reported in this study and in previous research) are presented in Figure 39 for illustrative purposes.

Figure 39 also shows the regional secular variation curve available for the last 47,000 years (Mahgoub et al., 2019a; 2019b). As can be observed in the enlarged yellow area, when the trend of the intensity data is analyzed using the value reported in Mahgoub et al. (2019b) for Rancho Seco volcano, an abrupt decay of the intensity value of ~40 μT is observed for a period of approximately 400 years, regarding the El Caracol intensity values, to later increase until the intensity values reported for Cd. Serdán.

Due to this abrupt intensity decay, one must be tempted to associate it with the Mono Lake geomagnetic excursion interval (e.g., Korte et al., 2019). However, we note that in the samples analyzed by Mahgoub et al. (2019b), their intensity determinations were carried out from room temperature until a maximum of 460 °C for two specimens and 340 °C for a third one. At these temperatures, the f parameter reaches values between 0.79 and 0.94, which indicates that the major magnetization portion is carried by minerals with medium Curie temperatures; this behavior is like that of the samples analyzed in this study (see Table 1). The use of the low to medium thermal fraction for PI determination in the research by Mahgoub et al. (2019b) could also be associated with the lack of thermal stability of the magnetic mineralogy in the samples at high temperatures, as was evidenced for most of the samples analyzed in the present study. However, no additional information is available to confirm this assumption.

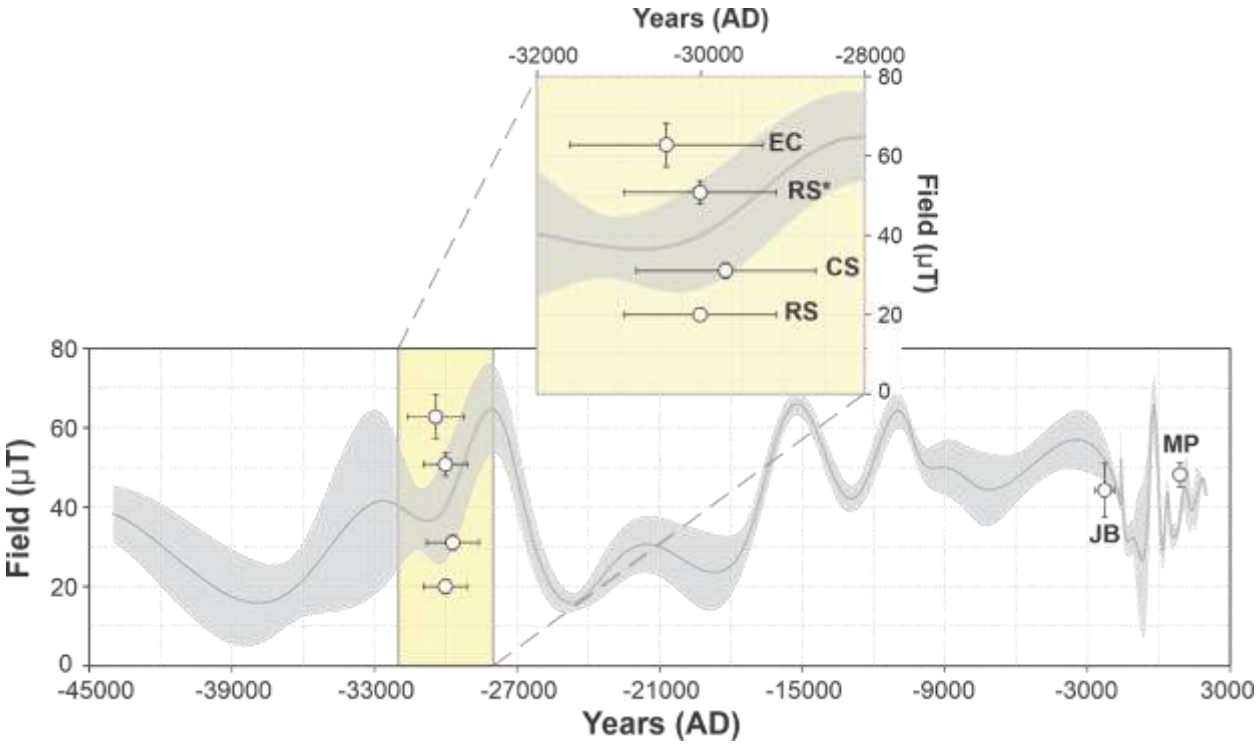

Figure 39 Intensities and age uncertainties of the two volcanoes reported in the literature with similar ages to Rancho Seco in a temporal range of ± 1 kyr. Paleointensity values reported in Mahgoub et al. (2019b): EC: El Caracol, CS: Cd. Serdán, RS: Rancho Seco. Paleointensity values obtained in the present study: RS* Intensity for samples RS03, RS05, and RS08 of Rancho Seco volcano, JB: Jabalí, MP: Malpaís Prieto. Grey line with the shaded area corresponds to the Mexican intensity paleosecular variation curve and its uncertainty for the last AD 47,000 years (Mahgoub et al., 2019a; 2019b).

Instead, when the Rancho Seco intensity value obtained in the present work is used, the secular variation pattern has a constant decay of the intensity value with time. However, only three data were used for an overview of the secular variation pattern over a period of ~1000 years, so conclusive comments cannot be made with the available information until now. It is also important to consider that although the intensity values reported are well constrained for the three sites compared, the uncertainty ages values are large, giving major imprecision to the comparison. The location of the samples taken in the present study and the site sampled in Mahgoub et al. (2019b) is shown in Figure 31b.

At this point, it is important to remember the results obtained from the MS – T curves of the samples from Rancho Seco volcano (see section 5.3.1 Rock magnetic behavior), where apparent reversibility was observed in the magnetic mineralogy of the RS10 sample at high temperatures (Figure 34f). However, the stepwise analysis of the κ - T curves applying increasing temperature steps shows a significant alteration in the mineralogy of the sample since the first heating step to 350 °C (Figure 34j). Accordingly, the low paleointensity values obtained by the IZZI method and by the MSP protocol could be related to an undetected thermal alteration of the sample, and to an unsuitable temperature choice (for RS10 the MSP experiment was carried out at 525 °C), respectively.

The data obtained with the Tsunakawa – Shaw method seem to support this hypothesis. When the samples from the Rancho Seco volcano are heated to temperatures at which their thermal stability is exceeded, their intensity values range between 15.8 and 27.3 μT (See Supplementary Material 2). This intensity range agrees with the results presented by Mahgoub et al. (2019b) and the results obtained in the present work for sample RS10. Additionally, results obtained with the Tsunakawa – Shaw method for the RS08 specimens at 300 °C, in which no significant alteration is observed in the magnetic mineralogy (see Figure 34i), are in good agreement with the results obtained with the MSP protocol for RS03, RS05, and RS08 samples (see Figure 38).

Under this evidence, an average intensity value was estimated employing MSP and Tsunakawa – Shaw results. As proposed by Calvo-Rathert et al. (2016), the weight of each MSP result corresponds to an individual Thellier-type or Tsunakawa - Shaw type data to obtain the average value. Following this proposal, a result of 45.3 ± 6.1 μT is obtained using five Tsunakawa -Shaw determinations and three MSP intensity estimations for Rancho Seco volcano.

5.8.2 Jabalí volcano intensities

The three intensity values estimated in the present study for the Jabalí volcano employing the Thellier-Coe (PI = 44.8 ± 5.9 μT; n = 5), the IZZI (PI = 40.3 ± 2.1 μT; n = 1), and the MSP (PI = 42.6 ± 3.5 μT; n = 2) protocols are in good agreement within their uncertainties, having a lower dispersion in the results obtained with the MSP protocol (see Figure 38). Previously, in the analysis of the secular variation for the last 30,000 years in central Mexico carried out by González et al. (1997), an intensity value for this volcano was obtained using the Shaw method (Shaw, 1974). In their final intensity results table, González et al. (1997) report an intensity value for the volcano of 28.9 ± 5.5 μT using a total of three specimens for the calculous of the mean paleointensity (n = 3), such value shows a difference of more than 10 μT with the values calculated in the present study.

As mentioned earlier (see section 5.1. Introduction), in the Shaw method the intensity is estimated from a comparison of the coercivity spectra of the samples obtained from the AF demagnetization of their NRM, with the coercivity spectra generated after printing them a TRM in a single heating step to the Curie temperature. The alteration of the magnetic mineralogy is monitored by the ratio of two anhysteretic remanent magnetizations (ARM), imparted one before and the other after the heating. However, in the original Shaw protocol (which was used by González et al., 1997) there is no control for the change in the TRM/ARM ratio during the laboratory heating, which may yield inaccurate paleointensity results (Tsunakawa and Shaw, 1994). Furthermore, it is worth noting that the data selection in González et al. (1997) lacks quality criteria, such as those used in the present work (see Supplementary Material 2), so this intensity value was considered unreliable.

A mean paleointensity value of 43.7 ± 5.1 μT (n = 8) was determined with the use of the Thellier-Coe, the IZZI, and MSP-DSC protocols for the Jabalí volcano.

5.8.3 Malpaís Prieto intensities

An optimal result for a multimethodological exercise focused on paleointensity determinations was obtained in the samples of the Malpaís Prieto lava flow, obtaining an excellent agreement between the intensity values got with three distinct methodologies. The volcanic samples were treated in the present

study with the Thellier-Coe and the MSP protocol. Also, these PI results were compared with the intensity obtained by the IZZI protocol in the research of Mahgoub et al. (2017).

The major dispersion is observed in the MSP determination (PI = 43.2 ± 6.8 μT; n = 2), which also reach the lowest paleointensity values. For the Thellier-Coe protocol, an intensity value of 47.9 ± 3.1 μT (n = 18) was obtained, while the most constrained result corresponds to the IZZI protocol (49.6 ± 1.5 μT; n = 5). As in the case of the Jabalí volcano, a mean paleointensity value for the three methodologies employed was estimated. For the determination of the mean intensity using the IZZI protocol (Mahgoub et al., 2017), the acceptance criteria set "A" and "B" proposed in the Thellier tool (Leonhardt et al., 2004) were employed. Such values are similar (although slightly stricter) than employed in the present study for the data selection of the Thellier- type experiments. The five specimens employed to obtain the average intensity in the IZZI method pass the selection criteria here used, so the quality of the results is analogous to that obtained with the Thellier-Coe method. Finally, a mean intensity value of 47.8 ± 3.1 μT (n = 25) was determined by employing three different methodologies for the Malpaís Prieto lava flow.

5.9 Conclusions

The magnetic properties of three volcanic structures belonging to the Michoacán-Guanajuato volcanic field were analyzed in detail and their intensity values were determined using several methods. These paleointensity values were contrasted with those previously published, where the concordance of the intensity values offers excellent quality data for the corresponding site, while the differences obtained by means of several methodologies were discussed.

The samples of Rancho Seco volcano were characterized by the lack of thermal stability, their main magnetization carriers are minerals with Curie temperatures lower than 350°C. During the characterization of the magnetic components of Rancho Seco using alternating field demagnetization experiments, the presence of strong secondary components was discovered, these were eliminated at maximum fields of 40 mT. According to the results obtained from the magnetic characterization of the samples, the MSP and the Tsunakawa – Shaw protocols were used for the determination of paleointensities, which yielded an average intensity value of 45.3 ± 6.1 μT for 3 of the 11 samples analyzed. This value represents more than twice the intensity reported in Mahgoub et al. (2019b) from this volcano (20.0 ± 1.4 μT). Both intensity values have good technical quality, i.e., they meet all the quality criteria

established in the literature to determine an accurate paleointensity value. However, the evidence found in the present work indicates that the low-intensity results could be associated with the alteration of the magnetic mineralogy of the sample caused by the heating in the experiments. When outlining the secular variation for an approximate period of 1000 years with the intensity values of the only two sites in the geomagnetic database with a similar age to the reported for Rancho Seco (30,010 BC), a constant decrease is observed for the trend using the intensity value obtained in the present study.

According to the results obtained for this volcano, it seems that the IZZI protocol does not warn about the changes in the magnetic mineralogy (observed in the κ - T experiments), when it has low thermal stability, giving erroneous results with an underestimation in the intensity values close to 50%.

Successful results were obtained from the comparison of intensity values with two and three different techniques for the Jabalí volcano, and Malpaís Prieto lava flows, respectively.

The samples from the Jabalí volcano showed a completely reversible behavior during the saturation magnetization versus temperature experiments, their component diagrams were characterized by a principal component directed towards the origin. The high Bcr / Bc ratio of their samples indicates the probable dominance of MD grains as the main magnetization carriers. This characteristic is also supported by the zig-zag trend in the points of the Arai diagram obtained with the IZZI method. Therefore, only one successful intensity determination could be performed with this protocol. Also, intensity values within the selected quality parameters could be obtained with the Thellier-Coe and MSP protocols. An average intensity value of 43.7 ± 5.1 μT was established for the Jabalí volcano.

Finally, the best result was obtained for the comparison of Malpaís Prieto lava flow intensities. Both sampled sites (MP01 and MP02) show irreversible behavior in the thermomagnetic curves, however, the pTRM checks show thermal stability during the heating steps of the Thellier-Coe protocol up to temperatures above 500 °C for the specimens of sample MP01. On the other hand, the distribution of points in the Arai diagram of the specimens of the MP02 sample is characterized by a curved trend, associated with the differences in the unblocking and blocking temperatures of the multidomain grains, for which Thellier-Coe intensity results were not obtained from this sample. In this sense, the multispecimen protocol fulfilled its objective of avoiding multidomain effects for a successful determination of paleointensities, and the samples from both sites achieved quality results. Additionally, the IZZI results (with quality comparable to Thellier-Coe results obtained in the present work) reported by Mahgoub et al. (2017) are in good agreement with the two protocols successfully tested in this research.

A mean paleointensity value of 47.8 ± 3.1 μT was established by employing three different methodologies in the Malpaís Prieto lava flow.

In accordance with the results obtained in this study, it is well noted that re-obtaining and/or re-evaluating the intensity data of previously sampled sites (whenever possible, considering for example the variable possibilities of access to the outcrops or the availability of the original measurements data) is an important goal to ensure the quality data. Especially for those samples whose intensities were determined with methodologies that are currently considered unreliable or that were evaluated under quality parameters that can be considered relaxed given the current theoretical development of the matter. An enhanced intensity database from Mexican geological and archeological materials implies the construction of regional secular variation curves with major quality, so the understanding of the Earth's magnetic field behavior and the use of such curves as a dating tool could be done in better terms.

In the present research, two previously published paleointensities were discarded as reliable data due to their inaccuracies and are replaced with new quality data. On the other hand, the quality of one previously published paleointensity data was reaffirmed.

5.10 Supplementary Material 1

Fieldwork record

Figure S1.1 Collection of photographs of the big sample plaster method and the Rancho Seco volcano sampling.

Figure S2.1 Collection of photographs of the Jabalí volcano sampling.

Figure S2.2 Collection of photographs of the Malpaís Prieto lava flow sampling.

5.11 Supplementary Material 2

Tsunakawa – Shaw results

Table S2.1 presents the results obtained by the Tsunakawa – Shaw method performed on samples of Rancho Seco volcano at different temperatures. The technical conditions of the experiment are described in section 4 (Laboratory procedures) of the main text. To classify the data according to their quality, the parameters established in Lloyd et al. (2021) were followed:

1. The linear segment of the paleointensity slope should include the maximum AF step identified as characteristic remanence.
2. The number of alternating field demagnetization steps used for the calculous of the paleointensity (N) ≥ 4.
3. Maximum angular deviation (MAD) $\leq 10°$.
4. The R^2 correlation of the paleointensity slope N (demagnetization spectra NRM/ TRM1*) > 0.990.
5. The complete coercivity spectra of TRM1 and TRM2 is used for the calculous of Slope T.
6. Slope T (demagnetization spectra TRM1/ TRM2*) = 1 ± 0.05 (Class A) and ± 0.10 (Class B).
7. The R^2 correlation of the slope T > 0.990.
8. Fraction of coercivity used in paleointensity determination (fN) ≥ 0.25 (Class A) and ≥ 0.20 (Class B).

Where:

$$\text{TRM1*} = \text{TRM1} \times \frac{\text{ARM0}}{\text{ARM1}} \text{ (Rolph and Shaw, 1985) ……. (1)}$$

and

$$\text{TRM2*} = \text{TRM2} \times \frac{\text{ARM1}}{\text{ARM2}} \text{ (Tsunakawa and Shaw, 1994) ……. (2)}$$

Figure S2.1 shows the procedure realized in one of the specimens for the paleointensity determination.

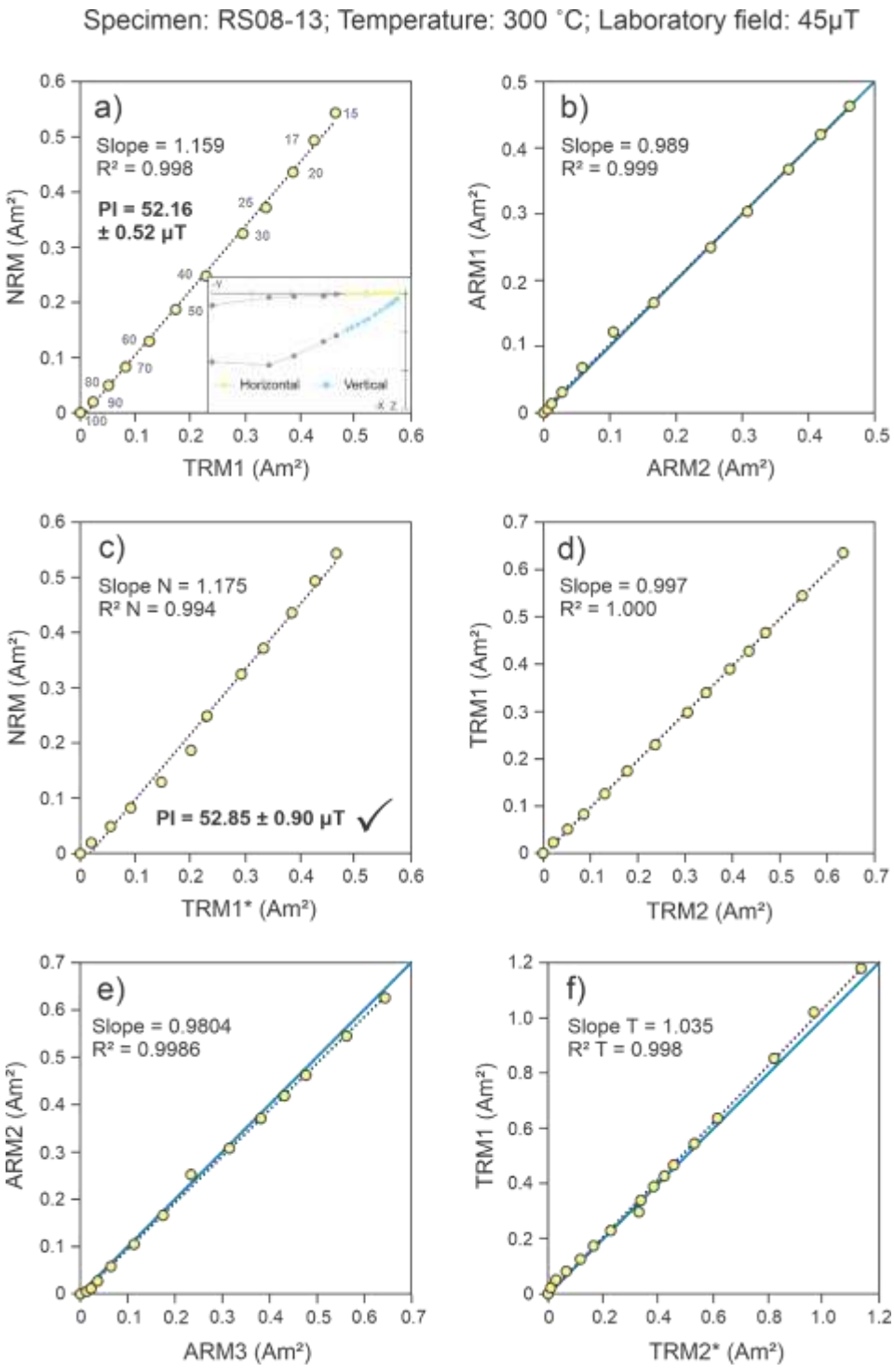

Figure S2.1 Example of data analysis realized for the paleointensity determination with the Tsunakawa – Shaw method. The paleointensity result shown in a) corresponds to the paleointensity estimation with the original Shaw method (Shaw, 1974), while the paleointensity value shown in c) corresponds to the Tsunakawa – Shaw method. Blue lines in b), e), and f) have slope = 1. The dashed lines are the slope line fitted to the paleointensity data. The Zijdelverd diagram in the a) panel represents the demagnetization spectra of the NRM; the yellow and blue dots correspond to the portion of the magnetization used to determine the paleointensity.

Table S2.1 Tsunakawa – Shaw paleointensity results for Rancho Seco samples. N: number of alternating field demagnetization steps used for the paleointensity calculation; f(N): fraction of the coercivity used in the paleointensity determination; MAD: maximum angular deviation; Slope N: slope of the demagnetization spectra NRM/ TRM1* (Yamamoto et al., 2003); R^2 N: correlation of the paleointensity slope N; Slope T: demagnetization spectra TRM1/ TRM2* (Yamamoto et al., 2003). Specimens' names and parameters with values out of the limits settled in the text are underlined, its corresponding paleointensity value was not used for mean intensity calculation.

Sample	Specimen	Temperature (°C)	N	f(N)	MAD (°)	Slope N	R^2 N	Slope T	R^2 T	Class	H
RS03	RS03-12	600	5	0.13	1.0	0.351	0.989	1.022	0.955	C	15.77
	RS03-13	300	7	0.18	1.5	1.015	0.944	1.107	0.997	C	45.67
	RS03-14	200	7	0.16	1.9	2.255	0.969	0.877	0.995	C	101.48
RS05	RS05-12	600	5	0.19	1.1	0.493	0.999	0.784	0.992	C	22.17
	RS05-13	300	5	0.17	1.1	0.606	0.998	0.966	0.998	C	27.28
	RS05-14	200	9	0.37	1.6	1.685	0.976	0.703	0.995	C	75.84
RS08	RS08-12	600	13	0.36	2.1	1.079	0.988	0.969	0.999	C	48.57
	RS08-13	300	12	0.29	1.4	1.175	0.994	1.035	0.998	A	52.85
	RS08-14	200	12	0.29	1.8	1.148	0.998	0.894	0.992	C	51.64
	RS08-15	300	13	0.37	1.4	0.814	1.000	1.072	0.996	B	36.61
	RS08-16	300	12	0.32	1.7	1.006	0.994	1.058	0.996	B	45.29
	RS08-17	300	11	0.29	1.9	0.821	0.993	1.051	0.994	B	36.95
	RS08-18	300	13	0.35	1.9	0.846	0.999	1.057	0.998	B	38.08
RS10	RS10-12	600	10	0.36	0.8	0.387	0.979	1.076	0.995	C	17.42
	RS10-13	300	7	0.28	1.5	4.213	0.988	0.892	0.996	C	189.56
										Mean	**41.96**
										Std	**5.69**

As can be seen from the data presented in Table S2.1, only the experiments carried out at 300 °C achieve results within the thresholds established for the quality parameters. These results are in good agreement with the paleointensity values obtained by the samples RS03, RS05, and RS08 with the multispecimen method (see main text). On the other hand, the samples that show alteration during the first and/or the second heating, have intensity values like those observed for the IZZI protocol and the RS10 sample treated with the multispecimen protocol.

5.12 Supplementary Material 3

Data set for the determination of the paleointensities values recorded in three Mexican Quaternary volcanoes using a multi-methodological approach

Modeling the evolution and variation of the geomagnetic field throughout the history of our planet requires the use of published paleomagnetic information for declination, inclination, and intensity values of the geomagnetic field. However, the fast and constant development of new paleointensity criteria to determine the data quality has led to discarding and/or using with great caution a large amount of the available information. The publication of raw paleointensity data allows overcoming this problem, since when new quality criteria appear in the literature, the raw data can be re-evaluated, thus enhancing the quality of a dataset.

We make available the information of the paleointensity experiments obtained for Rancho Seco volcano, El Jabalí volcano, and Malpaís Prieto lava flow in a public repository. The dataset includes both the raw and the analyzed data, and can be consulted in the following link:

https://data.mendeley.com/datasets/dk6frj4pjg/draft?a=8179a1d8-f2ae-400d-aea4-4fb2cca16579

The repository is made up of three main folders: Rancho Seco, Jabalí, and Malpaís Prieto. Each one contains the information corresponding to the different methods applied to determine the paleointensities of the samples of the three analyzed volcanoes.

The structure followed in the folders of the different paleointensity methods is described below:

1. Thellier Coe experiment / IZZI protocol (folder)

    a) Raw data (folder)

        i. Sample1.tdt (file)
        ii. Sample2.tdt (file)
        iii. Sample3.tdt (file)
        iv. Sample…

The format followed in the TDT files is the one proposed by Leonhardt et al., 2004 for the Thellier-type paleointensity data processing using the ThellierTool4.0 software.

        v. Cooling_rate.jr6 (file)

Files in JR6 format maintain the original structure assigned by the JR6 spinner magnetometer. The name of the specimen treated is indicated in the first column, and the procedure performed on the specimen is indicated in the second one. For details of the procedures performed in each experimental protocol, see section 2. Experiment design, material, and methods.

    b) Analyzed data (folder)

        i. Cooling rate.xls
        ii. Paleointensity_results.xls (file)

The XLS files, Paleointensity_results, contain three sheets. The first one shows the results obtained with the ThellierTool4.0 software, the second one describes the meaning of the parameters shown in the first sheet, and the third one has the threshold values used to establish the data quality.

2. Multispecimen protocol (folder)

    a) Raw data (folder)

        i. Site 1 (folder)
            1. M0.jr6 (file)
            2. M1.jr6 (file)
            3. M2.jr6 (file)
            4. M3.jr6 (file)
            5. M4.jr6 (file)
        ii. Site 2 (folder)
            1. M0.jr6 …

The data contained in M0 – M4 folders is described in detail in section 2. Experimental design, materials, and methods.

    b) Analyzed data (folder)

        i. Site 1.xlsm (file)
        ii. Site 2.xlsm (file)…

The analysis of the MSP data was realized by employing the VBA software by Monster et al. (2015).

3. Tsunakawa – Shaw method (folder)

    a) Raw data

        i. Specimens at 200 °C (folder)
            1. NRM.jr6
            2. ARM1.jr6
            3. TRM1.jr6
            4. ARM2.jr6
            5. TRM2.jr6
            6. ARM3.jr6

        ii. Specimens at 300 °C (folder)
            1. NRM…

        iii. Specimens at 600 °C (folder)
            1. NRM …

The Tsunakawa-Shaw experiments were performed at three different temperatures, and the data obtained were organized according to the temperatures employed in each set of specimens. The six JR6

files contained within each folder of specimens heated to different temperatures encompass information on the six steps involved in the Tsunakawa-Shaw method. For more details see section 2.

b) Analyzed data

i. Specimens at 200°C.xls (file)
ii. Specimens at 300°C.xls (file)
iii. Specimens at 600°C.xls (file)
iv. Paleointensity results.xls (file)

Files i – iii in the Analyzed data folder have the interpreted information from the Tsunakawa-Shaw experiment. The data is separated by the temperature employed for the experiment as in the Raw data folder. In the XLS files, two sections can be observed, the left section contains the processed data, and the right section presents the data in graphs for easy data visualization. Ten graphs per specimen are presented. The first five are useful to determine the intensity value of the sample, and the other five to ensure the stability of the magnetic mineralogy during the experiment.

File iv "Paleointensity results" contains the summary of the intensity values obtained with the Tsunakawa-Shaw protocol (sheet 1), the description of the parameters employed for their classification (sheet 2), and the criteria employed to determine the quality data.

6. Reassessment of the eruptive chronology of El Metate shield volcano (central-western Mexico) based on a comprehensive rock-magnetic, paleomagnetic and multi-approach paleointensity survey

https://doi.org/10.1016/j.quageo.2019.101031

Nayeli Pérez-Rodríguez, Juan Morales, Marie-Noëlle Guilbaud, Avto Goguitchaichvili, Rubén Cejudo-Ruiz, María del Sol Hernández-Bernal

Quaternary Geochronology

6.1 Resumen

Luego de un análisis detallado de las propiedades magnéticas, paleointensidades y paleodirecciones de las rocas obtenidas de siete de los trece flujos de lava que conforman al volcán en escudo "El Metate" (ubicado en el sector centro-occidente de México y reconocido como el volcán más voluminoso emplazado durante el Holoceno en el país), se cuestiona su naturaleza monogenética propuesto anteriormente en investigaciones vulcanológicas y paleomagnéticas.

En los trabajos previos se reconocieron dos etapas eruptivas del volcán diferenciadas por las características geoquímicas de los flujos de lava; durante la primera etapa se emplazaron cuatro flujos de lava (denominados como flujos tempranos), y en la segunda los nueve flujos restantes (flujos tardíos) y un domo. Tales diferencias también fueron apreciables durante el análisis de los datos de los experimentos de magnetismo de rocas. Basados en estas observaciones, se tomó la decisión de tratar los resultados paleomagnéticos dividiéndolos en dos grupos: flujos tempranos y tardíos, respectivamente.

Los valores de paleointensidades se obtuvieron con el método clásico de Thellier-Coe y con el método de múltiples especímenes. Las diferencias en los valores de intensidad dentro de los flujos de lava presentan un comportamiento similar a la tendencia seguida por la curva sintética de intensidad generada con el modelo global SHA.DIF.14k para el período AD 1000 – 1600. Por otro lado, las paleodirecciones de cada conjunto de lavas son estadísticamente diferentes; D = 346,4° e I = 32,1° (N = 34, R = 33,73, k = 121,74, $\alpha 95$ = 2,2) para los flujos tempranos (Flujo 1 - Flujo 3), y D = 359,2° e I = 29,6° (N = 9, R = 8.97, k = 294.6,

α95 = 3.0) para los flujos tardíos (Flujo 6a), lo que sugiere que transcurrió el tiempo suficiente entre las dos etapas eruptivas para registrar la variación secular del campo magnético terrestre en los flujos de lava del volcán. La asociación de edades a los conjuntos de flujos de lava con la ayuda del modelo SHA.DIF.14k sugiere un período sin actividad volcánica de aproximadamente 200 años entre el emplazamiento de las lavas tempranas y tardías, dicho período podría ser menor debido a que no todos los flujos de lava pudieron ser muestreados. Este trabajo demuestra la capacidad de las técnicas paleomagnéticas para analizar la evolución temporal del crecimiento de un volcán.

6.2 Abstract

We study seven out of the thirteen lava flows associated to El Metate shield volcano using paleomagnetic, absolute intensity and rock-magnetic experiments. Characteristic paleomagnetic directions were successfully determined from most of the flows. A combined mean direction of D = 346.4° and I = 32.1° (N = 34, R = 33.73, k = 121.74, α95 = 2.2) was obtained for the early flows (Flow 1 – Flow 3). Flow 6a (a flow from the late emplacement stage) yielded a statistically distinguishable mean paleomagnetic direction of D = 359.2° and I = 29.6° (N = 9, R = 8.97, k = 294.6, α_{95} = 3.0).

Furthermore, the significant between-flow variation of absolute paleointensity values obtained using two different methodologies, which resembles the trend followed by that of the global model SHA. DIF 14k intensity curve for the period 1000 AD 1600 AD, disagrees with previous hypothesis supporting a short emplacement period between 50 and 100 years for the whole sequence. Additionally, paleodirectional and paleointensity dating of the studied flows allowed to refine the eruptive chronology indicating that early flows were produced over a short time period, whereas at least two of the later flows were erupted 200 years later; the activity ending just prior to the arrival of the Spaniards in ~1520. Under these circumstances, and in light of the presented high quality paleomagnetic and paleointensity data, the assumed monogenetic nature of El Metate volcano seems to be questionable.

6.3 Introduction

Evaluation of volcanic hazard for an active area requires an accurate knowledge of the age of the associated lava flows and other volcanic products, which permits a reliable estimation of the eruptive rate

and the probability of occurrence of new eruptions. In the absence of historical records, dating of young structures (<40,000 yr.) is usually done by means of the radiocarbon (^{14}C) method. It requires, however, the existence of charred organic-material which can be, without doubt, related to the volcanic event. Often, this direct association is controversial, and the method may give erroneous results.

Alternatively, magneto-stratigraphy has long been used as a dating method for old rocks by direct correlation of their remanent magnetization with Geomagnetic Polarity Time Scale (GPTS) patterns. For younger rocks, the components of the past Earth's magnetic field (EMF) recorded in the rocks are compared against available paleosecular variation (PSV) curves for the last millennia, similarly to the ^{86}Sr dating method in carbonates (seawater curve). Through this method, it is possible to determine the most probable age of a rock through the combined analysis of the three components that characterize the past EMF (declination, inclination, and intensity).

The availability of detailed PSV, global models, and master curves for the last millennia (e.g., Gallet *et al.,* 2002; Gómez-Paccard *et al.,* 2006; Kovacheva *et al.,* 2009; Hagstrum and Blinman, 2010) has made it possible to apply this methodology for the dating of lava flows emplaced during the last few thousand years. This approach has been used to date lava flows emplaced during the last 10 ky in Mexico (e.g., Pérez-Rodríguez *et al.,* 2015; García-Quintana *et al.,* 2016; Urrutia-Fucugauchi *et al.,* 2016).

Monogenetic volcanoes, the most abundant edifices within a volcanic field, offer 'snapshots' of the direction and intensity of the geomagnetic field present during their formation. They are, however, time-discrete volcanic-rock logs due to the paused emanation of magnetically-recordable material of volcanic activity (Morales *et al.,* 2017). Medium-sized shields volcanoes that are larger than scoria cones but substantially smaller than stratovolcanoes, could provide a broader picture of the changes of the past geomagnetic field than the one offered by monogenetic volcanos due to their likely longer time span and hence polygenetic nature (Tchamabé et al., 2016; De Silva and Lindsay, 2015). Moreover, their multi-event eruption activity, contrary to that of monogenetic edifices, could pose hazards to human settlements established between two consecutive eruptive periods.

Within the ~400 medium-sized volcanoes within the Michoacán- Guanajuato Volcanic Field (MGVF), El Metate, located at the state of Michoacán, is considered as the youngest one, which produced the most voluminous eruption of the Trans-Mexican Volcanic Belt during the Holocene (Chevrel *et al.,* 2016a). Based on radiocarbon dates obtained from two paleosols located below early lava flows, Chevrel *et al.* (2016a) proposed the year AD 1250 as the onset of the eruptive episode of El Metate, which had to be

finished well before the invasion of the Spaniards in the 1520s due to the lack of colonial chronicles. According to this, the emplacement for the thirteen identified lava flows could have extended at the most for 275 years, while based on rheological determinations, a minimum of 35 years is proposed. However, as stated by Chevrel *et al.* (2016a), *"… active andesitic flows of the size of those emitted by El Metate have never been witnessed, which makes it difficult to make interpretations about their emplacement style".* Despite these limitations and the absence of direct exposure of the contact between separate flows, a monogenetic nature (*i.e.,* short time spans between individual effusive events) was proposed for El Metate by Chevrel *et al.* (2016a).

In order to further test the monogenetic nature of El Metate and its young age, Mahgoub *et al.* (2017) undertook a paleomagnetic study of five lava flows from El Metate to check the consistency of their paleomagnetic directions. Their results indicate an emplacement period which ranges in the interval 1150–1290 CE, supporting the hypothesis of Chevrel *et al.* (2016a). We carried out an independent paleomagnetic investigation of seven distinct lava flows from El Metate in order to test the short emplacement period suggested by Mahgoub *et al.* (2017). Differences in the archeomagnetic directions and associated calculated ages between three early flows and one late flow on one hand, and the compatibility of the paleointensity of two of the late flows (Flow 6 and Flow 11) with values for the Colonial period on the other hand, could suggest a two-stage effusive eruptive activity, with a period of relative quiescence between them, which yields an emplacement period for the thirteen flows that is longer than the one suggested by Mahgoub *et al.* (2017).

6.4 Location and geological background

El Metate volcano (19°32'19" N, 101°59'34" W, 2910 m.a.s.l.) is located in the Mexican state of Michoacán, 14 km NNE of Uruapan and 15 km NW of the archeological site of Tingambato (Figure 40). It is situated at the western rim of a plateau known as Meseta Tarasca, in the central part of the Michoacán-Guanajuato Volcanic Field (MGVF). The MGVF is the region of the Trans-Mexican Volcanic Belt (TMVB) with the highest concentration of volcanic vents. They cover an area of 40,000 km^2 and include >1000 small-volume edifices consisting mainly of scoria cones, with fewer lava flows and domes, and rare maar craters.

About 400 medium-sized shields, an extinct stratovolcano (Tancítaro) and a composite volcano (Patamban) are also found (Hasenaka, 1994; Hasenaka and Carmichael, 1985). According to Guilbaud *et al.* (2012), volcanism in the MGVF started ~5 Ma ago and the region is still active, as evidenced by the historic eruptions of Jorullo (1759–1774) and Paricutin (1943–1952).

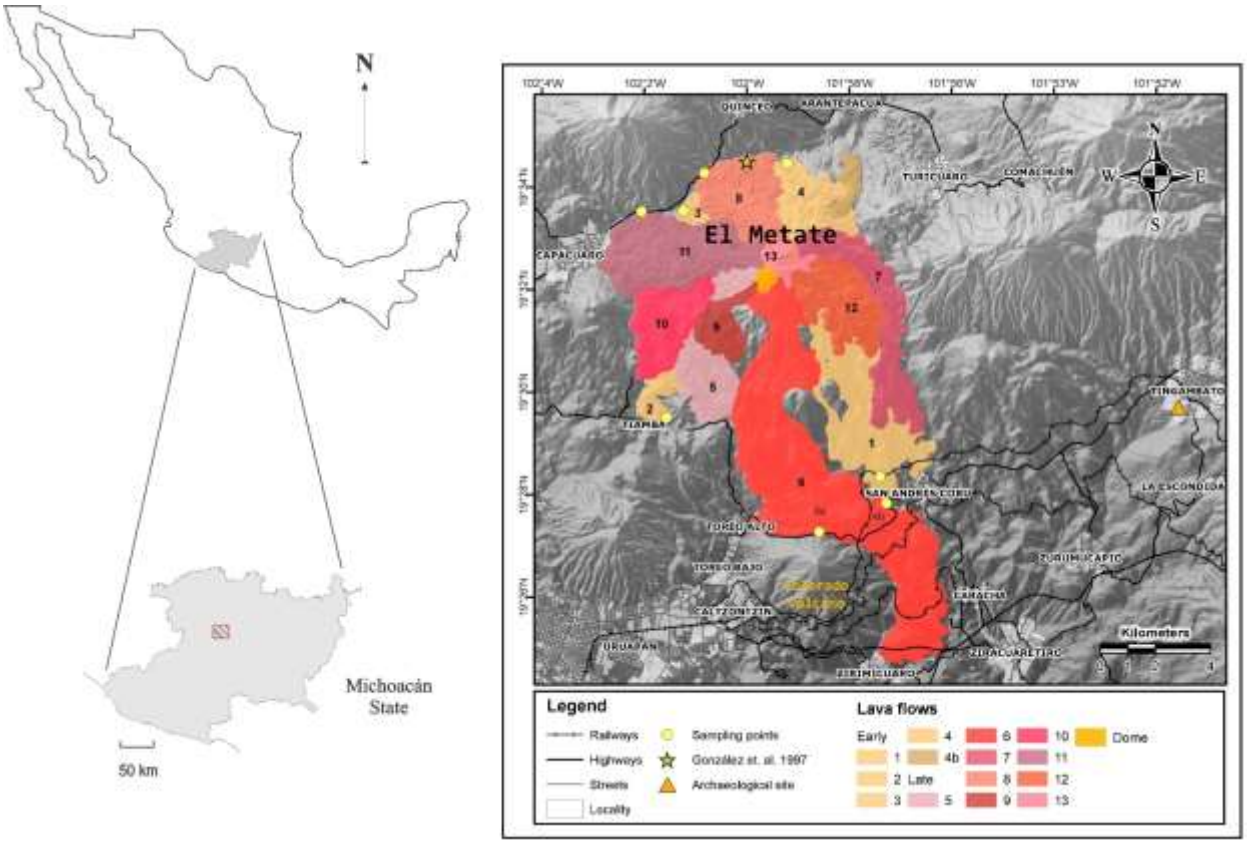

Figure 40 Digital elevation model of El Metate volcano and surroundings with sampling locations. The sequence of flows and their temporal relationship as from Chevrel *et al.,* (2016a).

El Metate displays a remarkably well-preserved morphology and is thus considered as the youngest one of the medium-sized volcanoes, representing the most voluminous eruption in Mexico (*ca.* 9 km^3 in Dense Rock Equivalent) during the Holocene (Chevrel *et al.,* 2016a). The eruption was entirely effusive and produced thirteen distinct lava units that flew radially from the vent (Figure 40, Chevrel *et al.,* 2016a). These lava flows units were separated into early and late ones based on stratigraphy, also corresponding to important differences in surface morphology, bulk chemical composition and mineralogy (Chevrel *et al.,* 2016a, 2016b).

6.5 Materials and sampling

Paleomagnetic sampling of lava flows was carried out in field by using a water-cooled portable gasoline-powered rock coring drill. An average of eight standard-diameter paleomagnetic cores (6–12 cm long) was obtained for each lava flow, which were distributed consistently both horizontally and vertically over the outcrop. Special care was dedicated to sampling only those blocks without evidence of post-emplacement dislodgment. Measurement of the azimuth and dip of in-place cores was carried out by means of a precision core orienting fixture, with coupled magnetic compass. Paired sun-compass orientation was carried out when possible. Paleomagnetic cores from the early eruptive stage – flows 1 to 4, with average thickness at the sampling site of 2, 5, 20 and 25 m respectively – and from the late eruptive stage – flows 6, 8 and 11, and average thickness at the sampling site from 2 to 4 m for the first one (sites F6a and F6b), and 40 and ~100 m respectively for the other two (Figure 40) – were obtained during a couple of field campaigns. Due to the good exposure of outcrops of Flow 6 along the highway, this flow was sampled at two different sites (Flow 6a and Flow 6b). For some sites, oriented blocks were also obtained when short cores and/or a minimum number of them were recovered, from which extra paleomagnetic cores were obtained in the laboratory. In total, 144 paleomagnetic cores were obtained.

6.6 Laboratory procedures

Paleomagnetic cores were cut into standard-dimensions (22 mm long x 25 mm diameter) paleomagnetic specimens with the help of an ASC Scientific dual blade rock saw, obtaining a total of 230 specimens. Rock magnetism experiments in air were carried out to identify the remanence carriers and to evaluate the thermal stability of magnetic mineralogy and the suitability of the material to obtain paleointensity (PI) determinations by using a variable field translation balance (AVFTB) from Magnetic Measurements Ltd. These experiments included: (i) progressive isothermal remanence magnetization (IRM) acquisition curves above 700 mT, (ii) hysteresis loops, (iii) backfield curves and (iv) thermomagnetic curves. Saturation remanent magnetizations (Mrs), saturation magnetizations (Ms) and coercivity fields (Bc) were retrieved after correction for paramagnetic contribution of hysteresis cycles up to ± 0.7 T. Coercivities of remanence (Bcr) were determined by applying progressively increasing backfield after saturation. Thermomagnetic

curves were obtained between room temperature and 600 °C. Analysis of the VFTB data was made using Rock-Mag Analyzer 1.0 (Leonhardt, 2006).

Additionally, detailed stepwise low-field susceptibility vs temperature (κ-T) curves were also obtained under an inert (Ar) atmosphere by means of an AGICO MFK1B Kappabridge with furnace for a precise monitoring of the irreversibility onset with temperature of the thermomagnetic curves. For these experiments a six-step protocol, with an initial temperature of 100 °C and first final temperature of 350 °C, was followed up to a maximum final temperature of 600 °C, with temperature increments of 50 °C. Susceptibility data were analyzed using Cureval 8.0.2 (Chadima and Hrouda, 2012).

Two pilot-specimens per flow (one from the outer and other from the inner part of the flow) were selected for detailed stepwise alternating field (AF). A similar selection of pilot-specimens was carried out for thermal demagnetization. AF demagnetization was carried out at a maximum AF field of 0.1 T by using an AGICO LDA 5 AF demagnetizer, while thermal demagnetization was performed up to a maximum temperature of 600 °C by means of an ASC Scientific TD48-SC furnace. Direction and intensity of the Natural Remanent Magnetization (NRM) remaining after each AF or thermal step was measured using an AGICO JR6 dual speed spinner magnetometer. Analysis of paleomagnetic data acquired during AF/thermal demagnetization procedures was accomplished by using the MS Windows application Remasoft (Chadima and Hrouda, 2006).

Worth of noting is that consistency of results obtained with procedures relying on distinct physical principles can be considered a way to strengthen the reliability of paleointensity determinations (e.g., De Groot *et al.,* 2015; Enterpinar *et al.,* 2016; Monster *et al.,* 2015b; Calvo-Rathert *et al.,* 2016). Accordingly, two different methods were used for absolute paleointensity determination. One set of experiments was carried out using a Thellier-type double heating method (Thellier and Thellier, 1959) as modified by Coe (1967). These experiments were carried out using a Magnetic Measurements Thermal Demagnetizer MMTD80A; heating/cooling runs were performed in air. Ten temperature steps were distributed through the entire temperature range (room temperature to 540 °C) with reproducibility better than 2 °C between two heating runs to the temperature in turn. The laboratory field strength was set to (45.0 ± 0.5) μT. Partial thermoremanent magnetization (pTRM) checks carried out every third temperature step, as well as pTRM tail checks (Riisager and Riisager, 2001) at 350 °C were also added to the protocol. Both natural and laboratory induced remanent magnetizations were measured by means of an AGICO JR6 dual speed spinner magnetometer. Calculations were performed using the ThellierTool4.0 software (Leonhardt *et al.,* 2004).

Bulk magnetic susceptibility of specimens after each double heating step was measured with a Bartington MS2B sensor coupled to a MS3 meter for mineralogic alteration monitoring.

A second set of paleointensity experiments was performed with the multispecimen (MS) method proposed by Dekkers and Böhnel (2006), including the extended protocols for fraction correction (FC) and domain state correction (DSC) proposed by Fabian and Leonhardt (2010). These experiments were carried out using an ASC Scientific TD48-SC furnace using laboratory fields from 10 to 70 μT, with increments of 10 μT, at a temperature of 525 °C. Calculations were performed by means of the VBA software implemented by Monster *et al.* (2015a).

6.7 Results

6.7.1 Rock-magnetic experiments

6.7.1.1 Thermomagnetic (Ms – T) and κ - T curves

We follow the common criteria based on the reversibility of the curves in order to describe the behavior of the magnetization with temperature (Ms-T curves). Three different kinds of behavior were recognized. Type H samples (Flow 1 and Flow 4, Figure 41) showed reversible curves with a single and a composite ferromagnetic phase, respectively, characterized by a high Curie temperature (T_C) close to 575 °C, which matches low-Ti titanomagnetite or slightly Al- or Mg-substituted magnetite. Samples were regarded as fitting this type when the same phases are present in both heating and cooling curves, and the difference between initial and final magnetization (at the beginning and at the end of the experiment, respectively) is within ± 20%.

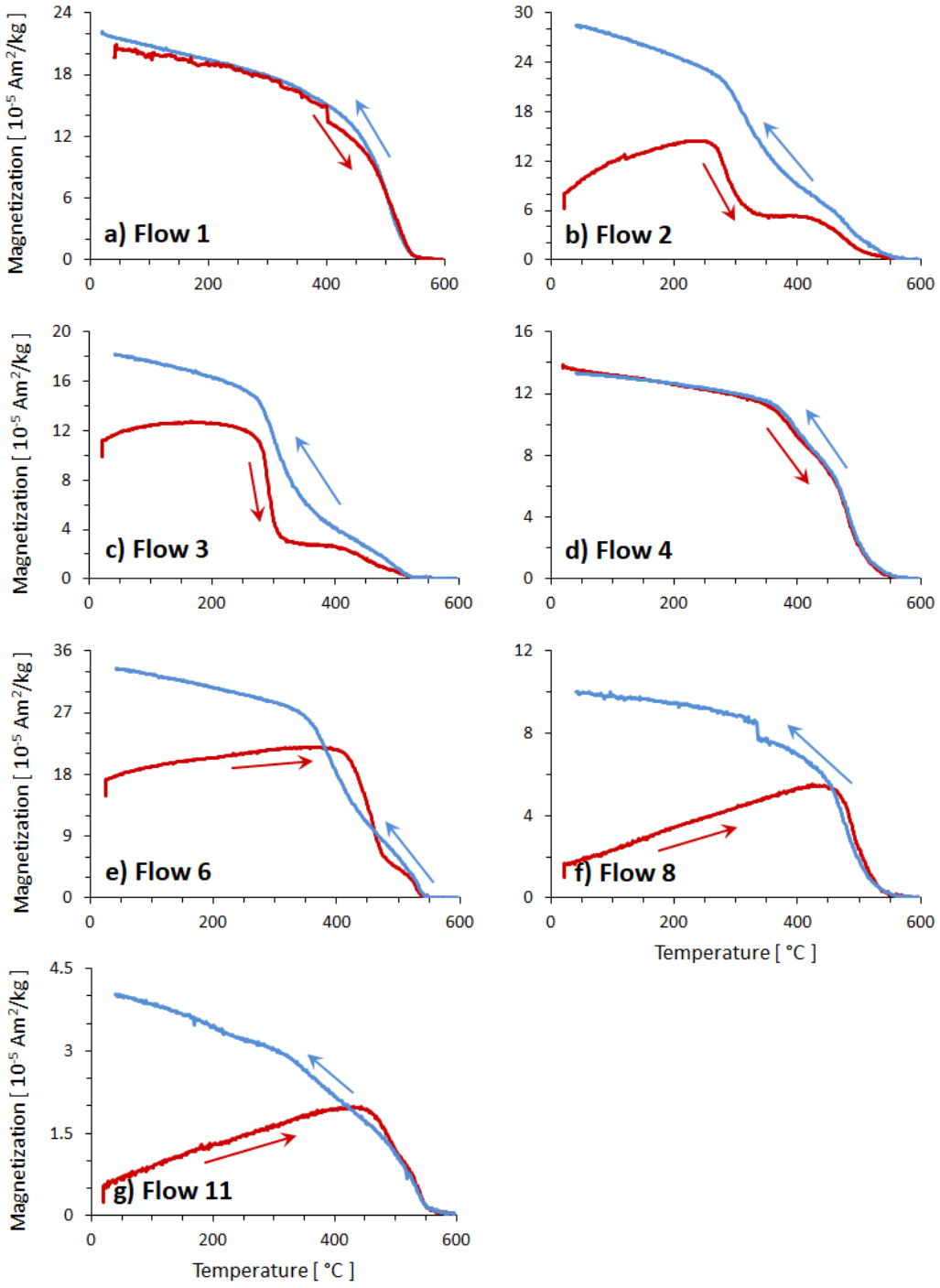

Figure 41 Thermomagnetic (M- T) curves for the different flows studied, showing the variation of magnetization vs temperature.

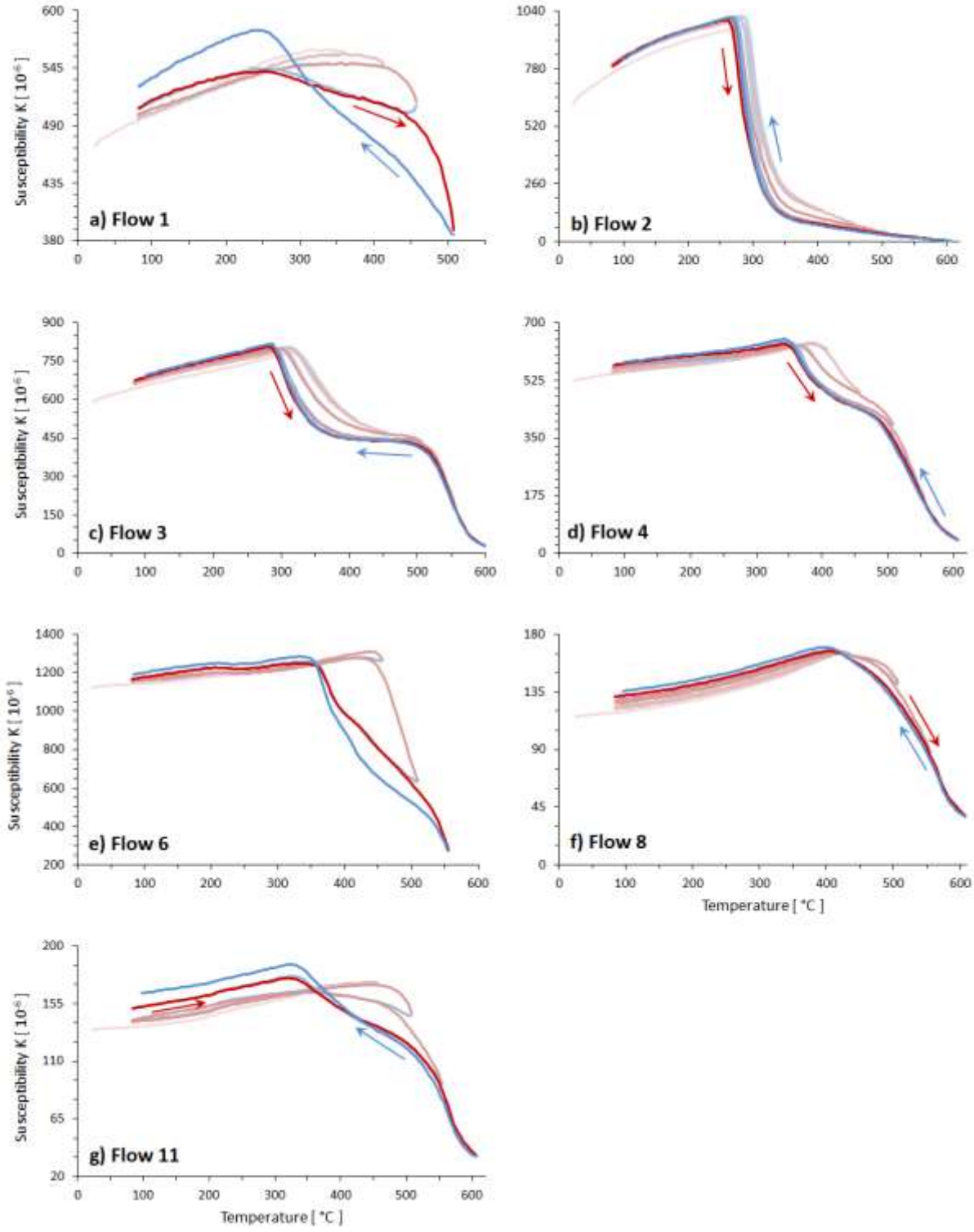

Figure 42 Stepwise low-field susceptibility vs temperature (κ- T) curves for the different flows studied.

Type L samples (Flow 2 and Flow 3, Figure 41) were characterized by irreversible curves with a low T_c (≈300 °C) and a high T_C phase (between 500 °C and 550 °C), in both the heating and the cooling curve. Low T_C phase appeared, however, less pronounced during the cooling. These two distinct phases could correspond to Ti-rich (x ≈ 0.5–0.7) and Ti-poor titanomagnetite, respectively.

Type M samples were also characterized by irreversible curves (Flow 6, Flow 8 and Flow 11, Figure 41), characterized by the presence of an intermediate T_C phase (between 450 °C and 500 °C) and a high T_C phase (between 500 °C and 580 °C) in both curves, which in some cases was accompanied by a very weak magnetite fraction. In the cooling curve a high T_C phase (low-Ti titanomagnetite) and in some cases a low T_C phase were observed.

Knowing the temperature range at which mineral alteration does take place is difficult by just examining the behavior of the Ms-T curves. Stepwise low-field susceptibility vs temperature (κ-T) curves are an alternative rock-magnetic tool suitable for this purpose. κ-T curves of Type H samples (Flow 1 and Flow 4, Figure 42 a & d) reveal the mineralogical alteration of these samples, not revealed by Ms-T curves, even under an inert (Ar) atmosphere, as well as the presence of two phases for Flow 4. Visible alteration appears to start at intermediate temperatures, between 400 °C and 500 °C. In the case of the Flow 1 sample, phase transformation does take place and the difference between initial and final magnetization can exceed 20%. Flow 4 sample behavior closely follows a reversible curve, except from a slightly alteration at ≈ 450 °C. Type L samples (Flow 2 and Flow 3, Figure 42 b & c), that have a two-phases magnetic mineralogy, display almost reversible curves under inert atmosphere conditions. A slight alteration appears at intermediate temperatures (400–500 °C). As expected, the curves obtained for Type M samples (Figure 46 e-g) are not as irreversible under the Ar atmosphere as in air. Mineral alteration takes place at intermediate temperatures (450–500 °C). While samples regarded as type H are the most suitable for PI determination experiments, only two samples belong to this type, and dealing with type L and type M samples is hence inevitable. Nonetheless, based on the magnetic mineralogy and their thermal stability on the one hand, and since mineral alteration occurs at high temperatures (above 450 °C) on the other hand, all 7 flows can be considered as suitable for paleodirectional and paleointensity determinations below alteration temperature.

6.7.1.2 IRM and hysteresis curves

As seen from the isothermal remanence magnetization (IRM) acquisition curves (Figure 43), most early flow samples reach saturation at fields between 270 and 480 mT, which suggests the dominance of medium coercivity slightly Al, Mg or Ti-substituted magnetite minerals of single domain (SD) and/or pseudo single domain (PSD) grain size. Sample from Flow 2, however, reached saturation at ~500 mT. Late flow samples reached saturation at fields close to 500 mT, pointing to high-coercivity minerals, like SD magnetite or hematite, as the carriers of remanence.

On the other hand, all samples present a pot-bellied shape, with different values of the paramagnetic contribution. Saturation magnetization Ms for early flows ranges from 5.2 to 9.2×10^{-4} Am^2kg^{-1}, in comparison with the range for late flows from 1.4 to 3.5×10^{-4} Am^2kg^{-1}. One exception is the sample coming from late Flow 6, which shows a higher Ms of 1.5×10^{-3} Am^2kg^{-1}.

In summary, dissimilar magnetic mineralogy – the dominant remanence carriers – between early and late lava flows are observed, but similar between lava flows coming from the same effusive event.

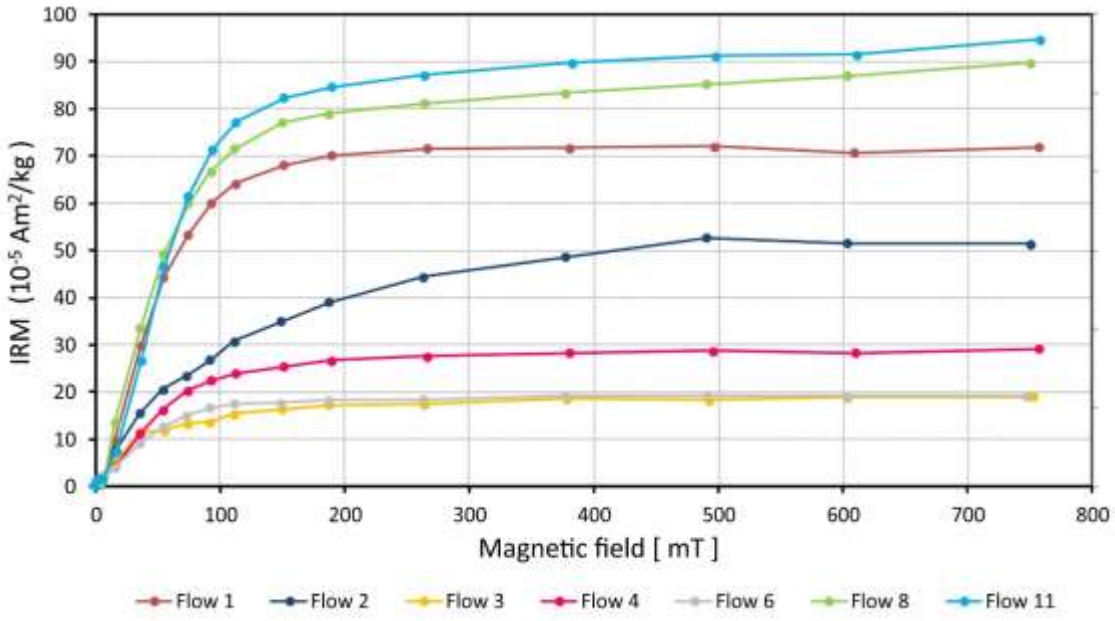

Figure 43 Representative examples of isothermal remanent magnetization (IRM) acquisition curves for the seven flows sampled.

6.7.2 Paleodirections

In all flows, samples display mainly a single main paleomagnetic component, frequently accompanied with an initial weak overprint, which could be removed at fields/temperatures below 10 mT / 300 °C (Figures 44 & 45). Table 16 reports the mean ChRM directions after correcting for the local declination value. Mean ChRM directions obtained for early flows (Flows 1 to 3) are well constrained and similar (Figure 46 a – c). Site-mean direction of Flow 4 is, however, slightly different from the previous flows (Figure 46 d), particularly for the inclination, which shows a steeper value of ~50°. We attribute such difference to the tilting of blocks at the front flow (thickness ~25 m at the sampling site) after their solidification, although no clear evidence of this was noticed at the field.

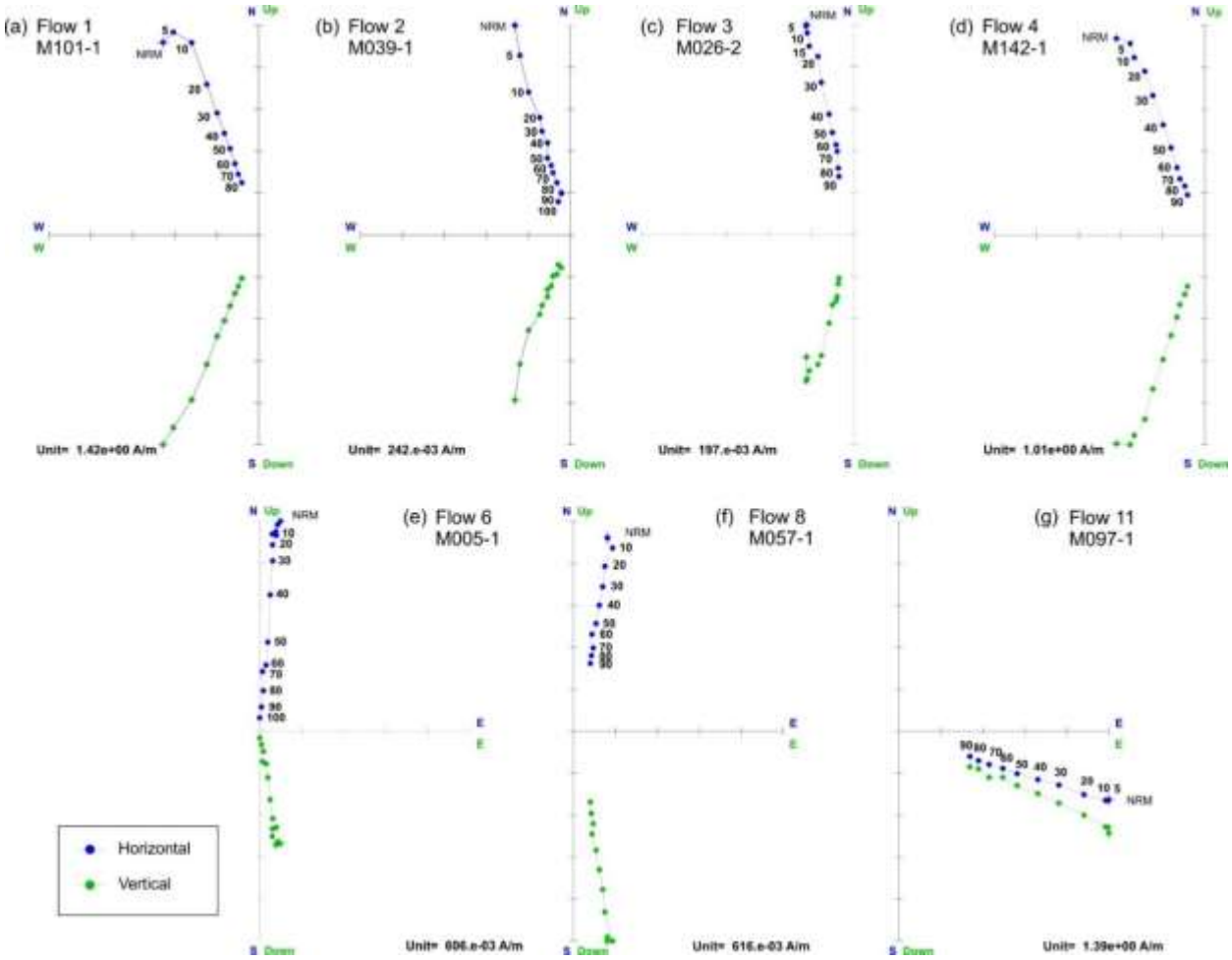

Figure 44 Representative Zijderveld plots of AF demagnetized samples from the studied lava flows. Labels along curves denote the maximum AF amplitude applied during the demagnetization process.

Table 15 Site-mean ChRM directions for the seven studied flows from El Metate volcano, and corresponding site coordinates; N, number of samples used for calculation of site-mean direction; Dec, declination; Inc, inclination; R, unit vector sum; k, precision parameter; α_{95}, radius of 95% confidence cone. Data in italics correspond to those blocks which likely experienced post-cooling tilting (Flow 4) or a combination of tilting plus a clockwise (Flow 8 and Flow 11) or anticlockwise (Flow 6b) rotation.

Site	Lat N	Long W	N	Dec (°)	Inc (°)	R	k	α_{95}
Flow 1	19°28.363’	101°57.398’	15	347.2	30.7	14.86	97.85	3.9
Flow 2	19°29.371’	102°01.678’	7	344.4	31.9	6.97	199.23	4.3
Flow 3	19°33.414’	102°01.293’	13	346.6	34.6	12.90	118.12	3.8
Flow 4	19°34.679’	101°59.687	12	337.1	49.3	11.97	300.46	2.4
Flow 6a	19°27.270’	101°58.608’	9	359.2	29.6	8.97	294.60	3.0
Flow 6b	19°27.688’	101°57.145’	8	329.2	48.9	7.83	42.06	8.6
Flow 8	19°34.285’	102°00.840’	7	14.3	46.7	6.99	533.67	2.6
Flow 11	19°33.523’	102°02.084’	9	113.5	36.3	8.91	93.74	5.3

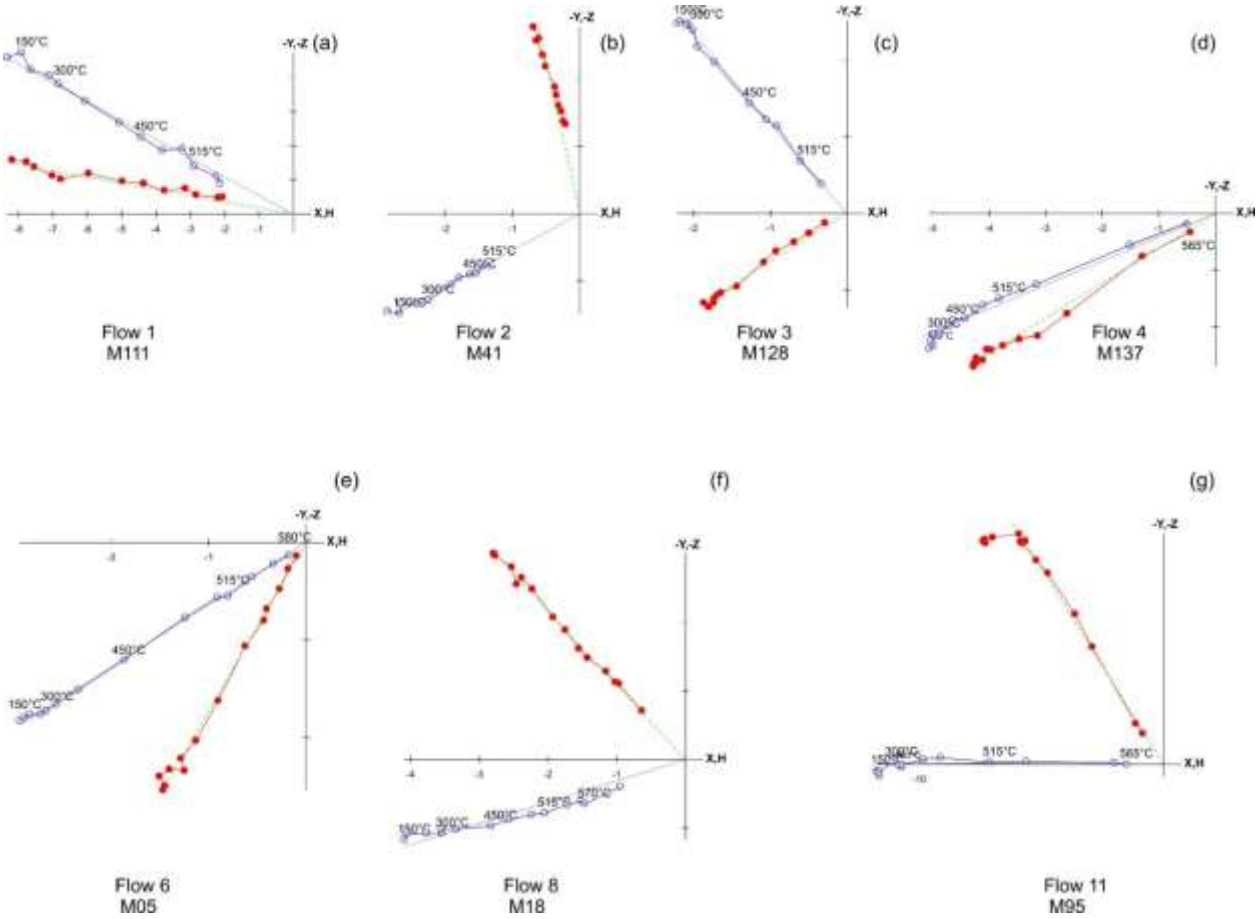

Figure 45 Representative Zijderveld plots of thermal demagnetized samples from the studied lava flows. Labels along curves denote the temperature steps during the demagnetization process.

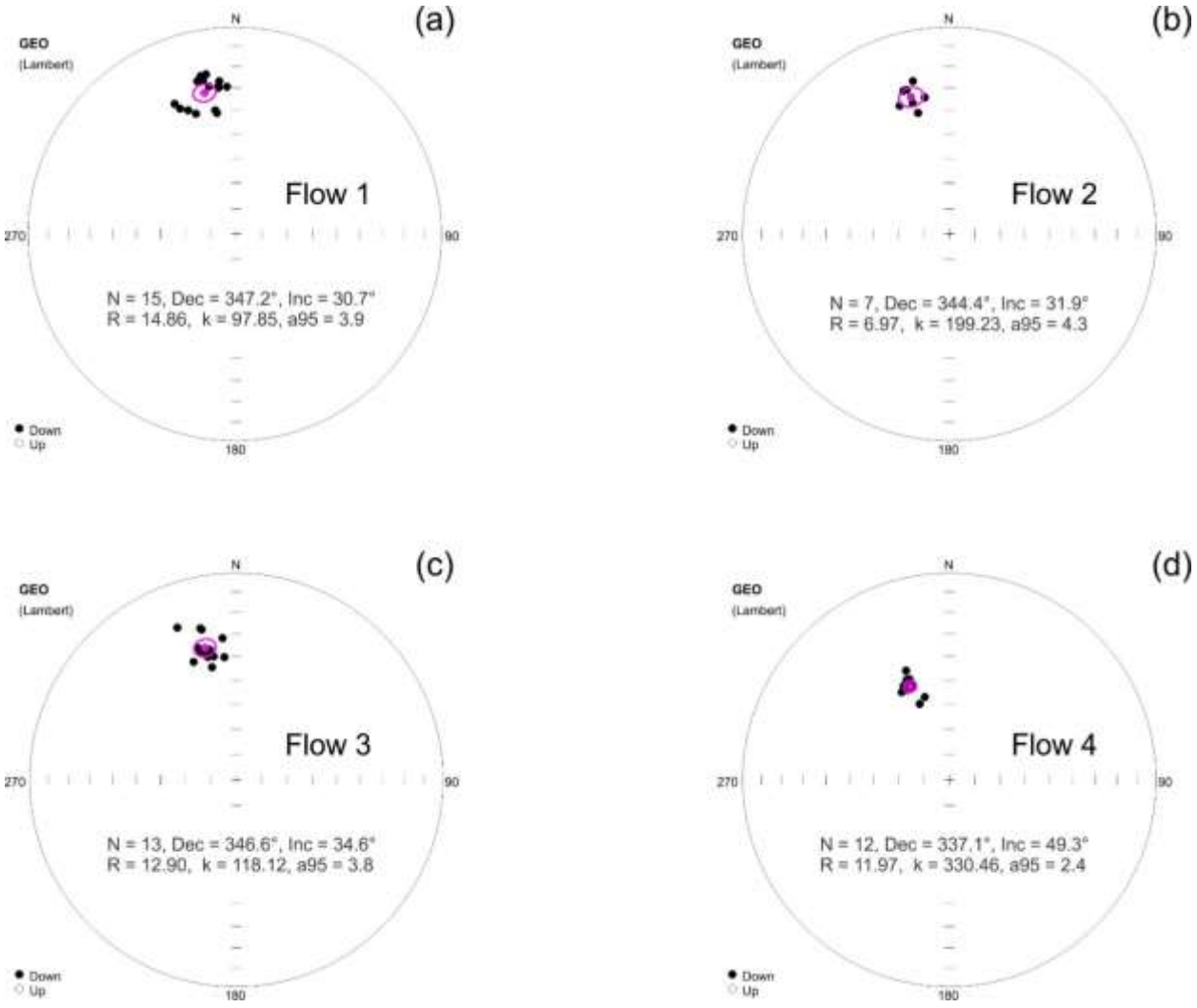

Figure 46 Stereo plots showing the characteristic remanent magnetization (ChRM) directions for the early lava flows. Flow mean directions are shown by the red dots, together with their corresponding 95% confidence angles. (For interpretation of the references to color in this figure legend, the reader is referred to the Web version of this article.)

Samples from late flows present more variations. Flow 6a and Flow 8 show higher declination values (359.2° and 14.3°, respectively) (Figure 47 a & c) than the early flows, but the inclination for Flow 8 is significantly high (~50°), being comparable to that of Flow 4. Notably, Gonzalez *et al.* (1997) obtained also a high inclination value of 41.5° for Flow 8. The mean direction of Flow 6b (Figure 47b) displays lower declination and steeper inclination values (see the discussion section for an interpretation about dissimilar mean directions obtained for Flow 6). In case of Flow 11, declination is abnormally high (113.5°), while its inclination value is slightly higher than that of Flow 6 (Figure 47d). These anomalous late-flows site-mean directions deserve some comments. Both northern lava flow (Flow 4 and Flow 8) fronts appear to have

experienced post-cooling tilting. This hypothesis seems realistic considering the steepness and high thickness (up to 200 m) of the front of the flows. These movements occurring after the acquisition of the magnetic footprint by the solidified lava should have deviated the magnetic record.

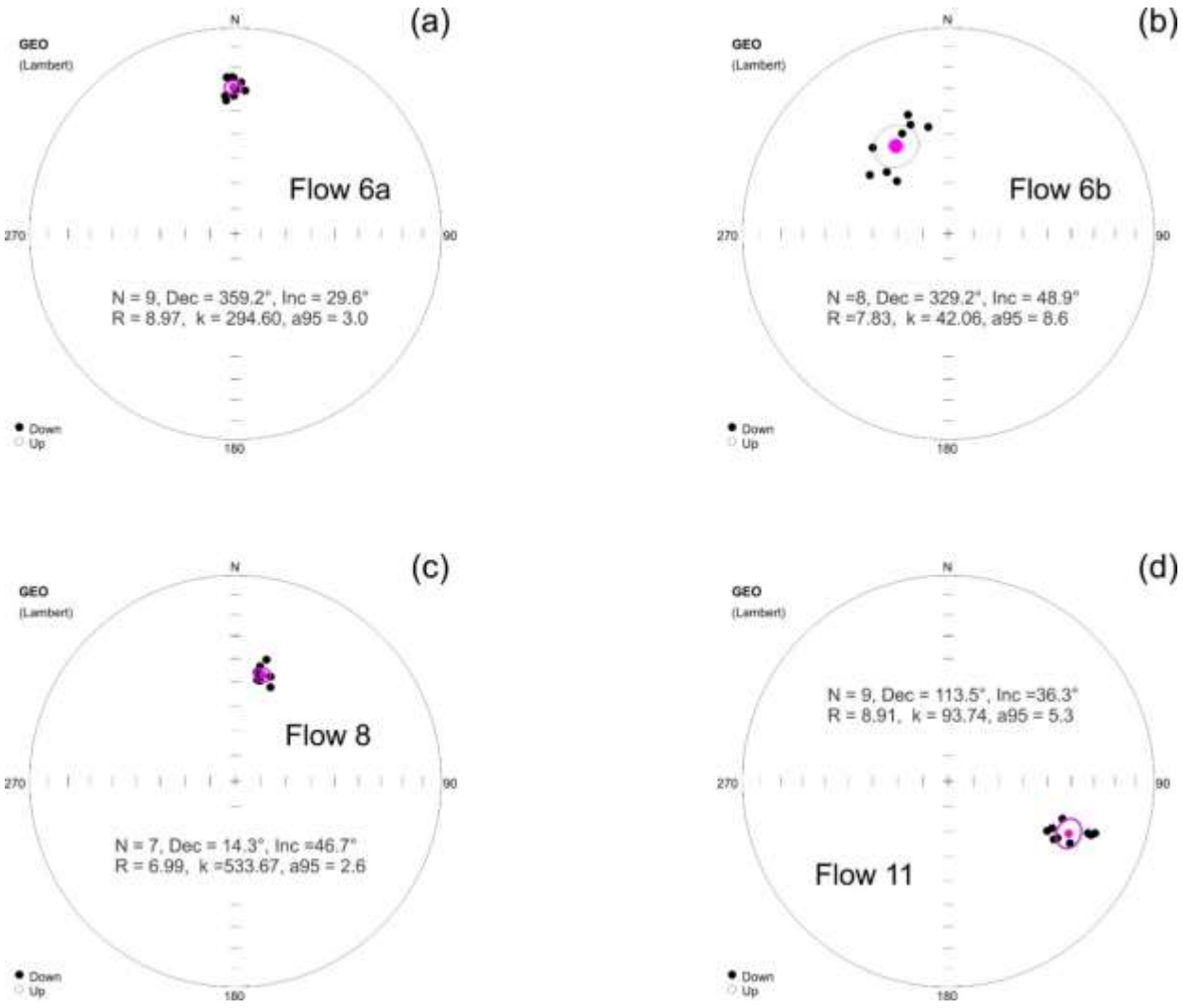

Figure 47 Stereo plots showing the characteristic remanent magnetization (ChRM) directions for the late lava flows. Flow mean directions are shown by the red dots, together with their corresponding 95% confidence angles. (For interpretation of the references to color in this figure legend, the reader is referred to the Web version of this article.)

In order to assess the similarity in paleomagnetic direction, and hence calculated age of early flows, F-distribution tests were carried out on the site mean directions from these flows. The F parameters calculated for the three possible combinations (Flow 1 vs Flow 2, Flow 1 vs Flow 3 and Flow 2 vs Flow 3)

yielded values lower than the critical value (95% confidence level), validating the null hypothesis H_0 that states that both samples have the same variance. On the contrary, F value obtained by applying the F test to any early flow against Flow 6 yielded a higher value that the critical one, thus rejecting H_0 and indicating that the mean paleomagnetic direction of Flow 6 (late flow) is significantly different from that of the early flows. The combined mean direction obtained for the early flows is: D = 346.4°, I = 32.1° (N = 34, R = 33.73, k = 121.74, α_{95} = 2.2) (see also Supplementary material SM1).

6.7.3 Paleointensities

6.7.3.1 Thellier-Coe method

Paleointensity determinations were considered as reliable record of the past geomagnetic field strength based on three criteria: (i) Quality of the checks and the statistical parameters of the linear fit, (ii) Correspondence between the selected temperature segment for intensity analyses and the temperature range which carries the characteristic remanent magnetization of the sample, and (iii) Applied experimental checks. Accordingly, we used a modified (stricter) criterion set to that included in the ThellierTool4.0 software (Leonhardt *et al.,* 2004) (Table 16). These criteria comprise three quality levels (Class A, Class B and Class C) of different stringency. See please caption of this table for more details. Under the application of these reliability criteria, 41 analyzed specimens yield successful paleointensity determinations (Table 18); 10 (24.4%) fulfil all class A criteria, 23 (56.1%) class B criteria and 8 (19.5%) class C criteria.

Table 16 Selection criteria and threshold values for class A, class B and class C determinations for Thellier-Coe experiments. Class: quality class A, B or C of each determination (see text); N: number of NRM-pTRM points used for paleointensity determination; f: fraction of extrapolated NRM used. f is referred to the so-called "true NRM", which is the intersection between linear fit and y-axis (Leonhardt *et al.,* 2004); σ/slope: Ratio of the standard error of the slope and the slope of the NRM-TRM diagram; q: quality factor (Coe *et al.,* 1978); MAD: Maximum angular deviation of NRM end-point directions at each step obtained from paleointensity experiments; α: angle between the vector average of the data selected for paleointensity determination and the principal component of the data; δ(CK): Difference between the pTRM check and original TRM value at a given temperature normalized to the TRM (Leonhardt et al., 2000); δ(pal): cumulative check error (Leonhardt *et al.,* 2003); δ(TR): relative intensity difference in pTRM-tail check; δ(t*): normalized tail of pTRM (Leonhardt *et al.,* 2004).

Class	**A**	**B**	**C**
N	≥ 8	≥ 6	≥ 5

f	≥ 0.35	≥ 0.35	≥ 0.35
σ/slope	≤ 0.1	≤ 0.15	≤ 0.15
q	≥ 6	≥ 1	≥ 1
MAD	≤ 5	≤ 8	≤ 10
α	≤ 15	≤ 15	≤ 15
δ(CK)	≤ 5	≤ 7	≤ 20
δ(pal)	≤ 5	≤ 10	≤ 15
δ(TR)	≤ 5	≤ 7	≤ 7
δ(t*)	≤ 3	≤ 30	≤ 30

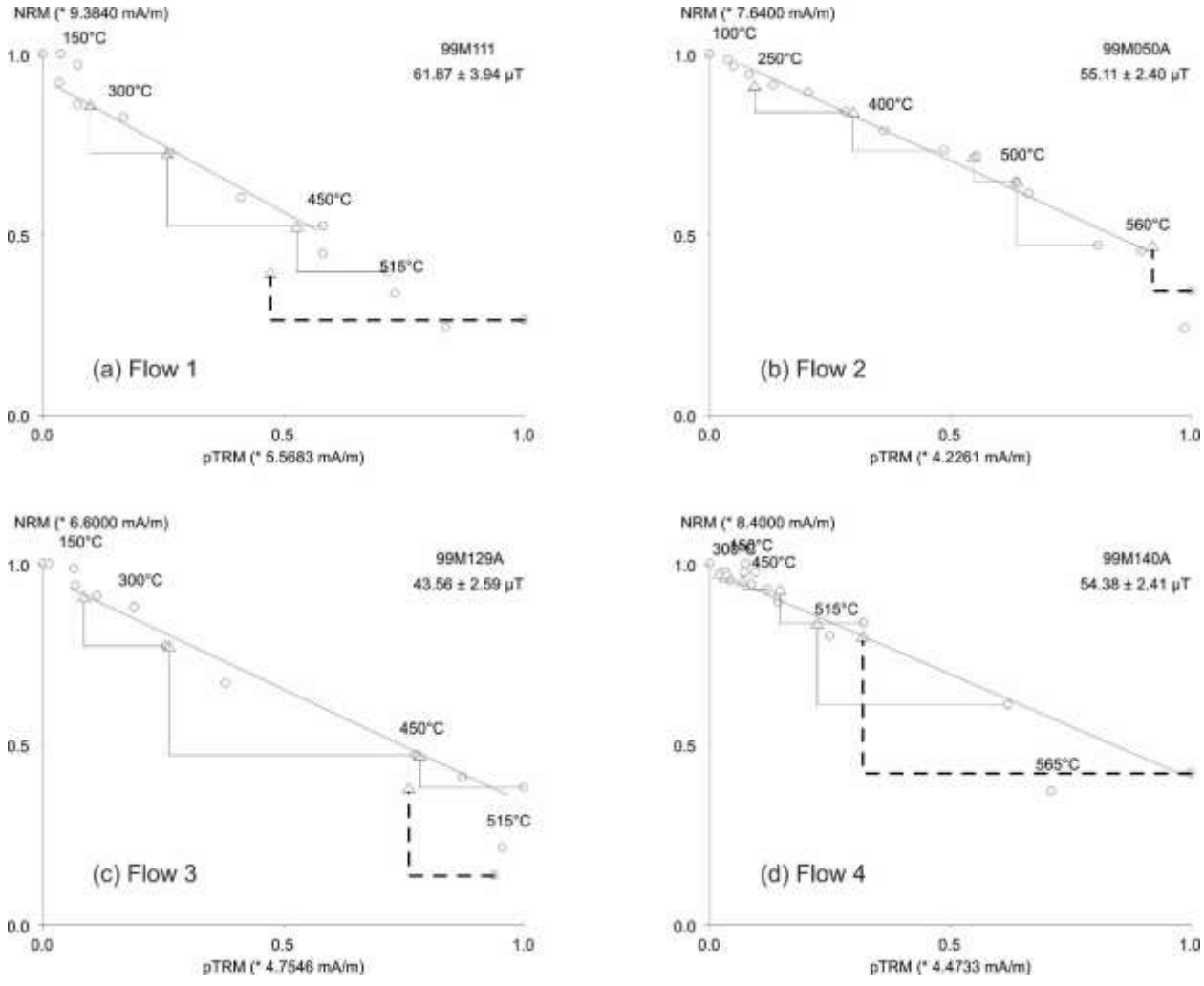

Figure 48 Representative Thellier-Coe NRM-lost vs pTRM-gained (Arai) plots for the early flows.

Thellier-Coe paleointensity (PI) results for all the seven flows studied together with their associated quality parameters are listed in Table 17, and representative Arai plots are shown in Figures 48 and 49. 41 out of 56 specimens analyzed yielded successful determinations. This means an almost 73% of success rate. Alteration both in nature or during laboratory heating and the influence of multidomain (MD) grains seem to be the main factors of failure for paleointensity determinations.

Table 17 Thellier-Coe paleointensity results for all seven studied flows. Paleoint: paleointensity; σ: standard deviation; Tmin/max: minimum/maximum temperature; N: number of point included for the linear best-fit; β: σ/slope; f: fraction of extrapolated NRM used for intensity determination; g: gap factor; q: quality factor as defined by Coe *et al.* (1978); MAD anc: anchored maximum angular deviation; α: angular difference between anchored and non-anchored best solution; Class: A, B or C; CK-error: relative check error; CK-diff: cumulative check difference; Drat: differential ratio; d(t*): normalized tail of pTRM; d(TR), tail check. Underlined specimen-names are those specimens discarded for the mean intensity calculation due to exceeding of at least one of the threshold values (also underlined) stablished for the corresponding Class assigned.

Name	Paleoint	σ	Tmin	Tmax	N	β	*f*	*g*	*q*	MAD anc	α	Class	CK-error	CK-diff	Drat	d(t*)	d(TR)
Flow 1																	
99M101A	68.1	5.9	400	540	6	0.09	0.77	0.47	4.1	1.4	1.5	C	11.0	17.9	8.5	0.7	4.5
99M102A	78.6	4.6	350	560	8	0.06	0.87	0.67	10.1	1.8	2.6	C	10.1	13.7	6.3	1.0	2.8
99M103A	91.4	8.5	450	560	6	0.09	0.52	0.67	3.7	2.5	5.2	C	7.0	27.6	6.5	0.0	1.1
99M104A	92.2	11.1	475	560	5	0.12	0.31	0.68	1.8	1.1	0.5	C	5.0	20.8	7.6	9.9	3.4
99M111	61.9	3.9	200	450	6	0.06	0.43	0.78	5.2	1.2	2.1	B	2.0	4.6	2.9	3.7	4.7
99M119A	83.2	8.3	450	540	5	0.10	0.24	0.64	1.6	0.6	0.6	C	5.1	8.1	11.0	3.6	3.2
Mean =	**69.5**	**1 σ =**	**8.4**														
Flow 2																	
99M041A	46.5	4.2	150	450	7	0.09	0.36	0.75	3.0	0.7	1.2	B	1.3	2.7	2.7	0.0	0.1
99M042A	49.4	5.0	150	450	7	0.10	0.36	0.71	2.6	1.3	2.6	B	2.6	8.9	5.1	1.4	0.1
99M043A	54.5	7.1	200	450	6	0.13	0.34	0.62	1.6	1.9	4.0	B	3.2	3.4	6.4	6.3	0.0
99M047A	48.5	1.3	150	515	10	0.03	0.33	0.87	10.8	1.8	5.2	B	3.0	5.1	6.6	4.4	0.9
99M049A	NR																
99M050A	55.1	2.4	150	560	12	0.04	0.51	0.88	10.3	4.7	14.9	B	6.8	3.0	9.0	0.0	3.0
Mean =	**49.9**	**1 σ =**	**3.7**														
Flow 3																	
99M078A	62.6	6.1	350	540	6	0.10	0.41	0.76	3.2	2.2	4.1	C	7.1	1.4	10.9	1.0	0.9
99M079A	49.7	2.4	150	475	8	0.05	0.49	0.60	6.1	3.3	10.0	C	8.6	0.9	12.4	0.0	4.0
99M080A	39.1	0.9	150	500	9	0.02	0.29	0.79	9.6	3.7	14.7	C	0.6	2.4	1.7	0.3	5.2
99M127A	37.9	2.0	200	500	8	0.05	0.61	0.76	9.0	2.7	5.7	B	2.9	3.7	3.9	3.2	2.2
99M128A	34.4	1.3	150	500	9	0.04	0.55	0.78	11.4	2.7	6.5	A	1.8	1.4	2.6	0.4	3.0
99M129A	43.6	2.6	200	500	8	0.06	0.59	0.78	7.7	3.0	6.9	B	1.8	0.5	2.2	3.6	1.6
99M130A	45.5	2.6	200	500	8	0.06	0.61	0.79	8.4	3.7	8.9	A	1.2	3.2	1.5	1.3	2.0
99M131A	43.0	2.5	200	500	8	0.06	0.57	0.79	7.9	2.4	5.7	A	1.4	1.8	1.8	0.8	3.3
Mean =	**40.9**	**1 σ =**	**4.6**														
Flow 4																	

99M083A	53.7	2.5	350	540	7	0.05	0.19	0.59	2.4	1.9	2.9	C	8.6	33.3	31.4	0.0	1.7
99M085A	43.7	2.1	200	540	10	0.05	0.38	0.71	5.8	1.5	4.5	C	7.7	19.8	15.4	0.4	1.4
99M086A	45.8	5.4	250	540	9	0.12	0.59	0.70	3.5	1.2	2.3	B	5.6	7.8	7.1	1.5	1.1
99M135A	52.6	3.5	350	560	8	0.07	0.45	0.77	5.2	1.4	3.6	C	1.9	11.0	2.9	4.9	2.4
99M137A	57.5	3.0	200	560	11	0.05	0.72	0.68	9.5	1.5	2.1	C	12.6	14.4	11.6	0.0	0.0
99M139A	70.4	4.9	200	540	10	0.07	0.64	0.59	5.5	1.4	2.3	C	17.3	21.9	15.5	3.9	2.2
99M140A	54.4	2.4	300	560	9	0.04	0.56	0.70	8.9	1.2	1.2	B	5.8	7.7	7.0	0.0	1.2
99M142A	40.4	2.5	300	560	9	0.06	0.34	0.71	4.0	0.8	1.0	B	2.8	5.0	6.4	2.2	1.3
99M143A	51.0	3.2	300	560	9	0.06	0.25	0.76	2.9	0.9	2.5	C	2.3	1.7	6.4	2.7	2.4
Mean =	**48.8**	**1 σ =**	**5.7**														
Flow 6																	
99M002A	51.43	3.80	200	515	9	0.07	0.70	0.79	7.5	2.2	1.7	C	10.4	7.6	10.4	3.2	2.7
99M003A	58.70	4.21	200	515	9	0.07	0.68	0.73	6.8	3.5	5.6	C	8.3	9.5	8.0	0.9	1.9
99M004A	59.69	4.65	150	500	9	0.08	0.67	0.75	6.4	4.3	8.1	A	4.1	1.1	4.0	1.1	2.8
99M005A	54.71	2.73	150	475	8	0.05	0.56	0.71	7.9	1.2	0.8	B	3.9	3.9	4.7	3.3	2.3
99M007A	47.99	3.18	300	500	6	0.07	0.56	0.56	4.7	2.9	2.6	C	12.0	8.3	15.6	0.0	6.0
99M008A	49.54	5.25	150	475	7	0.11	0.60	0.74	4.2	7.4	11.4	B	3.0	1.3	3.6	20.0	1.3
99M009A	46.52	2.22	150	475	8	0.05	0.56	0.62	7.3	1.5	1.9	B	2.0	2.4	2.6	8.4	2.5
99M010A	54.65	3.64	150	475	8	0.07	0.57	0.66	5.6	3.1	6.0	B	2.5	4.5	3.0	5.3	5.9
99M011A	55.47	3.19	150	475	8	0.06	0.62	0.69	7.4	1.1	1.7	B	0.4	0.9	0.4	4.1	3.7
Mean =	**53.6**	**1 σ =**	**4.7**														
Flow 8																	
99M015A	108.29	14.55	150	580	13	0.13	0.79	0.79	4.6	3.1	5.2	B	5.4	8.2	2.9	5.7	2.1
99M016A	38.89	1.55	150	580	13	0.04	0.83	0.86	17.9	1.7	2.5	A	3.6	1.1	3.5	0.0	0.7
99M018A	47.84	1.67	150	570	13	0.03	0.62	0.89	15.9	2.2	5.9	A	3.0	4.8	3.5	0.0	0.9
99M021A	59.56	1.65	150	560	12	0.03	0.62	0.77	17.4	1.5	3.1	A	4.5	3.9	4.7	0.0	0.9
99M052A	53.35	1.35	150	540	11	0.03	0.61	0.85	20.7	1.6	4.3	B	5.4	9.9	6.0	0.0	1.1
99M056A	51.68	2.43	200	500	8	0.05	0.39	0.80	6.7	0.7	1.8	B	2.0	9.3	3.6	1.8	1.0
99M061A	54.26	1.58	150	540	11	0.03	0.60	0.87	17.8	1.5	3.7	A	1.7	4.4	2.0	0.0	1.0
99M067A	55.3	2.33	150	540	11	0.04	0.61	0.87	12.6	2.3	5.8	A	1.7	1.9	1.9	0.0	1.7
99M071A	55.61	3.15	150	475	8	0.06	0.50	0.81	7.2	2.3	6.5	A	1.5	3.6	2.0	0.0	0.3
Mean =	**52.1**	**1 σ =**	**6.3**														
Flow 11																	
99M087A	40.64	2.10	400	540	6	0.05	0.36	0.77	5.4	5.5	13.1	B	4.1	8.4	8.7	0.0	2.9
99M088A	33.09	1.12	300	515	7	0.03	0.34	0.73	7.4	4.5	12.8	B	1.6	3.1	3.8	0.0	2.5
99M089A	35.04	1.92	250	515	8	0.05	0.35	0.69	4.4	4.1	13.2	B	1.7	1.0	3.9	0.0	2.5
99M090A	38.33	3.34	300	540	8	0.09	0.29	0.84	2.8	4.9	14.7	C	4.4	2.4	11.9	2.4	0.0
99M091A	38.46	3.18	300	540	8	0.08	0.30	0.83	3.0	5.1	16.8	C	3.5	11.5	9.2	0.0	5.0
99M093A	32.00	3.64	250	540	9	0.11	0.22	0.84	1.6	4.6	17.3	C	1.6	10.1	6.2	0.0	5.2
99M094A	33.08	4.70	200	540	10	0.14	0.34	0.81	1.9	4.5	18.9	C	5.6	32.0	13.7	0.0	0.0
99M095A	42.65	3.43	250	540	9	0.08	0.51	0.79	5.1	2.2	3.8	B	1.7	8.6	2.5	0.1	6.6
99M096A	53.09	2.25	200	500	8	0.04	0.34	0.78	6.2	2.4	3.9	B	2.5	8.3	5.1	1.1	3.1
99M100A	35.31	2.24	150	500	9	0.06	0.31	0.67	3.3	1.8	4.7	B	2.0	6.7	5.2	0.0	5.9
Mean =	**39.7**	**1 σ =**	**6.8**														

PI values of (69.5 ± 8.4) µT, (49.9 ± 3.7) µT, (40.9 ± 4.6) µT and (48.8 ± 5.7) µT were obtained for Early flows (Flow 1 – Flow 4), respectively. In the case of Late flows (Flow 6 – Flow 11), PI values of (53.6 ± 4.7) µT, (52.1 ± 6.3) µT and (39.7 ± 6.8) µT, respectively, were obtained. These differences are evident in Figure 50a. At first sight, an atypical high PI obtained from Flow 1 stands out. Although no evidently concave-up behavior – characteristic of large multidomain (MD) magnetic grains – is appreciated from Arai plots, slightly high percentage pTRM tails above 10% are observed for most samples coming from this flow, which could suggest a considerably contribution MD magnetic grains to the remanence within this flow, thus overestimating the PI value. We note, however, that pTRM tails might be also an indication of alteration. Therefore, these intensities have been discarded for further determinations.

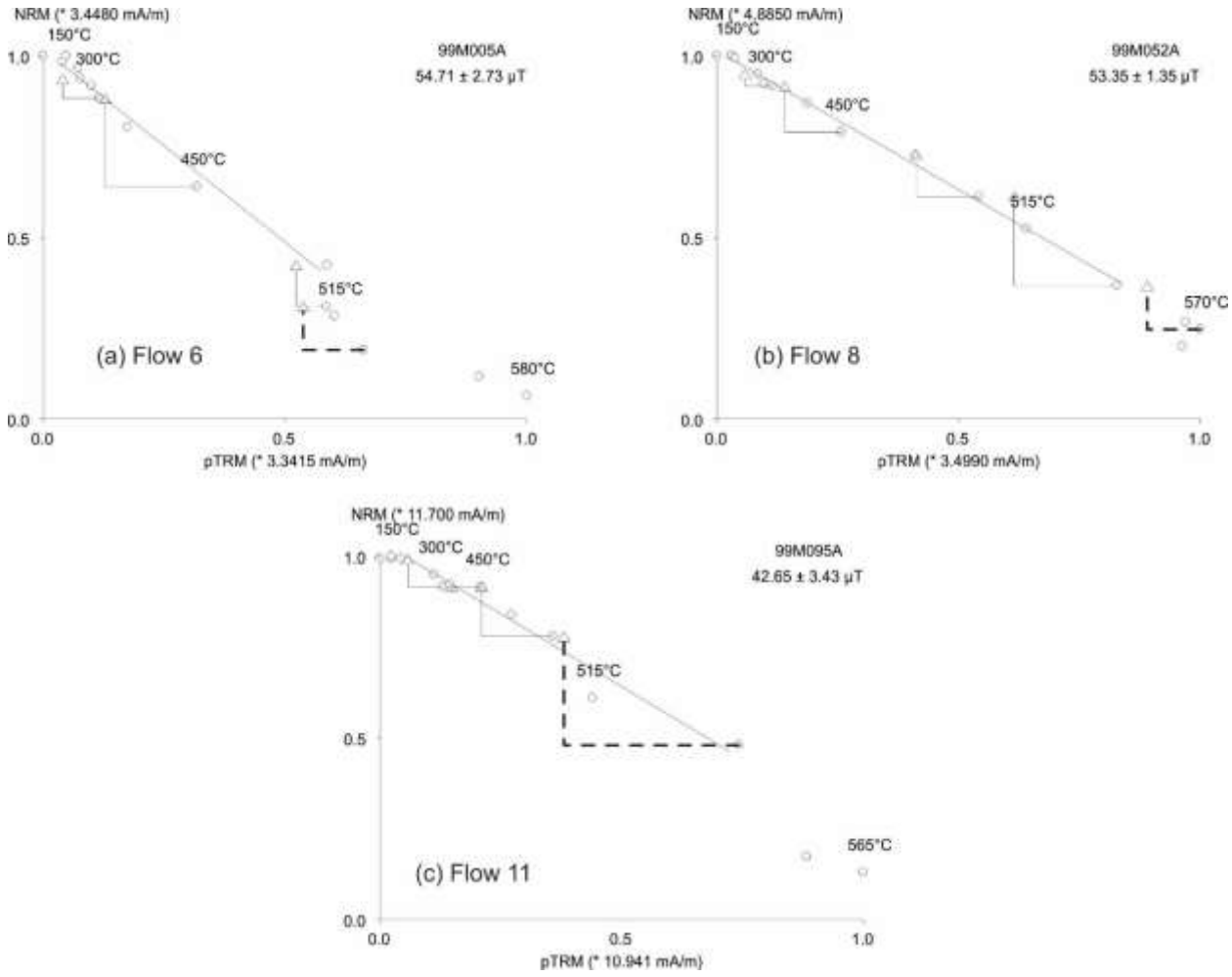

Figure 49 Representative Thellier-Coe NRM-lost vs pTRM-gained (Arai) plots for the late flows.

With the purpose of estimating whether there are significantly differences (at the 95% confidence limit) between the mean PI values obtained for different flows, a series of two-tailed Student's t-test was applied to the different mean PI flow's combinations. Considering pairs of consecutive flows, only the results between Flow 1 and Flow 2 and between Flow 8 and Flow 11 are significantly different at the 95% confident limit, indicating that their mean PI values are statistically different. The same can be concluded between the non-consecutive pairs: Flow 3 and Flow 6, and Flow 6 and Flow 11. Accordingly, large PI differences between-flows do not allow to calculate an overall mean PI value, caused likely by an incipient secular variation recorded by the different flows.

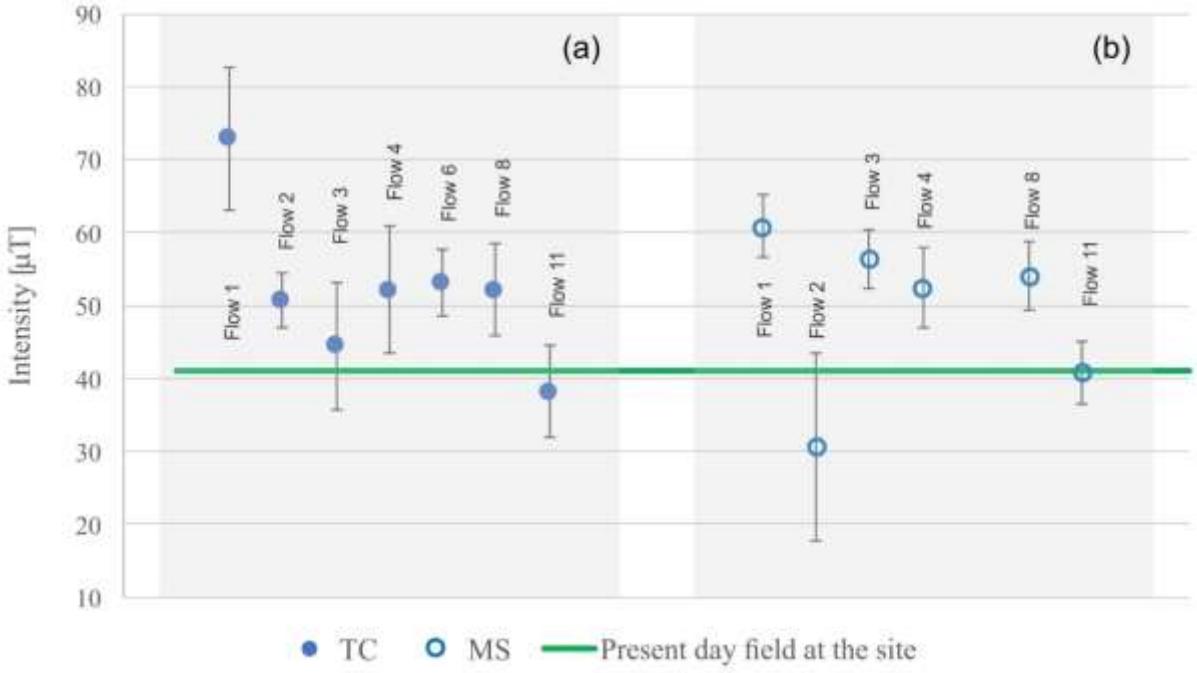

Figure 50 Plot showing the different PI values obtained by the Thellier-Coe (TC) and multispecimens (MS) paleointensity experiments. Error bars for TC data represent the corresponding standard deviation (σ), while error bars for MS data correspond to the difference between the Min and Max values reported on Table 18.

6.7.3.2 Multispecimen method

Multispecimen paleointensity results for each studied flow along with associated quality parameters are listed in Table 18, and representative PI plots are shown as Supplementary material (SM2 – SM7). An

acceptable angular deviation (AAD) of 10° and α=0.5 were chosen for the calculations by the VBA software, while the overprint check (Δdec and Δinc < 10°), the amount of progressive alteration ($\varepsilon_{alt} \leq$ 10%), and the intersection with the y axis (0 < Δb < -1) were all considered as reliability criteria. Domain state corrected results (DSC) are systematically lower than fraction corrected (FC) and DB values at different proportion.

Table 18 Multispecimen (Q_{DSC}) paleointensity results for each studied flow. Min and Max: Minimum and maximum estimated paleointensity values. Overprint check (Δdec and Δinc < 10°) - the difference between declinations and inclinations of the isolated NRM remaining and the isolated pTRMs-, the amount of progressive alteration ε_{alt} - a systematic (alteration-induced) error-, and the intersection with the y axis (- 1 < Δb < 1) were considered as reliability criteria. r^2: correlation coefficient of the linear regression. Data in italics denote rejected results due to ε_{alt} > 10%.

Site	Q_{DSC} [μT]	Min [μT]	Max [μT]	Avg ε_{alt}	Δb	r^2
Flow 1	60.9	58.4	62.6	-8.4	0.18	0.966
Flow 2	30.6	21.1	34.0	-7.1	-0.14	0.902
Flow 3	56.4	54.5	58.5	-18.0	-0.45	0.971
Flow 4	52.5	48.7	54.1	-14.6	-0.09	0.967
Flow 6	N/R					
Flow 8	54.1	52.2	57.0	-0.8	0.05	0.976
Flow 11	40.8	38.8	43.1	-2.9	0.03	0.978

As in the case of Thellier-Coe method, MS paleointensity for distinct flows are different (Figure 50b). However, MS trend resembles the one follow by the Thellier-Coe data (Figure 50a). Flow 4 has a similar PI value (52.5 μT) as Flow 8, while Flow 11, however, presents a much lower PI value of 40.8 μT than the preceding flows, but very similar to the one obtained by the TC method. Although methodological issues are not the aim of this study, it is worth noting that for Flow 1, the PI value calculated by using Thellier-Coe method (which is likely overestimated because of the contribution of MD remanence) is distinct from the value calculated by DSC MS method, which has been corrected for the MD remanence. Instead, these two methods give similar results for Flow 11. It is worth of noting that Early flows (Flow 1 - Flow 3) present the highest differences between both methods, while Flow 4, Flow 8 and Flow 11 the ones with the lowest intra-method differences (see Figure 50 a & b).

Finally, we stand out the fact that paleointensity results obtained with both the Thellier-Coe and the multispecimen method agree in some cases – percent relative differences (%RDiff) of 7.0%, 3.7% and 2.7%

for flows 4, 8 and 11, respectively– should be considered as an alternative robust reliability criterion for the correct paleointensity determination.

6.7.4 Paleomagnetic dating

The determination of the most probable date for the cooling of the analyzed lava flows was carried out by assessing the corresponding probability density function (PDF) obtained by the use the Matlab tool *archaeo_dating* developed by Pavón-Carrasco *et al.* (2011), along with the global model SHA. DIF.14k of Pavón-Carrasco *et al.* (2014) (calculated for the geographical position of the site). This model is the latest developed using all the available paleomagnetic data for their corresponding time intervals and applying the classical modeling approach, *i.e.,* the spherical harmonic analysis in space and the penalized cubic B-splines in time.

It is well known that there are more factors that affect the intensity retrieval of the ancient geomagnetic field than its direction. Paleomagnetic sampling of *in situ* blocks is, by itself, a premise for obtaining reliable directions, after elimination of secondary magnetizations, if present. Moreover, due to the scatter of PI values for distinct samples within a single flow and differences in the PI values obtained by the two methods used (Thellier-Coe and multispecimens), we decided, as a first approach, to carry out the paleomagnetic dating of early (using the mean direction (see Supplementary material SM1)) and late (Flow 6) flows separately based on directional data.

The outcomes can be summarized as follows. The emplacement of the first three early flows could have occurred any time between AD 990 and AD 1130 (Figure 51), which represent an ~140 years period. This maximum interval age is in good agreement with the ^{14}C-dating (840 ± 30 yr BP) of a paleosol sample (no. 14285) collected directly under Flow 1 (Chevrel *et al.,* 2016a).

Paleomagnetic dating of Flow 6, the next dated flow in the stratigraphy, yield three possible age intervals: [685AD 875AD], [900AD 941AD] and AD 1431–1600 (Figure 53). However, because of the ^{14}C-dating above mentioned on the one hand, and to the upper stratigraphic position of this flow on the other hand, the two first age intervals can be straightforwardly discarded, suggesting a period of ~300 years between the emplacement of this flow and the early ones. During this time-gap flows 4 and 5 were emplaced, but their age could not be constrained due to the post-cooling tilting of blocks at the flow front of Flow 4 (see above) and the inaccessibility of Flow 5. The age of Flow 6 can be further restricted as prior to AD 1530,

date at which the region was colonized (this eruption was not reported in historical documents hence it must have ended prior to the arrival of the Spaniards: see Chevrel *et al.,* 2016a). The scenario above presented could be graphically represented by means of a video with the sequence of the different directional dating (Lava flows timing.MP4).

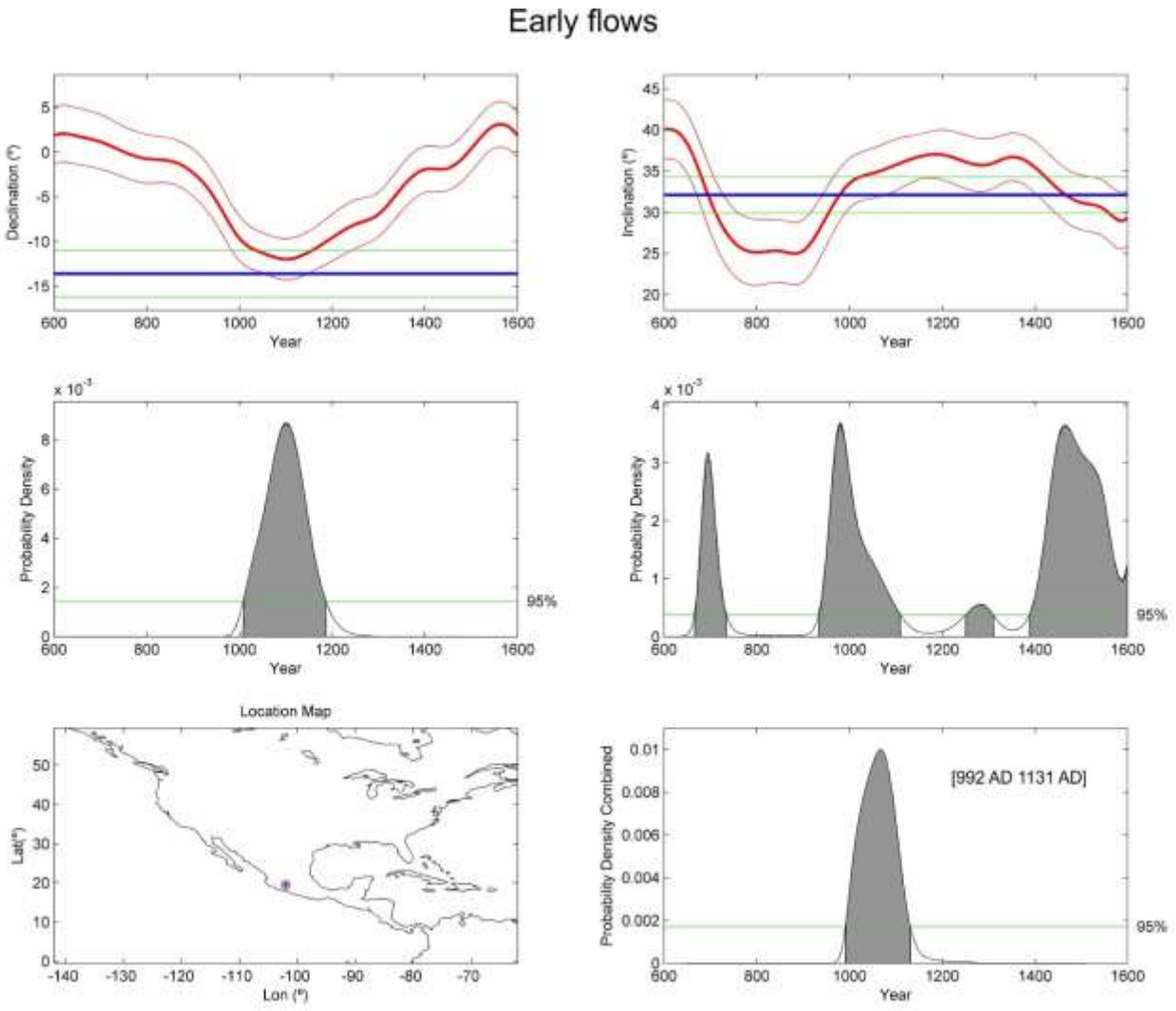

Figure 51 Directional paleomagnetic dating of early flows of El Metate's lava flows. Upper panels: Red thick curves show the variation in time of the directional components of the paleomagnetic field as determined from the SHA. DIF.14k model (Pavon-Carrasco *et al.,* 2014), while blue thick horizontal lines represent the mean declination and inclination of the ancient field determined for the early flows (F1 – F3) of El Metate volcano; all curves and lines are shown with their corresponding 95% confidence intervals (thin lines above and below the corresponding thick line). Central panels: The corresponding probability density function is shown as shaded peaks, together with the 95% confidence level highlighted by horizontal green lines. The combined (Dec and Inc) probability density is shown at the lower most panel. (For interpretation of the references to color in this figure legend, the reader is referred to the Web version of this article.)

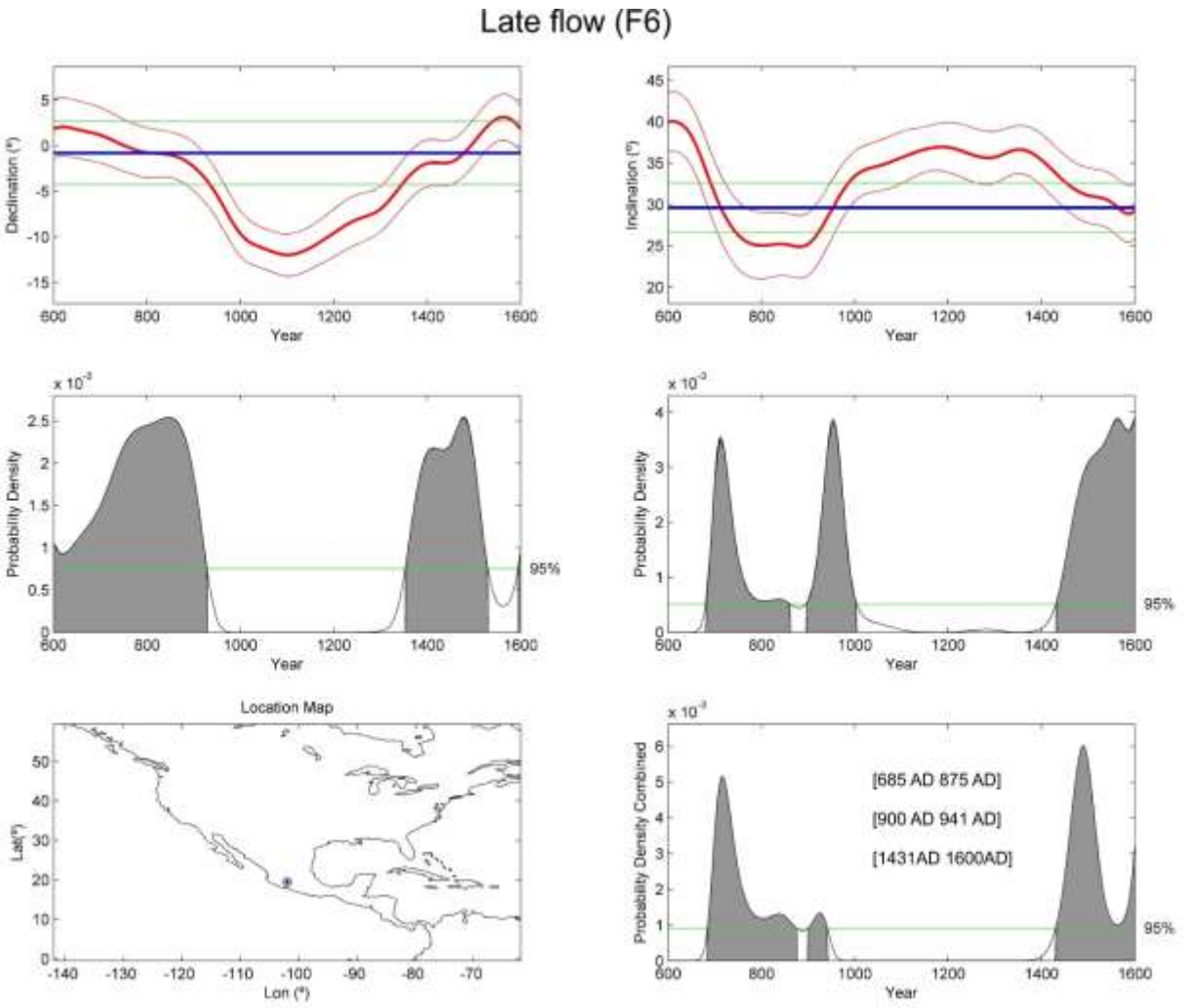

Figure 52 Directional paleomagnetic dating of late flow F6 of El Metate. Description of panels as in Figure 52.

Supplementary video related to this article can be found at https://doi.org/10.1016/j.quageo.2019.101031.

Models based on flow morphology indicate that the latest flows, Flow 6, 7, 8 and 11 were emplaced during the course of 1.6, 1.3, 2.0, and 6.7 years, respectively (Chevrel *et al.,* 2016a), but the interval of time between the emission of each of these distinct flow units could not be constrained by previous studies (Chevrel *et al.,* 2016a; Mahgoub *et al.,* 2017). In any case, this indicates a minimum of 12 years emplacement period for all the late flows.

The age of all late flows except Flow 6 could not be constrained by their magnetic direction because of post-cooling block movement. Accordingly, and as a second approach, we used individual paleointensity

values for the paleomagnetic dating of late flows since this parameter is unaffected by post-cooling displacements of the lava blocks. Consequently, the age of Flow 11 – for which similar PI were obtained by the two methods applied – could be constrained to AD 1480–1600 by the paleointensity dating carried out, coinciding likely with the arrival of the Spaniards. We note, however, that a single-component (intensity) is less reliable than a two-, or even three-, components dating.

It is worth noting that the full vector paleomagnetic dating (using both direction and intensity) of Flow 6 yields a similar result (AD 1429 AD 1559) to the one obtained using only the mean paleomagnetic direction, validating this technique, and supporting the hypothesis that El Metate eruption spread a much longer-time span (*ca.* 200 years) than previously thought.

6.8 Discussion

Based on the outcomes of two independent methods, both requiring the knowledge of the average length, width, and thickness of the fully exposed lava flows, Chevrel *et al.* (2016a) inferred emplacement periods between 1.3 and 6.7 years for four of the fully exposed lava flows (F6, F7, F8, and F11, as designated in that study). Under these considerations, they estimate that the emplacement of the entire edifice would have taken at least 34 years. As properly mentioned there, this estimate assumes a continuously and sequentially activity between the emplacements of each of the different lava flows, one after the other. They note also, however, that *"… the efficiency of the lava to retain heat might allow the flow to keep advancing for months (Manley, 1992) after the cessation of the effusion at the vent".* Taking into consideration this fact it is suggested that a "*Maximum emplacement duration of the volcano must have been less than ~275 years, the time that elapsed between the start of the eruption in AD 1250 and the arrival of the Spaniards in that region in the 1520s*", due to the lack of colonial chronicles. However, the time that elapsed between the extrusion of each of El Metate's lava flows remains unknown. Additionally, a monogenetic origin was proposed for El Metate based on field observations.

In order to test its monogenetic origin, Mahgoub *et al.* (2017) undertook a paleomagnetic study of five lava flows from El Metate. With the aim of estimating the directional independence between the obtained early (MT1, MT2, MT4) and late (MT6) flow mean directions (as designated in their study) the F-distribution test (McFadden and Lowes, 1981) was applied to the different possible flow combinations, being all of them positive. Since a positive result implies that two mean directions are statistically

indistinguishable at a chosen confidence level (in this case 95%), they concluded that "… *all studied flows recorded the same field and thus probably represent the same instance in time*".

Moreover, in order to ascertain whether the mean-PI values for El Metate lava flows were similar, Mahgoub *et al.* (2017) performed a two-sample Student's t-test assuming equal variance and using a pooled estimate of the variance μ, concluding no significant differences between flow mean PI values.

However, it is worth noting that the calculation of an overall mean flow using such an uneven number of early and late data seems to bias the result to that of early flows, masking a likely incipient secular variation record by the different flows.

As in the case of consistent results obtained by two (or more) independent paleointensity methods, consistent directions for different paleomagnetic sites got by different groups reinforce the reliability of paleomagnetic methods, and particularly of paleomagnetic dating of lava flows. This was accomplished in the case of the early flows. In the case of late flows, the situation is somewhat different. All four paleomagnetic sites from Flow 6 (MT6.1 and MT6.2 from Mahgoub *et al.* (2017) and Flow 6a and Flow 6b from this study) yielded significantly different directions (Figure 53).

However, based on the consistency between the retrieved mean direction from site MT6.1 and the other (early) flows, Mahgoub *et al.* (2017) assumed that this result represents the El Metate flow MT6 mean direction and discarded the one retrieved from site MT6.2.

As properly noted by Chevrel *et al.* (2016a), lava flows directed to the south reached longer distances (<15 km) than those emitted to the N due to different topographical gradients and the presence of the older prominent Paracho shield to the N. Likewise, topographical gradients and preexisting structures (particularly the Colorado volcano to the S) deviated the advance of Flow 6, altering its original southern trajectory to an eastern one (see Supplementary material SM8). As stated by Glaze *et al.* (2014), in such circumstances, the angular momentum generated by this change in trajectory results in some form of circulation, eddying, or vortex formation within the flow or at its margins. In the case of Flow 6, this situation should had resulted in some form of a counter-clockwise circulation within the flow. Bearing in mind the broad thickness of El Metate lava flows, and that a lava flow cools from the outer to the inner part, the solidified upper part of the flow – with a temperature below enough as to block a remanent magnetization – , lying over a hotter lava core, should alter its original position due to the further advance and circulation of the flow, modifying its magnetic record.

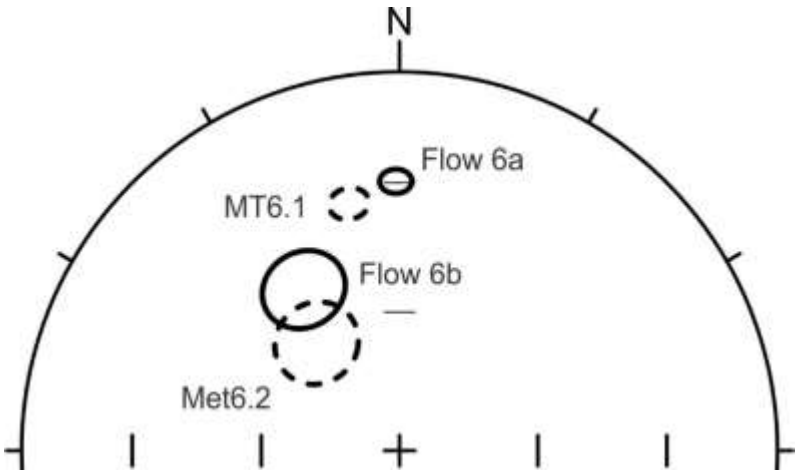

Figure 53 Mean flow direction for the four different sites of Flow 6 - MT6.1 and MT6.2 from Mahgoub *et al.* (2017) and Flow 6a and Flow 6b from this study.

Sites MT6.1 and MT6.2 of Mahgoub *et al.* (2017) locate just within this "disturbed" area. Site Flow 6b is located in the same front flow of that of Mahgoub *et al.* (2017), with a mean direction (declination) close, but shallower, to that of site MT6.2. On the contrary, site Flow 6a is located in a front flow within a *"free flowing"* area, just where the flow stopped its flowing to the S, before the occurrence of any counterclockwise circulation.

Given the potential rotations at this area, the possibility of small rotations of the individual site mean directions should not be excluded. Taking into consideration the counter-clockwise circulation inferred, if the declination of flow MT6.1 from Mahgoub *et al*. is rotated by ±5° (*i.e.,* 5° clockwise) the inferred age ranges become [944 AD – 1069 AD] and [1165 AD – 1458AD] (see Supplementary material SM9). Moreover, a declination rotation of ±10° (entirely feasible for this region) shifts forwards the most probable age range to [1307 AD – 1542 AD] (see Supplementary material SM10), which would bring the results more compatible with the ones obtained in this study. We note, however, that the opposite situation (a clockwise rotation) would shift backwards the most probable age range for Flow 6a to a result more in accordance with that of Mahgoub *et al.* (2017); however, such an opposite rotation seems not feasible according to the observed lava flow patterns.

Although far from ideal averaging out local disturbances, the combination of a southern and northern edge sampling site would result in a more representative paleomagnetic direction. Combining the here reported Flow 6a result with that of MET6.1 from Mahgoub *et al.* (2017), the resulting paleodirection is D = 353.9°, I = 31.8°, a95 = 3.2° (N = 18, R = 17.86, k = 119.3). Because both results come from different sites

of the same flow, small local rotations should be smoothed. This mean direction yields three possible age ranges: [921 AD - 1029 AD], [1220 AD - 1361 AD], and [1400 AD-1481 AD] (see Supplementary material SM11). Worth of noting is the upper bond age, adjacent to the age interval of [1498 AD -1625 AD] determined for Flow 11.

Taking into consideration the constraining above mentioned arguments for dating Flow 6 - ^{14}C dating of paleosol sample- the first age interval should be discarded, suggesting that the paleomagnetic age of Flow 6 cannot be unambiguously estimated, giving rise to the possibility of a much longer-time span effusive activity of El Metate.

Previous paleomagnetic studies of young lava flows have documented anomalously shallow remanence inclination (e.g., Castro and Brown, 1987; Tanguy, 1990). Shallow inclinations, up to 6° compared with nearby geomagnetic observations, were reported for the 1950 lava from Mauna Loa and the 1972 lavas from Kilauea, Hawaii. Urrutia-Fucugauchi (1996) reported the occurrence of shallow inclinations in the historic lava flow from the cinder cone volcano in the southern basin of Mexico, as well as in the historic lava flow from the Paricutin volcano (Urrutia-Fucugauchi *et al.,* 2004). Among the different explanations proposed for anomalous inclinations, the one that explain them in terms of internal deformation of lava and movement of lava front after cooling of magma below the blocking temperature spectra during emplacement is the one, we consider pertinent for this case study.

Direction from Flow 8 determined in this study, and that of Flow 11 – this study and MT11 from Mahgoub *et al.* (2017)- seem to come from moved blocks. As noticed by Mahgoub *et al.* (2017), "… *the site-mean direction of MT11 corresponds to one big block exposed at the upper part of the front of flow, which we suspected already during fieldwork to have moved after cooling*". However, at first sight from the image of their outcrop, it is evident that their paleomagnetic site consists of several brecciated blocks over an altered substrate. Though our site Flow 11 comes also from a similar dimensions big block exposed at the upper part of the front of flow, it is a single massive non-fragmented vesicle-free block. While its declination value seems to have experienced a clockwise rotation, its corresponding inclination value is in good agreement within the *"expected"* interval.

As mentioned above, the >220 years difference suggested between the emplacement of Flow 3 and Flow 6 extends the eruptive activity of El Metate to just before the arrival of the Spaniards (AD 1530). Although no colonial chronicles exist which witnessed the prolonged effusive activity of El Metate, a clear occupation interruption between AD 900 and 1250 has already been documented for the Zacapu area

(~30 km to the NE of El Metate), located at the western border of the Zacapu lacustrine basin in the Michoacan-Guanajuato Volcanic Field (MGVF), central-western Mexico, with a known human occupation which extended back to AD 550 and forth AD 1550. As mentioned by Michelet *et al.* (2005), "*The construction of thousands of buildings in the Malpaís de Zacapu, shortly after AD 1250, constitutes a process both sudden and innovative in several respects*". This process is normally explained (according to the data provided by the Relación de Michoacán (Alcalá, 1988) - a document that describes the customs of the inhabitants of Michoacán, Mexico, before the Spanish conquest. It was elaborated towards 1540, most likely by the Franciscan friar Jerónimo de Alcalá, at the request of the first viceroy of the Nueva España, Don Antonio de Mendoza, with the information provided to him by old indigenous priests-) by the arrival of a chichimeca group (Uacusecha, *i.e.*, Eagles) to the Zacapu region during the 13th century, which marks the onset of a socio-political process that culminated, two centuries later, with the rise of the reino Tarasco (Michelet *et al.,* 2005).

Alternatively, however, this sudden process, and the corresponding displacements within the Zacapu basin area, could be well explained in terms of the volcanic impact caused by the effusive activity of El Metate.

Results from a recent investigation carried out at the El Estribo Volcanic Complex (EVC, Pola *et al.,* 2015) have questioned the classic interpretation of small size edifices as produced by short-lived monogenetic eruptions (*i.e.,* what type of volcanic structure should be considered monogenetic?) and their paused or continuous deposition character of the different eruptive phases. Cerro Negro volcano in Nicaragua, morphologically similar to any scoria cone, and which has been reactivated several times during its life span (Viramonte and Di Scala, 1970; Hill *et al.,* 1998), exemplifies well this situation. In fact, at least 23 historical eruptions have been described, posing a serious doubt to the monogenetic character of all these structures. In particular, the eruptive style that produced the Mexican shields (e.g., purely effusive or partly Strombolian) and their monogenetic or polygenetic nature remain under debate (Chevrel *et al.,* 2016a).

Finally, Pola *et al.* (2015) conclude by casting an alert on this classic interpretation of monogenetic volcanism because the potential volcanic risk of the MGVF (based on this classical interpretation) could be different as previously thought because of the occurrence of complex structures that could have formed as a result of several eruptive events (e.g., EVC, Cerro Grande, Cerro El Metate, Cerro Buenavista Tomatlán, Cerro Cuates, and Cerro Capaxtiro).

6.9 Conclusions

Seven out of the thirteen lava flows from El Metate volcano, central-western Mexico, were studied in detail by using conventional rock-magnetic, paleomagnetic, and paleointensity methods. Rock-magnetic results of IRM acquisition curves, hysteresis plots and thermomagnetic curves indicate dissimilar magnetic mineralogy between lava flows from the early and late eruptive stages, but similar magnetic mineralogy between lava flows coming from the same event, in good agreement with petrological observations reported.

Obtained mean-flow paleomagnetic directions from three out of the four early-flows (Flow 1- Flow 3) are statistically indistinguishable at the 95% confidence level. With the exception of Flow 6a, no consistent mean paleomagnetic directions could be obtained from late flows due to post-cooling movement of the blocks sampled. Flow 6a, however, yielded a slightly different - statistically distinguishable- mean paleomagnetic direction from that of the overall mean early-flows.

Between-flow differences of PI values obtained by the Thellier-Coe method (and in some cases supported by the alternative multispecimen PI method), which resembles the trend followed by the intensity curve predicted by the global model SHA. DIF.14k for the period 1000 AD 1600 AD, and which preclude the determination of an overall mean PI value, hardly supports the short emplacement period of between 50 and 100 years that was suggested previously. Moreover, individual paleodirectional dating of the studied flows lets propose a reasonable short-duration eruptive chronology of the early flows, not available otherwise by lava rheology considerations, as well as a likely difference of ~200 years between the early flows and some of the late flows, which extends the eruptive activity of El Metate to just prior to the arrival of the Spaniards.

Consequences of the prolonged effusive activity of El Metate could be found likely in the repopulation of the Zacapu area around AD 1250, which could have resulted from the massive displacements of inhabitants of the Metate area to this region.

As pointed out by Chevrel *et al.* (2016a), the eruptive style that produced the Mexican shields (e.g., purely effusive or partly Strombolian) and their monogenetic or polygenetic nature remain under debate. Under these circumstances, and in light of present high quality paleomagnetic data, the monogenetic nature of El Metate volcano seems to be questionable.

6.10 Supplementary material

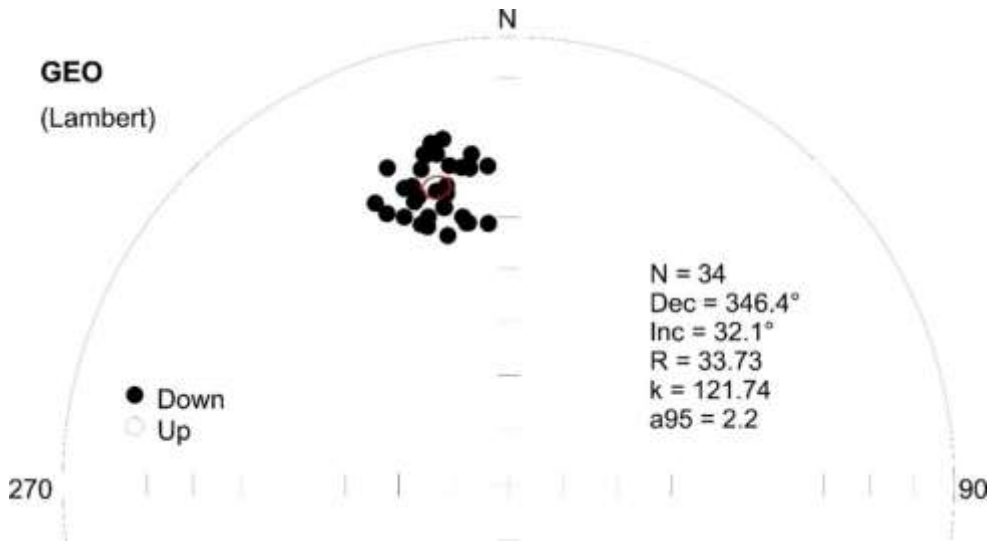

SM1 Mean paleomagnetic direction for early flows (Flow 1 – Flow 4).

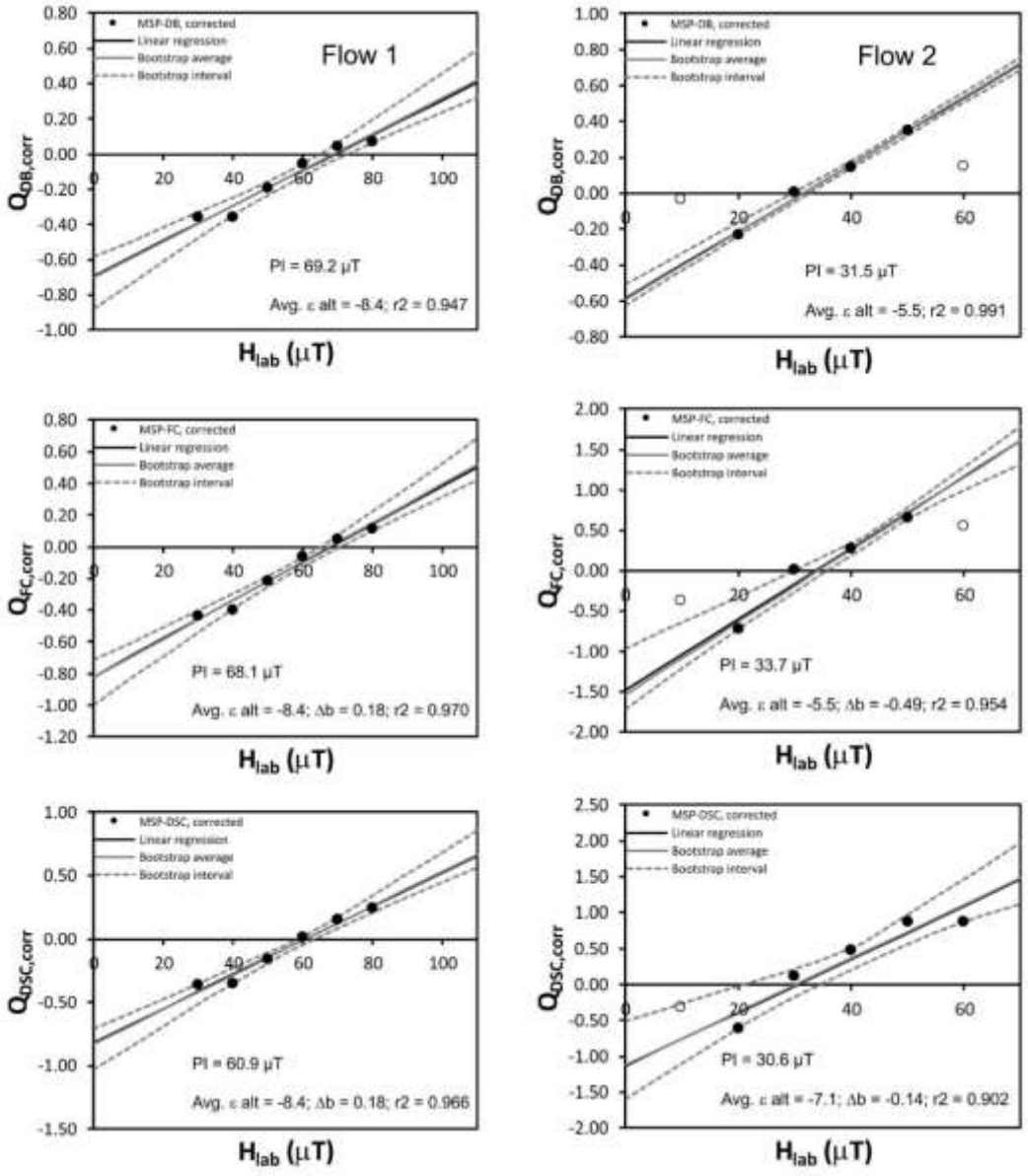

SM2 & SM3 Multispecimen PI plots for Flow 1 and Flow 2.

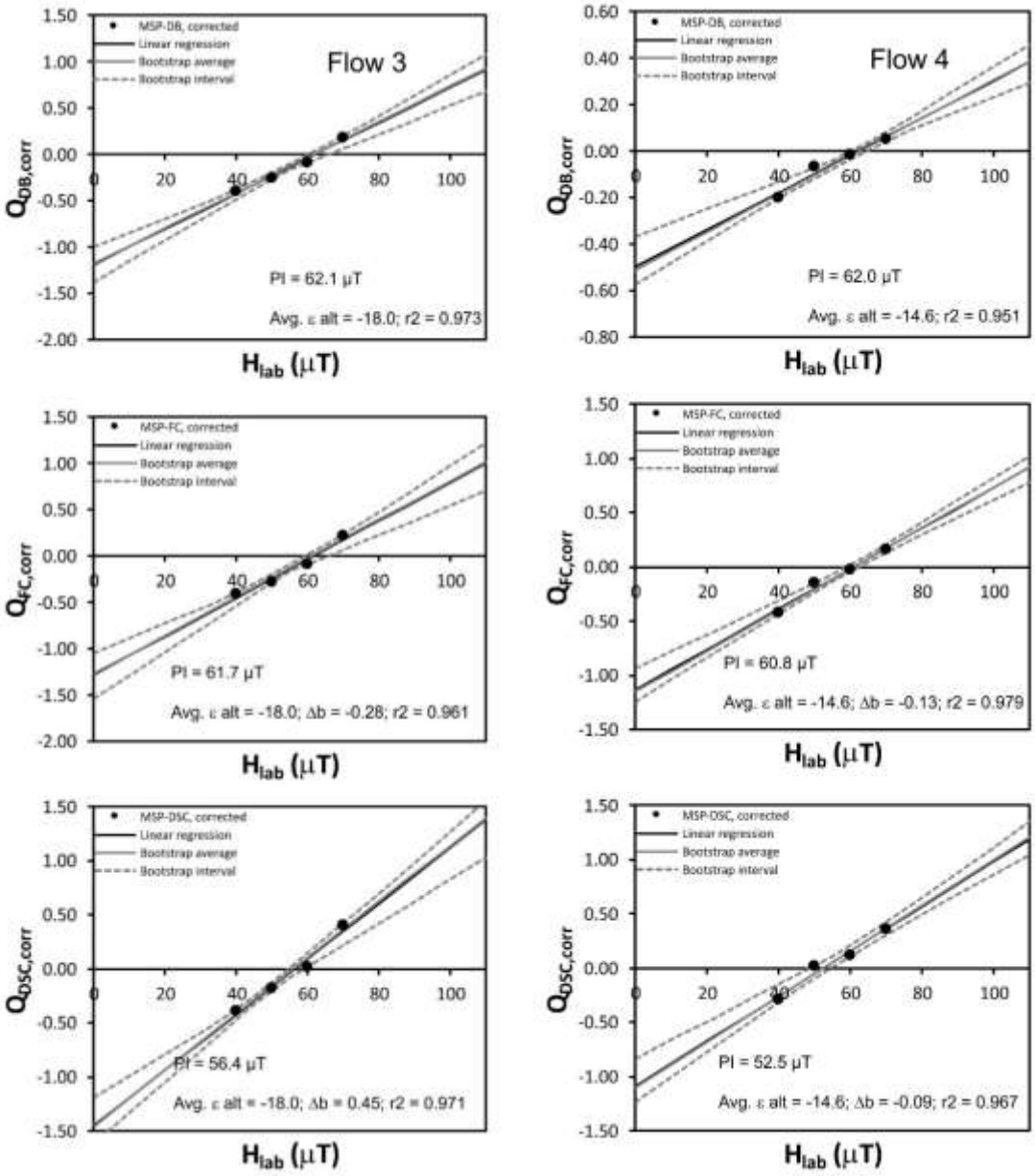

SM4 & SM5 Multispecimen PI plots for Flow 3 and Flow 4.

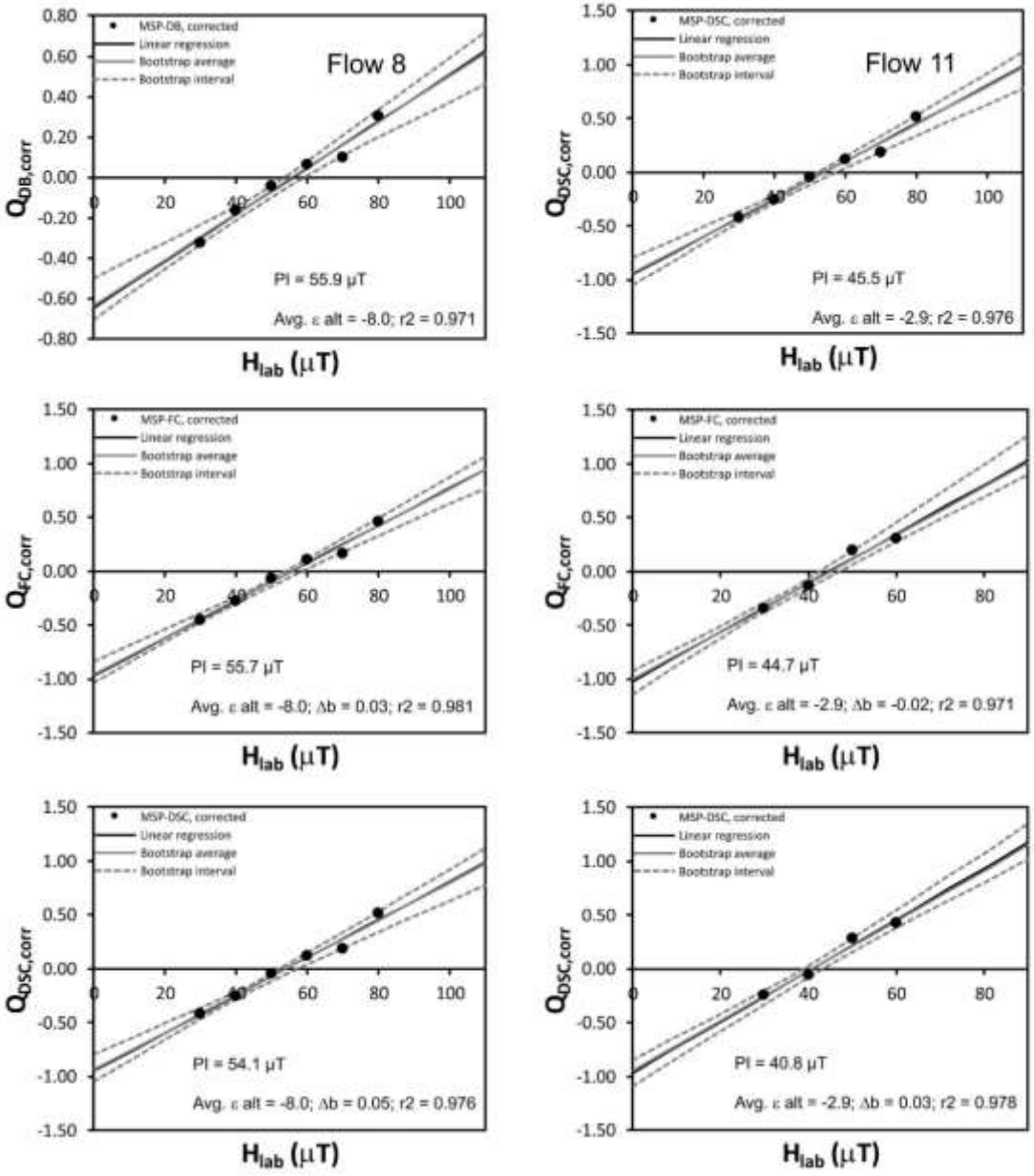

SM6 & SM7 Multispecimen PI plots for Flow 8 and Flow 11.

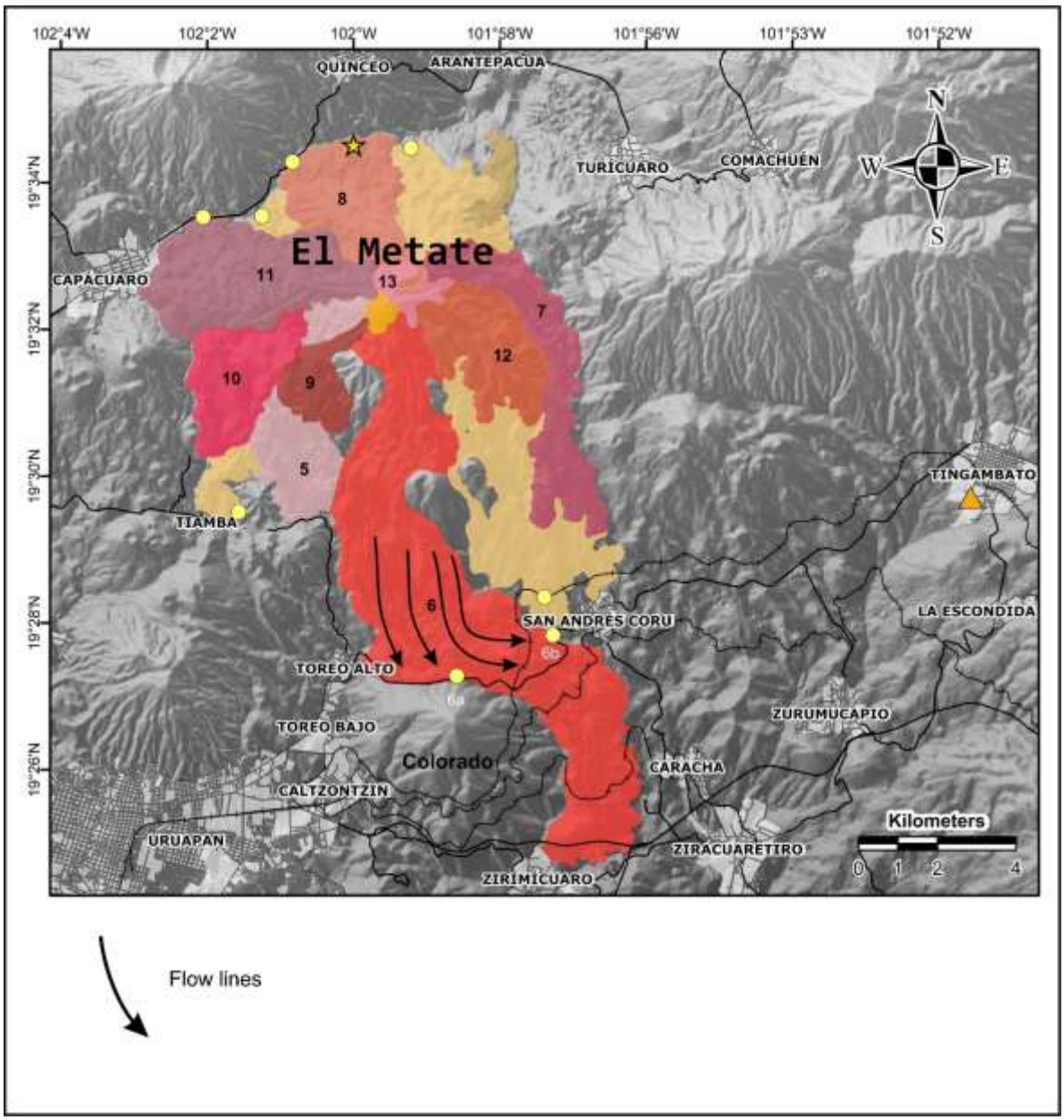

SM8 Topographical gradients and preexisting structures (particularly the Colorado volcano to the S) deviated the advance of Flow 6, altering its original southern trajectory to an eastern one.

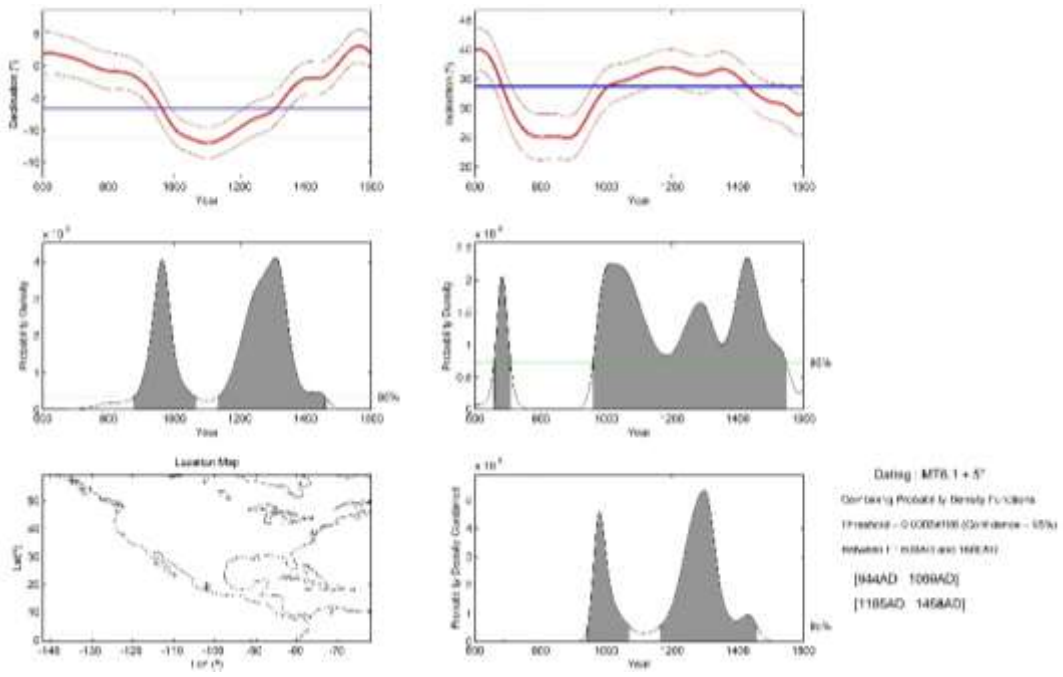

SM9 Paleomagnetic dating of Flow MT6.1 rotated 5° clockwise.

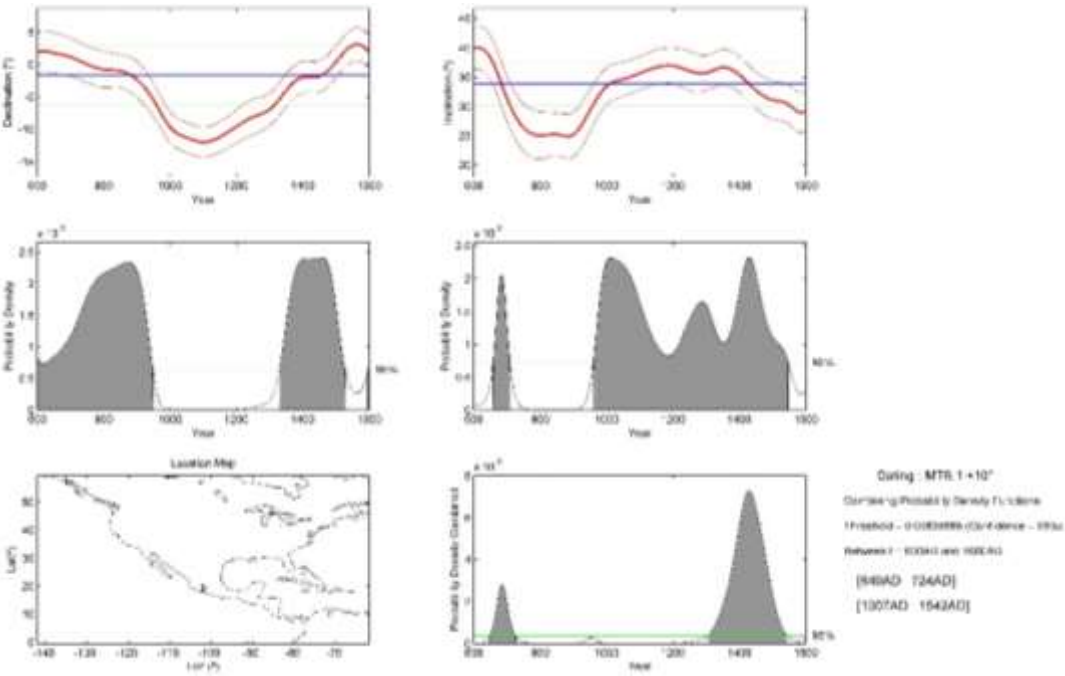

SM10 Paleomagnetic dating of Flow MT6.1 rotated 10° clockwise.

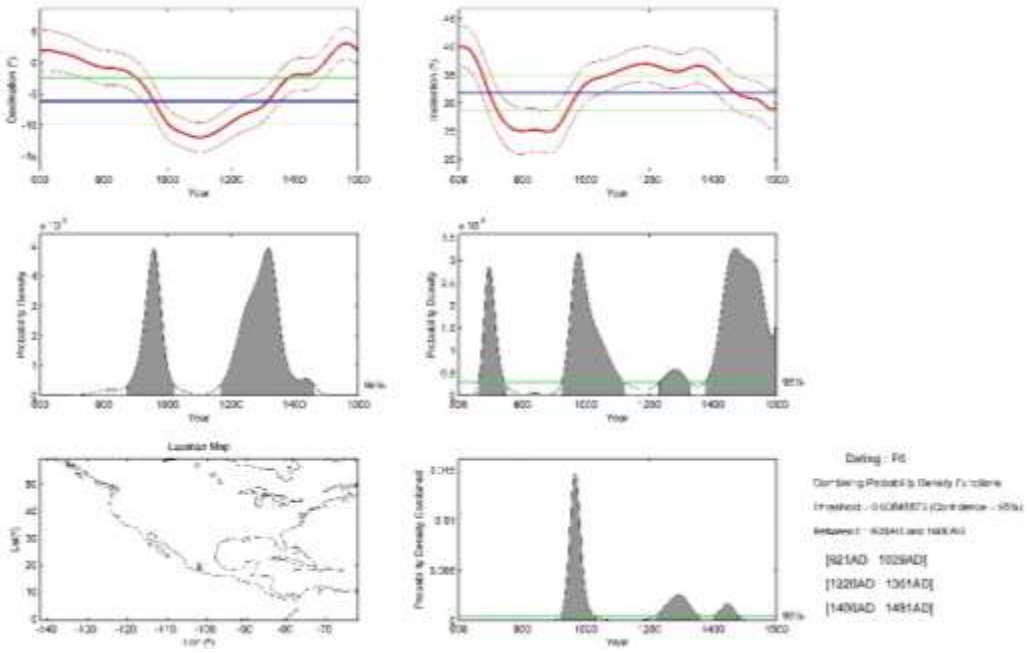

SM11 Paleomagnetic dating of Flow 6 using a combined direction (Flow 6a and MET6.1).

7. Consideraciones generales

Como se aprecia en el desarrollo de los capítulos 2 a 6, y como se puede consultar en la literatura desde los trabajos pioneros enfocados en la determinación de paleointensidades (PI), existe una gran cantidad de factores que influyen en la determinación certera de un valor de intensidad del campo magnético terrestre antiguo. Muchos de estos factores han sido representados de manera cuantitativa a través de criterios que han ido incrementando y/o evolucionando conforme los desarrollos teóricos y experimentales lo han requerido. Dada la variabilidad que existe con respecto a la cantidad de minerales magnéticos presentes en una roca y/o material arqueológico, así como su tipo, tamaño e historia térmica, es difícil, si no que prácticamente imposible, establecer un conjunto de parámetros que nos permitan predecir el éxito de un protocolo experimental para la determinación de PI considerando únicamente el tipo de material a tratar. Sin embargo, una primera caracterización de las muestras basada en experimentos de magnetismo de rocas (curvas de histéresis, campo inverso, curvas de magnetización remanente isotérmica, magnetización de saturación contra temperatura y/o susceptibilidad contra temperatura, etc.), permite realizar en un tiempo mínimo la caracterización de las muestras a partir de la cual se obtiene un panorama general de sus portadores de magnetización, por lo que se puede inferir el o los protocolos con los que se van a alcanzar las mejores estimaciones de intensidad. Aunado a esto, la implementación de (des)magnetizaciones térmicas y/o por campos alternos en muestras piloto ayudan a caracterizar las distintas componentes magnéticas registradas en los materiales de estudio; sus temperaturas de (des)bloqueo y la presencia de minerales de baja y alta coercitividad, cuyo conocimiento es también de utilidad al momento de seleccionar las técnicas más adecuadas para la determinación de paleointensidades, además de que permiten determinar si la remanencia es o no de origen térmico. Asimismo, como los resultados de la tesis lo sugieren, siempre que sea posible se recomienda realizar las determinaciones de PI empleando más de un protocolo experimental, lo cual puede conducir principalmente a dos caminos (ver resultados de los capítulos 4 a 6):

1. Obtener los mismos valores de intensidad (dentro de sus rangos de incertidumbre) con las distintas metodologías empleadas, aumentando la confiabilidad de los resultados obtenidos;
2. Obtener resultados distintos que requieran de análisis adicionales para justificar la disparidad en los valores.

En el segundo caso se puede implementar el uso de un método de PI adicional a los ya empleados para soportar alguno de los valores previamente obtenidos. Si adicionalmente se realiza un análisis a detalle de los minerales portadores de la magnetización empleando técnicas de microscopia junto con su caracterización geoquímica, se pueden determinar con mayor certeza las causas de la falla de alguno de los experimentos aplicados.

Por otra parte, tanto el análisis de la base de datos realizado para el desarrollo de la curva de variación secular de la intensidad en México para los últimos 3000 años (presentada en el apéndice A), como el análisis de las características de todas las curvas de variación secular de intensidad disponibles al año 2021 para el país (ver capítulo 2), permitieron realizar una evaluación de la calidad de los datos de PI publicados desde la década de los 60's del siglo pasado, hasta aquellos publicados recientemente. Como se mencionó de manera previa, los criterios que se emplean para determinar la calidad de los datos han ido incrementando con el tiempo, por lo que mientras más antiguas son las publicaciones, menor es la cantidad de parámetros reportados y por tanto aumenta la incertidumbre con respecto a su calidad. Esto no implica que los procedimientos empleados hayan sido incorrectos o que no se hayan realizado con el cuidado suficiente. Sin embargo, al no existir mayor posibilidad de evaluar su calidad se opta por descartarlos para su uso futuro en otros procedimientos como la elaboración de curvas de variación secular, por lo que se requiere que estos sitios sean analizados nuevamente para volver a determinar las propiedades del paleocampo registradas en ellos. Una forma de evitar que este problema se siga propagando es mediante la publicación de artículos con la mayor cantidad de información posible, incluyendo incluso las mediciones en crudo realizadas en laboratorio para que, al desarrollarse nuevos criterios de evaluación, se cuente con la información suficiente para realizar las determinaciones de dichos criterios sin la necesidad de volver a realizar todo el trabajo.

En el análisis realizado se observa que los datos de intensidades de los pasados 3 ka se encuentran concentrados principalmente dentro de la Faja Volcánica Transmexicana. Adicionalmente, de los 240 datos disponibles para esta temporalidad, únicamente 115 pueden ser considerados aceptables al ser evaluados utilizando uno de los conjuntos de parámetros de calidad vigentes (Paterson et al., 2014). Tomando en cuenta el año de publicación, el dato aceptado más antiguo pertenece al trabajo de Gratton *et al.,* 2005, obtenido para el volcán Jorullo mediante el método de microondas.

Cabe señalar además que la falta de consenso general dentro de la comunidad paleomagnética para homogenizar tanto la cantidad de parámetros a emplear para estipular la calidad de una determinación de PI, así como el valor umbral de estos, influye en la cantidad de datos que pueden ser o no considerados

de calidad, lo cual explica las diferencias en los comportamientos de las curvas de variación secular publicadas para México al observar un mismo rango temporal. Estas diferencias, a su vez, influyen en la determinación de edades al aplicar las curvas de variación secular como herramienta de datación. Sin embargo, como se observa en los resultados presentados en el capítulo 2, mientras mayor sea la cantidad de datos existente para una temporalidad específica, mejor será la descripción del comportamiento del parámetro del campo magnético terrestre que se esté representando (inclinación, declinación o intensidad), sin importar los criterios empleados para la determinación de la calidad de los datos. En este sentido es importante mencionar que el número de datos empleados para la elaboración de las curvas de variación secular en otros países (ej., la curvas de variación secular de la península ibérica de Molina Cardín *et al.*,2018, y la curva Italiana de Tema y Lanos 2020) es similar a la empleada en la construcción de las curvas de variación secular publicadas para México, por lo que se puede considerar que el trabajo realizado por los distintos grupos de paleomagnetistas en el país, aunque con muchas posibilidades de mejorar y una gran variedad de oportunidades por ser explotadas, va por un buen camino y a la par del desarrollo de la materia a nivel global.

A pesar de las discrepancias recién discutidas, parece ser más acertado el uso de las curvas de variación secular regionales en lugar de los modelos globales para la determinación de edades en un material, ya que de manera general se ha observado que los modelos globales muestran valores sobreestimados de la intensidad del campo magnético al ajustarlos al área que cubre el territorio mexicano.

Con todo lo descrito hasta este punto dentro de los párrafos anteriores, se pretende resaltar la importancia de la disponibilidad de datos de buena calidad para la descripción del comportamiento de la intensidad del campo magnético terrestre antiguo durante los últimos milenios, lo cual es muy valioso dada la gran variedad de aplicaciones que esto tiene dentro de las ciencias de la Tierra, abarcando desde la datación de artefactos geológicos y arqueológicos hasta el entendimiento de la evolución del interior de nuestro planeta y, como consecuencia, probablemente también de la evolución de los organismos en su superficie (ver Kravchinsky *et al.,* 2021: Qin *et al.,* 2022).

Como último punto se recomienda que conforme se vayan agregando datos a las curvas de variación secular, y estas tengan una mejor resolución, se realice una reevaluación de las edades obtenidas con el método paleomagnético para validar tanto las edades que se asociaron a estos materiales como las interpretaciones que de ellas se obtuvieron. Por otra parte, es importante considerar que aunque el trabajo que se presenta en esta tesis está enfocado en la determinación y uso de valores de intensidad del campo geomagnético antiguo, la adición de los valores de declinación, inclinación o ambos, a la

determinación de edades (los datos direccionales únicamente se pueden obtener de materiales que se encuentran *in situ* desde el momento en que adquirieron su registro de magnetización, ej.: flujos de lava o pisos quemados) aumenta la certidumbre en las dataciones debido a las restricciones temporales que se obtienen al combinar las curvas de variación secular de los parámetros que describen el comportamiento del campo magnético terrestre, por lo que se requiere también de un incremento en los esfuerzos para desarrollar curvas de variación secular de calidad para describir estos parámetros.

8. Conclusiones generales

En la presente tesis fueron analizados de manera detallada un total de 5 estructuras volcánicas y 18 fragmentos cerámicos pertenecientes a dos sitios arqueológicos. El trabajo realizado emplea todos los criterios que actualmente se consideran dentro de la literatura para realizar determinaciones de valores de PI de gran calidad, haciéndolos útiles para formar parte de la base de datos global (Geomagia50.v3; Brown *et al.,* 2015). Gracias al análisis riguroso y sistemático de estas muestras se llegó a las siguientes conclusiones:

- De las 11 cerámicas analizadas del sitio arqueológico de Tingambato se obtuvieron determinaciones de intensidades fiables para 4 de ellas. Las cerámicas recolectadas de los estratos superiores presentan dos componentes de magnetización, la primera asociada con el momento de elaboración de las cerámicas y la segunda con el incendio que probablemente llevó al abandono del sitio arqueológico hacia el año 900 de nuestra era. Con el análisis de la segunda componente de magnetización se estimaron temperaturas de entre 350 y 475 °C, dando un primer indicio de las temperaturas que se alcanzaron durante el incendio. Esta información puede ser de utilidad para que dentro de futuros estudios arqueológicos se comiencen a realizar inferencias sobre las probables causas de este evento.
- Aunque la falta de control estratigráfico de las cerámicas recolectadas sobre el flujo de lava "El Caracol" (zona del Malpaís de Zacapu, estado de Michoacán) limita las interpretaciones que se pueden derivar de las edades obtenidas de estas con respecto a su contexto arqueológico, los valores de intensidad bajos (~20 μT) registrados en dos de las cerámicas y las dataciones derivadas de tales valores sugieren que estos utensilios fueron elaborados antes de la edad que se había estipulado para el desarrollo de grupos humanos sobre este flujo de lava (~ AD 1200). Esto implica que el sitio pudo haber sido ocupado durante dos etapas: la primera antes del emplazamiento del Malpaís Prieto, estimado hacia el año 900 de nuestra era y correspondiente con las edades determinadas en la presente tesis, y la segunda posterior a dicho evento eruptivo, correspondiente con los datos de las investigaciones arqueológicas disponibles.
- En los dos trabajos en que se involucraron materiales arqueológicos se empleó por primera vez en México el método de la doble pendiente de Yu y Dunlop (2002) para la determinación de los valores de intensidad de dos momentos distintos en la historia térmica de un mismo material. De manera general este método ha sido muy poco empleado, y aunque los resultados obtenidos

tanto en esta tesis como en trabajos previos (ej., Lisé-Pronovost *et al.,* 2020) son coherentes y ofrecen una buena solución para resolver los problemas en que se ha implementado, se requiere de una revisión a detalle del método empleando materiales sintéticos con propiedades específicas y en condiciones controladas de laboratorio para asegurar su validez, especialmente para aquellas componentes que adquirieren su magnetización a bajas temperaturas y que poseen, por tanto, una mayor inestabilidad dado que son susceptibles a ser alteradas por procesos geológicos, antrópicos, e incluso por el mismo campo magnético terrestre después de registrar las magnetizaciones asociadas a los procesos que se consideren de interés en el diseño de la investigación.

Adicionalmente, al haber determinado los rangos de temperatura entre los que se encuentra cada una de las componentes de magnetización, se podría hacer uso del método de múltiples especímenes (empleando especímenes hermanos), para realizar determinaciones de intensidades dentro de las temperaturas asociadas a cada una de las componentes. Esto permitiría verificar la validez tanto del método de múltiples especímenes para componentes de alta y baja temperatura, como la validez del método de la doble pendiente.

- Con los experimentos llevados a cabo en las muestras de lava del volcán Xitle se puede apreciar que al utilizar un conjunto de parámetros de selección más estricto para evaluar los resultados de los experimentos de paleointensidades de tipo Thellier es posible reducir la dispersión en los valores de intensidad obtenidos por espécimen, reduciendo también la incertidumbre del valor de PI medio determinado. Adicionalmente, los distintos flujos de la lava analizados de la unidad V del volcán Xitle, muestran diferencias significativas entre los valores de intensidad de las lavas 1 y 2 con respecto a los valores registrados en las lavas 3 a 6, por lo que se puede inferir que estos conjuntos de lavas corresponden a eventos eruptivos diferentes, en donde no necesariamente ambos surgieron del volcán Xitle.
- En el estudio multimetodológico realizado sobre tres estructuras volcánicas pertenecientes al campo volcánico Michoacán-Guanajuato presentado en el capítulo 5, se aprecia la utilidad de la aplicación de distintas metodologías para la determinación de paleointensidades en un mismo sitio como un factor adicional para verificar la veracidad de los resultados obtenidos. En este trabajo además se hace evidente la falta de rigurosidad en los criterios de calidad empleados en trabajos publicados durante el siglo pasado, por lo que al volver a determinar los valores de intensidades del campo magnético terrestre antiguo registrados en estas lavas empleando criterios más actuales, los resultados tienden a variar. Para el flujo de lava del Malpaís Prieto y el

volcán monogenético el Jabalí se obtuvieron resultados congruentes a través del análisis multimetodológico, ofreciendo información de gran calidad para estas estructuras. Por otra parte, del material analizado del volcán Rancho Seco se obtuvieron valores de intensidad con una variación de aproximadamente 20 µT entre el método de múltiples especímenes y el protocolo IZZI. Aunque el valor obtenido al emplear el método de múltiples especímenes presenta una mayor concordancia con los valores de intensidad reportados para temporalidades similares, la determinación realizada con el protocolo IZZI es técnicamente correcta, por lo que se requiere de un análisis a detallado de los minerales portadores de la magnetización para dar una respuesta fundamentada a este hecho.

- El análisis de las propiedades magnéticas registradas en siete de los trece flujos de lava que conforman al volcán El Metate lleva al cuestionamiento de su naturaleza monogenética propuesta durante los primeros trabajos realizados sobre este volcán. De acuerdo con los estudios vulcanológicos publicados previamente, las lavas fueron separadas en dos grupos de acuerdo con sus características geoquímicas, los flujos 1 a 4 fueron reconocidos como la fase temprana y el resto de los flujos como la fase tardía. Las componentes direccionales registradas en estos flujos coinciden con la clasificación realizada mediante el análisis geoquímico, es decir, los valores de declinación e inclinación de las lavas de la fase tardía son distintos a los valores hallados en las lavas de la fase temprana. Esto sugiere el registro de variación secular sobre las lavas del volcán el Metate, fenómeno que es percibido en una escala de tiempo que comprende varias decenas de años, por lo que se infiere que el volcán tuvo más de un periodo eruptivo quedando fuera de la definición tradicional de un volcán monogenético.
- En los experimentos en que se emplearon los protocolos IZZI y Thellier-Coe para especímenes hermanos del mismo sitio (ver capítulos 4 y 5), se puede observar una menor tasa de éxito en los resultados obtenidos con el protocolo IZZI, así como menor dispersión en las paleointensidades obtenidas por espécimen, esto puede estar asociado a la mayor sensibilidad que tienen el protocolo IZZI para detectar la presencia de granos multidominio dentro de las muestras (Yu *et al.,* 2004).

Apéndice A: On the absolute geomagnetic intensity fluctuations in Mexico over the last three millennia

https://doi.org/10.1016/j.jsames.2020.102927

Rafael García, **Nayeli Pérez-Rodríguez**, Avto Goguitchaichvili, María Rodríguez Ceja, Juan Morales, Ana Maria Soler, Jaime Urrutia-Fucugauchi

Journal of South American Earth Sciences

A.1 Resumen

El Campo Magnético Terrestre (CMT) se caracteriza por presentar variaciones continuas en términos de dirección e intensidad a lo largo del tiempo. Estas fluctuaciones ocurren con periodicidades del orden de años a decenas de miles de años y constituyen una de las principales características del campo geomagnético. Revelar tales variaciones a escala regional tiene un impacto significativo dentro de la geofísica, dónde dicho conocimiento permite acercarse al entendimiento del origen y evolución del CMT, pero también tiene relevancia dentro de otras ciencias como la arqueología, ya que la disponibilidad de una curva de variación secular regional es útil como herramienta de datación. Por lo tanto, los estudios sobre las variaciones del CMT representan un claro ejemplo de investigación interdisciplinaria.

Debido a la importancia de las componentes no dipolares del campo geomagnético en la variación secular, las curvas de referencia únicamente se pueden construir para áreas limitadas, comúnmente dentro de un área con radio máximo de 1200 km. Actualmente se encuentran disponibles tres curvas de variación paleosecular elaboradas con información de las variaciones de paleointensidad dentro de Mesoamérica para los últimos tres milenios. Las curvas muestran tendencias contradictorias probablemente asociadas con la selección inapropiada de datos, así como con los criterios de calidad aplicados a las determinaciones de intensidades individuales.

En el presente trabajo se realiza la reevaluación crítica de los datos de intensidades publicados en artículos científicos, así como de los datos reportados en tesis de grado con especial énfasis en muestra correspondientes a los últimos 3600 años. La información fue utilizada en la elaboración de una curva de

variación secular regional considerando únicamente aquellos datos dentro de los criterios de calidad establecidos.

A.2 Abstract

Earth Magnetic Field is characterized by continuous variations in terms of direction and intensity. These fluctuations occur with periodicities of the order of years to tens of thousands of years and constitute the principal characteristic of the geomagnetic field. Revealing such variations at a regional scale has a significant impact in geophysics, but also in archaeology and thus represents a clear example of interdisciplinary research. Due to the importance of non-dipole field components in the secular variation, reference curves can only be constructed for limited areas, commonly within less than 1200 km radius. Three recently reported paleosecular variation curves for most Mesoamerica show contradictory trends, probably due to inappropriate selection of data and the criteria applied to individual intensity determinations. The use of unpublished data, essentially reported in thesis, may lead the discrepancy over the reported curves. Here, we report a critical revaluation of existing published and unpublished data with particular emphasis on the sample-radiometric age relationship for the last 3600 years.

A.3 Introduction

Regional-scale paleosecular variation curves (PSVC), obtained from directional and intensity data with varying degrees of detail in different regions of the world, describe geomagnetic field variations over the past centuries or millennia and can also be used as an archaeological dating tool (e.g., Lanos, 2004; Schnepp and Lanos, 2006; Pavón-Carrasco *et al.,* 2011). Currently, many areas in Europe have regional PSVC curves for archeomagnetic dating, such as Germany (Schnepp and Lanos, 2005), Austria (Schnepp and Lanos, 2006), Bulgaria (Kovacheva *et al.,* 2009, 2014), France (Gallet *et al.,* 2002), Greece (De Marco *et al.,* 2008, 2014), Hungary (Márton and Ferencz, 2006; Marton, 2010), Iberian Peninsula (Gómez-Paccard *et al.,* 2006a; Molina Cardín *et al.,* 2018), Italy (Tema *et al.,* 2006) or the United Kingdom (Zananiri *et al.,* 2007; Batt *et al.,* 2017). These paleosecular variation records also help to elucidate the fine characteristics of the Earth's Magnetic Field through archaeological times.

From the analysis of spherical harmonics, global models of the Earth's Magnetic Field (EMF) have been constructed using burned archaeological artefacts, volcanic flows and lake sedimentary records (e.g., Korte *et al.,* 2009; 2011a, b; Nilsson *et al.,* 2014). These types of models allow determining a secular variation curve for a given place within the study region, avoiding relocation errors. The main problem of many available models for the Holocene is that they incorporate sedimentary data. The magnetization registered by lake sediments is detrital and, thus, is subjected to effects that generate errors in the paleomagnetic record, such as shallow inclination values (Narumoto *et al.,* 2006). For this reason, Pavón-Carrasco *et al.* (2014) proposed a global model based exclusively on archeomagnetic and volcanic data, spanning the past 14,000 years (SHA.DIF.14 k), but with still important geographic and temporal gaps.

Recently, a great effort was paid to construct regional paleosecular variations curves in Mesoamerica (Goguitchaichvili *et al.,* 2018, Mahgoub et al., 2019b and Hervé *et al.,* 2019b). While Goguitchaishvili *et al.* (2018b) used available, selected intensities from Mexico and Southern United States, both Mahgoub *et al.* (2019a and 2019b) and Hervé *et al.* (2019a, 2019b) limited to mainly Mexican Mesoamerican sites. The discrepancies found with these studies motivated to perform a new, critical revaluation of both available data and model construction-techniques paying special attention to values retrieved from unpublished thesis. The record covers the last 3600 years, while only lava flows, burned archaeological artefacts and direct historical geomagnetic measurements (Goguitchaichvili *et al.,* 2020) were considered.

A.4 Database and selection criteria

The intensity values for the last 3600 years were recollected from GEOMAGIA50.v3 (Brown *et al.,* 2015) database providing a total of 243 intensities complemented with the most recent studies (Herve *et al.,* 2019b; Mahgoub *et al.,* 2019b; Pérez-Rodríguez *et al.,* 2020; Morales *et al.,* 2020). Moreover, some previous works were revaluated in light of new criteria for individual determinations (Ichikaantijo data reported in Goguitchaichvili *et al.,* 2018). Numerous datasets reported in PhD thesis on Teotihuacan ceramics (Rodriguez-Ceja *et al.,* 2012) were completely revaluated, which allowed increasing the density of archeointensities. The great majority of these studies used Thellier type protocols (Thellier and Thellier, 1959; Coe *et al.,* 1978). Other techniques consisted of microwave (Hill and Shaw, 2000) and Multiple Specimens protocols (Dekkers and Bohnel, 2006) in their extended form (Fabian and Leonhardt, 2010), considered as the most reliable methodologies. It should be noted that about 95% of the intensity data

available for Mexico were obtained well before (1970–2010) the current stringent acceptance criteria were proposed (Kissel and Laj, 2004; Biggin *et al.,* 2007; Leonhardt *et al.,* 2004; Paterson *et al.,* 2014) using some variant of the Thellier-Thellier methods. In this context, we established several selection criteria for datasets obtained using the Thellier and Microwave protocols. First, we ensured that intensities obtained from archaeological artefacts have been corrected by both the cooling rate (Chauvin *et al.,* 2000) and anisotropy corrections. The archeomagnetic studies of Mexico employed two primary types of anisotropy correction: Thermoremanence (ATRM) and Anhysteretic Remanent Magnetization (AARM) (McCabe and Jackson, 1985; Veitch *et al.,* 1984; Jackson, 1991). Many studies, however, used the so-called XYZ mean method (Morales *et al.,* 2009) to mitigate the remanence anisotropy effect. Mahgoub *et al.* (2019b) and Poletti *et al.* (2016) considered this approach as an imprecise method without performing any adequate experimentation to prove it. Hervé *et al.* (2019a), however, carried out an experimental analysis on modern bricks under actual conditions observing that the six specimens at different axis in the XYZ mean method may reduce the risk of anisotropy inaccuracy. In addition, detailed intensity acquisition simulation studies under modern conditions performed on ceramic and brick samples (Morales *et al.,* 2011; Calvo-Rathert *et al.,* 2019) showed a minor difference between values obtained from ATRM and XYZ mean approaches. Thus, we accepted these determinations if they were performed on 6 specimens. The intensities obtained using the microwave and Thellier methods may be tentatively divided into two groups; the first represents all intensities with the anisotropy and cooling rate corrections obeying some classical selection criteria: pTRM checks, $N \geq 5$ for temperature steps, fraction parameter (f) ≥ 0.5, the quality factor (q) ≥ 5, standard deviation (std) ≤ 5 μT for average intensity. The second group also considers the cooling rate and the anisotropy correction mentioned above, but additionally involves the parameters that allow quantifying thermal alteration ($\delta CK/\delta pal$) through the pTRM checks and the stability of the NRM directions during archeointensity experiments (MADanc, α, and DANG). Such approaches have been developed and implemented during the last decade, so a large percentage of the intensity data reported in Mexico does not provide such parameters. For this group, we decided to use a flexible criterion similar to the one used by Mahgoub *et al.* (2019b) with $N \geq 4$ temperature steps (per specimen), $f \geq 0.4$, $q \geq 5$, $MAD \leq 10$, $\delta CK \leq 10$, with the only differences in the average intensities with $N \geq 3$ number of specimens and std ≤ 5 μT. Finally, the quality of the intensities determined using the Multiple Specimen protocol (~3% of the intensity data in the database) were evaluated considering that all steps in the extended protocol (fraction and multidomain corrections; Fabian and Leonhardt, 2010) were carried out. In summary, 110 reliable intensities were selected for the last 3600 years (Figure A.1). As an additional exercise, we selected archeointensities from the Southern United States to compare them with the

Mexican record and evaluate whether non-dipole features of the geomagnetic field may result in a significant difference. In this way, 115 intensity values were selected applying the above-described selection criteria.

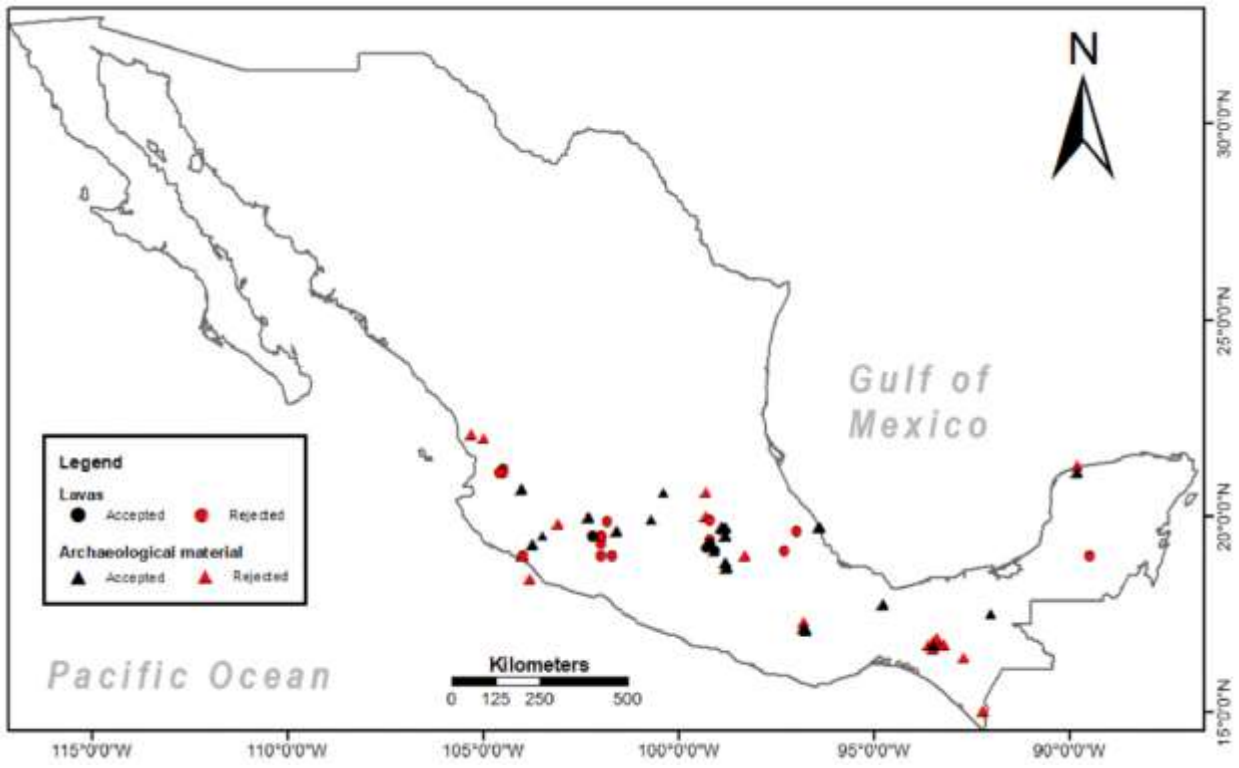

Figure A. 1 Archeointensites for the last 3600 years along of territory of Mexico for volcanic lava flows and burned archaeological artefacts.

A.5 Methodology

Developing a PSVC is a complex process that needs a high density of well-dated and homogeneous information concentrated in a relatively small area. Moreover, all data need to be readjusted to a common location (Mexico City in our case) by the pole reduction method of Noël and Batt (1990). We assume a dipolar field from the area of study using the VADM, where the original intensity *Fs* is relocated *FR* using the co-latitude in situ θ_S and the co-latitude of the common site θ_R

$$F_R = F_S\sqrt{\frac{1+3\cos\theta_R^2}{1+3\cos\theta_S^2}} \quad (1)$$

The necessary methodology to build a PSVC should mandatorily detect the presence of outliers, reduce the effect of the anomalous data in intensity values and ages in order to obtain a consistent and well-defined PSVC. The method developed by Thebault and Gallet (2010) has proven to be an extremely reliable way to build PSVCs (e.g., Goguitchaishvili *et al.,* 2018; Mahgoub *et al.,* 2019b; Kapper *et al.,* 2020). Thus, in the present study, we chose the bootstrap method to generate a collection of master curves interpolated by cubic penalized splines (Equation (2)) to mitigate the anomalies of information by a second-order matrix and the use of a smoother parameter to finally generate a master PSVC.

$$\hat{f} = (A^T W A + \lambda D)^{-1} A^T W^T f \quad (2)$$

Intensity estimated *f*, diagonal weighting matrix *W*, which involves the uncertainties of the intensities σf and for the ages σT, following the sum of variance $\sigma^2 = \sigma^2_f + \sigma^2_T$, the matrix based on a set of B-splines *A*, the matrix of penalty function which depends on the second time derivatives *D* and the damping parameters. λ.

A.6 Main results and discussion

The revaluation of Teotihuacan data (unpublished PhD thesis, Rodríguez-Ceja, 2009) was achieved based on the criteria established in the *Database* section using Thellier-Tool4.0 by Leonhardt *et al.* (2004). In total, 51 ceramic fragments belonging to three different sites within the Teotihuacan zone were re-evaluated; 7 of them come from Cuanalan (three selected data), 29 from Teopancazco (no selected data) and 15 from Xalla (three selected data). Significant differences were found between the originally reported and the re-evaluated data under this investigation. The most critical case was observed for the potshard of Teopancazco AA30, where Rodríguez-Ceja (2009) reported an archeointensity value of 25.59 ± 1.85 μT, while our revaluated data yields a value of 47.3 ± 3.3 μT (see database in supplementary material) which implies a difference greater than 20 μT. Previously published models of the PSVC in Mexico

(Mahgoub *et al.,* 2019b; Hervé *et al.,* 2019b) considered the original, unpublished dataset of Teotihuacan, generating an artificial deviation of the curve towards lower values. In this context, archeointensity values obtained for the Cuanalan (Mahgoub *et al.,* 2019b) should be considered as reliable.

The present selection criteria are quite similar to those established by Mahgoub *et al.* (2019b); the difference comes from the direct revision of the original articles and unpublished thesis where the archaeointensity data were reported. The selection parameters used in Mahgoub *et al.* (2019b) are as follows: $N \geq 5$ temperature steps, $\beta \leq 1$, $f \geq 0.5$, $q \geq 5$, $MAD_{anc} \leq 10$, $\alpha \leq 10$, $\delta CK \leq 10$, $\delta pal \leq 10$, $|K'| \leq 10$, average intensity with $N \geq 2$ and std ≤ 5. Additionally, they mentioned that when any of these parameters were not reported in the publications, the value should not be considered for modelling the PSVC. However, in a detailed review of the Mahgoub *et al.* (2019b) database, we noticed some discrepancies:

A. Although a cut-off value for the standard deviation is less than 5, 5 out of 38 accepted values in their database have a standard deviation > 5.
B. Some archeointensity values were rejected arguing that authors do not report MAD data, which is not true in the case of the study by Morales *et al.* (2013). Besides, archeointensity values were accepted when MAD data were not reported (e.g., data reported in Fanjat *et al.* (2013) and Duran *et al.* (2010), see please Supplementary Material for more details).
C. Archeointensity data with $f < 0.5$ are considered acceptable (e.g., CHAL02, CHAL22 and CHAL40 of Hervé et al. (2019a)).

In the present study, we compare the PSVCs for Mexico and Southern USA separately using the same mathematical procedure in order to reveal possible lateral, non-dipolar contribution mentioned by Mahgoub et al. (2019b). The Mexican curve covers the last 3600 years, while S-USA record goes up to the last 2000 years (Figure A.2).

Both PSVCs (Figure A.2) show a similar general trend for the last two millennia, sharing very similar amplitudes from 350 to 1250 AD, despite the difference of data and the distance between both regions. This similarity emphasizes that the variation of the intensity between Mexico and S-USA is too low to be considered, as already reported in Goguitchaishvili *et al.* (2018) using the relocation exercise with a maxima error lower than 3 μT. This finding evidences the suitability of using S-USA intensities to be incorporated into the Central Mexico curve. It is also obvious that when a rigorous selection is performed, there is no evidence of strong non-dipole contribution.

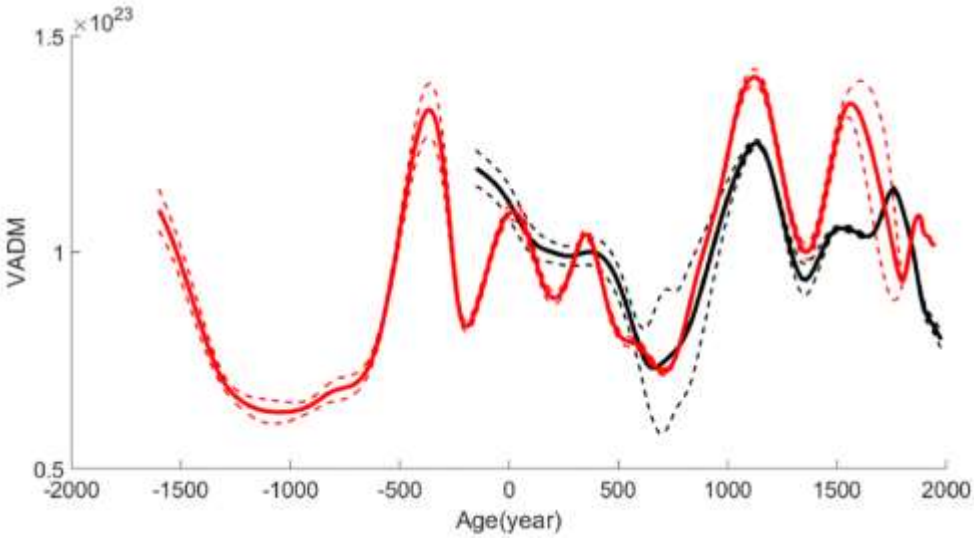

Figure A. 2 PSVC of Intensity from Mexico for the last 3600 years (red) vs. PSVC from S-USA for the last two millennia(black). (For interpretation of the references to color in this figure legend, the reader is referred to the Web version of this article).

The PSVC reported in Figure A.3 represents only selected data exclusively from Mexico, resulting in 110 archeointensities for the last 3600 years. This dataset has a maximum gap of 250 years, which is lower than the presented in the study of Mahgoub *et al.* (2019b). The archaeointensities present relatively high fluctuation between 45 µT to 24 µT for 1600 to 1000 BCE, following an increase until 500 BCE, and continuing with a marked periodic behavior until 348 AD, where the maximum reaches around 45 µT, with a minimum of 40 µT between its peaks. This is followed by a decreasing trend until 750 AD to reach a minimum of 33 µT. Another periodic trend with increasing intensities to 45.5 µT is detected from 1150 to 1576. Finally, a well-defined decrease is recorded using historical data from direct geomagnetic measurements (Goguitchaichvili *et al.,* 2020). The curve presents relatively low dispersion, which is probably due to the strict selection criteria, and thus high technical quality determinations (Figure A.3).

During the last years, the question of remanence anisotropy correction application raised many debates and criticism. The great inconvenience of Thellier and Thellier (1959) method and modifications (Coe *et al.,* 1978 among others) is the numerous heating (commonly more than 25). In addition, at least four pTRM checks and three additional heating for the cooling rate experiments are required, which definitively alter some way the original remanent magnetization (please see the discussion in Goguitchaichvili *et al.,* 2015 also mentioned below). The anisotropy correction suggested by some authors requires at least six additional heating at the high temperatures when usually less than 10% of original magnetization survives. Thus, there are almost ideal conditions for the eventual magneto-mineralogical

alteration. To try to overcome these circumstances, Morales *et al.* (2009) used an approach, which at least experimentally proved to be a reasonably good alternative to mitigate the anisotropy effect (Goguitchaichvili *et al.,* 2015). For each of the studied samples, small fragments of pottery are arbitrarily marked with parallel arrows on its internal or external flattening plane to create a reference orientation. Then, each ceramic fragment is broken into *"oriented"* specimens of different sizes. Six specimens with the same type of shape and volume (approx. 1 cm^3) are chosen per ceramic fragment and are then embedded in salt (NaCl) pellets compressed with a non-magnetic hydraulic press in order to treat them as standard paleomagnetic cores.

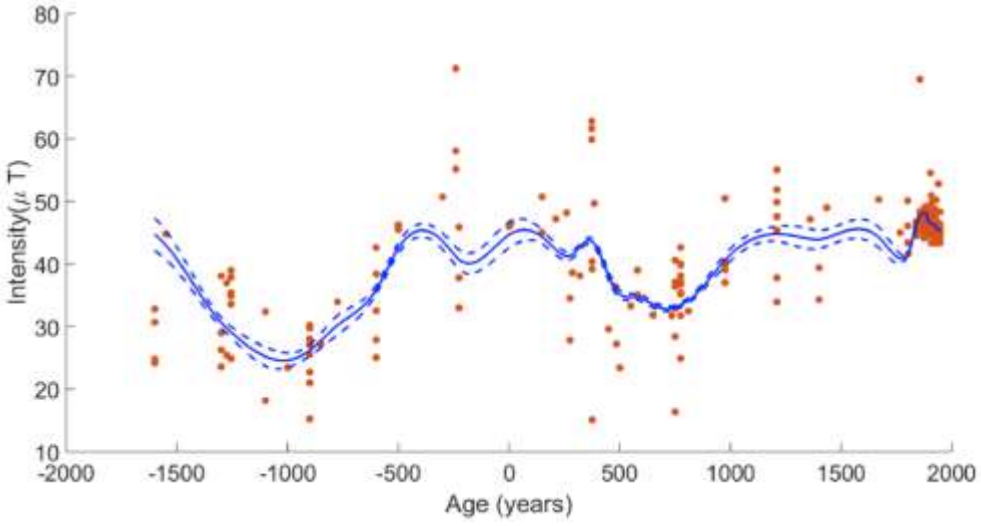

Figure A. 3 PSVC (blue) of the intensities selected for the last 3600 years exclusively from Mexico. (For interpretation of the references to color in this figure legend, the reader is referred to the Web version of this article).

Some authors, however, have criticized this approach. Poletti *et al.* (2016) presented some experimental evidence that the method suggested by Morales *et al.* (2009) should be abandoned. However, the comparison between results from both methodologies was carried out in only 5 out of 11 fragments. While the percent standard difference between the Mean (XYZ) intensity and the TRM tensor intensity - the so-called IE by Hervé *et al.* (2019a, 2019b), see below- is between 0.1 and 4.2% for 4 out of the 5 comparisons carried out, only one sample yielded a difference of 14.2% (selected as a proof of failure of the 'Mean (XYZ)' method).

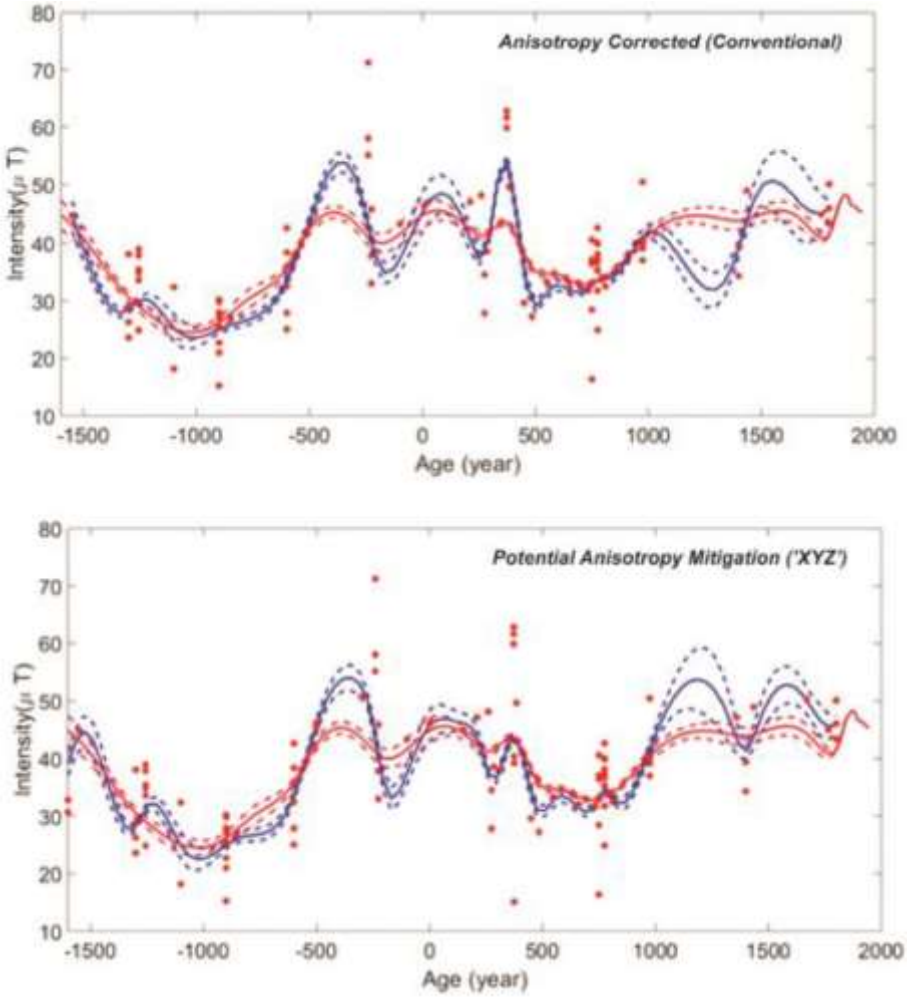

Figure A. 4 Comparison between the secular variation (blue) curves using anisotropy corrected values in a conventional way (upper panel) and those using the so-called 'XYZ' anisotropy mitigation approach (lower panel). SHA.DIF.14k (red curve) of Pavón-Carrasco *et al.* (2014) in both panels. Please see text for more details. (For interpretation of the references to color in this figure legend, the reader is referred to the Web version of this article.)

From the experiments carried out by Hervé *et al.* (2019a, 2019b), a maximum difference (which they denote as IE) of 5.6% was obtained by analyzing a couple of small baked bricks, and 3.8% for three pottery sherds. Archeomagnetic investigations, and particularly archeointensity studies, are normally carried out on various pottery sherds or specimens from a single sherd. Thus, from the integral analysis of the results presented by Herve et al. (2019a, 2019b) (Table 3S, Supplementary Material), a maximum IE of 3.7% for the baked bricks, and 0.5% in the case of the pottery sherds, respectively, are obtained. As properly noted by Hervé *et al.* (2019a, 2019b), averages should be calculated from six specimens with an equal contribution of the three axes. However, they overcame this premise and made an extreme hypothesis in

which the NRM would lie close to one axis: *"if the NRM were close to x-axis, the true palaeointensity would have been around 102–103 μT, whereas the average of the six specimens is 85.5 ± 11.5 μT".*

Summarizing, although in some cases data obtained using the method proposed by Morales *et al.* (2009) could be less precise and accurate, there are no justified reasons at all for considering it as unreliable. Figure A.4 shows the paleosecular variation curves for Mexico using anisotropy (conventional way) corrected data and those obtained by an anisotropy mitigation approach. Both curves show essentially similar trends, and some minor differences are due to unequal data distribution rather than methodology issues.

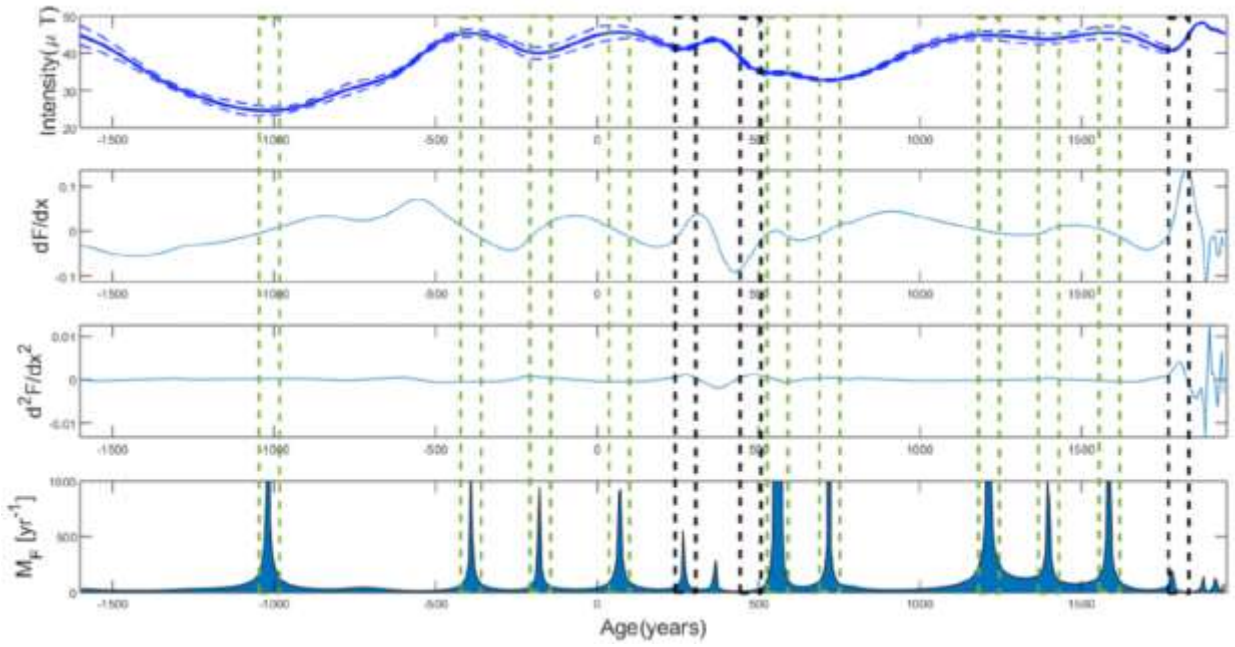

Figure A. 5 PSVC and its first and second derivatives with respect to time and MF (Pavón-Carrasco *et al.,* 2010), the black dotted lines are the most significant changes by its second derivative, the green dotted lines are the possible jerks detected (please see text for more details). (For interpretation of the references to color in this figure legend, the reader is referred to the Web version of this article.)

The PSVC was analyzed by its first and second derivative with respect to time and the exchange rate between them (Figure A.5). Parameter Mf (t) was used to find the most abrupt changes and jerks (Pavón-Carrasco *et al.,* 2010). The present PSVC has three rapid variations detected by its second derivative at 273, 467, and 1808 A.D., but the Mf (t) detected nine possible jerks at - 1024, - 384, - 184, 79, 574, 711, 1200, 1401, and 1589 A.D. However, only four coincides with jerks detected in Europe: three of them -

1024, 574, and 1589 coincide with jerks of the Balkans (Tema and Kondopolou, 2011) and one of 1401 AD for France (Gallet *et al.,* 2009), which represents the first jerks detected in America. The potential geomagnetic jerks detected should be considered with caution and need to be verified comparing with directional PSVC in future studies.

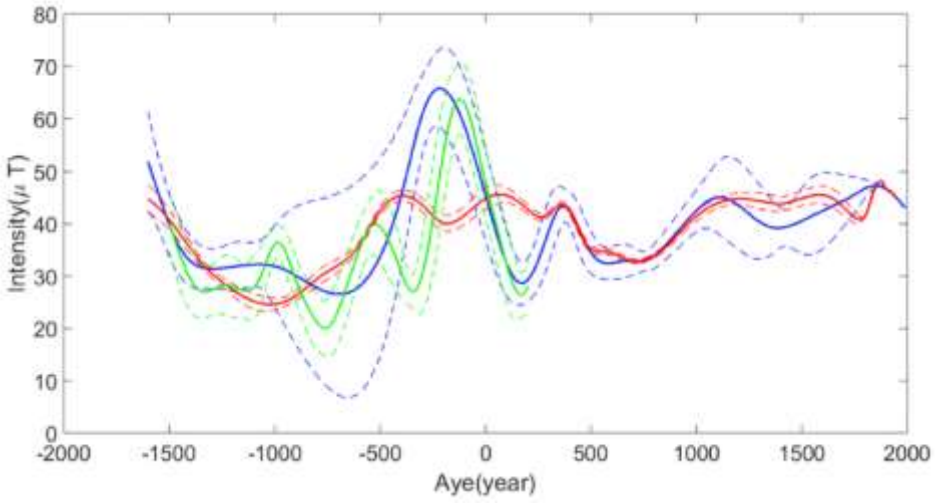

Figure A. 6 PSVC's from Mexico: Mahgoub *et al.* (2019b) (blue), Hervé *et al.* (2019b) (green), and the present study (red). (For interpretation of the references to color in this figure legend, the reader is referred to the Web version of this article).

The Mexican PSVC was compared with the previous curves for Mexico (Figure A.6) developed by Mahgoub *et al.* (2019b) using a bootstrap method following the methodology of Thebault and Gallet (2010), and the PSVC for the last 3500 years of Hervé *et al.* (2019b), constructed under a Bayesian framework (Lanos, 2004). A significant difference is observed between 1600 BCE and 350 AD. First, it should be noted that significant uncertainties observed in both previous models are not present in our curve. Second, the most important feature is a well-marked maximum around 250 BCE, which is completely absent in our curve.

The corresponding Virtual Dipole Moment (VADM) evolution in Mexico was compared to recently reported PSVC's for Africa (Kapper *et al.,* 2020) and Europe (Figure A.7, Gómez-Paccard *et al.,* 2016; Tema and Kondopolou, 2011). This comparison is valid because the authors used a similar mathematical procedure, excepting the PSVC of the Balkans, where Bayesian statistics was applied (Lanos, 2004). The interesting feature of this confrontation is that the several maxima detected on the respective PSVC's do not match at exactly the same age. Finally, the PSVC was compared with the SHA.DIF.14 k model (Pavón-Carrasco et al., 2014) for Mexico, attesting that both curves show essentially similar trends from 1600 BCE

to 500 AD, and a marked difference between 500 AD and present (Figure A.8). Both CALSK10k (Korte *et al.,* 2011a,b) and PFM9K (Nilsson *et al.,* 2014) models, however, show marked differences for several time intervals.

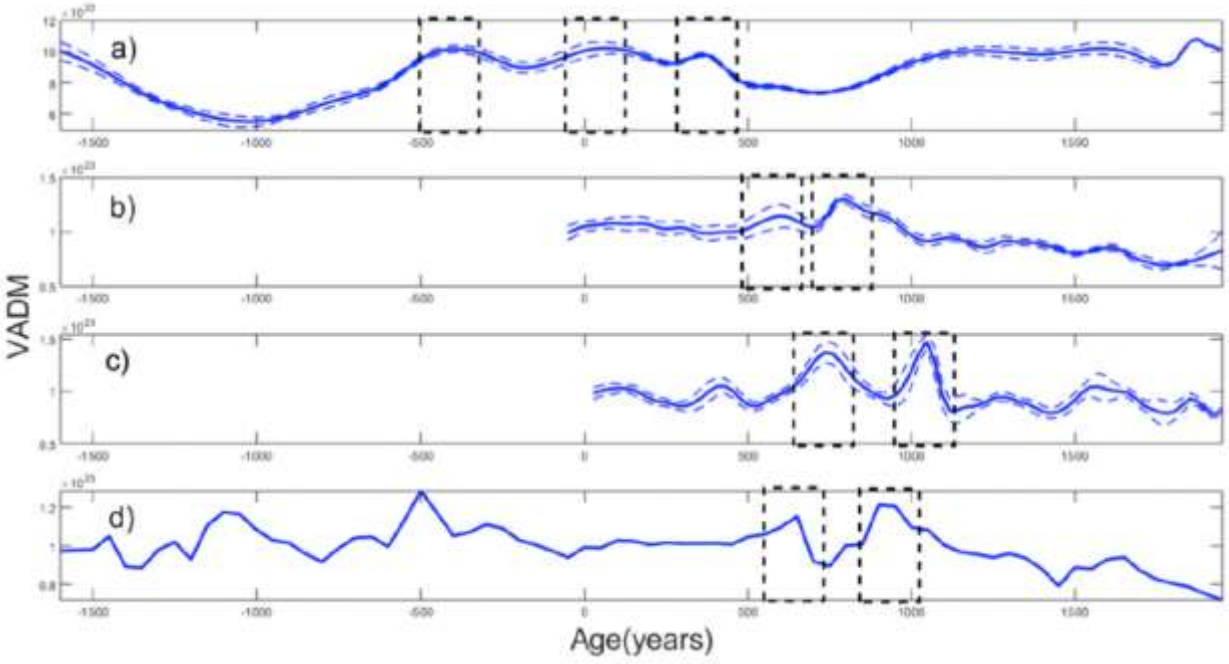

Figure A. 7 PSVC from a) Mexico, present study, b) North Africa (Kapper *et al.,* 2020), c) Paris (Gómez-Paccard *et al.,* 2016) and d) Balkans (Tema and Kondopolou, 2011).

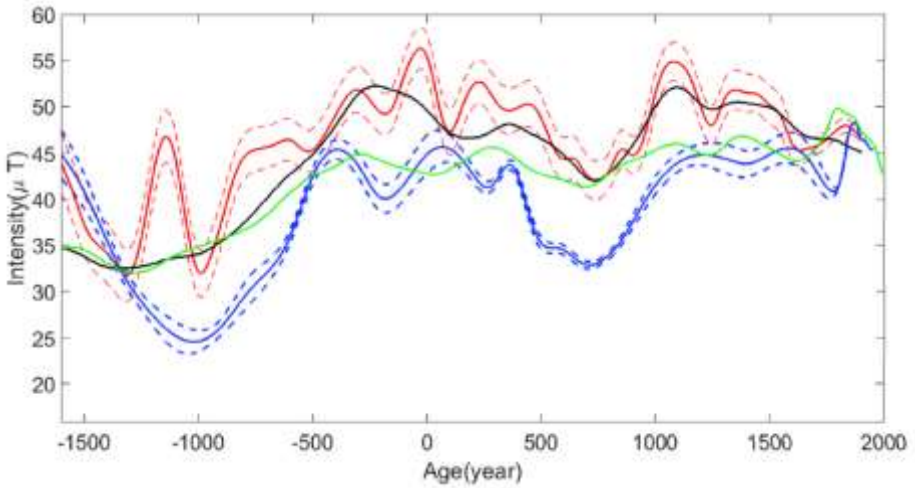

Figure A. 8 PSVC of the present study (blue) vs. SHA.DIF.14k (red) of Pavón-Carrasco *et al.* (2014). Also shown are the Pfm9k (black) and Cals10 k (green) models (Nilsson *et al.,* 2014; Korte *et al.,* 2011a, b). (For interpretation of the references to color in this figure legend, the reader is referred to the Web version of this article).

A.7 Conclusions

- A carefully selected absolute geomagnetic intensity data, which are homogeneously distributed throughout the last 3600 years in Mexico, allowed the development of a reliable paleosecular variation curve.

- Similar archaeointensity trends are observed between central Mexico and Southern United States, which excludes the existence of strong non-dipole contribution.

- The current paleosecular variation curve detected nine potential jerks, three of them have similarities to those detected in the Balkans and one for France, and thus probably correspond to global geomagnetic phenomena.

- The peak values detected within the present paleosecular variation curve show a possible west-drift movement attributed to some alteration within the Earth's outer core.

- The present curve shows a significant difference with previously reported trends. Because the data are distributed homogeneously and present low uncertainties, we believe that it should be used as a preferred dating tool for the involved region.

Referencias bibliográficas

AGICO, P., 2018. AARM – A Brief Practical Guide (Measurement of Anisotropy of Magnetic Remanence using JR-6 and LDA5/PAM1). AGICO Prints. https://www.agico.com/text/support/agicoprints/agicoprints.php Accessed September 6, 2018.

Aitken, M.J., 1970. Dating by archaeomagnetic and thermoluminescent methods. Philos. Trans. R. Soc. London, Ser. A 269, 77–88.

Aitken, M.J., 1983. Basic techniques for archaeointensity determination. Geomagnetism of Baked Clays and Recent sediments. Elsevier, pp. 86–87.

Aitken, M.J., Alcock, P.A., Bussell, G.D., Shaw, C.J., 1981. Archaeomagnetic determination of the past geomagnetic intensity using ancient ceramics: allowance for anisotropy. Archaeom. 23 (1), 53–64. https://doi.org/10.1111/j.1475-4754.1981.tb00954.x.

Aitken, M.J., Allsop, A.L., Bussell, G.D., Winter, M.B., 1988. Determination of the intensity of the Earth's magnetic field during archaeological times: reliability of the Thellier technique. Rev. Geophys. 26 (1), 3–12.

Alcalá fray Jerónimo de, 1988. La Relación de Michoacán, versión paleográfica, separación de textos, ordenación coloquial, estudio preliminar y notas de Francisco Miranda, México, secretaria de Educación Pública, Consejo Nacional para la Cultura y las Artes (Cien de México).

Alcalá, J., 1977. La relación de Michoacán. Colección Estudios Michoacanos V. Fimax Publicistas, Morelia, Michoacán.

Alva-Valdivia, L. M., 2005. Comprehensive paleomagnetic study of a succession of Holocene olivine-basalt flow: Xitle Volcano (Mexico) revisited. Earth Planets Space 57, 839–853. https://doi.org/10.1186/BF033 51862

Alva-Valdivia, L.M., Bravo-Ayala, M.A., Camps, P., Poidras, T., Mahgoub, A.N., 2020. Reassessment of paleointensity estimated of a single lava flow from Xitle volcano, Mexico, by means of multispecimen domain-state corrected, Journal of South American Earth Sciences 100, 102549

Alva-Valdivia, L.M., Rodríguez-Trejo, A., Cruz-Antillón, R., Hervé, G., Perrin, M., Salgado-Saito, M.M., Mahgoub, A.N., 2021. Archaeomagnetic dating and magnetic characterization of ceramics from the paquimé, casas grandes region, Chihuahua, Mexico. J. Arch. Sci. Rep. 37, 103. https://doi.org/10.1016/j.jasrep.2021.103040.

Arnauld, C., Carot, P., Fauvet-Berthelot, M.F., 1993. Arqueología De Las Lomas de La Cuenca Lacustre De Zacapu, Michoacán, México. Cuadernos De Estudios Michoacanos, 5. Centre de Etudes Mexicaines et Centroamericaines, México.

Arnold, J.T., Libby, W.F. (1951) Radiocarbon dates. Science, 113:111–120.

Ban, M., Hasenaka, T., Delgado-Granados, H., Takaoka, N., 1992. K–Ar ages of lavas from shield volcanoes in the Michoacan-Guanajuato volcanic field, Mexico. Geofis. Int. 31, 467–473.

Batt C.M., Brown M.C., Clelland S.J., Korte M., Linford P., Outram Z., 2017. Advances in archaeomagnetic dating in Britain: New data, new approaches and a new calibration curve. J. Archaeol. Sci., 85:66–82, https://doi.org/10.1016/j.jas.2017.07.002

Batt, C.M., 1998. Where to draw the line? The calibration of archaeomagnetic dates. Phys. Chem. Earth 23 (9–10), 991–995.

Béguin, A., Paterson, G.A., Biggin, A.J., de Groot, L.V., 2020. Paleointensity.org: an online, open source, application for the interpretation of paleointensity data. Geoch. Geoph. Geosys 21, e2019GC008791. https://doi.org/10.1029/2019GC008791.

Berger M.E., 2019. From a Cave near Tehuacán'. An attempt to reassemble post-classic mesoamerican ritual deposits that were separated by the art market C.G. Tremain, D. Yates (Eds.), The Market for Mesoamerica: Reflections on the Sale of Pre-Columbian Antiquities, University Press of Florida, Gainesville, 112-135

Biggin A.J., Perrin M., Dekkers M.J., 2007. A reliable absolute paleointensity determination obtained from a non-ideal recorder. Earth and Planetary Science Letters, 257:545–563, https://doi.org/10.1016/j.epsl.2007.03.017.

Biggin, A. J., Paterson, G. A., 2014. A New Set of Qualitative Reliability Criteria to Aid Inferences on Palaeomagnetic Dipole Moment Variations through Geological Time. Front. Earth Sci. 2, 1–9. https://doi.org/10.3389/feart.2014.00024

Biggin, A. J., Poidras, T., 2006. First-order symmetry of weak-field partial thermoremanence in multi-domain ferromagnetic grains. 1. Experimental evidence and physical implications. Earth Planet. Sci. Lett. 245, 438–453.

Böhnel, H. N., Dekkers, M. J., Delgado-Argote, L. A., Gratton, M. N., 2009. Comparison between the microwave and multispecimen parallel difference pTRM palaeointensity methods, Geophys. J. Int., 177, 383–394. doi: 10.1111/j.1365-246X.2008.04036.x

Böhnel, H., Biggin, A.J., Walton, D., Shaw, J., Share, J.A., 2003. Microwave palaeointensities from a recent Mexican lava flow, baked sediments and reheated pottery. Earth Planet Sci. Lett. 214, 221–236.

Böhnel, H., Morales, J., Caballero, C., Alva, L., McIntosh, G., Gonzalez, S., Sherwood, G., 1997. Variation of rock magnetic parameters and paleointensities over a single Holocene lava flow. J Geomag. Geoelectr. 49, 523–542. https://doi.org/10.5636/jgg.49.523

Boschman L.M., van der Wiel E., Flores K.E., Langereis C.G., van Hinsbergen D.J.J., 2019. The Caribbean and Farallon Plates Connected: Constraints From Stratigraphy and Paleomagnetism of the Nicoya Peninsula, Costa Rica. Journal of Geophysical Research: Solid Earth, 124(7). https://doi.org/10.1029/2018JB016369

Brown M.C., Donadini F., Korte M., Nilsson A., Korhonen K., Lodge A., Lengyel S.N., Constable C.G., 2015. GEOMAGIA50.v3: 1. General structure and modifications to the archeological and volcanic database. Earth, Planets and Space, 67(83), doi:10.1186/s40623-015-0232-0.

Brown, M.C., Donadini, F., Nilsson, A., Panovska, S., Frank, U., Korhonen, K., Schuberth, M., Korte, M., Constable, G.C., 2015. GEOMAGIA50.v3: 2.A new paleomagnetic database for lake and marine sediments. Earth Planets Space 67 (70). https://doi.org/10.1186/s40623-015-0233-z.

Brown, M.C., Hervé, G., Korte, M., Genevey, A., 2021. Global archaeomagnetic data: The state of the art and future challenges. Physics of the Earth and Planetary Interiors, https://doi.org/10.1016/j.pepi.2021.106766

Bullard, F.M., 1976. Volcanoes of the Earth. University of Queensland Press, Saint Lucia.

Bush, J., 2012. Architectural Patterning in the Purépecha Heartland: An Intrasite Settlement Study at the Urban Center of Sacapu Angamuco, Michoacán, México. Master's thesis, Department of Anthropology, Colorado State University, Fort Collins.

Butler, R.F., 1992. Paleomagnetism: Magnetic Domains to Geologic Terrains. Blackwell Science.

Butzer, K.W., 2013. Prehispanic Settlement Patterns in the Northwestern Valley of Mexico: The Zumpango Region. Journal of Historical Geography, 39.

Calvo, M., Prévot, M., Perrin, M., Riisager, J., 2002. Investigating the reasons for the failure of paleointensity experiments: a study on historical lava flows from Mt. Etna (Italy). Geophys. J. Int. 149, 44–63. https://doi.org/10.1046/j.1365-246X.2002.01619.x.

Calvo-Rathert, M., Morales-Contreras, J., Carrancho, A., Camps, P., Goguitchaichvili, A., Hill, M.J., 2019. Reproducibility of archaeointensity determinations with a multimethod approach on archaeological material reproductions. Geophys. J. Int. 218, 1719–1738. https://doi.org/10.1093/gji/ggz246.

Calvo-Rathert, M., Morales-Contreras, J., Carrancho, Á., Gogichaishvili, A., 2016. A comparison of Thellier-type and multispecimen paleointensity determinations on Pleistocene and historical lava flows from Lanzarote (Canary Islands, Spain). Geochem., Geophys., Geosystems, https://doi.org/10.1002/2016GC006396

Carot, P., 2005. Reacomodos demográficos del Clásico al Postclásico en Michoacán: el retorno de los que se fueron. En Reacomodos demográficos del Clásico al Posclásico en el centro de México. Universidad Nacional Autónoma de México, Instituto de Investigaciones Antropológicas, pp. 103–122.

Carvallo, C., Roberts, A.P., Leonhardt, R., Laj, C., Kissel, C., Perrin, M., Camps, P., 2006. Increasing the efficiency of paleointensity analyses by selection of samples using first-order reversal curve diagrams. J. Geophys. Res. 11, B12103. https://doi.org/10.1029/2005JB004126.

Casas, L., Auguet, C., Cantoni, G., López-Vilar, J., Guasch, N., Prevosti, M., 2018. Using archaeomagnetism to improve the dating of three sites in Catalonia (NE Spain). J. Cult. Herit. 31, 152–161. https://doi.org/10.1016/j.culher.2017.11.004.

Casas, L., Tema, E., 2019. Investigating the expected archaeomagnetic dating precision in Europe: a temporal and spatial analysis based on the SCHA.DIF.3K geomagnetic field model. J. Archaeol. Sci. 108, 15. https://doi.org/10.1016/j.jas.2019.104972.

Castro, I., Brown, L., 1987. Shallow paleomagnetic directions from historic lava flows, Hawaii. Geophys. Res. Lett. 14, 1203–1206.

Cejudo-Ruiz, R., García-Ruiz, R., Pelz-Marín, A., Goguitchaichvili, A., Morales, J., Cervantes-Solano, M., Bautista-Zuñiga, F., 2019. Intervención arqueomagnética en el Ocote (Aguascalientes, México): Implicaciones cronológicas absolutas. Arqueol. Iberoam. 44, 3–9.

Cervantes-Solano, M., Cifuentes-Nava, G., Caballero-Miranda, C.I., Goguitchaichvili, A., López-Loera, H., Delgado-Granados, H., Morales-Contreras, J., Urrutia-Fucugauchi, J. (2019) Estudio magnético

integral de flujos de lava del volcán Xitle: implicaciones arqueológicas sobre el abandono de Cuicuilco. Bol. Soc. Geol. Mex., 71(2):397–411. http://dx.doi.org/10.18268/BSGM2019v71n2a10

Chadima, M., 2018. Anisoft5. Anisotropy data browser. Version 5.1.01. https://www.agico.com/text/softw_are/anisoft/anisoft.php. Agico company. Accessed April 6 2018.

Chadima, M., Hrouda, F., 2006. Remasoft 3.0—a user-friendly paleomagnetic data browser and analyzer. Travaux Géophysiques XXVII, 20–21.

Chadima, M., Hrouda, F., 2012. Cureval 8.0.2: Thermomagnetic Curve Analyzer for Windows. Agico, Inc.

Chauvin, A., García, Y., Lanos, Ph., Laubenheimer, F., 2000. Paleointensity of the geomagnetic field recovered on archaeomagnetic sites from France. Phys. Earth Planet. Inter. 120, 111–136. https://doi.org/10.1016/S0031-9201(00)00148-5.

Chauvin, A., Guerrero-Suarez, S., Pérez-Fuentes, J.C., McIntosh, G., Catanzariti, G., Sastre-Blanco, J.C., Larrazabal, J., Fernández-Martínez, V.M., Martín-Viso, I., García-Rubert, D., 2018. Updated iberian archaeomagnetic catalogue: new full vector paleosecular variation curve for the last three millenia. G-cubed 19. https://doi.org/10.1029/2018GC007781.

Chernov, N., 2020. Circle fit (Pratt method). https://www.mathworks.com/matlabcentral/fileexchange/22643-circle-fit-pratt-method. MATLAB Central File Exchange. Accessed January 28, 2020.

Chevrel, M.O., Guilbaud, M.-N., Siebe, C., 2016. The ~AD 1250 eruption of El Metate shield volcano (Michoacan, Mexico): magma source, crustal storage, eruptive dynamics, and lava rheology. Bull. Volcanol. 78 (4), 1–18, 32.

Chevrel, M.O., Siebe, C., Guilbaud, M.-N., Salinas, S., 2016. The AD 1250 El Metate shield volcano (Michoacan): Mexico's most voluminous Holocene eruption and its significance for archeology and hazards. Holocene 26 (3), 471–488.

Coe, R. S., Grommé, S., Mankinen, E. A., 1978. Geomagnetic paleointensities from radiocarbon-dated lava flows on Hawaii and the question of the Pacific nondipole low. J. Geophys. Res. 83, 1740–1756. https://doi.org/10.1029/JB083iB04p01740.

Coe, R.S., 1967. The determination of paleointensities of the Earth's magnetic field with emphasis on mechanisms which could cause non-ideal behavior in Thellier's method. J. Geomagn. Geoelectr., 19(3):157–179. https://doi.org/10.5636/jgg.19.157

Cohen, A. S., 2016. Creating an Empire: Local Political Change at Angamuco, Michoacan, Mexico. PhD's thesis, Department of Anthropology, University of Washington, Seattle.

Connor, C. B., 1987. Structure of the Michoacán-Guanajuato volcanic field, Mexico. J. Volcanol. Geotherm. Res. 33, 191–200. https://doi.org/10.1016/0377-0273(87)90061-8.

Constable, C., Korte, M., Panovska, S. (2016) Persistent high paleosecular variation activity in southern hemisphere for at least 10000 years. Earth Planet. Sci. Lett.453, 78–86. https://doi .org /10 .1016/j.epsl.2016.08.015.

Cromwell, G., Tauxe, L., Staudigel, H., Ron, H., 2015. Paleointensity estimates from historic and modern Hawaiian lava flows using glassy basalt as a primary source material. Phys. Earth Planet. Interiors, 241, 44–56. doi: 10.1016/j.pepi.2014.12.007

Cruz, L.M., Landa, O., 2013. Tingambato. Un sitio del Occidente de México y una tuba real. Arqueol. Mex. 21 (123), 43–46.

Darin, M. H., Bennett, S.E.K., Dorsey R.J., Oskin, M.E., Iriondo, A., 2016. Late Miocene extension in coastal Sonora, México: Implications for the evolution of dextral shear in the proto-Gulf of California oblique rift. Tectonophysics, 693 (B), https://doi.org/10.1016/j.tecto.2016.04.038

Darras, V., 1998. Presentación. Genesis, Culturas y Espacios en MICHOACAN. Centro de Estudios Mexicanos y Centroamericanos, pp. 11–12. V.

Day, R., Fuller, M., Schmidt, V. A., 1977. Hysteresis properties of titanomagnetites: grainsize and compositional dependence. Phys. Earth Planet. Inter. 13, 260–267. https://doi.org/10.1016/0031-9201(77)90108-X.

De Groot, L. V., Biggin, A. J., Dekkers, M. J., Langereis, C. G., Herrero-Bervera, E., 2013. Rapid regional perturbations to the recent global geomagnetic decay revealed by a new hawaiian record. Nat. Commun. 4, 1–7. https://doi.org/10.1038/ncomms3727

De Groot, L.V., Béguin, A., Kosters, M.E., van Rijsingen, M., Struijk, E.L.M., Biggin, A.J., Hurst, E.A., Langereis, C.G., Herrero Dekkers, M.J., 2015. High paleointensities for the Canary Islands constrain the Levant geomagnetic high. Earth Planet. Sci. Lett. 419, 154–167. https://doi.org/10.1016/jepsl.2015.03.020.

De Marco E., Spassov S., Kondopoulou D., Zananiri I. Gerofoka E., 2008. Archaeomagnetic study and dating of a Hellenistic site in Katerini (N. Greece). Phys.Chem. Earth, 33(6):481–495, doi: 10.1016/j.pce.2008.02.017

De Marco E., Tema E., Lanos P., Kondopoulou D., 2014. An updated catalogue of Greek archaeomagnetic data for the last 4500 years and a directional secular variation curve. Studia Geophysica et Geodaetica, 58(1):121–147, https://doi.org/10.1007/s11200-013-0910-y

De Silva S., Lindsay J.M., 2015. Primary Volcanic Landforms. Sigurdsson, H. (2 Ed.), In: The Encyclopedia of Volcanoes. Academic Press, pp. 274–295.

Dekkers, M.J., Böhnel, H.N., 2006. Reliable absolute palaeointensities independent of magnetic domain state. Earth Planet Sci. Lett. 284, 508–517.

Delgado-Granados, H., Molinero, R., Cervantes, P., Nieto-Obregón, J., Lozano-Santa Cruz, R., Macías-González, H.L., Méndoza-Rosales, C., Silva-Romo, G. (1998) Geology of Xitle volcano in southern Mexico City -A 2000-year-old monogenetic volcano in an urban área. Revista Mexicana de Ciencias Geológicas 15(2):115–131.

Demant, A., 1992. Marco geológico regional de la laguna de Zacapu, Michoacán, México. In: Demant A., Labat J. N., Michelet D., Tricart J., (editors), El Proyecto Michoacán 1983 – 1987. Medio Ambiente e Introducción a los trabajos Arqueológicos. CEMCA, México, D.F. Collect. Etudes Mesoam. II (11), 53–72.

DuBois, R.L., 1975. Secular variation in southwestern United States as suggested by archaeomagnetic studies. In: Fischer, R.M., Fuller, M., Schmidt, V.A., Wasilewski, P. J. (Eds.), Takesi Nagata Conference - Magnetic Fields: Past and Present. Goddard Space Flight Center, Greenbelt, Maryland.

Dumberry M., Finlay C.C., 2007. Eastward and westward drift of the Earth's magnetic field for the last three millennia. Earth and Planetary Science Letters, 254:146–157, https://doi.org/10.1016/j.epsl.2006.11.026

Dunlop, D. J., Özdemir, Ö., 2015. 5.08 Magnetization in Rocks and Minerals. In: Schubert, G. (Ed.), Treatise on Geophysics (Second Edition) Elsevier, Oxford, 255 – 308. http://dx.doi.org/10.1016/B978-0-444-53802-4.00102-0

Dunlop, D., 2002. Theory and application of the Day plot (Mrs/Ms versus Hcr/Hc) 1. Theoretical curves and test using titanomagnetite data. J. Geophys. Res. 10 (B3) https://doi.org/10.1029/2001JB000486.

Enterpinar, P., Langereis, C.G., Biggin, A.J., de Groot, L.V., Kulakoglu, F., Osmura, S., Süel, A., 2016. Full vector archaeomagnetic records from Anatolia between 2400 and 1350 BCE: implications for geomagnetic field models and the dating of fires in antquity. Earth Planet. Sci. Lett. 434, 171–186.

Espejel-Carbajal, C., 2014. Las Investigaciones Arqueológicas En Michoacán: Avances, Problemas y Perspectivas. El Colegio de Michoacán, Zamora Michoacán.

Fabian K., Leonhardt R., 2010. Multiple-specimen absolute paleointensity determination: An optimal protocol including pTRM normalization, domain-state correction, and alteration test. Earth and Planetary Science Letters, 297:84–94, https://doi.org/10.1016/j.epsl.2010.06.006

Fabian, K., 2001. A theoretical treatment of paleointensity determination experiments on rocks containing pseudo-single or multi domains magnetic particles. Earth Planet Sci. Lett 188, 45–58. https://doi.org/10.1016/S0012-821X(01)00313-2.

Fabian, K., 2003. Some additional parameters to estimate domain state from isothermal magnetization measurements. Earth Planet. Sci. Lett. 213, 337–345. https://doi.org/10.1016/S0012-821X(03)00329-7.

Fabian, K., Leonhardt, R., 2010. Multi-specimen absolute paleointensity determination: an optimal protocol including pTRM normalization, domain-state correction and alteration test. Earth Planet. Sci. Lett. 297, 84–94. doi:10.1016/j.epsl.2010.06.006

Fergusson, G.S, Libby, W.F. (1963) UCLA radiocarbon dates 11. Radiocarbon 5: 1–22.

Fisher, C. T., Cohen, A. S., Fernandez-Diaz, J. C., Leisz, S. J., 2017. The Application of Airborne Mapping LiDAR for the Documentation of Ancient Cities and Regions. Quat. Int. 448, 129–138. http://dx.doi.org/10.1016/j.quaint.2016.08.050

Fisher, C. T., Cohen, A. S., Solinis-Casparius, R., Pezzutti, F. L., Bush, J., Forest, M., Torvinen, A., 2019. A Typology of Ancient Purépecha (Tarascan) Architecture from Angamuco, Michoacán, Mexico. Lat. Am. Antiq. 30 (3), 510 – 528. https://doi.org/10.1017/laq.2019.50

Fox, J.M.W., Aitken, M.J., 1980. Cooling rate dependence of the thermoremanent magnetization. Nature 283, 462–463. https://doi.org/10.1038/283462a0.

Francés-Negro, M., Carrancho, A., Pérez-Romero, A., Arsuaga, J.L., Carretero, J.M., Iriarte, E., 2019. Storage or cooking pots? Inferring pottery use through archaeomagnetic assessment of palaeotemperatures. J. Archaeol. Sci. 110 https://doi.org/10.1016/j.jas.2019.104992.

Frank, U., Nowaczyk, N. R., 2008. Mineral magnetic properties of artificial samples systematically mixed from haematite and magnetite. Geophys. J. Int. 175, 449 – 461. https://doi.org/10.1111/j.1365-246X.2008.03821.x

Gallet Y., Genevey A., Le Goff M., 2002. Three millennia of directional variation of the Earth's magnetic field in western Europe as revealed by archaeological artefacts. Phys. Earth Planet. Inter. 131:81–89, https://doi.org/10.1016/S0031-9201(02)00030-4

García – García, G., 2017. El estudio cerámico de Tingambato, Michoacán, como un indicador de desarrollo local. Bachelor thesis. Veracruzana University, Xalapa, Veracruz.

García, R., Pérez-Rodríguez, N., Goguitchaishvili, A., Rodríguez-Ceja, M., Morales, J., Soler, A.M., Urrutia-Fucugauchi, J., 2021. On the absolute geomagnetic intensity fluctuations in Mexico over the last three millennia. J. South Am. Earth Sci. https://doi.org/10.1016/j.jsames.2020.102927.

García-Pimentel, A., Goguitchaichvili, A., Torreblanca, C., Cejudo-Ruiz, R., Kravchinsky, V., García, R., Morales, J., Cervantes, M., 2020. The memory of fire in El Coporo (Northern Mesoamerica): apogee and abandonment. J. Archaeol. Sci. Rep. 30 https://doi.org/10.1016/j.jasrep.2020.102274.

García-Quintana, A., Goguitchaichvili, A., Morales, J., Cervantes-Solano, M., Osorio-Ocampo, S., Macías, J.L., Urrutia-Fucugauchi, J., 2016. Datación magnética de rocas volcánicas formadas durante el Holoceno: caso de flujos de lava alrededor del lago de Pátzcuaro (campo volcánico Michoacán-Guanajuato). Rev. Mex. Ciencias Geol. 33 (2), 209–220.

Gasco, J., Masson, M.A., Rosenswig, R.M., Smith, M.E., 2016. Prehispanic Mesoamerica. In: Carmack, R.M., Gasco, J. (Eds.), The Legacy of Mesoamerica: History and Culture of a Native American Civilization, second ed., pp. 38–77.

Genevey, A., Gallet, Y., Constable, G.C., Korte, M., Hulot, G., 2008. ArcheoInt: an upgrade compilation of geomagnetic field Intensity data for the past ten millennia and its application to the recovery of the past dipole moment. Geochem. Geophys. Geosyst. 9 https://doi.org/10.1029/2007GC001881.

Glaze, L.S., Baloga, S.M., Fagents, S.A., Wright, R., 2014. The influence of slope breaks on lava flow surface disruption. J. Geophys. Res. Solid Earth 119, 1837–1850. https://doi.org/10.1002/2013JB010696.

Goguitchaichvili A., García-Ruiz R., Echeverria-Castillo S., Morales J., Ortiz S., Urrutia-Fucugauchi J., 2018a. Last two millenia Earth's Magnetic Field strength: New archaeointensity determinations from Ichkaantijo, Early to Late Maya Classic period. J. Arch. Sci.: Reports, 18:292–299, https://doi.org/10.1016/j.jasrep.2018.01.023

Goguitchaichvili A., Hernández-Quintero E., García-Ruiz R., Cejudo R., Cifuentes G., Cervantes M., 2020. Fluctuation of the Earth's magnetic field elements in Mexico revealed by archive documents since 1587. Physics of the Earth and Planetary Interiors, 300, https://doi.org/10.1016/j.pepi.2020.106433

Goguitchaichvili, A., Morales, J., Schavelzon, D., Vásquez, C., Gogorza, C.S.G., Loponte, D., Rapalini, A., 2015. Variations of the Earth's magnetic field strength in South America during the last two millennia: new results from historical buildings of Buenos Aires and re-evaluation of regional data. Phys. Earth Planet. In. 245, 15–25.

Goguitchaichvili, A., Ortega, V., Archer, J., Morales, J., Terán-Guerrero, A., 2017. Absolute geomagnetic intensity record from pre-Columbian pottery dates elite Tlailotlacan Woman in ancient Teotihuacan. J. Archaeol. Sci.: Reports 14, 141–146.

Goguitchaishvili A., García-Ruiz R., Pavón-Carrasco F.J., Morales-Contreras J.J., Soler- Arechalde A.M., Urrutia-Fucugauchi J., 2018b. Last Three millennia Earth's magnetic field strength in Mesoamerica and southern United States: Implications in geomagnetism and archaeology. Physics of the Earth and Planetary Interiors, 279:79–91, https://doi.org/10.1016/j.pepi.2018.04.003

Gómez-Paccard M., Lanos P., Chauvin A., McInstosh G., Osete M.L., Catanzariti G., Ruiz-Martínez V.C., Núñez J.I., 2006. The first Archaeomagnetic secular variation curve for the Iberian Peninsula. Comparison with other data from Western Europe and with global geomagnetic field models. Geochem. Geophys. Geosyst., 7(12), https://doi.org/10.1029/2006GC001476

Gómez-Paccard M., Osete M.L., Chauvin A., Pavón-Carrasco F.J., Pérez-Asencio M., Jiménez P., Lanos P., 2016. New constraints on the most significant paleointensity change in Western Europe over the last two millennia. A non-dipolar origin? Earth Planet. Sci. Lett. 454:55–64, http://dx.doi.org/10.1016/j.epsl.2016.08.024

Gómez-Tuena, A., Orozco-Esquivel, M., Ferrari, L., 2005. Petrogénesis ígnea de la faja Volcánica Transmexicana. Bol. Soc. Geol. Mex. LVII, 227–283.

González, S., Pastrana A., Siebe, C., Duller, G., 2000. Timing of the prehistoric eruption of Xitle Volcano and the abandonment of Cuicuilco Pyramid, Southern Basin of Mexico. Geological Society, London, Special Publications (Geol. Soc. London Sp. Pub.) 171: 205–224.

González, S., Sherwood, G., Böhnel, H., Schnepp, E., 1997. Paleosecular variation in central Mexico over the last 30,000 years: the record from lavas. Geophys. J. Int.130, 201–219.

González-Huesca, I.S., 1992. La variación secular en México central durante los últimos 30,000 años por medio del estudio magnético de lavas. Doctoral Thesis, National University of Mexico, Mexico City.

Grabowski J., Lakova I., Petrova S., Stoykova K., Inanova D., Wójcik-Tabol P., Sobien K., Schnabl P., 2016. Paleomagnetism and integrated stratigraphy of the Upper Berriasian hemipelagic succession in the Barlya section Western Balkan, Bulgaria: Implications for lithogenic input and paleoredox variations. Palaeogeography, Palaeoclimatology, Palaeoecology, 461(1). https://doi.org/10.1016/j.palaeo.2016.08.018

Gratton, M.N., Goguitchaichvili, A., Conte, G., Shaw, J., Urrutia-Fucugauchi, J., 2005. Article Navigation Microwave palaeointensity study of the Jorullo volcano (Central Mexico). Geophysical Journal International, 161, 3: 627–634, https://doi.org/10.1111/j.1365-246X.2005.02619.x

Guilbaud, M. N., Siebe, C., Layer, P., Salinas, S., 2012. Reconstruction of the volcanic history of the Tacámbaro-Puruarán area (Michoacán, México) reveals high frequency of Holocene monogenetic eruptions. Bull. Volcanol. 74, 1187–1211. https://doi.org/10.1007/s00445-012-0594-0.

Guilbaud, M. N., Siebe, C., Layer, P., Salinas, S., Castro-Govea, R., Garduño-Monroy, V. H., Le Corvec, N., 2011. Geology, geochronology, and tectonic setting of the Jorullo Volcano region, Michoacán, México. J. Volcanol. Geotherm. Res. 201, 97–112. https://doi.org/10.1016/j.jvolgeores.2010.09.005.

Gyarmati J., Maróti B., Kasztovszky Z., Donczo B., Szikzai Z., Aradi L.E., Mihaly J., Koch G., Szilagyi V., 2022. Hidden behind the mask: An authentication study on the Aztec mask of the Museum of Ethnography, Budapest, Hungary, Forensic Science International, 333.

Hagstrum, J.T., Blinman, E., 2010. Archeomagnetic dating in western North America: an updated reference curve based on paleomagnetic and archeomagnetic data sets. Geochem. Geophys. Geosyst. 11, Q06009. https://doi.org/10.1029/2009GC002979.

Hasenaka, T. E., Carmichael, I. S. E., 1985. A compilation of location, size, and geomorphological parameters of volcanoes of the Michoacan-Guanajuato volcanic field, central Mexico. Geofis. Int. 24, 577–607.

Hasenaka, T., 1994. Size, distribution and magma output rates for shield volcanoes of the Michoacán-Guanajuato volcanic field, Central Mexico. J. Volcanol. Geotherm. Res. 63, 13–31.

Hasenaka, T., Carmichael, I.S.E., 1985. The cinder cones of Michoacán-Guanajuato, central Mexico: their age, volume and distribution, and magma discharge rate. J. Volcanol. Geotherm. Res. 25, 105–124.

Heizer, R.F., Bennyhoff, J.A. (1958) Archeological investigations of Cuicuilco, Valley of Mexico, 1957. Science, 127(3292):232–233. doi: 10.1126/science.127.3292.232

Herrero-Bervera, E., Urrutia-Fucugauchi, J., Martin-del Pozzo, A.L., Böhnel, H., Guerrero, J. (1986) Normal amplitude Brunhes paleosecular variation at low latitudes: a paleomagnetic record from the Trans-Mexican Volcanic Belt. Geophysical Research Letters 13(13):1442–1445. https://doi.org/10.1029/GL013i013p01442

Hervé G., Chauvin A., Lanos P., Rochette P., Perrin M., Perron d'Arc, M., 2019a. Cooling rate effect on thermoremanent magnetization in archaeological baked clays: An experimental study on modern bricks. Geophysical Journal International, 217:1413–1424, https://doi.org/10.1096/gji/ggz076.

Hervé, G., Faβbinder, J., Gilder, S. A., Metzner-Nebelsick, C., Gallet, Y., Genevey, A., Schnepp, E., Geisweid, L., Pütz, A., Reuβ, S., Wittenborn, F., Flontas, A., Linke, R., Riedel, G., Walter, F., Westhausen, I., 2017. Fast geomagnetic field intensity variations between 1400 and 400 BCE: New archaeointensity data from Germany. Phys. of the Earth and Planet. Int. 270, 143-156. https://doi.org/10.1016/j.pepi.2017.07.002.

Hervé, G., Perrin, M., Alva, Valdivia L., Madingou, Tchibinda B., Rodríguez, Trejo A., Hernández, Cardona A., Córdova, Tello M., Mezza, Rodríguez C., 2019a. Critical analysis of the Holocene palaeointensity database in Central America: impact on geomagnetic modelling. Geophys. J. Int. 289, 1–10.

Hervé, G., Perrin, M., Alva-Valdivia, L., Rodríguez-Trejo, A., Hernández-Cardona, A., Córdova-Tello, M., Meza-Rodríguez, C., 2019b. Secular variation of the intensity of the geomagnetic field in Mexico during the first millennium BCE. G-cubed 20 (12), 6066–6077. https://doi.org/10.1029/2019GC008668.

Hill M.J., Shaw J., 2000. Magnetic field intensity study of the 1960 Kilauea lava flow, Hawaii, using the microwave palaeointensity technique. Geophys. J. Int., 142:487–504, https://doi.org/10.1046/j.1365-246x.2000.00164.x

Hill, B.E., Connor, C.B., Jarzemba, M.S., La Femina, P.C., Navarro, M., Strauch, W., 1998. 1995 Eruptions of Cerro Negro volcano, Nicaragua, and risk assessment for future eruptions. Geol. Soc. Am. Bull. 110 (10), 1231–1241.

Hodgson, E., Grappone, J.M., Biggin, A.J., Hill, M.J., Dekkers, M.J., 2018. Thermoremanent behavior in synthetic samples containing natural oxyexsolved titanomagnetite. Geochem. Geophys. Geosyst. 19, 1751–1766. https://doi.org/10.1029/2017GC007354.

Hoffman, K. A., Constantine, V. L., Morse, D. L., 1989. Determination of absolute palaeointensity using a multi-specimen procedure. Nat. 339, 295–297. https://doi.org/10.1038/339295a0

Huang W., van Hinsbergen D.J.J., Maffione M., Orme D.A., Dupont-Nivet G., Guilmette C., Ding L., Guo Z., Kapp P., 2015. Lower Cretaceous Xigaze ophiolites formed in the Gangdese forearc: Evidence from paleomagnetism, sediment provenance, and stratigraphy. Earth and Planetary Science Letters, 415. https://doi.org/10.1016/j.epsl.2015.01.032

Jackson, A., Jonkers, A.R.T., Walker, M.R., 2000. Four centuries of geomagnetic secular variation from historical records. Phil. Trans. Roy. Soc. Lond. 358, 957–990. https://doi.org/10.1098/rsta.2000.0569.

Jadot, E., Testard, J., 2020. Artefactos cerámicos y otros pequeños objetos. ARCHAEOPRESS. In: El Palacio: Historiography and New Perspectives on a Pre-Tarascan City of Northern Michoacán, Mexico, 53. Paris Monographs in American Archaeology, pp. 135–171, 9781789697964.

Kapper L., Serneels V., Panovska S., García-Ruiz R., Hellio G., de Groot L., Goguichaishvili A., Morales J., Cejudo-Ruiz R., 2020. Novel insights on the geomagnetic field in West Africa from new intensity curve 0-2000 A.D. Scientific Reports, 10(1121) | https://doi.org/10.1038/s41598-020-57611-9

Kirschvink, J. L., 1980. The least-squares line and plane and the analysis of palaeomagnetic data, Geophys. J. Roy. Astron. Soc., 62, 699–718.

Kissel C., Laj, C., 2004. Improvements in procedure and paleointensity selection criteria (PICRIT-03) for Thellier and Thellier determinations: applications to Hawaii basaltic long cores. Physics of Earth and Planetary Interiors, 147(2-3):155–169, https://doi.org/10.1016/j.pepi.2004.06.010

Kitahara, Y., Yamamoto, Y., Ohno, M., Kuwahara, Y., Kameda, S., Hatakeyama, T., 2018. Archeointensity estimates of a tenth-century kiln: first application of the Tsunakawa-Shaw paleointensity method to archeological relics. Earth Planets Space 70, 79. https://doi.org/10.1186/s40623-018-0841-5

Korte M., Constable C., Donadini F., Holmes R., 2011. Reconstructing the Holocene geomagnetic field. Earth Planet. Sci. Lett, 312:497–505, https://doi.org/10.1016/j.epsl.2011.10.031

Korte M., Donadini F., Constable C.G., 2009. Geomagnetic field for 0-3 ka: 2. A new series of time-varying global models Geochem. Geophys. Geosyst., 10(6) doi:10.1029/2008GC002297.

Korte, M., Brown, M. C., Panovska, S., Wardinski, I., 2019. Robust Characteristics of the Laschamp and Mono Lake Geomagnetic Excursions: Results From Global Field Models. Frontiers in Earth Science. https://doi.org/10.3389/feart.2019.00086

Korte, M., Brown, M.C., Gunnarson, S.R., Nilsson, A., Panovska, S., Wardinski, I., Constable, C.G., 2019. Refining Holocene geochronologies using palaeomagnetic records. Quat. Geochronol. 50, 47–74. https://doi.org/10.1016/j.quageo.2018.11.004.

Korte, M., Constable, C., 2003. Continuous global geomagnetic field models for the past 3000 years. Phys. Earth Planet. In. 140, 73–89.

Kosterov, A.A., Prévot, M., 1998. Possible mechanisms causing failure of Thellier palaeointensity experiments in some basalts. Geophys. J. Inter. 134, 554–572.

Kovacheva M., Boyadziev Y., Kostadinova-Avramova M., Jordanova N., Donadini F., 2009. Update archaeomagnetic data set of the past 8 millennia from the Sofia laboratory, Bulgaria. Geochem. Geophys. Geosyst., 10(5), https://doi.org/10.1029/2008GC002347

Kovacheva M., Kostadinova-Avramova M., Jordanova N., Lanos P., Boyadzhiev Y., 2014. Extended and revised archaeomagnetic database and secular variation curves from Bulgaria for the eight millennia. Physics of the Earth and Planetary Interiors, 236:79–94, https://doi.org/10.1016/j.pepi.2014.07.002

Kovacheva, M., Chauvin, A., Jordanova, N., Lanos, Ph., Karloukovski, V., 2009. Remanence anisotropy on the paleointensity results obtained from various archaeological materials, excluding pottery. Earth Planets Space 61, 711–732. https://doi.org/10.1186/BF03353179.

Krása, D., Heunemann, C., Leonhardt, R., Petersen, N., 2003. Experimental procedure to detect multidomain remanence during Thellier-Thellier experiments. Phys. Chem. Earth 28 (16–19), 681–687. https://doi.org/10.1016/S1474-7065(03)00122-0.

Kravchinsky, V.A., Zhang, R., Borowiecki, R., Tarasov, P.E., Van der Baan, M., Anwar, T., Goguitchaichvili, A., Muller, S., 2021. Centennial scale climate oscillations from southern Siberia in the Last Glacial Maximum. Quaternary Science Reviews, 270. https://doi.org/10.1016/j.quascirev.2021.107171

Lanos P., 2004. Bayesian inference of calibration curves: Application to archaeomagnetism. In Buck C.E., & Millard A.R., (Eds.), Tools for Constructing Chronologies: Crossing Disciplinary Boundaries, London: Springer, 43–82.

Lanos, P., 1987. The effects of demagnetizing field on thermoremanent magnetization acquired by parallel-sided baked clay blocks. Geophy. J. R. Astron. Soc. 91, 985–1012. https://doi.org/10.1111/j.1365-246X.1987.tb01676.x.

Larson E.E., Patterson P.E., Curtis G., Drake R., Mutschler F.E., 1985. Petrologie, paleomagnetic, and structural evidence of a Paleozoic rift system in Oklahoma, New Mexico, Colorado, and Utah. Geologycal society of American Bulletin, 96, 1364 – 1372.

Lenhardt, N., Böhnel, H., Wemmer, K., Torres-Alvarado, I.S., Hornung, J., Hinderer, M., 2010. Petrology, magnetostratigraphy and geochronologyof the Miocene volcaniclastic Tepoztlán Formation:implications for the initiation of the TransmexicanVolcanic Belt (Central Mexico). Bull Volcanol, 72: 817-832, DOI 10.1007/s00445-010-0361-z

Leonhardt R., Heunemann C., Krasa D., 2004. Analyzing absolute paleointensity determinations: Acceptance criteria and the software ThellierTool4.0. Geochemistry, Geophysics, Geosystems, 5(12), https://doi.org/10.1029/2004GC00807

Leonhardt, R., 2006. Analyzing rock magnetic measurements: the Rock-MagAnalyzer 1.0 software. Comput. Geosci. 32, 1420–1431. https://doi.org/10.1016/j.cageo.2006.01.006.

Leonhardt, R., Hufenbecher, F., Heider, F., Soffel, H., 2000. High absolute paleointensity during a mid-Miocene excursion of the Earth's magnetic field. Earth Planet. Sci. Lett. 184 (1), 141–154, 30.

Leonhardt, R., Matzka, J., Menor, A., 2003. Absolute paleointensities and paleodirections from Fernando de Noronha, Brazil. Phys. Earth Planet. Int. 139, 285–303.

Levi, S., 1977. The effect of magnetite particle size on paleointensity determinations of the geomagnetic field. Phys. Earth Planet. Inter., 13:245–259. https://doi.org/10.1016/0031-9201(77)90107-8

Lewchuk M.T., Al-Aasm I.S., Symons D.T.A., Gillen K.P., 1998. Dolomitization of Mississippian carbonates in the Shell Waterton gas field, southwestern Alberta: insights from paleomagnetism, petrology and geochemistry. Bulletin of Canadian Petroleum Geology 46(3), 387 -410.

Libby, W.F., 1955. Radiocarbon Dating. 2nd ed., Chicago University Press, Chicago, USA.

Licht, A., Hulot, G., Gallet, Y., Thébault, 2013. Ensembles of low degree archeomagnetic field models for the past three millennia. Phys. Earth Planet. Inter. 224, 38–67.

Lisé-Pronovost, A., Mallett, T., Herries, A.I.R., 2020. Archaeointensity of nineteenth century Scottish firebricks from a foundry in Melbourne, Australia: comparisons with field models and magnetic observatory data. In: Geomagnetic Field Variations in the Past. New Data, Applications and Recent Advances, vol. 497. Geological Society, London, Special Publications, pp. 27–45. https://doi.org/10.1144/SP497-2019-72.

Lloyd, S.J., Biggin, A.J., Halls, H., Hill, M., 2021. First palaeointensity data from the cryogenian and their potential implications for inner core nucleation age. Geophysical Journal International. https://doi.org/10.1093/gji/ggab090

López-Delgado, V., Goguitchaichvili, A., Torreblanca, C., Cejudo, R., Jiménez, P., Morales, J., Soler, A.M., 2019. La Quemada: decline and abandonment in two stages on the classic period northern frontier of Mesoamerica. J. Archaeol. Sci. Rep. 24, 574–581. https://doi.org/10.1016/j.jasrep.2019.02.013.

Luhr, J. F., Simkin, T., Cuasay, M., 1993. Parícutin: The Volcano Born in a Mexican Cornfield. US Geoscience Press.

Mahgoub A.N., Juarez-Arriaga E., Böhnel H., Manzanilla L., Cyphers A., 2019b. Refined 3600 years palaeointensity curve for Mexico. Physics of the Earth and Planetary Interiors, 296. https://doi.org/10.1016/j.pepi.2019.106328

Mahgoub A.N., Juárez-Arriaga E., Böhnel H., Siebe C., Pavón-Carrasco F.J., 2019a. Late-Quaternary secular variation data from Mexican volcanoes. Earth and Planetary Science Letters, 519:28–39, https://doi.org/10.1016/j.epsl.2019.05.001

Mahgoub, A. N., Reyes-Guzmán, N., Böhnel, H., Siebe, C., Pereira, G., Dorison, A., 2017. Paleomagnetic constraints on the ages of the Holocene Malpaís de Zacapu lava Flow eruptions, Michoacán (Mexico): implications for archeology and volcanic hazards. The Holocene. 28 (2), 229–245. https://doi.org/10.1177/0959683617721323

Mahgoub, A.N., Böhnel, H., Siebe, C., Chevrel, M.O., 2017. Paleomagnetic study of El Metate shield volcano (Michoacán, Mexico) confirms its monogenetic nature and young age (~1250 CE). J. Volcanol. Geotherm. Res. https://doi.org/10.1016/j.jvolgeores.2017.02.024.

Manley, C.R., 1992. Extended cooling and viscous flow of large, hot rhyolite lavas: implications of numerical modeling results. J. Volcanol. Geotherm. Res. 53 (1), 27–46.

Martin-Del Pozzo, A.L., Cordoba, C., López, J. (1997) Volcanic impact on the southern Basin of Mexico during the Holocene. Quaternary International 43-44:181–190. https://doi.org/10.1016/S1040-6182(97)00034-7

Márton P., 2010. Two thousand years of geomagnetic field direction over central Europe revealed by indirect measurements. Geophys. J. Int. 181(1):261–268, https://doi.org/10.1111/j.1365-246X.2010.04507.x

Márton P., Ferencz, E., 2006. Hierarchical versus stratification statistical analysis of archaeomagnetic directions: the secular variation curve for Hungary, Geophys. J. Int., 164(3): 484–489, https://doi.org/10.1111/j.1365-246X.2006.02873.x

McCabe C., Jackson M., 1985. Magnetic anisotropy in the Trenton Limestone: Results of a new technique, anisotropy of Anhysteretic susceptibility. Geophysical Research Letters, 12(6):333–336, https://doi.org/10.1029/GL012i006p00333

McFadden, P.L., Lowes, F.J., 1981. The discrimination of mean directions drawn from Fisher distributions. Geophys. J. R. Astron. Soc. 67, 19–33.

Michalk, D. M., Biggin, A. J., Knudsen, M. F., Böhnel, H. N., Nowaczyk, N. R., Ownby, S., López-Martínez, M., 2010. Application of the multispecimen palaeointensity method to Pleistocene lava flows from the Trans-Mexican Volcanic Belt. Phys. of the Earth and Planet. Inter., 179, 139–156. https://doi.org/10.1016/j.pepi.2010.01.005

Michalk, D. M., Muxworthy, A. R., Böhnel, H. N., Maclennan, J., Nowaczyk, N., 2008. Evaluation of the multispecimen parallel differential pTRM method: A test on historical lavas from Iceland and Mexico. Geophys. J. Int., 173, 409–420. https://doi.org/10.1111/j.1365-246X.2008.03740.x

Michelet, D., 1988. La Céramique du Project Michoacán : quelques considérations sur son évolution séquentielle. CEMCA, México, p. 17.

Michelet, D., 2018. El Apogeo Tarasco. In: La Ciudad Perdida. Raíces de los soberanos Tarascos. Pereira G. and Padilla Gutiérrez E. F. Coor. (First edition) CEMCA. Secretaría de cultura. INAH. Museo Nacional de Antropología, 91 – 97.

Michelet, D., Demant, A., Labat, J.N., Michelet, D., Tricart, J., 1992. El Centro – Norte de Michoacán: características generales de su estudio regional. El Proyecto Michoacán 1983 –1987. Medio Ambiente e Introducción a los Trabajos Arqueológicos. CEMCA, México. D.F. Collection Etudes Mésoaméricaines II (11): 9 –52.

Michelet, D., Pereira, G., Migeon, G., 2005. La llegada de los uacusechas a la región de Zacapu, Michoacán: datos arqueológicos y discusión. In: Manzanilla, L. (Ed.), Reacomodos demográficos del Clásico al Posclásico en el centro de México. IIA, UNAM, Mexico, pp. 137–153.

Migeon, G., 2016. Patrones de asentamiento del Malpaís de Zacapu (Michoacán, México) y de sus alrededores en el Posclásico. Paris Monographs In: Am. Archaeol. 46, 23–124

Molina-Cardín A.,Campuzano S.A., Osete M.L., Rivero-Montero M., Pavón-Carrasco F.J., Palencia-Ortas A., Martín-Hernández F., Gómez-Paccard M., Chauvin A., Guerrero-Suárez S., Pérez-Fuentes J.C., McIntosh G., Catanzariti G., Sastre-Blanco J.C., Larrazabal J., Fernández-Martínez V.M., Álvarez-Sanchís J.R., Rodríguez-Hernández J., Martín-Viso I., Garcia-Rubert D.. 2018. Updated Iberian archeomagnetic catalogue: New full vector paleosecular variation curve for the last three millennia. Geochemistry, Geophysics, Geosystems, 19(10):3637–3656, https://doi.org/10.1029/2018GC007781

Monster, M.W.L., de Groot, L.V., Biggin, A.J., Dekkers, M.J., 2015b. The performance of various palaeointensity techniques as a function of rock-magnetic behaviour - a case study for La Palma. Phys. Earth Planet. Inter. 242:36–49. doi: 10.1016/j.pepi.2015.03.004

Monster, M.W.L., de Groot, L.V., Dekkers, M.J., 2015a. MSP-Tool: A VBA-based software tool for the analysis of multispecimen paleointensity data. Frontiers in Earth Science 3(86). doi: 10.3389/feart.2015.00086.

Morales, J., Alva-Valdivia, L.M., Goguitchaichvili, A., Urrutia-Fucugauchi, J., 2006. Cooling Rate Corrected Paleointensities From the Xitle Lava Flow: Evaluation of Within-Site Scatter for Single Spot-Reading Cooling Units. Earth Planets and Space, 58(10):1341–1347. doi: 10.1186/BF03352630

Morales, J., Fernández Martínez, G., Gogichaisvilli, A., Cárdenas, E., Hernández-Bernal, M.S., 2015. Archeomagnetic dating of some pre-columbian pottery fragments from northern mesoamerica: implications for the chronology of central Mexico during the epiclassic period. J. Arch. Sci. Rep. 4, 32–43. https://doi.org/10.1016/j.jasrep.2015.08.027.

Morales, J., Goguitchaichvili, A., Acosta, G., González-Morán, T., Alva-Valdivia, L., Robles-Camacho, J., Hernández-Bernal, M.S., 2009. Magnetic properties and archeointensity determination on Pre-Columbian pottery from Chiapas, Mesoamerica. Earth Planets Space 83–91. https://doi.org/10.1186/BF03352887.

Morales, J., Goguitchaichvili, A., Aguilar Reyes, B., Pineda, M., Carvallo, C., Baramendi Orozco, L., González Hernández, G., Oliveros, A., 2012. A detailed rock-magnetic and archeointensity investigation on some pottery relics and burned floors from Tzintzuntzan archeological site, western Mesoamerica. Geoarchaeology 27 (issue 6), 521–537. https://doi.org/10.1002/gea.21426, 2012.

Morales, J., Goguitchaichvili, A., Aguilar-Reyes, B., Pineda-Duran, M., Camps, P., Carvallo, C., Calvo-Rathert, M., 2011. Are ceramics and bricks reliable absolute geomagnetic intensity carriers? Phys. Earth Planet. Inter. 187, 310–321. https://doi.org/10.1016/j.pepi.2011.06.007.

Morales, J., Goguitchaichvili, A., Olay, A., Carvallo, C., Aguilar Reyes, B., 2013. Archeointensity investigation on pottery vestiges of puertas de rolón, capacha culture: in search for affinity with other mesoamerican prehispanic cultures. Stud. Geophys. Geod. 57, 605–626. https://doi.org/10.1007/s11200-012-0878-z.

Morales, J., Goguitchaichvili, A., Urrutia-Fucugauchi, J., 2001. A rock-magnetic and paleointensity study of some Mexican volcanic lava flows during the Latest Pleistocene to the Holocene. Earth Planets Space53 (9), 893–902.

Morales, J., Hernández-Bernal, M.S., Goguitchaichvili, A., Punzo-Díaz, J.L., 2017. An integrated magnetic, geochemical and archeointensity investigation of casting debris from ancient metallurgical sites of Michoacan, western Mesoamerica. Stud. Geophys. Geod. 61, 290–309. https://doi.org/10.1007/s11200-016-1033-z.

Morales, J., Pérez-Rodríguez, N., Goguitchaichvili, A., Cervantes-Solano, M., 2020. A multimethod paleointensity approach applied to the historical Xitle lava flows (Central Mexico): towards the accurate paleointensity determination. Earth, Planets and Space, 72 (101). https://doi.org/10.1186/s40623-020-01232-z

Morales, J., Smith-Márquez, S.M., Goguitchaichvili, A., Cárdenas-García, E., 2020. Estudio Arqueomagnético del sitio arqueológico El Palacio de Ocomo (Noreste de Mesoamérica): evidencia de su abandono en el Posclásico. Arqueol. Iberoam. 46, 64–71.

Morales-Contreras, J.J., 1995. Determinación de paleointensidades del campo geomagnético para el Cuaternario en la Sierra Chichinautzin, Ms.Sc. Thesis, UNAM, México.

Moskowitz, B.M., 1981. Methods for estimating Curie temperatures of titanomaghemites from experimental Js-T data. Earth Planet Sci. Lett. 53 (1), 84–88. https://doi.org/10.1016/0012-821X(81)90028-5.

Muxworthy, A. R., Taylor, S. N., 2011. Evaluation of the domain-state corrected multiple-specimen absolute palaeointensity protocol: a test of historical lavas from Iceland. Geophys. J. Int. 187,118–127. doi:10.1111/j.1365-246X.2011.05163.x

Nagata, T., Arai, Y., Momose, K., 1963. Secular variation of the geomagnetic total force during the last 5000 years. J. Geophys. Res. 68, 5277–5281. https:// doi. org/ 10. 1029/j. 2156- 2202. 1963. tb000 05.x

Nagata, T., Arai, Y., Momose, K., 1965b. Secular variation of the geomagnetic total force during the last 5000 years. J. Geophys. Res., 68, 5277-5282.

Nagata, T., Kobayashi, K., Schwarz, E.J., 1965a. Archeomagnetic intensity studies of South and Central America. J. Geomagn. Geoelectr., 17:399–405. https://doi.org/10.5636/jgg.17.399

Newton, A. J., Metcalfe, S. E., Davies, S. J., Cook, G., Barker, P., Telford, R. J., 2005. Late Quaternary volcanic record from lakes of Michoacan, central Mexico. Quat. Sci. Rev., 24, 91–104. doi:10.1016/j.quascirev.2004.07.008

Nilsson, A., Holme, R., Korte, M., Suttie, N., Hill, M., 2014. Reconstructing Holocene geomagnetic field variation: new methods, models and implications. Geophys. J. Int. 198 (1), 229–248. https://doi.org/10.1093/gji/ggu120.

Ohi, K., 2005. Tinganio. Memoria de un sitio arqueológico de la Sierra Purépecha. Universidad de Estudios Extranjeros de Kyoto, Japón, p. 103.

Olay Barrientos, M.A., Cejudo, R., Goguitchaichvili, A., Morales, J., Soler, A.M., 2020. The temporality of the funerary spaces of the Colima valley through the determination of the absolute geomagnetic archaeointensity of its archaeological pottery. Arq. Iberoam. 45, 64–92. ISSN 1989-4104.

Ortega-Guerrero, B., Urrutia-Fucugauchi, J., Nieto-Obregón, J. (1993) Geología y edades C-14 del derrame del Pedregal de San Ángel: México City, Universidad Nacional Autónoma de México, Instituto de Geofísica, Internal report (unpublished).

Osorio-Campos, S., Macías, J. L., Pola, A., Cardona-Melchor, S., Sosa-Ceballos, G., Garduño-Monroy, V. H., Layer, P. W., García-Sánchez, L., Perton, M., Benowitz, J., 2018. The eruptive history of the Pátzcuaro Lake area in the Michoacán Guanajuato Volcanic Field, central México: Field mapping, C-14 and 40Ar/39Ar geochronology. J. of Volcanol. and Geotherm. Res., 358. https://doi.org/10.1016/j.jvolgeores.2018.06.003

Panovska, S., Korte, M., Finlay, C.C., Constable, C.G., 2015. Limitations in paleomagnetic data and modelling techniques and their impact on Holocene geomagnetic field models. Geophys. J. Int. 202, 402–418. https://doi.org/10.1093/gji/ggv137.

Paterson, G. A., Biggin, A. J., Hodgson, E., Hill, M. J., 2015. Thellier-type paleointensity data from multidomain specimens. Phys. Earth and Plan. Int. 117 – 133. http://dx.doi.org/10.1016/j.pepi.2015.06.003

Paterson, G. A., Zhao, X., Jackson, M., Heslop, D., 2018. Measuring, processing, and analyzing hysteresis data, Geochem. Geophys. Geosyst., 19, doi:10.1029/2018GC007620.

Paterson, G., 2011. A simple test for the presence of multidomain behavior during paleointensity experiments. J. Geophys. Res. 116 (B10104) https://doi.org/10.1029/2011JB008369.

Paterson, G.A., Tauxe, L., Bigging, A.J., Shaar, R., Jonestrask, L., 2014. On improving the selection of Thellier-type paleointensity data. Geochem. Geophys. Geosyst. 15, 1180–1192. https://doi.org/10.1002/2013GC005135.

Paterson, G.A., Zhao, X., Jackson, M., Heslop, D., 2018. Measuring, processing, and analyzing hysteresis data. Geochem. Geophys. Geosyst. 19 https://doi.org/10.1029/2018GC007620.

Pavón-Carrasco F.J., Osete M.L., Torta J.M., De Santis A., 2014. Geomagnetic Field Model for the Holocene based on archaeomagnetic and lava flows data. Earth Planet. Sci. Lett., 388:98–109, https://doi.org/10.1016/j.epsl.2013.11.046

Pavón-Carrasco F.J., Osete M.L., Torta M.J., 2010. Regional modeling of the geomagnetic field in Europe from 6000 to 1000 B.C. Geochemistry, Geophysics and Geosystems, 11(11), doi: 10.1029/2010GC003197.

Pavón-Carrasco, F.J., Rodríguez-González, J., Osete, M.L., Torta, J.M., 2011. A matlab tool for archeomagnetic dating. J. Archaeol. Sci. 38, 408–419. https://doi.org/10.1016/j.jas.2010.09.021.

Pereira, G., Michelet, D., Gillot, C., Quesada, O., 2019. El Rinc´on de las flores: un asentamiento monumental de la región de Zacapu en el epiclásico. In conference. IV Coloquio de la Arqueología en Michoacán y sus áreas vecinas. Urbanismo y Arquitectura. [Unpublished results].

Pérez-Rodríguez N., Morales J., Guilbaud M.N., Goguitchaichvili A., Cejudo-Ruiz R., Hernández-Bernal M.S., 2020. Reassessment of the eruptive chronology of El Metate shield volcano (central-western Mexico) based on a comprehensive rock-magnetic, paleomagnetic and multi-approach paleointensity survey. Quaternary Geochronology, 55. https://doi.org/10.1016/j.quageo.2019.101031.

Pérez-Rodríguez, N., Morales, J., Goguitchaichvili, A., García-Tenorio, F., 2019. A comprehensive paleomagnetic study from the last Plinian eruptions of Popocatepetl volcano: absolute chronology of lavas and estimation of emplacement temperatures of PDCs. Earth, Planets and Space, ttps://doi.org/10.1186/s40623-019-1059-x

Pérez-Rodríguez, N., Morales, J., Rangel-Campos, D., Goguitchaichvili, A., Punzo-Diaz, J.L., 2021. An inter-comparison exercise for the Mexican intensity secular variation curves: case study of the tingambato archaeological site (central-western Mexico). Quat. Geochronol. 65 https://doi.org/10.1016/j.quageo.2021.101195.

Pérez-Rodríguez, N., Morales-Contreras, J., García-Tenorio, F., Gogishaishvili, A., 2015. Fechamiento arqueomagnético de las últimas tres erupciones plinianas del volcán Popocatépetl. In: En Rapalini, A.E., Caballero-Miranda, C., Goguitchaichvili, A. (Eds.), Proceedings Sao Paulo, Brasil, Latinmag Letters, Special Issue, vol. 6, pp. 1–7 C11.

Perrin, M., Alva-Valdivia, L.M., Lopez-Martinez M., Rosas-Elguera, J., Benammi, M., Gonzalez-Rangel, J.A., Camps, P., 2013. Palaeomagnetism of the upper volcanic supergroup, southern part of the Sierra Madre Occidental, Mexico. Geophysical Journal International, 3, 193: 1250-1264.

Piña-Chan, R., Ohi, K., 1982. Exploraciones Arqueológicas en Tingambato, Michoacán. Instituto Nacional de Antropología e Historia de México, México, p. 106.

Pola, A., Macías, J.L., Osorio-Ocampo, S., Sosa-Ceballos, G., Gardu˜no-Monroy, V.H., Martínez-Martínez, J., 2015. El Estribo volcanic complex: evolution from a shield volcano to a cinder cone, Pátzcuaro lake, Michoacán, México. J. Volcanol. Geotherm. Res. https://doi.org/10.1016/j.jvolgeores.2015.07.032.

Poletti W., Trinidade R.I., Hartman G.A., Damian N., Rech R.M., 2016. Archaeomagnetism of Jesuits Missions in South Brazil (1657-1706 AD) and assessment of South American database. Earth Planet. Sci. Lett., 445:36–47, https://doi.org/10.1016/j.epsl.2016.04.006

Pratt, V., 1987. Direct least-squares fitting of algebraic surfaces. ACM SIGGRAPH Comput. Graph. 21 (4), 145–152. https://doi.org/10.1145/37401.37420.

Principe, C., Tanguy, J. C., Arrighi, S., Paiotti, A., Le Goff, M., Zoppi, U., 2004. Chronology of Vesuvius' activity from A.D. 79 to 1631 based on archaeomagnetism of lavas and historical sources. Bull. Volcanol., 66, 703-724. doi: 10.1007/s00445-004-0348-8

Punzo-Díaz J.L., in press. Revisitando las exploraciones arqueológicas en el sitio de Tingambato, Michoacán. Nuevos datos, nuevas tecnologías. Lat. Am. Antiq.

Punzo-Díaz, J.L., 2016. Nueva evidencia de la ocupación de Tingambato durante el Clásico y el Epiclásico en el occidente de México. Arqueol. Iberoam. 30, 10–15.

Qin, J., Zhang, R., Kravchinsky, V., Valet, J.P., Sagnotti, L., Li, J., Xu, Y., Anwar, T., Yue, L., 2022. 1.2-million-year band of Earth–Mars obliquity modulation on the evolution of cold late Miocene to warm early Pliocene climate. ESSOAr, https://doi.org/10.1002/essoar.10510387.2

Ramírez-Uribe, I., Siebe, C., Chevrel, M. O., Fisher, C. T., 2021. Rancho Seco monogenetic volcano (Michoacán, Mexico): Petrogenesis and lava flow emplacement based on LiDAR images. J. of Volcanol. and Geotherm. Res. https://doi.org/10.1016/j.jvolgeores.2020.107169

Ramírez-Uribe, I., Siebe, C., Salinas, S., Guilbaud, M. N., Layer, P., Benowitz, J., 2019. 14C and 40Ar/39Ar radiometric dating and geologic setting of young lavas of Rancho Seco and Mazcuta volcanoes hosting archaeological sites at the margins of the Pátzcuaro and Zacapu lake basins (central Michoacán, Mexico). J. Volcanol. Geotherm. Res. 388, 1–22. https://doi.org/10.1016/j.jvolgeores.2019.106674

Rangel-Campos, D., 2018. Datación de la cerámica de Tingambato mediante la técnica de arqueomagnetismo. Bachelor Thesis. ENAH, Mexico City.

Reyes-Guzmán, N., Siebe, C., Chevrel, M. O., Guilbaud, M. N., Salinas, S., Layer, P., 2018. Geology and radiometric dating of Quaternary monogenetic volcanism in the western Zacapu lacustrine basin (Michoacán, México): implications for archeology and future hazard evaluations. Bull. of Volcanol. 80 (18). https://doi.org/10.1007/s00445-018-1193-5

Riisager, P., Riisager, J., 2001. Detecting multidomain magnetic grains in Thellier palaeointensity experiments. Phys. Earth Planet. Inter. 125, 111–117.

Roberts, A.P., Tauxe, L., Heslop, D., Zhao, X., Jiang, Z., 2018. A critical appraisal of the "day" diagram. JGR Solid Earth 123, 2618–2644. https://doi.org/10.1002/2017JB015247.

Roberts, A.P., Winklhofer, M., 2004. Why are geomagnetic excursions not always recorded in sediments? Constraints from post-depositional remanent magnetization lock-in modelling. Earth Planet Sci. Lett. 227, 345–359.

Rodríguez-Ceja M.G., 2009. Propiedades Magnéticas y arqueointensidades de Cerámicas Teotihuacanas. PhD Thesis, Instituto de Geofísica, UNAM

Rodríguez-Ceja M.G., Soler-Arechalde A.M., Morales J.J., Goguichaishvili A., 2012. Estudios de arqueointensidad y propiedades magnéticas de céramicas teotihuacanas. Una aportación a la cronología de Mesoamérica. Estudios arqueométricos del centro del barrio de Teopancazco en Teotihuacan, First edition, Instituto de Investigaciones Antropológicas, UNAM, ISBN, 978-607-02-3605- 1

Rojas-Navarrete, L.L., 1995. Desarrollo de un vidriado sin plomo de baja temperatura para la alfarería tradicional Mexicana. M. Sc. thesis, Universidad Autónoma Metropolitana. Unidad Iztapala 127.

Rolph, T. C., Shaw, J., 1985. A new method of paleofield magnitude correction for thermally altered samples and its application to lower carboniferous lavas. Geophys. J. R. Astron. Soc. 80, 773–781 doi: 10.1111/j.1365-246X.1985.tb05124.x

Roperch, P., Chauvin, A., Lara, L.E., Moreno, H., 2015. Secular variation of the Earth's magnetic field and application to paleomagnetic dating of historical lava flows in Chile. Phys. Earth Planet. In. 242, 45–78. https://doi.org/10.1016/j.pepi.2015.03.005.

Ruíz-González V., Renda E.M., Vizán H., Ganerod M., Puigdomenech C.G., Zaffarana C.B., 2022. Deformation along the Deseado Massif (Patagonia, Argentina) during the Jurassic Period and its relationship with the Gondwana breakup: paleomagnetic and geochronological constraints. Tectonophysics, 834(5). https://doi.org/10.1016/j.tecto.2022.229389

Sánchez-Moreno, E. M., Calvo-Rathert, M., Goguitchaichvili, A., Vashakidze, G. T., Camps, P., Morales-Contreras, J., Vegas-Tubía, N., Lebedev, V. A., 2021. Paleointensity Results From Pliocene Lavas of the Lesser Caucasus Obtained Using the Multispecimen Parallel Differential pTRM Method: A Comparison With Thellier-Thellier and IZZI Data. J. of Geophys. Res.: Solid Earth, 126. https://doi.org/10.1029/2020JB019682

Santini L.M., Weber S.L., Marston J.M., Runggaldier A., 2022. First archaeological identification of nixtamalized maize, from two pit latrines at the ancient Maya site of San Bartolo, Guatemala. Journal of Archaeological Science, https://doi.org/10.1016/j.jas.2022.105581

Schnepp E., Lanos P., 2005. Archaeomagnetic secular variation in Germany during the past 2500 years. Geophys. J., Int., 163(2):479–490, https://doi.org/10.1111/j.1365-246X.2005.02734.x

Schnepp E., Lanos P., 2006. A preliminary secular variation reference curve for archaeomagnetic dating in Austria. Geophysical Journal International, 166(1):91–96, https://doi.org/10.1111/j.1365-246X.2006.03012.x.

Schnepp, E., Brüggler, M., 2016. Archaeomagnetic investigation of a Roman glass workshop in Goch-Asperden, Germany. J. of Archaeol. Sci.: Rep. 10, 322-330. http://dx.doi.org/10.1016/j.jasrep.2016.10.015

Schnepp, E., Thallner, D., Arneitz, P., Mauritsch, H., Scholger, R., Rolf, C., Leonhardt, R., 2020. New archaeomagnetic secular variation data from Central Europe. I: directions. Geophysical Journal International, 220, 1023-1044. doi: 10.1093/gji/ggz492

Selkin, P. A., Tauxe, L., 2000. Long-term variations in palaeointensity. Philos. Trans. R. Soc. Lond. A. 358, 1065–1088. http://doi.org/10.1098/rsta.2000.0574

Shaw, J., 1974. A new method of determining the magnitude of the paleomagnetic field. Application to five historical lavas and five archaeological samples. Geophys. J. R. Astr. Soc., 76, 637 – 651.

Siebe, C., 2000. Age and archaeological implications of Xitle volcano, southwestern Basin of Mexico-City. J. Volcanol. Geoth. Res. 104, 45–64. https://doi.org/10.1016/S0377- 0273(00)00199-2.

Singer, B.S., Jicha, B.R., Mochizuki, N., Coe, R.S., 2019. Synchronizing volcanic, sedimentary, and ice core records of Earth's last magnetic polarity reversal. Sci. Adv. 5, eaaw4621. https://doi.org/10.1126/sciadv.aaw4621.

Suganuma, Y., Haneda, Y., Kameo, K., Kubota, Y., Hayashi, H., Itaki, T., Okuda, M., Head, M.J., Sugaya, M., Nakzato, H., Igarashi, A., Shikoku, K., Hongo, M., Watanabe, M., Satoguchi, Y., Takeshita, Y., Nishida, N., Izumi, K., Kawamura, K., Kawamata, M., Okuno, J., Yoshida, T., Ogitsu, I., Yabusaki, H., Okada, M., 2018. Paleoclimatic and paleoceanographic records of marine isotope stage 19 at the chiba composite section, central Japan: a reference for the early-middle pleisotocene boundary. Quat. Sci. Rev. 191, 406–430. https://doi.org/10.1016/j.quascirev.2018.04.022.

Tanguy, J.C., 1990. Abnormal shallow paleomagnetic inclinations from the 1950 and 1972 lava flows, Hawaii. Geophys. J. Int. 103, 281–283.

Tauxe, L., 2010. Essentials of Paleomagnetism. University of California Press, 489 p.

Tauxe, L., Mullender, T.A.T., Pick, T., 1996. Potbellies, wasp-waists, and superparamagnetism in magnetic hysteresis. J. Geophys. Res. 10 (B1), 571–583. https://doi.org/10.1029/95JB03041.

Tauxe, L., Staudigel, H., 2004. Strength of the geomagnetic field in the Cretaceous Normal Superchron: New data from submarine basaltic glass of the Troodos Ophiolite. Geochemistry Geophysics Geosistems 5(2). doi:10.1029/2003GC000635

Tauxe, L., Yamazaki, T., 2015. 5.13 Paleointensities. In: Schubert, G. (Ed.), Treatise on Geophysics (Second Edition) Elsevier, Oxford, 461–509. http://dx.doi.org/10.1016/B978-0-444-53802-4.00107-X

Tchambé B.C., Kereszturi G., Németh K., Carrasco-Nuñez G., 2016. How Polygenetic are Monogenetic Volcanoes: Case Studies of Some Complex Maar-Diatreme Volcanoes. Meneth, K. (Ed.). In: Updates in Volcanology. From Volcano modelling to Volcano Geology, pp. 355 – 390.

Tema E., Kondopolou D., 2011. Secular variation of the Earth's magnetic field in the Balkan region during the last eight millennia based on archaeomagnetic data. Geophysical Journal International, 186:603–614, doi:10.1111/j.1365-246X.2011.05088.x

Tema, E., 2009. Estimate of the magnetic anisotropy effect on the archaeomagnetic inclination of ancient bricks. Phys. Earth Planet. Inter. 176, 213–223. https://doi.org/10.1016/j.pepi.2009.05.007.

Tema, E., Camps, P., Ferrara, E., Poidras, T., 2015. Directional results and absolute archaeointensity determination by the classical Thellier and the multi-specimen DSC protocols for two kilns excavated at Osterietta, Italy. Stud. Geophys. Geod. 59, 554–577. https://doi.org/10.1007/s11200-015-0413-0

Tema, E., Ferrara, E., Camps, P., Conati-Barbaro, C., Spatafora, S., Carvallo, C., Poidras, T., 2016. The Earth's magnetic field in Italy during the Neolithic period: new data from the Early Neolithic site of Portonovo (Marche, Italy). Earth Planet Sci. Lett. 448, 49–61. http://dx.doi.org/10.1016/j.epsl.2016.05.003

Tema, E., Hedley I., Lanos P., 2006. Archaeomagnetism in Italy: a compilation of data including new results and a preliminary Italian secular variation curve. Geophys. J. Int. 167(3):1160–1171, https://doi.org/10.1111/j.1365-246X.2006.03150.x

Tema, E., Lanos, P., 2020. New Italian directional and intensity archaeomagnetic reference curves for the past 3000 years: insights on secular variation and Implications on dating. Archaeometry. https://doi.org/10.1111/arcm.12603.

Terán-Guerrero, A.G., Soler-Arechalde, A.M., Goguitchaichvili, A., Caballero- Miranda, C., Morales, J., Urrutia-Fucugauchi, J., 2016. Dataciones arqueomagnéticas en la ciudadela de Teotihuacan, Sierra de las Navajas y Xalasco. Arqueol. Iberoam. 29, 15–20.

Terres R.R., Luyendyk B. P., 1985. Neogene tectonic rotation of the San Gabriel Region, California, suggested by paleomagnetic vectors. Journal of Geophysical Research: Solid Earth, 90(B14). https://doi.org/10.1029/JB090iB14p12467

Thebault E., Gallet Y., 2010. A bootstrap algorithm for deriving the archeomagnetic field intensity variation curve in the Middle East over the past 4 millennia BC. Geophys. Res. Lett., 37. https://doi.org/10.1029/2010GL044788

Thébault, E., Finlay, C., Beggan, C. D., Alken, P., Aubert, J., Barrios, O., Bertrand, F., Bondar, T., Boness, A., Brocco, L., Canet, E., Chabodut, A., Chulliat, A., Coïsson, P., Civet, F., Du, A., Fournier, A., Fratter, I., Gillet, N., Hamilton, B., Hamoudi, M., Gauthier, H., Jager, T., Korte, M., Kuang, W., Lalanne, X., Langlais, B., Léger, J. M., Lesur, V., Lowes, F. J., Macmillan, S., Mandea, M., Manoj, C., Maus, S., Olsen, N., Petrov, V., Ridley, V., Rother, M., Sabaka, T. J., Saturnino, D., Schachtsneider, R., Sirol, O., Tangborn, A., Thomson, A., Toffner-Clausen, L., Vigneron, P., Wardinski, I., Zereva, T., 2015. International geomagnetic reference field: the 12th generation. Earth Planets Space, 67. https://doi.org/10.1186/s40623-015-0228-9.

Thellier E., Thellier O., 1959. Sur l'intensite du champ magnetique terrestre dans la passe historique et geologique. Ann. Geophys. 15:285–376.

Thellier, E., 1938. Sur l'aimantation des terres cuites et ses applications géophysiques. Ann. Inst. Globe Univ. Paris 16, 157–302.

Thellier, E., 1981. Sur la direction du champ magnétique terrestre, en France, durant les deux derniers millenaires. Phys. Earth Planet Inter. 24, 89–132.

Torreblanca, C., Goguitchaichvili, A., L´opez, V., Cejudo, R., Morales, J., Bautista, F., Kravchinsky, V., García, R., 2020. Mesoamerica: absolute chronological contributions through the archeomagnetic study of associated fire pits. J. Archaeol. Sci. Rep. 33 https://doi.org/10.1016/j.jasrep.2020.102558.

Tsunakawa, H., Shaw, J., 1994. The Shaw Method of Palaeointensity Determinations and its Application to Recent Volcanic Rocks. Geophys. J. Int. 118, 781–787. doi:10.1111/j.1365246X.1994.tb03999.x

Urrutia-Fucugauchi, J., 1996. Paleomagnetic study of the Xitle-Pedregal de San Angel lava flow, southern basin of Mexico. Phys. Earth Planet. Inter. 97, 177–196.

Urrutia-Fucugauchi, J., Alva-Valdivia, L.M., Goguitchaichvili, A., Rivas, M.L., Morales, J., 2004. Paleomagnetic, Rock-magnetic and microscopy studies of historic lava flows from the Paricutin volcano, Mexico: implications for the deflection of paleomagnetic directions. Geophys. J. Int. 156, 431–442.

Urrutia-Fucugauchi, J., Goguitchaichvili, A., Pérez-Cruz, L., Morales, J., 2016. Archaeomagnetic dating of the eruption of Xitle volcano, basin of Mexico - implications for the mesoamerican centers of Cuicuilco and Teotihuacan. Arqueol. Iberoam. 30, 23–29. http://laiesken.net/arqueologia/archivo/2016/30/4.PURL.

Urrutia-Fucugauchi, J., Martin-del Pozzo, A.L., 1993. Implicaciones de los datos paleomagnéticos sobre la edad de la Sierra de Chichinautzin, Cuenca de México. Geofísica Internacional 32:523–533.

Valentine, G.A., Connor, C.B., 2015. Basaltic volcanic fields. Sigurdsson, H. (2 Ed.), In: The Encyclopedia of Volcanoes. Academic Press, pp. 423–439.

Valet, J.P., 2003. Time variations in geomagnetic intensity. Rev. Geophys. 41 (1), 44. https://doi.org/10.1029/2001RG000104.

Veitch, R.J., Hedley, I.G., Wagner, J.J., 1984. An investigation of the intensity of the geomagnetic field during Roman times using magnetically anisotropic bricks and tiles. Archaeol. Sci. Gen`eve 37 (3), 359–373.

Viramonte, J.G., Di Scala, L., 1970. Summary of the 1968 eruption of Cerro Negro, Nicaragua. Bull. Volcanol. 34, 347–351.

Williams, E., 2005. El antiguo occidente de México: un área cultural mesoamericana. [online] Foundation for the Advancement of Mesoamerican Studies, Inc., http://www.famsi.org/spanish/research/williams/wm_geography.html Accessed 15 January 2020.

Williams, H., 1950. Volcanoes of the Parícutin Region Mexico. Geological investigations in the Paricutin area, Mexico. United States Printing office, Washington. Geol. Surv. Bull. 965 – B, 165-279.

Wilson, R.L., 1961. Paleomagnetism in Northern Ireland. Part I. The Thermal Magnetization of Natural Magnetic Moments in Rocks. Geophysical Journal International, 5, 1: 45–58, https://doi.org/10.1111/j.1365-246X.1961.tb02928.x

Wolfman D., 1990, Mesoameric chronologies and archaeomagnetic dating, AD 1-1200. Archaeomagnetic dating Eghmy J.L. and R.S. Stern editors, University of Arizona Press, Tucson.

Yamamoto, Y., Tsunakawa, H., Shibuya, H.,2003. Paleointensity study of the Hawaiian 1960 lava: implications for possible causes of erroneously high intensities. Geophys. J. Int. 153, 263–276 doi: 10.1046/j.1365-246X.2003.01909.x

Yamamoto, Y., Yamaoka, R., 2018. Paleointensity Study on the Holocene Surface Lavas on the Island of Hawaii Using the Tsunakawa–Shaw Method. Frontiers in Earth Science. 6:48, doi: 10.3389/feart.2018.00048

Yu, Y., Dunlop, D.J., 2002. Multivectorial paleointensity determination from the cordova gabbro, southern ontario. Earth Planet Sci. Lett. 203, 983–998.

Yu, Y., Tauxe, L., 2005. Testing the IZZI protocol of geomagnetic field intensity determination, Geochem. Geophys. Geosyst., 6 (5). doi:10.1029/2004GC000840.

Yu, Y., Tauxe, L., Genevey A., 2004. Toward an optimal geomagnetic field intensity determination technique. Geochem. Geophys. Geosyst., 5 (2). doi:10.1029/2003GC000630

Zananiri I., Batt C.M., Lanos P., Tarling D.H., Linford P., 2007. Archaeomagnetic secular variation in the UK during the past 4000 years and its application to archaeomagnetic dating. Phys. Earth Planet. Int., 160(2):97–107, https://doi.org/10.1016/j.pepi.2006.08.006

Zijderveld, J., 1967. AC demagnetization of rocks: analysis of results. In Methods in paleomagnetism. Editors Collison, D. W., Creer, K. M., and Runcorn, S. K. (New York, NY: Elsevier), 245–286.